Computer Simulation Studies of Multi-Component Melts and Ionic Liquids

Thesis Submitted for the Degree of

Doctor of Philosophy (Science)

of

Jadavpur University

By

Tamisra Pal

Department of Chemical, Biological and Macromolecular Sciences

S. N. Bose National Centre for Basic Sciences

Block-JD, Sector-III, Salt Lake City

Kolkata-700098, INDIA

July 2014

Dedicated to

My Father Sri Tarak Nath Pal

And

Mother Smt. Sumita Pal

CENTRE FOR BASIC SCIENCES 1986
S. N. BOSE NATIONAL
1894 - 1974
विज्ञानेन परिपश्यन्ति धीराः

सत्येन्द्र नाथ बसु राष्ट्रीय मौलिक विज्ञान केन्द्र
SATYENDRA NATH BOSE NATIONAL
CENTRE FOR BASIC SCIENCES
সত্যেন্দ্র নাথ বসু জাতীয় মৌল বিজ্ঞান কেন্দ্র

CERTIFICATE FROM THE SUPERVISOR(S)

This is to certify that the thesis entitled **"Computer Simulation Studies of Multi-Component Melts and Ionic Liquids"** submitted by **Smt. Tamisra Pal** (Index no. 19/12/Chem./21) , who got her name registered on 18th April 2012 for the award of Ph. D. (Science) degree of Jadavpur University, is absolutely based upon her own work under the supervision of **Prof. Ranjit Biswas** and that neither this thesis nor any part of it has been submitted for either any degree /diploma or any other academic award anywhere before.

Ranjit Biswas 22/07/14

Dr. Ranjit Biswas

Professor,

Department of Chemical , Biological and Macromolecular Sciences

S. N. Bose National Centre for Basic Sciences

Block – JD , Sector – III, Salt Lake , Kolkata – 700098 , West Bengal , India

DR. RANJIT BISWAS
Professor
Dept. of Chemical, Biological & Macromolecular Sciences
S. N. Bose National Centre for Basic Sciences
Block - JD, Sector - III, Salt Lake, Kolkata - 700 098, India

Acknowledgement

I have spent about five years at the S. N. Bose National Centre for Basic Sciences (SNBNCBS) , as a research scholar in the department of Chemical , Biological and Macromolecular Sciences (CBMS) . It is a great pleasure to acknowledge the cooperation I have received from many people. The thesis would not have been possible without their efforts and blessings .

First of all , I would like to take this opportunity to express my sincere thanks and humble gratitude to my supervisor , Prof. Ranjit Biswas . His untiring help , immense support and encouragement motivated me to achieve the best . His constant enthusiasm in work with fruitful and illuminating discussions , have helped me to learn the ways of dealing scientific problems intelligently . Besides academics , he has always incited my creative skills . I am extremely fortunate to have worked with a good person like him , whose suggestions during different phases in Ph. D. tenure have been priceless.

I am obliged to Prof. Arup Kumar Raychaudhuri , the Director , S. N. Bose National Centre for Basic Sciences , for providing the latest computational facilities and excellent research environment . My sincere thanks to Prof. G. Gangopadhyay , Prof. J. Chakrabarti , Prof. S. K. Pal and other faculty members of the department for their help and advice . I also thank Prof. Priya Mahadevan for her whole-hearted assistance regarding computational facilities during those early days of my Ph. D. career. I am indebted to the prompt technical assistance provided by engineers at the computer centre. I thank all the members of my Thesis Committee for devoting their valuable time for me .

I express my profound sense of gratitude to Prof. Biman Bagchi , IISc , Bangalore , India and Prof. Mark Maroncelli , Pennsylvania State University , USA for many comments and suggestions , which have always been helpful in strengthening my manuscripts. My sincere thanks to Prof. Pradip K. Ghorai , IISER, Kolkata, and Dr. Rajesh K. Murarka , IISER , Bhopal, for their great assistance during my simulation work . Prof . Charusita Chakrabarty and her student Shadrack Jabes , IIT, Delhi , deserve lots of appreciation for their help.

Great appreciation extends to all the non-academic staffs of the Centre for their help. I am grateful to the security personnel , canteen-boys during my stay at SNBNCBS.

Thanks to my present labmates (PCCP group) : Anuradha , Sandipa , Suman and Kallol , who shared the same work place for a long time . They provided me such a homely environment and cheered me up with great fun moments , during those difficult times at work . I am indebted to the ex-lab members of this group : Dr. Tuhin Pradhan , Dr. Hemant K. Kashyap , Dr. Harun Al. Rasid Gazi , Dr. Biswajit Guchhait , Dr. Snehasis Daschakraborty and Dr. Mainak Sadhukhan for their tremendous help in various academic and non-academic matters . I would also like to mention the good times spent with project students : Kaustubh , Bibek , Krishna ,Prabhat and Sudhanshu . Needless to say , I have received great favours from all my M.Sc. batchmates as well as friends from my centre and other institutes , especially with whom I started my research career.

I express my sincere regards to Dr. Parijat Das for her extreme caring attitude , while my visit to her home. I'll always cherish the sweet moments I've spent with Rwitoban and Arshaman.

I will be ever grateful to my late grandfather , maternal grandmother , "mamu" and "monti pisi" for their blessings . Their memories will always be with me. And finally , I pay my high regards to my mother and my father for their devotion , encouragement , moral support and blessings . I owe a special thanks to my uncles, aunts and "bibi pisi" for their deep affection. Whenever I needed , my cousins Sagnick , Monojit , Basabdatta and Subhajit always stood by my side. I am also grateful to my elder cousins Dr. P. Nag , P. Dutta ,C. Pal and Dr. S. Pal for motivating me in different ways.

Finally , I thank S. N. Bose National Centre for Basic Sciences for providing me the research fellowship , and the computational facilities made available at the centre via the UNANST project.

Abstract

In this Thesis we have presented a detailed computer simulation studies and theoretical investigation on the structural and dynamical aspects in liquids possessing long-ranged interactions. We have considered (acetamide + electrolyte) deep eutectics and room temperature ionic liquids (RTILs), which resemble each other via ion-ion, ion-dipole and dipole-dipole interactions. Both of these media possess tremendous potential for application in industry as reaction media owing to their less hazardous nature. These systems show signatures of pronounced spatial and temporal heterogeneities constructing a kinship to supercooled liquids near glass transition. For example, time-resolved fluorescence measurements of (acetamide + electrolyte) deep eutectics have reported a strong decoupling of both solute and solvent dynamics from medium viscosity. Our model simulation studies of the same deep eutectics have indicated pronounced non-Gaussian particle displacements and dynamic heterogeneity. In addition, decoupling of translational diffusion coefficient from medium viscosity has been observed. The heterogeneity aspect in RTILs and its impact on dynamics have been investigated in a subsequent all-atom simulation study. This study have revealed the interconnection between the slow solvation timescales observed in dynamic Stokes shift measurements and the inherent heterogeneity timescales arising via non-Gaussian ion movements. In addition, the roles for correlated ion motions and correlated domains have been investigated. In a way, this particular study complements earlier study in explaining the full solvation response in RTILs which extends from sub-picosecond to nanosecond timescales. The impact of ion-ion interaction and spatial heterogeneity on rotational motion of dipolar ion of a given RTIL has been explored in an all-atom simulation study which explored the rank dependence of ion orientational dynamics. In another simulation study we have explored the connection between the single particle and collective orientational dynamics in RTILs that possess dipolar ions. Very recently, we have developed a semi-molecular theory for studying dynamic solvent response in (non-dipolar IL + dipolar solvent) binary mixtures which is expected to stimulate experimental and simulation studies for these systems. The role of co-solvent on the spatial and temporal heterogeneities in a mixture of RTIL possessing longer alkyl chains and subsequent effects on solution dynamics

have been explored via all-atom simulations in another study. All these results have been described in the Thesis that consists of seven chapters, beginning with an Introduction and concluding with a list of exciting new problems that may be studied in future.

List of Publications

1. *"Heterogeneity and Viscosity Decoupling in (Acetamide + Electrolyte) Molten Mixtures: A Model Simulation Study"* by **Tamisra Pal** and Ranjit Biswas, ***Chemical Physics Letters*, 517**, 180 (2011).

2. *"Rank Dependent Orientational Relaxation in an Ionic Liquid: An All-atom Simulation Study"* by **Tamisra Pal** and Ranjit Biswas, ***Theoretical Chemistry Accounts*, 132**, 1348 (2013) .

3. * *"Stokes shift Dynamics of Ionic Liquids: Solute Probe Dependence, and Effects of Self-Motion, Dielectric Relaxation Frequency Window and Collective Intermolecular Solvent Modes"* by Snehasis Daschakraborty, **Tamisra Pal** and Ranjit Biswas, ***Journal of Chemical Physics*, 139**, 164503 (2013) .

4. *"Slow Solvation in Ionic Liquids: Connections to Non-Gaussian Moves and Multi-point Correlations"* by **Tamisra Pal** and Ranjit Biswas , ***Journal of Chemical Physics*,** (2014) (under revision)

5. *"Stokes Shift Dynamics in (Non-Dipolar Ionic Liquid + Dipolar Solvent) Binary Mixtures: A Semi-Molecular Theory"* by **Tamisra Pal** and Ranjit Biswas , ***Journal of Chemical Physics*,** (2014) (under revision)

6. *"Exploring Onsager-Glarum Relation in an Imidazolium Ionic Liquid: Insights from All-Atom Molecular Dynamics Simulation"* by **Tamisra Pal** and Ranjit Biswas , ***Journal of Physical Chemistry B*,** (2014) (submitted)

7. *"Role of co-solvent on the interaction and dynamics of long alkyl chain Ionic Liquids :Simulation Study"* by **Tamisra Pal** and Ranjit Biswas ***Journal of Chemical Physics*,** (2014) (in preparation)

* not included in this Thesis

Contents

Chapter 1: Introduction..……**1**

Chapter 2: Heterogeneity and Viscosity Decoupling in (Acetamide + Electrolyte) Molten Mixtures: A Model Simulation Study

2.1 Introduction ……...**8**

2.2 Simulation Details ……...**10**

2.3 Results and Discussion ……....**11**

2.4 Conclusion ……..…**27**

Chapter 3: Rank Dependent Orientation Relaxation in an Ionic Liquid : An All-atom Simulation Study

3.1 Introduction ……..**31**

3.2 Force Field and Method ……**32**

3.3 Present Simulations: Fidelity Check and New Results ……**35**

3.3.1. Thermodynamic Quantities …….....……**36**

3.3.2. Structural Properties …….....…**36**

3.3.3. Diffusion Coefficient …….....**41**

3.3.4. Viscosity …….....**47**

3.3.5. Temporal Heterogeneity ……....**48**

3.4 Rank Dependence of Reorientational Time Correlation Function…….……..**52**

3.5 Conclusion …….…….....**55**

Chapter 4 : Exploring Onsager-Glarum Relation in an Imidazolium Ionic Liquid: Insights from All-Atom Molecular Dynamics Simulation

4.1 Introduction …….....**60**

4.2 Methodology and Simulation Details …….....**63**

4.3 Results and Discussion…….....**64**

4.3.1. Reorientation Time Correlation Function…….....**64**

4.3.2. Viscosity Coefficient …….....**69**

4.3.3. Testing the validity of the Onsager-Glarum relation : Collective and single particle rotation …….....**72**

4.3.4. Hydrodynamic explanation : Effective volume of the rotating dipolar ion …….....**75**

4.4 Conclusion ……**76**

Chapter 5 : Slow Solvation in Ionic Liquids: Connections to Non-Gaussian Moves and Multi-point Correlations

5.1 Introduction …….....**81**

5.2 Theoretical Background and Simulation Details …….....**85**

5.2.1 Simulation Details …….....……**85**

5.2.2 Data Analyses: Relevant Expressions and Theoretical Background…….....**86**

5.3 Results and Discussion…….....**89**

5.3.1. Temperature Dependent Dynamic Heterogeneity in Neat [Bmim][PF_6] and the Associated Timescales: Simulation Results…….....…..**90**

5.3.1.1. Non-Gaussian and New Non-Gaussian Parameters: Signature of Slower Moves **90**

5.3.1.2. Displacement (δr) Distribution: Bimodality, Ion Hopping and Connection to Slow Solvation.....**94**

5.3.1.3. Overlap Function and Self Dynamic Structure Factor: Inherent Slow Timescales.....**98**

5.3.1.4. Four-Point Dynamic Susceptibility and Correlation Length: Time-and Length-scales of Correlated Ion Motions.....**100**

5.3.2. Temperature Dependent Solvation Response in [Bmim][PF_6]: Reflection of DH Timescales in Simulated Slow Solvation **104**

5.4 Conclusion **109**

Chapter 6 : Stokes Shift Dynamics in (Non-Dipolar Ionic Liquid + Dipolar Solvent) Binary Mixtures: A Semi-Molecular Theory

6.1 Introduction **116**

6.2 Theory and Calculation Details **119**

6.2.1. Separate Medium (SM) Treatment **119**

6.2.2. Effective Medium (EM) Treatment **124**

6.3 Numerical Results and Discussion.....**125**

6.3.1. Composition Dependent Dynamic Stokes Shift: Comparison Between SM and EM Predictions **127**

6.3.2. Stokes Shift Dynamics : Composition Dependence **131**

6.4 Conclusion.....**137**

Chapter 7 : Concluding Remarks and Future Problems.....**143**

7.1 Future Problems.....**143**

7.1.1. Investigation of particle spatial and temporal correlations in (IL+dipolar solvent) binary mixtures.....**144**

7.1.2. Cluster size and their life-time distributions
in (IL+water) binary mixtures …….....**144**

7.1.3. Orientational jump dynamics in (IL+solvent)
binary mixture …….....**145**

7.1.4. Potential energy landscape view of Ionic Liquids ……..…**145**

7.1.5. Alkyl chain length and anion dependence of Stokes
shift Dynamics in ILs…….....**146**

Appendix A…….……..…...**150**

Appendix B…….…….....**158**

Appendix C…….…….....**164**

Appendix D…….……...**168**

Addendum I …….....**176**

Chapter 1

Introduction

Presence of long-range interactions in a reaction medium can have profound effects on outcome of a chemical reaction as dynamic solvent response changes dramatically in presence of such interactions.[1-11] Charge-charge and charge-dipole interactions between species can introduce spatial and temporal heterogeneities in such a medium, making simple interpretations of medium effects untenable. Ionic deep eutectics (DEs) composed of amides and electrolytes,[12-24] and room-temperature ionic liquids [25-41] (RTILs) are examples of such systems which contain ion-ion ($\propto r_{ij}^{-1}$), ion-dipole ($\propto r_{ij}^{-2}$) and dipole-dipole ($\propto r_{ij}^{-3}$) interactions. Similarity in interactions, therefore, builds a kinship between DEs and RTILs which represent two different classes of media. Both these media possess application potential in industry[42,43] as suitable replacements for volatile organic solvents. Ionic amide DEs are molten mixtures of constituents which are individually high temperature solids but become liquids near or at room temperature upon mixing at certain proportions. These DEs have been found to exhibit signatures commonly observed for supercooled liquids.[44-48] Interestingly, spatial and temporal heterogeneities have emerged as common features in many experimental and simulation studies of RTILs and DEs.

Medium heterogeneity has important consequences on transport properties and relates to the activation energy barrier crossing. [46,49-51] Spatial heterogeneity[44,52-63] refers to distinct regions in a given medium, whereas temporal heterogeneity (dynamical heterogeneity) [38,64-67] is connected to spatially varying relaxation rates. Interestingly,

temporal heterogeneity may arise as a consequence of spatial heterogeneity but the observation of temporal heterogeneity does not necessarily indicate presence of spatial heterogeneity in a given system. Note dynamic heterogeneities has been diagnosed for inducing breakdown of the hydrodynamic relations.[21,23,24,68-70]

As already mentioned, RTILs are salts that are fused near room temperature and composed of large organic cations and relatively small inorganic anions. RTILs have been found to sustain long-range spatial correlations, alkyl tail aggregation and long-lived domains.[30,71-75] Interestingly, relaxation time constants obtained via time-resolved fluorescence measurements[25,27,76,77] of solute dynamics in a number of ionic liquids have been found to follow the conventional hydrodynamics, although dielectric relaxation measurements[78-80] have signalled non-hydrodynamic moves for the rotation dipolar ionic species. DEs, in contrast, have revealed a strong fractional viscosity dependence of solute solvation and rotational times.[21-24] The central focus of the present Thesis is, therefore, exploration of the dynamic mechanism that gives rise to solute-medium decoupling and deviation from hydrodynamics in these systems possessing ion-ion, ion-dipole and dipole-dipole interactions. In addition, the relationship between slow solvation and dynamic heterogeneity timescales is investigated here although existing studies with RTILs [25,27,32,34,74,81] and mixtures of RTILs with conventional polar solvents[36,80,82-86] have not touched upon this important aspect.

The research work that has been carried out for this thesis is presented in the next six chapters. Chapter 2 contains a detailed molecular dynamics study on the structural and temporal aspects of (acetamide+ electrolyte) DEs using a model potential. Simulation codes developed at home has been employed for performing the study described here. Sodium and potassium thiocyanates (Na/KSCN) have been considered as electrolytes. Note Na^+ is known to induce the maximum depression of freezing point among the various ions studied.[87] In chapter 3 we have expanded the above investigation for RTILs. Here all-atom molecular dynamics simulations have been performed to study orientational relaxation in a given RTIL, 1-butyl-3-methylimidazolium hexafluorophosphate ([Bmim][PF_6]) at 298 K and 450 K. Heterogeneity aspects and their impact on relaxation have been explored here. Chapter 4 explores the relationship

between single particle and collective reorientational relaxation dynamics in RTILs via carrying out all-atom molecular dynamics simulations. Chapter 5 investigates the interconnection between timescales of dynamic heterogeneity (DH) in a neat ionic liquid and slow solvation of a dipolar solute in it. Molecular dynamics simulations employing realistic interaction potentials for both the IL and the solute have been performed. DH timescales have been obtained from non-Gaussian (NG) and new non-Gaussian[64] (NNG) parameters, and four-point dynamic susceptibilities ($\chi_4(k,t)$) and overlap functions ($Q(t)$)[52,53,57,60]. Simulated ion displacement distributions exhibit pronounced deviations from Gaussian behaviour and develop bimodality in the timescales of structural relaxation[65], τ_α, indicating ion hopping at long-time. In chapter 6 , a semi-molecular theory for studying composition dependent Stokes shift dynamics of a dipolar solute in a binary mixture of (non-dipolar ionic liquid + common dipolar solvent) is developed. The theory provides microscopic expressions for solvation response functions in terms of static and dynamic structure factors of the mixture components and solute-solvent static correlations. In addition, the theory provides a framework for examining the interrelationship between the time dependent solvation response in and frequency dependent dielectric relaxation of a binary mixture containing electrolyte. The thesis then ends in chapter 7 with a discussion on several interesting future problems. Appendices and preliminary results from some of our studies involving RTILs are provided after chapter 7 for the sake of completeness.

References :

1. E. W. Castner Jr., C. J. Margulis, M. Maroncelli, and J. F. Wishart ,Annu. Rev. Phys. Chem. **62** ,85 (2011).
2. J. T. Hynes, Annu. Rev. Phys. Chem. **36**,573 (1985).
3. R. F. Grote and J. T. Hynes, J. Chem. Phys. **73**,2715(1980).
4. Y. Nagasawa and H. Miyasaka Phys. Chem. Chem. Phys. **(**2014**)** DOI: 10.1039/C3CP55465A
5. X. Li, M. Liang, A. Chakraborty, M. Kondo, and M. Maroncelli, J. Phys. Chem. B **115**, 6592 (2011).
6. B. Bagchi, Annu. Rev. Phys. Chem. **40**,115 (1989).
7. G. van der Zwan and J. T. Hynes , Chem. Phys. **152**,169 (1991).
8. G. A. Voth and R. M. Hochstrasser , J. Phys. Chem. **100**, 13034(1996).
9. M. T. Klein, L. A. Torry, B. C. Wu, S. H. Townsend, S. C. Paspek, J. Supercrit. Fluids. **3** , 222(1990).
10. A. Warshel , J. Phys. Chem., **86** , 2218(1982).
11. M. Liang, A. Kaintz, G. A. Baker, and M. Maroncelli , J. Phys. Chem. B **116**, 1370(2012).
12. A. Amico, G. Berchiesi, C. Cametti, and A. D. Biasio, J. Chem. Soc. Faraday Trans. 2, **83** 619(1987).
13. G. Berchiesi, M. D. Angelis, G. Rafaiani, and G. Vitali, J. Mol. Liq. **51** ,11(1992).
14. G. Berchiesi, F. Farhat, M. D. Angelis, J. Mol. Liq. **54**,103(1992).
15. G. Berchiesi, J. Mol. Liq. **83** , 271(1999).
16. F. Catellani, G. Berchiesi, F. Pucciarelli, V. Bartocci, J. Chem. Eng. Data **26** ,150(1981).
17. G. Kalita, N. Rohman, S. Mahiuddin, J. Chem. Eng. Data **43**, 148(1998).
18. G. Kalita, K. G. Sarma, S. Mahiuddin, J. Chem. Eng. Data **44** , 222(1999).
19. G. Berchiesi, G. Rafaiani, G. Vitali, F. Farhat, J. Therm. Anal. **44**,1313(1995).
20. S. Mahiuddin, J. Chem. Eng. Data , **41** , 231(1996).
21. B. Guchhait, H. A. R. Gazi, H. K. Kashyap, and R. Biswas, J. Phys. Chem. B **114** ,5066 (2010).

22. H. A. R. Gazi, B. Guchhait, S. Daschakraborty, and R. Biswas, Chem. Phys. Lett. **501** , 358 (2011).
23. B. Guchhait, S. Daschakraborty, and R. Biswas , J. Chem. Phys. **136** , 174503 (2012).
24. A. Das, S. Das, and R. Biswas, Chem. Phys. Lett. **581**, 47 (2013).
25. A. Samanta, J. Phys. Chem. B , **110**, 13704 (2006).
26. A. Samanta, J. Phys. Chem. Lett. **1**, 1557 (2010).
27. X.-X. Zhang, M. Liang, N. P. Ernsting, and M. Maroncelli, J. Phys. Chem. B **117**, 4291(2013).
28. H. Jin, X. Li, M. Maroncelli, J. Phys. Chem. B **111** ,13473(2007).
29. J. A. C. Lopes, A. A. H. Padua, J. Phys. Chem. B **110** ,3330(2006).
30. A. Triolo, O. Russina, B. Fazio, R. Triolo, E. D. Cola, Chem. Phys. Lett. **467** ,362(2008).
31. P. K. Mandal, M. Sarkar, A. Samanta, J. Phys. Chem. A **108** , 9048 (2004).
32. D. K. Sasmal, A. K. Mandal, T. Mondal, K. Bhattachrayya, J. Phys. Chem. B. **115**,7781 (2011).
33. S. Arzhantsev, H. Jin, N. Ito, and M. Maroncelli , Chem. Phys. Lett. **417**, 524 (2006).
34. H. K. Kashyap and R. Biswas , J. Phys. Chem. B , **114**, 254, (2010).
35. H. K. Kashyap and R. Biswas , J. Phys. Chem. B , **114**, 16811, (2010).
36. S. Daschakraborty and R. Biswas, J. Phys. Chem. B, **115**, 4011 (2011).
37. S. Daschakraborty, T. Pal, and R. Biswas, J. Chem. Phys. **139**, 164503 (2013).
38. S. S. Sarangi, W. Zhao, F. Muller-Plathe, S. Balasubramanian, Chem. Phys. Chem. **11**,2001 (2010).
39. D. A. Turton, J. Hunger, A. Stoppa, G. Hefter, A. Thoman, M. Walther, R. Buchner, K. Wynne, J. Am. Chem. Soc. **131**,11140(2009).
40. J. K. Shah, J. F. Brennecke, and E. J. Maginn, Green Chem. **4**,112(2001).
41. D. Roy, N. Patel, S. Conte, M. Maroncelli, J. Phys. Chem. B **114** , 8410(2010).
42. M.J. Earle, K.R. Saddon, Ionic liquids. Green solvents for the future, in: Ionic Liquids:Green Solvents for the Future, ACS Sym. Ser., Belfast, 10 (2002).
43. R. D. Rogers, K. R. Seddon, Ionic Liquids: Industrial Application for Green Chemistry. ACS Symposium Series 818; American Chemical society, Washington DC (2002).

44. M. D. Ediger, Annu. Rev. Phys. Chem. **51,** 99(2000).
45. H. Sillescu , J. Non – Cryst. Solids , **243** , 81 (1999).
46. P. G. Debenedetti and F. H. Stillinger , Nature , **410** , 259 (2001).
47. M. D. Ediger, C. A. Angell ,and S. R. Nagel , J. Phys. Chem. **100**, 13200(1996).
48. M S. Shell, P. G Debenedetti, and F. H Stillinger , J. Phys. Condens. Matter **17** ,S4035 (2005).
49. D. Chakrabarti and B. Bagchi , Phys. Rev. Lett. **96**, 187801 (2006).
50. A. Heuer, J. Phys. Condens. Matter **20** , 373101 (2008).
51. S. Sastry, P. G. Debenedetti and F. H. Stillinger , Nature , **393** , 554 (1998).
52. S. C. Glotzer, J. Non-Cryst. Solids, **274**, 342 (2000).
53. N. Lacevic, F. W. Starr, T. B. Schroder, and S. C. Glotzer, J. Chem. Phys. **119**, 7372 (2003).
54. G. Szamel and E. Flenner, Europhys. Lett. **67**, 779 (2004).
55. E. Flenner and G. Szamel, Phys. Rev. E **70**, 052501 (2004).
56. J.-P. Hansen, Physica A **201**, 138 (1993).
57. C. Toninelli, M. Wyart, L. Berthier, G. Biroli, and J.-P. Bouchaud, Phys. Rev. E **71**, 041505 (2005).
58. C. Bennemann, C. Donati, J. Baschnagel, and S. C. Glotzer, Nature **399**, 246 (1999).
59. S. C. Glotzer, V. N. Novikov, and T. B. Schroder, J. Chem. Phys. **112**, 509 (2000).
60. N. Lacevic, F. W. Starr, T. B. Schroder, V. N. Novikov, and S. C. Glotzer, Phys. Rev. E **66**, 030101(R) (2002).
61. K. Kim and S. Saito, J. Chem. Phys. **138**, 12A506 (2013).
62. C. Donati, S. Franz, G. Parisi, and S. C. Glotzer, J. Non-Cryst. Solids **307**, 215 (2002).
63. S. Karmakar, C. Dasgupta, and S. Sastry , Phys. Rev. Lett. **105**, 015701 (2010).
64. K. Kim and S. Saito, J. Chem. Phys. **133**, 044511 (2010).
65. E. Flenner and G. Szamel, Phys. Rev. E. **72**, 011205 (2005).
66. T. Pal and R. Biswas, Chem. Phys. Lett. **517**, 180 (2011).
67. T. Pal and R. Biswas, Theor. Chem. Acc. **132**,1348 (2013).
68. J. P. Hansen and I. R. McDonald, Theory of Simple Liquids 3rd ed. (Academic, London, 2006).

69. J. R. Lakowicz , Principles of Fluorescence Spectroscopy, Kluwar Academic , Plenum :New York ,1999.
70. B. Guchhait, S. Das, S. Daschakraborty, and R. Biswas, J. Chem. Phys. **140**, 104514 (2014).
71. M. Kofu, M. Nagao, T. Ueki, Y. Kitazawa, Y. Nakamura, S. Sawamura, M. Watanabe, and O. Yamamuro, J. Phys. Chem. B **117**, 2773 (2013).
72. Y. Wang and G. A. Voth, J. Am. Chem. Soc. **127**,12192(2005).
73. M. G. Del Popolo and G. A. Voth, J. Phys. Chem. B **108**,1744(2004).
74. A. M. Funston, T. A. Fadeeva, J. F. Wishart, and E. W. Castner, Jr., J. Phys. Chem. B. **111**, 4963 (2007).
75. Z. Hu and C. J. Margulis, Proc. Natl. Acad. Sci. USA **103**,831(2006).
76. N. Ito, S. Arzhantsev, M. Heitz, and M. Maroncelli, J. Phys. Chem. B ,**108**,5771 (2004).
77. H. Jin, G. A. Baker, S. Arzhantsev, J. Dong, and M. Maroncelli,J. Phys.Chem. B, **111**, 7291 (2007).
78. J. Hunger, A. Stoppa, S. Schrödle, G. Hefter, and R. Buchner, Chem. Phys. Chem **10**, 723 (2009).
79. A. Stoppa , J. Hunger , R. Buchner , G. Hefter , A. Thoman, and H. Helm , J. Phys. Chem. B. Lett. **112** , 4854 (2008).
80. M. Liang, X.-X. Zhang, A. Kaintz, N. P. Ernsting, and M. Maroncelli, J. Phys. Chem. B. **118**, 1340 (2014).
81. M. N. Kobrak and V. Znamenskiy , Chem. Phys. Lett. **395**,127(2004)
82. X.-X. Zhang, M. Liang, J. Hunger, R. Buchner, and M. Maroncelli, J. Phys. Chem. B. **117**, 15356 (2013).
83. S. Daschakraborty and R. Biswas , J. Phys. Chem. B.,**118**,1327 (2014).
84. M. B. Rogac, A. Stoppa, and R. Buchner , J. Phys. Chem. B.,**118,** 1426 (2014)
85. C. Schröder, J. Hunger, A. Stoppa, R. Buchner, and O. Steinhauser , J. Chem. Phys. **129**, 184501 (2008).
86. H. Shirota, and R. Biswas , J. Phys. Chem. B, **116**, 13765 (2012).
87. G. Berchiesi, G. Gioia Lobbia, V. Bartocci and G. Vitali, Thermochim. Acta, **70**, 317, (1983).

Chapter 2

Heterogeneity and Viscosity Decoupling in (Acetamide + Electrolyte) Molten Mixtures: A Model Simulation Study

2.1 Introduction

Binary and ternary mixtures of acetamide with electrolytes are well-known examples of supercooled melts around room temperature[1-7]. These melts are characterized by pronounced microscopic solution heterogeneities [2-4,8] and glass transition temperatures (T_g) in the range, $\sim 190 < T_g(K) < 250$ [6,7, 9-10]. Depending on mixture composition and temperature, viscosity (η) of these melts varies between ~4 - 250 cP, and exhibits, as typical for fragile glass formers, a non-Arrhenius temperature dependence [6,7]. Recent time-resolved fluorescence measurements have revealed a strong decoupling of both solute and solvent dynamics from medium viscosity[11-13]. This is quite reminiscent of frequent observations in deeply supercooled neat liquids [14-16] and, therefore, the observed non-hydrodynamic behavior might be linked to the spatial and temporal heterogeneities of these melts. Interestingly, eventhough presence of strong spatial heterogeneities in these melts have been suggested by several earlier experimental studies [1-4, 8], no measurements or simulations, similar to those for ionic liquids [17-22], have been carried out so far to better understand the heterogeneity and their effects on chemical events in these multi-component mixtures. Needless to say, a quantitative understanding of heterogeneities and their implications on transport properties is necessary for developing these melts into useful dielectric materials and subsequent applications in technology.

In this chapter , we report results from our molecular dynamics simulations on viscosity decoupling of diffusion in binary and ternary molten mixtures of acetamide (CH_3CONH_2) with sodium thiocyanate ($NaSCN$) and potassium thiocyanates ($KSCN$) at 318 K. Three different mixtures of the following general formula, $0.75CH_3CONH_2 + 0.25[fKSCN + (1-f)NaSCN]$ with f (fraction of K^+) = 0, 0.2 and 0.6, have been considered. Note that these are the melt compositions and temperature at which the fluorescence experiments reported in Ref. 11 have been carried out. Composition dependence of the spatial distributions of the ions and solvent particles, their diffusion coefficients, and mixture viscosities have been simulated in order to understand the ion-solvent interactions present in these systems. Dynamic heterogeneity is reflected in the large values of non-Gaussian parameter ($\alpha(t)$) and pronounced deviations from the Gaussian distribution (with respect to particle displacement) of the self part of the van Hove correlation function ($G_s(\mathbf{r},t)$) in the simulated particle motions [23,24]. Eventhough strong non-Gaussian characteristics have been found in the particle motions, no rattling within a cage, as typically seen in supercooled systems [25,26] and ionic liquids [27,28], could be detected in the present model simulations. Moreover, similar to earlier findings for mixed alkali silicate glasses [29-31], addition of foreign ion (here K^+) suppresses the long-range motions of other ions (Na^+ and SCN^-) and solvent particles, the extent of suppression being the largest at the lowest K^+ concentration considered.

Note here that the pair potential between two acetamide molecules is approximated by that between two dipolar L-J spheres, whereas pair interaction between ions is assumed to be given that between two singly-charged L-J spheres. Such modeling of pair potentials completely neglects shape anisotropy, molecular flexibility and other atomic details and therefore excludes the possibility of reproducing the static heterogeneity revealed by various experiments with these melts [2-4,8]. This will have implications on various properties of this melt, most directly on the viscosity, because structural heterogeneity is known to substantially affect this transport quantity[32,33]. However, longer-ranged ion-ion ($u_{ii} \propto r^{-1}$), ion-dipole ($u_{id} \propto r^{-2}$) and dipole-dipole ($u_{dd} \propto r^{-3}$) interactions are expected to dominate the energetic and dynamic aspects of these melts

and thus a qualitative understanding of the $D-\eta$ relationship may be achieved even without considering the detailed chemical interactions. Moreover, the model considered here for (acetamide + electrolyte) melts is similar in spirit to a recent coarse-grained representation of an idealized ionic liquid[27] which produced not only reasonable agreement between simulations and experiments on liquid structural and energetic properties but also on solute-based dynamics. In addition, consideration of only L-J interaction between particles in a simulation study [34] has been found to generate a qualitative understanding of the physical picture behind the cooperative blockage and jump dynamics [29,30] associated with the conductivity in mixed alkali glasses. Therefore, use of simple model potentials for studying dynamics in complex systems is not new. Our primary motivation here is to generate a qualitative understanding of the experimentally observed fractional viscosity dependence (of the medium dynamics) in these melts while being computationally economical.

2.2 Simulation Details

A mixture of 384 acetamide molecules and 64 ion pairs (a total of 512 particles) were simulated by using a home-developed code in the canonical (*NVT*) ensemble at 318 K (Nose-Hoover thermostat) with box-length adjusted to produce the experimental density [6] of these melt mixtures at a given composition. Such compositions correspond to solutions with electrolyte present at ~10^{-3} moles/litre concentration. Here *N* denotes the total number of particles in the system, *V* the volume and *T* the absolute temperature. Periodic boundary conditions were employed and equations of motion integrated following the Verlet leapfrog integration scheme using a time step of ~2 fs. Equilibration was done for 1 ns and the production run for 3 ns. Longer-ranged interactions were treated via the standard Ewald method [35,36]. The interaction potentials between a pair of ions, a pair of dipolar solvent molecules, and between a solvent dipole and an ion were respectively approximated as

$$u_{ion-ion}(r_i, r_j) = 4\varepsilon_{ij}\left[\left(\frac{\sigma_{ij}}{r_{ij}}\right)^{12} - \left(\frac{\sigma_{ij}}{r_{ij}}\right)^{6}\right] + \frac{q_i q_j}{r_{ij}}, \qquad (2.1)$$

$$u_{dipole-dipole}(\mu_i,\mu_j) = 4\varepsilon_{ij}\left[\left(\frac{\sigma_{ij}}{r_{ij}}\right)^{12} - \left(\frac{\sigma_{ij}}{r_{ij}}\right)^{6}\right] + \frac{\mu_i\mu_j}{r_{ij}^3}, \qquad (2.2)$$

and $$u_{ion-dipole}(q_i,\mu_j) = 4\varepsilon_{ij}\left[\left(\frac{\sigma_{ij}}{r_{ij}}\right)^{12} - \left(\frac{\sigma_{ij}}{r_{ij}}\right)^{6}\right] + \frac{q_i\mu_j}{r_{ij}^2}. \qquad (2.3)$$

In the above expressions q and μ represent charge and dipole moment respectively, *i* and *j* different particles (ion or/and solvent dipole) and r_{ij} distance between two such particles. The L-J lengthscales (σ_{ij}) and energy parameters (ε_{ij}) were obtained by using the Lorentz-Berthelot [35] combination rule (that is, $\sigma_{ij} = \frac{\sigma_i + \sigma_j}{2}$ and $\varepsilon_{ij} = \sqrt{\varepsilon_i \varepsilon_j}$) from the known individual L-J parameters [11,37-39]. μ = 3.7 D [11].

2.3 Results and Discussion

We present in Fig. 2.1 the simulated $Na^+ - Na^+$ and $CH_3CONH_2 - CH_3CONH_2$ radial distribution functions ($g(r)$) at $f = 0$, 0.2 and 0.6 for the melt $0.75CH_3CONH_2 + 0.25[fKSCN + (1-f)NaSCN]$ at 318 K. $K^+ - K^+$, $SCN^- - SCN^-$, Cation-anion and ion-solvent $g(r)$ are shown in Figs. A1 and A2 (See Appendix A). Data in these figures clearly indicate that the addition of K^+ influences the spatial distribution of particles, the effect being the strongest at the lowest concentration of *KSCN*. Note that while the addition of K^+ enhances the first peak height and broadens the simulated $g(r)$ for $Na^+ - Na^+$, $SCN^- - SCN^-$, $Na^+ - SCN^-$ and $CH_3CONH_2 - CH_3CONH_2$, increase in K^+ concentration in melt reduces and narrows those for $Na^+ - CH_3CONH_2$ and $K^+ - CH_3CONH_2$. Moreover, $K^+ - K^+$ and $K^+ - SCN^-$ radial distribution functions (RDFs) do not show any appreciable change upon increasing the *KSCN* concentration. The enhancement and broadening of ion-ion and solvent-solvent RDFs along with the insignificant changes in

those for $K^+ - K^+$ and $K^+ - SCN^-$ suggest enhanced interactions between these species upon addition of $KSCN$ and thus much less ideal mixing. The reduction by a factor of ~2 of the first peak height of $Na^+ - CH_3CONH_2$ RDF upon addition of K^+ (see Fig. A1) seems to suggest stronger interaction between acetamide and K^+ than that between Na^+ and acetamide. A decrease in diffusion coefficient of acetamide upon increase in f and a relatively smaller diffusion coefficient for K^+ than Na^+ (shown later) further support this view as mobility of these alkali metal ions in common polar solvents shows quite the opposite trend [40]. The second peak of the simulated $CH_3CONH_2 - CH_3CONH_2$ $g(r)$ at f =0 appears non-regular and suggests presence of slight disorder [41,42]. Interestingly, experimental studies with this melt at f =0 have indicated presence of substantial disorder in solution structure [4]. Simulations incorporating detailed atomic interactions are therefore required for a better understanding of the static disorder (and thus spatial heterogeneity) of these systems.

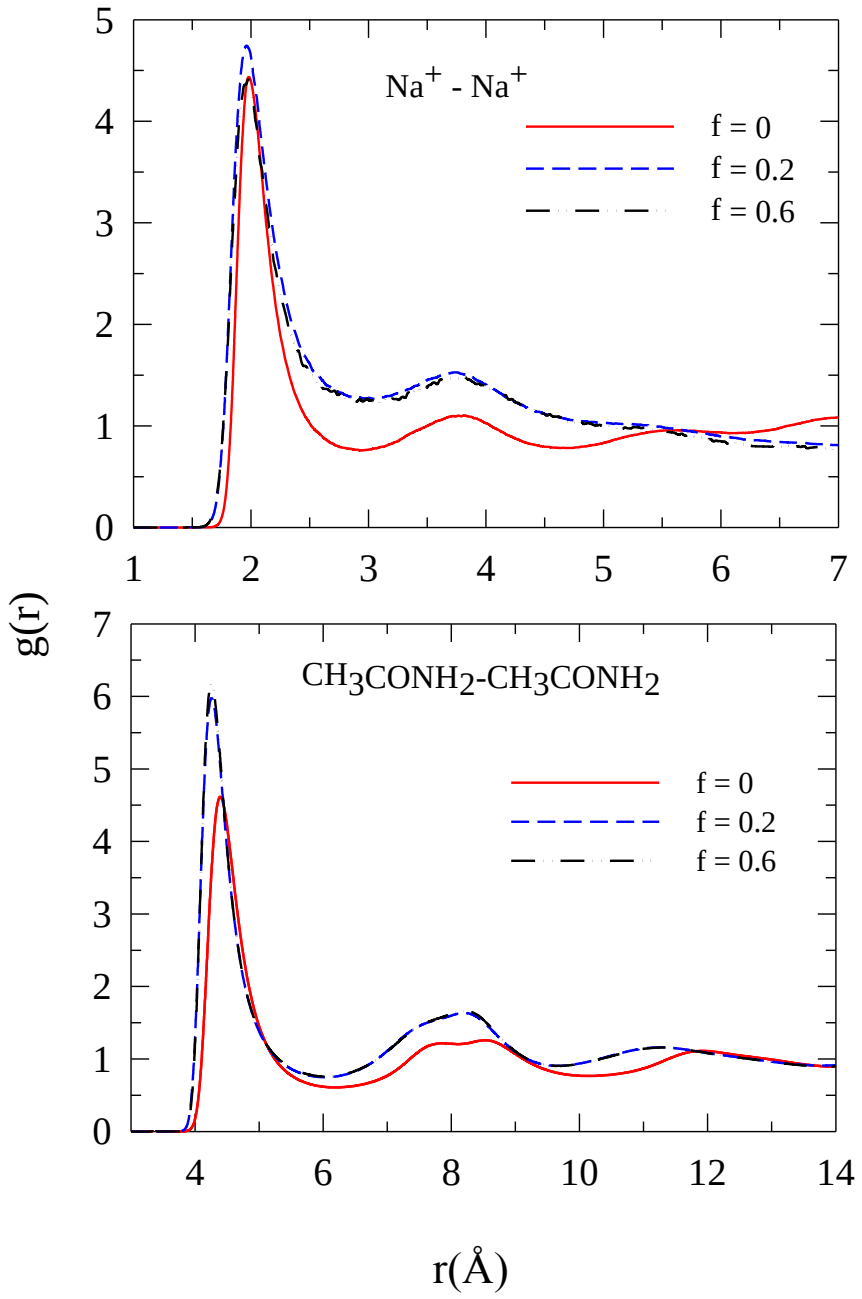

Figure. 2.1 : Composition dependence of the centre-of-mass radial distribution function (RDF), $g(r)$ for Na^+ and solvent (acetamide) particles present in the (acetamide + sodium/potassium thiocyanate) melt at 318 K. Solid, dashed and dash-dot lines represent RDFs at $f = 0,0.2,0.6$, respectively (also indicated in each of the panels). The RDFs are color-coded . See Figs. A1 and A2 of Appendix A for $g(r)$ of other species in the melt.

Next we present in Fig. 2.2 the composition dependent mean squared displacments (MSDs) for Na^+ and solvent particles. MSDs for the other species are provided in the Appendix A (Fig. A3). The MSDs have been calculated from the time-dependent centre-of-mass positional vectors $(\vec{r}_i^{\,c}(t))$, $\left\langle \left|\Delta\vec{r}(t)\right|^2 \right\rangle = \frac{1}{N}\left\langle \sum_{i=1}^{N} \left|\vec{r}_i^{\,c}(t) - \vec{r}_i^{\,c}(0)\right|^2 \right\rangle$. Note that none of the MSDs shown here exhibit 'rattling in a cage' motion so typical for alkali glasses [25], supercooled systems [26] and ionic liquids [27,28]. It is again evident that the addition of K^+ influences the MSDs and thus the diffusion coefficient (because $D = \left[\frac{1}{6t}\left(\left\langle \left|\Delta\vec{r}(t)\right|^2 \right\rangle\right)\right]_{t\to\infty}$) of each of the species present in the melt, the most affected being those of the acetamide molecules. The corresponding velocity autocorrelation function (Fig. A4, upper panel, in Appendix A) also shows a similar effect.

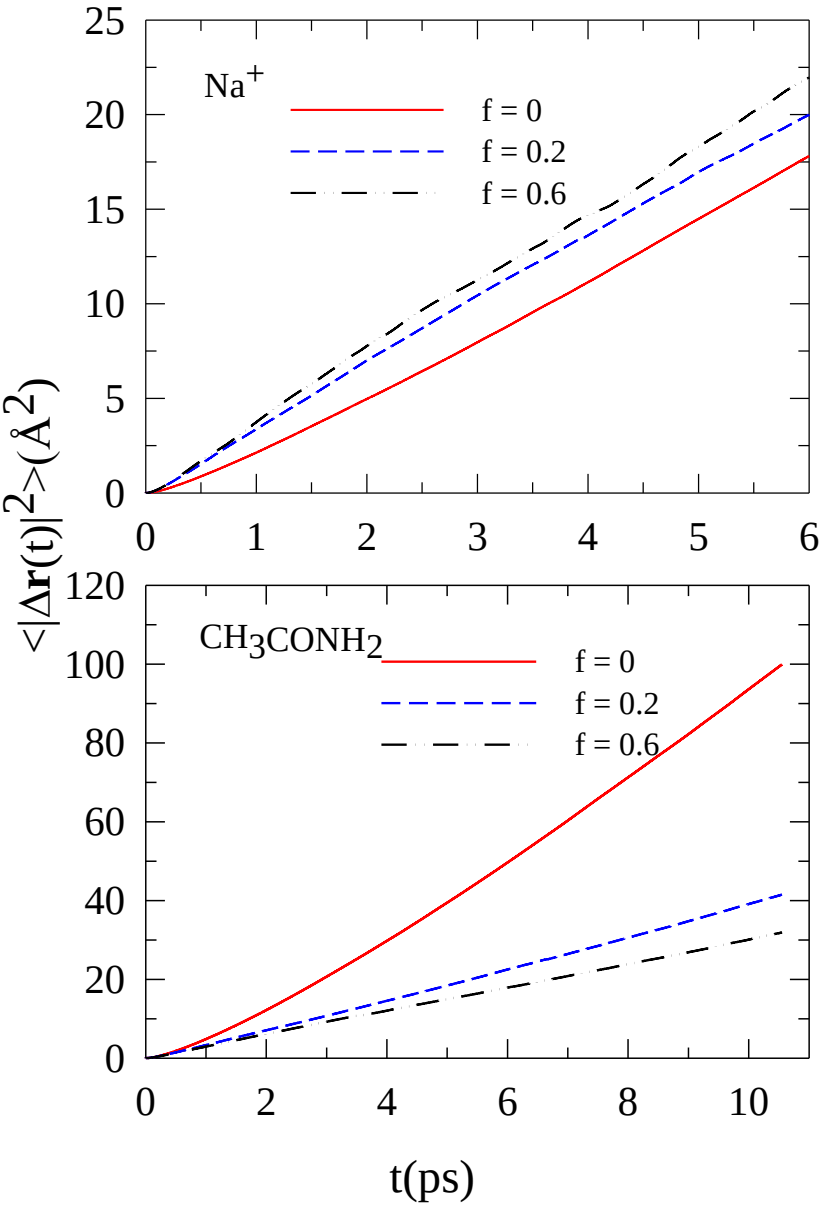

Figure. 2.2: Composition dependent centre-of-mass mean squarred displacements (MSD) for Na^+ and acetamide for the melt under study. The curves are color-code . MSDs for K^+ and SCN^- are provided in Fig. A3 of Appendix A.

Simulated diffusion coefficients (D) summarized in Table 2.1 reveals that SCN^- is the most efficient among the diffusing ions in this melt. Moreover, while D for acetamide reduces substantially, an over-all increase (small though) in D for the ions is observed for changing f from 0 to 0.6 in this melt. This is in qualitative agreement with experiments [43] which report enhancement of electrical conductivity upon replacement of Na^+ by K^+ in this melt (see Fig. A4, lower panel). However, simulated diffusion coefficients for K^+, present in the current melt at milli-molar concentration, is ~5 times larger than that estimated from the measured conductivity of centi-molar solutions of potassium chloride in molten acetamide at ~367 K [44] . Also, simulated D for Na^+ (also present at milli-molar concentration) is more than an order of magnitude larger than the measured value in N-methylacetamide (NMA) at ~313 K [45]. These results contradict the hydrodynamic predictions because η_{melt} at 318 K is larger than η_{NMA} at ~313 K [45] and $\eta_{Acetamide}$ at ~367 K [11] and, therefore, suggest participation of non-hydrodynamic mechanism for particle movement.

Table 2.1: Composition dependent simulated diffusion coefficients for ions and acetamide particles in $0.75CH_3CONH_2 + 0.25[fKSCN + (1-f)NaSCN]$ at 318 K. Diffusion coefficients have been calculated from both the MSD and VACF routes. The error bars (standard deviation about the mean) have been estimated from block averaging.

	D **(*f* = 0.0)** **X 10^4 (cm^2/sec)**			***D*** **(*f* = 0.2)** **X 10^4 (cm^2/sec)**			***D*** **(*f* = 0.6)** **X 10^4 (cm^2/sec)**		
	MSD	VACF	Average	MSD	VACF	Average	MSD	VACF	Average
CH_3CONH_2	1.79 ± 0.19	1.94± 0.40	1.87± 0.29	0.68 ± 0.19	0.73± 0.37	0.71± 0.28	0.50 ± 0.22	0.51± 0.27	0.51± 0.25
Na^+	0.54 ± 0.15	0.51± 0.13	0.53± 0.14	0.53 ± 0.19	0.53± 0.15	0.53± 0.17	0.59 ± 0.13	0.54± 0.16	0.57± 0.15
K^+				0.51 ± 0.10	0.50± 0.15	0.51± 0.13	0.56 ± 0.19	0.52± 0.15	0.54± 0.17
SCN^-	1.46 ± 0.28	1.44± 0.40	1.45± 0.34	1.53 ± 0.22	1.55± 0.19	1.54± 0.21	1.59 ± 0.26	1.71± 0.22	1.65± 0.24

A comparison in Table 2.2 among the simulated diffusion coefficients (D_{simu}) and those from hydrodynamics (D_{cal}) calculated after using the simulated and measured viscosities (η_{simu} and $\eta_{\exp t}$, respectively) further reflects the inefficiency of the hydrodynamics in describing the particle diffusion in the present melt. The comparison is a representative one (shown only for f =0) and the viscosity has been simulated from

the stress tensor autocorrelation function as described in the literature [24]. At this composition (f =0), we find η_{simu} = 20 cP, a value more than an order of magnitude less than in experiments (η_{expt} = 235 cP) [6]. This underestimation is expected because of the non-consideration of the atomistic details in the interaction potentials but the simualated value will be sufficient to show the break-down of the hydrodynamic description for particle diffusion in this melt. Note that the simulated diffusion coefficients for CH_3CONH_2, Na^+ and SCN^- are larger by factors of ~4300, ~500, ~3100 respectively than the corresponding hydrodynamic (Stokes-Einstein) [24] predictions using η_{expt}. These differences are reduced by the factor, $\eta_{expt}/\eta_{simu} \approx 12$, when the simulated viscosity replaces the experimental one in the Stokes-Einstein relation. The simulated diffusion coefficients are still much larger than the hydrodynamic predictions and strongly indicate partial decoupling from the medium viscosity.

Table 2.2 : Break-down of Stokes-Einstein relation for particle diffusion in (acetamide + sodium/potassium thiocyanates) molten mixtures at $f = 0$ and 318 K. Error bars have been calculated by following the method as mentioned for Table 2.1.

Species	$D_{cal} = \frac{k_B T}{6\pi\eta r}$ (cm^2/sec)X10^7 From $\eta_{simu} = 20cP$	$D_{cal} = \frac{k_B T}{6\pi\eta r}$ (cm^2/sec)X10^7 From $\eta_{expt} = 235cP$	D_{simu} (cm^2/sec) X 10^7
CH_3CONH_2	5.1533	0.438	1870.65 ± 290
$Na+$	12.0066	1.022	525.83 ± 140
$SCN-$	5.4169	0.461	1453.40 ± 340

Next we explore the dynamic heterogeneity as a probable reason for the observed break-down of the Stokes-Einstein relation via examining the time-evolution of the self-part of the van Hove correlation function, defined as [24]

$$G_s(\vec{r},t) = \frac{1}{N}\left\langle \sum_{i=1}^{N} \delta\left(\vec{r}_i^{\,c}(t) - \vec{r}_i^{\,c}(0) - \vec{r}\right)\right\rangle, \tag{2.4}$$

which describes the probability of locating the centre-of-mass of a particle at r^c at time t given that it was at the origin $r^c(0)$ at $t = 0$. Because of the Maxwell-Boltzmann velocity distribution in the free particle limit (that is, $\Delta r \to 0$ and $t \to 0$) and hydrodynamic behavior at $t \to \infty, G_s(\vec{r},t)$ exhibits Gaussian distribution with particle displacement, $\Delta\vec{r}(t)$. Additionally, $G_s(\vec{r},t)$ for most liquids at normal condition retains the Gaussianity at all times [28]. Traditionally, strong deviations from Gaussian behavior in supercooled liquids at intermediate times have been attributed to dynamic heterogeneity [46] and quantified by the following non-Gaussian parameter [23]

$$\alpha(t) = \frac{3}{5}\frac{\left\langle \left|\Delta\vec{r}(t)\right|^4 \right\rangle}{\left\langle \left|\Delta\vec{r}(t)\right|^2 \right\rangle^2} - 1. \tag{2.5}$$

For a Gaussian $G_s(\vec{r},t)$ as in the cases of random walk or homogeneous harmonic vibrations [26], $\alpha(t) = 0$. For hot liquids, $\alpha(t) = 0$ for both at $t = 0$ and $t = \infty$ but $\alpha(t) = 0.2$ (a maximum) at intemediate times [26].

Fig. 2.3 depicts the composition dependence of $\alpha(t)$ simulated for Na^+ and K^+ ions present in the current melt. Simulated $\alpha(t)$s for SCN^- and acetamide are shown in the Appendix A (Fig. A5). Eventhough the data are noisy because of insufficient averaging, the multi-peak (or peak *plus* a shoulder) structure of $\alpha(t)$ is evident. Large values of $\alpha(t)$ at intermediate times ($\sim 10 \le t/ps \le 1000$) indicate presence of varying rates of motion for the particles (dynamic heterogeneity) at each of the compositions considered. Note $\alpha(t)$ for SCN^- at $f = 0.6$ has not decayed to zero even after ~2ns,

indicating extremely sluggish dynamics for this ion and warrants a much longer simulation run. The multi-peak (or peak + shoulder) structure has already been observed in simulations of mixed alkali silicate glasses and explained in terms of localization of jumps of shorter and longer lengthscales at short and long times respectively[29]. Also note that the scales of $\alpha(t)$ for different species are strikingly similar to those reported in Ref. 29 but quite different from the simulated results for an ionic liquid, 1-ethyl-3-methylimidazolium nitrate [47]. Additionally, the effects on $\alpha(t)$ is the most dramatic at f =0.2, and dilution of one of the alkali metal ions by the other moves the peak of $\alpha(t)$ towards shorter times. However, increase of f shifts the peak for SCN^- towards longer times and leads to an emergence of a shoulder for CH_3CONH_2 around 10 ps. The $\alpha(t)$ profiles shown here therefore indicate that dynamic heterogeneity in this melt is present over a wide range of timescale, and motions of different lengthscales for each of the particles (ions and solvent) contribute to the observed partial decoupling of D from η.

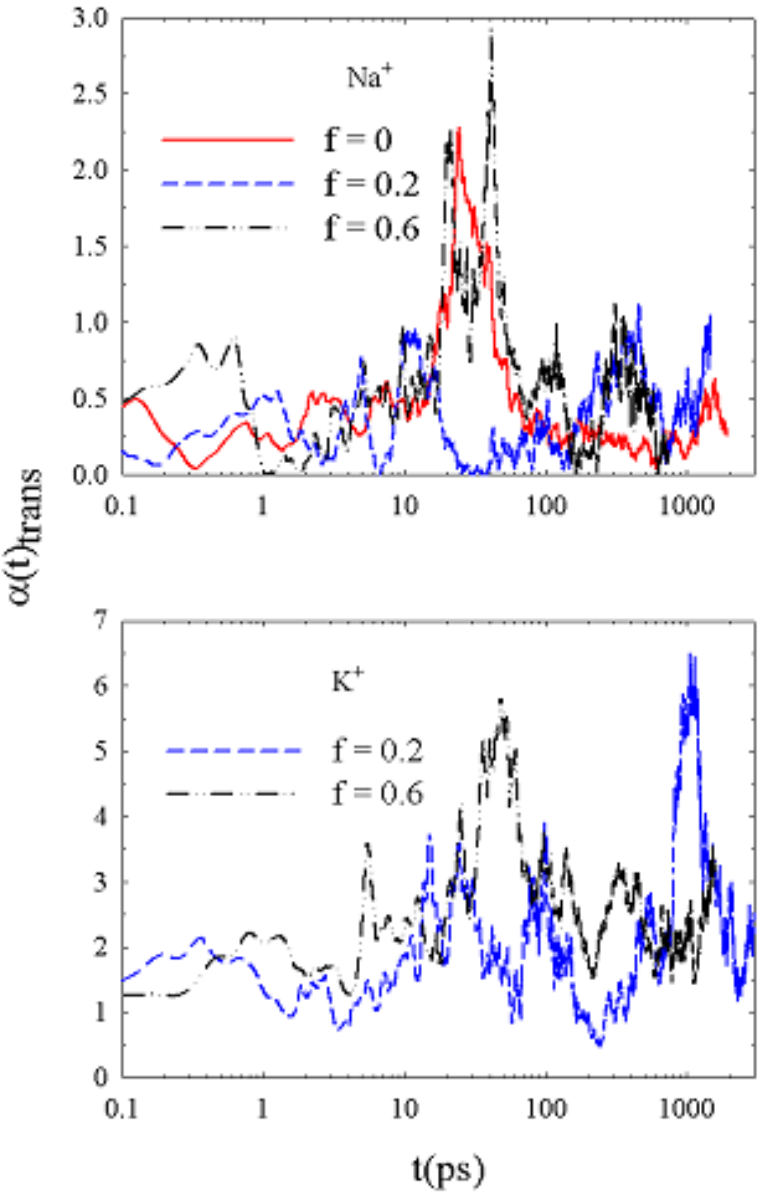

Figure. 2.3: Composition dependence of the non-Gaussian parameter, $\alpha(t)$, for alkali metal ions present in the melt, $0.75CH_3CONH_2 + 0.25[\,fKSCN + (1-f)NaSCN\,]$ at 318 K. $\alpha(t)$ has been calculated by using Eq. 2.5 described in the text. Simulated data are noisy because of insufficient averaging. See Fig. A5, in Appendix A, for $\alpha(t)$s associated with SCN^- and acetamide. Note that better averaging via longer runs will remove the noise but not alter the qualitative understanding generated by the present curves.

The deviation from the Gaussian distribution with particle displacement is further elaborated in Fig. 2.4 where the simulated composition dependent self-part of the van Hove function, $G_s(\vec{r},t)$, for each of the ions and acetamide are shown, for a time where the respective $\alpha(t)$ s exhibit maxima in the intermediate time scale, and compared with the corresponding Gaussian approximation [28], $G_s^0(\vec{r},t) = \left[3/2\pi\left\langle|\Delta\vec{r}(t)|^2\right\rangle\right]^{3/2} \exp\left(-3r^2/(2\left\langle|\Delta\vec{r}(t)|^2\right\rangle)\right)$. Note that at these times the deviation from Gaussian distribution is expected to be the most pronounced. It is clear that simulated distributions deviate strongly from the Gaussian approximation and show significant composition dependence. Of particular interest is the supression of the large lengthscale motions for K^+ with f which is qualitatively similar to that found for mixed alkali silcate glasses [29] and can be attributed to the 'cooperative blockage' of the large jumps. In fact, relatively large lengthscale motions are increasingly becoming non-accessible with varying degree for all the ions and acetamide with f in this melt. A comparison between the simulated and calculated curves also reveal that the most pronounced effects are felt by those ions which are present at the dilute limit. Previous studies [30,34] have shown that presence of foreign ions at higher concentration leads to the suprression of both jump length and collective dynamics. This might be the reason behind the drastic deviation of $G_s(\vec{r},t)$ for Na^+ from Gaussian distribution at f =0.6 around 40 ps but much tender one for K^+ at the same composition and similar time. The role of concentration is further supported by the relatively weaker deviation of simulated $G_s(\vec{r},t)$ from the Gaussian ones for SCN^- and CH_3CONH_2 whose concentrations remained unaltered during the change of mixture composition. Figures 2.3 and 2.4 might therefore jointly suggest that the addition of K^+ pushes the medium dynamics towards faster timescales via localising the jumps between neighboring regions and thereby effectively shortening the timescales of dynamical events. This is probably the reason for the experimental observation of faster solute and solvent dynamics with f in this melt [11].

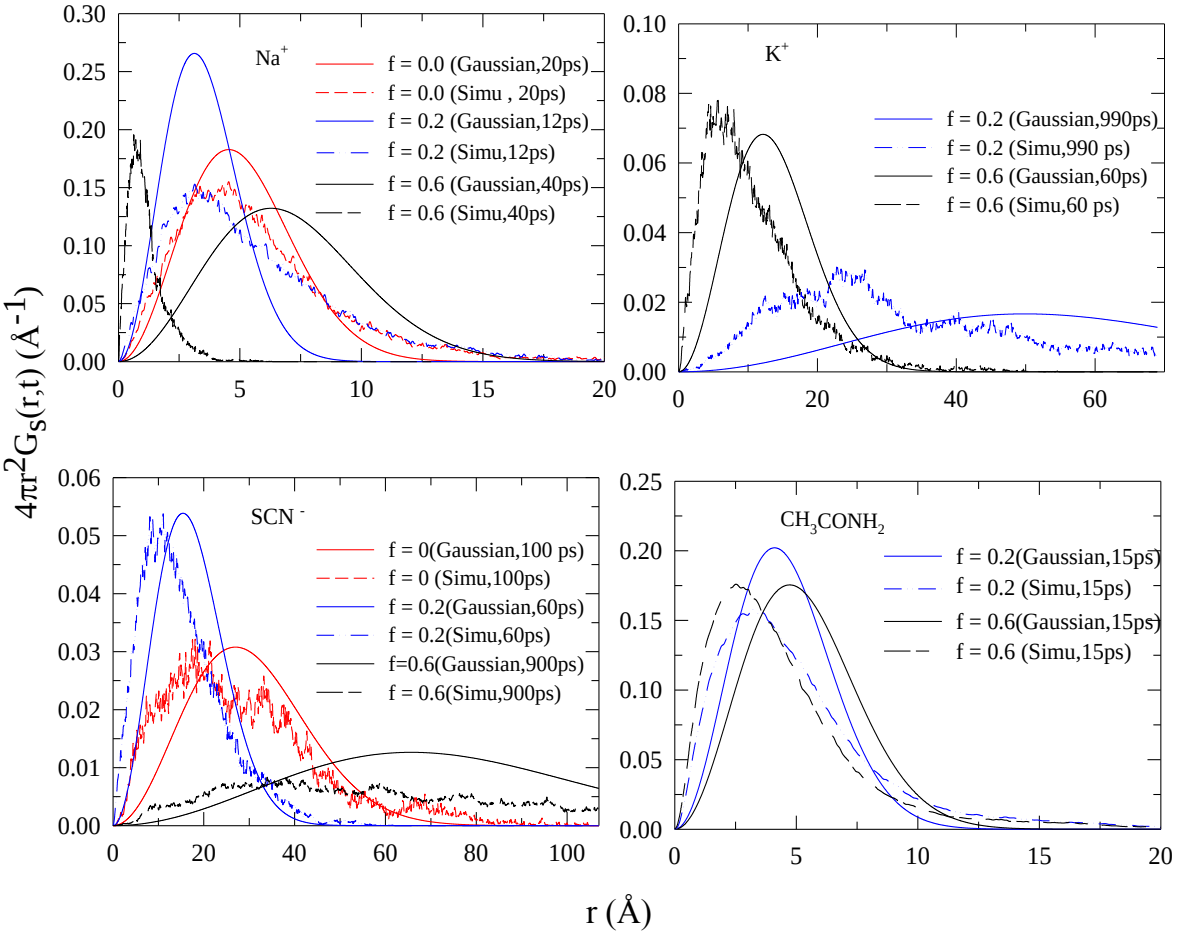

Figure. 2.4: Effects of K^+ concentration on the self-part of the van Hove function, $G_s(\vec{r},t)$, for each of the species present in the molten mixtures of (acetamide + sodium/potassium thiocyanate) at 318 K. Smooth solid lines denote the calculated $G_s(\vec{r},t)$ assuming Gaussian distribution with respect to the particle displacement as described in the text. Simulated and calculated $G_s(\vec{r},t)$ are shown at times where the corresponding $\alpha(t)$ attains a maximum value. These times are indicated in the legends. Note the simulated data for ions appear noisy which become nearly smooth for acetamide because of better averaging due to relatively larger number of particles.

A visual sense of the heterogeneity in particle motion is presented in Figs. A6 and A7 (Appendix A) where 1 ns trajectories associated with the centre-of-mass motions of a few arbitrarily selected ions (Na^+, K^+ and SCN^-) and CH_3CONH_2 particles are shown for this melt at $f = 0.2$ and 318 K. These representative trajectories clearly

indicate jump motions for ions (particularly for Na^+ and K^+) and heterogeneity in translational motion of all the particles. Note that in accordance with the time profile of MSDs presented in Fig. 2.2, these trajectories also do not suggest any presence of rattling in a cage motion. However, some particles are seen to be more mobile (judged by the length covered in 1 ns) than others. The slow and fast particles in these mixtures, as in supercooled systems [14] and ionic liquids [28], might also be spatially correlated. This requires further investigation.

We next explore the timescales associated with the solvent dipolar rotation via following the relaxation of the normalized collective dipole moment autocorrelation function defined as [24]

$$\Phi(t) = \frac{\left\langle \vec{M}(0).\vec{M}(t) \right\rangle}{\left\langle \left| \vec{M}(0) \right|^2 \right\rangle}, \qquad (2.6)$$

where the time dependent collective dipole moment ($\vec{M}(t)$) is the sum over all the molecular dipole moments, $\vec{M}(t) = \sum_i^N \vec{\mu}_i(t)$. Note that $\Phi(t)$ is connected to the exerimentally measured frequency dependent dielectric function ($\varepsilon(\omega)$) via the relation, $\varepsilon(\omega) = 1 + \frac{4\pi}{3Vk_BT} L\left[-\frac{d}{dt}\Phi(t) \right]$, where L denotes Fourier-Laplace transform. In addition, $\varepsilon(\omega)$ and polar solvation energy relaxation measured via time-resolved fluorescence experiments are intimately connected [11]. Since the available dielectric relaxation data [1] cannot provide any information regarding the short time dynamics of this melt because they were obtained via using rather a narrow frequency coverage (10^{-1} - 10^8 Hz), we have followed the time evolution of $\Phi(t)$ mainly to justify the ultrafast solvation timescale suggested by our recent experiments [11]. We cannot, however, explore the reported slow timescale (>10 ns) [1] as they are too slow to be accessed by the present simulations. Fig. 2.5 demonstrates this aspect where the simulated $\Phi(t)$ at f =0 are shown for different temperatures. Note the decays shown in this figure are fitted lines through the actual simulated data (presented in the Appendix A, Fig. A8).

The short time $\Phi(t)$ decays are shown separately in the bottom panel for better representation of the extremely fast relaxation at the early stage. It is evident from this figure that eventhough none of the $\Phi(t)$ decays are complete within the present time window, both ultrafast and ultraslow timescales exist in this melt, particularly at lower temperatures. Moreover, the longtime decay shows the expected temperature dependence. Bi-exponential fit to these incomplete decays have been found to produce one timescale roughly in the 2-10 ps range and the other in the 0.3 – 1 ns range. Although the incomplete decay suggests presence of an even longer timescale, the simulated short time dynamics qualitatively support the experimental suggestion [11] that early part of the solvation energy relaxation of a laser-excited polar dye in this melt occurs in picosecond or even faster timescale. According to the simulated decay of $\Phi(t)$, an extremely rapid component of the dipolar solvent rotation provides a channel for such a fast solvation energy relaxation in this melt.

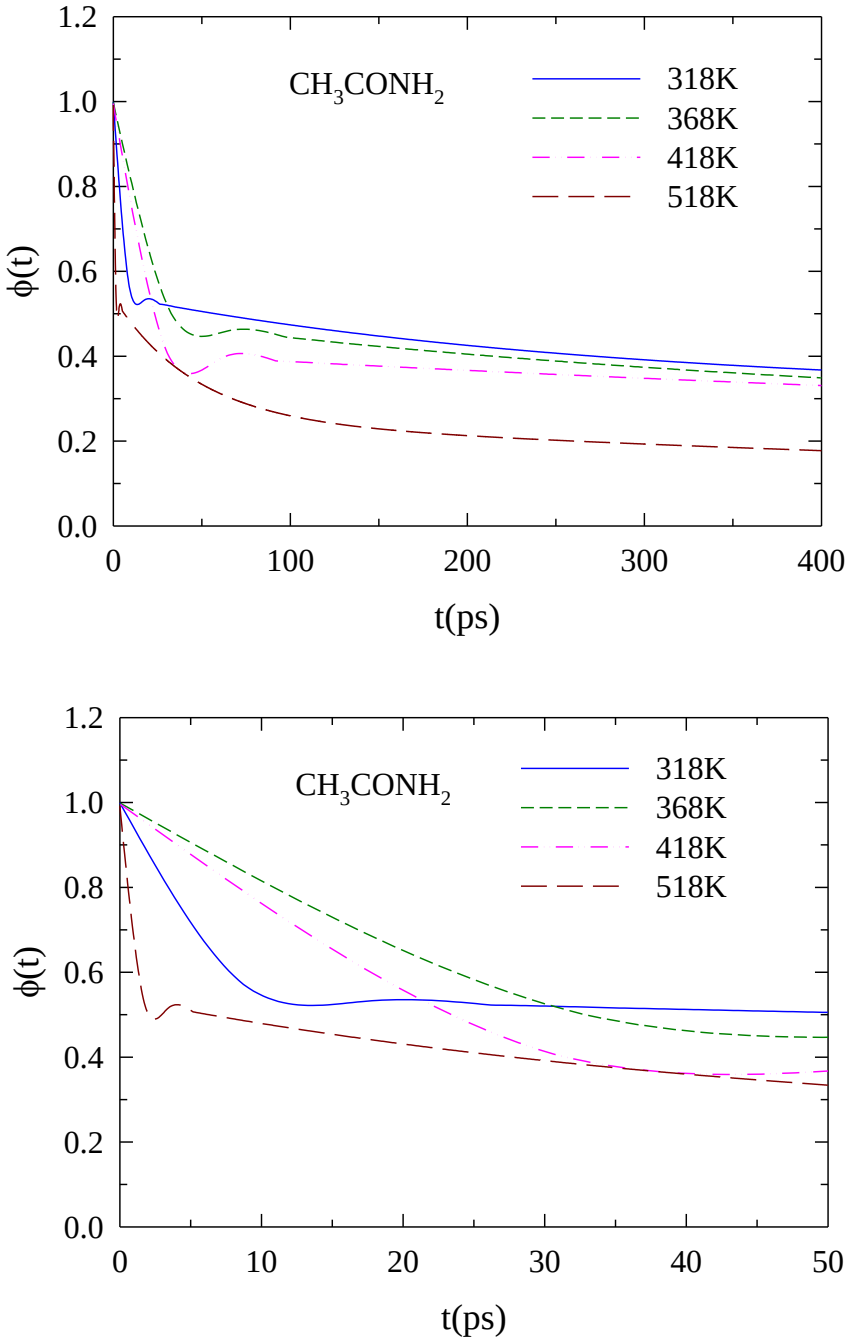

Figure. 2.5 : Temperature dependence of the relaxation of the collective dipole moment autocorrelation function, $\Phi(t)$, for acetamide in this melt at $f = 0$ and 318 K. Note the fitted data through the simulated curves (shown in Fig. A8, Appendix A) are presented to avoid cluttering due to noise. While the upper panel shows the data for the full time window accessed by the present simulations, the lower panel specifically shows the early time dynamics. Data representations are indicated inside each of the panels and colors coded.

2.4 Conclusion

In summary, the present work shows that the dynamic heterogeneity is one of the responsible factors for the partial decoupling between the diffusion and viscosity coefficients in these melts. The decoupling of average solvation and rotation times for a polar solute in this melt at various compositions reflected in recent experiments [11, 13] may be explained in terms of the dynamic heterogeneity observed in the present model simulation studies. The simulated decay of the collective dipole moment autocorrelation function indicate the presence of ultrafast polarization relaxation in this melt which was not explored before. It should, however, be kept in mind that eventhough various aspects of non-Gaussian parameter and the self-part of the van Hove correlation function for this melt are qualitatively similar to those found in mixed alkali silicate glasses, the simulated mean squared displacements for the ions or solvent particles never showed any indication of rattling within a cage. Simulations with more number of particles than considered here are not likely to alter the qualitative character of these results as evidences for secondary or no system size effects on ion motions in glassy systems already exist [25,30]. The role of the spatial heterogeneity remained unexplored because of the use of model interaction potentials in the present work. Limited simulation runs did not allow to access the slowest timescales associated with the dipolar relaxation in these systems. Moreover, relations between particle jump, local stress relaxation and wavenumber dependence of it [48-50] needs to be explored.

References :

1. A. Amico, G. Berchiesi, C. Cametti, and A. D. Biasio, J. Chem. Soc. Faraday Trans. 2, **83,** 619 (1987).
2. G. Berchiesi, M. D. Angelis, G. Rafaiani, and G. Vitali, J. Mol. Liq. **51,** 11 (1992).
3. G. Berchiesi, F. Farhat, and M. D. Angelis, J. Mol. Liq. **54,** 103 (1992).
4. G. Berchiesi, J. Mol. Liq. **83,** 271 (1999).
5. F. Catellani, G. Berchiesi, F. Pucciarelli, and V. Bartocci, J. Chem. Eng. Data **26,** 150 (1981).
6. G. Kalita, N. Rohman, and S. Mahiuddin, J. Chem. Eng. Data **43,** 148 (1998).
7. G. Kalita, K. G. Sarma, and S. Mahiuddin, J. Chem. Eng. Data **44** , 222 (1999).
8. G. Berchiesi, G. Rafaiani, G. Vitali, and F. Farhat, J. Therm. Anal. **44** , 1313 (1995).
9. S. Mahiuddin, J. Chem. Eng. Data . **41,** 231 (1996).
10. G. E. McManis, A. N. Fletcher, D. E. Bliss, and M. H. Miles, J. Electroanal. Chem. **190** , 171 (1985).
11. B. Guchhait, H. A. R. Gazi, H. K. Kashyap, and R. Biswas, J. Phys. Chem. B **114** , 5066 (2010).
12. H. A. R. Gazi, B. Guchhait, S. Daschakraborty, R. Biswas, Chem. Phys. Lett. **501,** 358 (2011).
13. B. Guchhait, S. Daschakraborty, R. Biswas, J. Phys. Chem. B,**136**,174503 (2012) .
14. M. D. Ediger, Annu. Rev. Phys. Chem. **51,** 99 (2000).
15. W. Huang and R. Richert, Phil. Mag. **87** , 371 (2007).
16. D. Chakrabarti and B. Bagchi, Phys. Rev. Lett. **96,** 187801 (2006).
17. Y. Wang and G. A. Voth, J. Am. Chem. Soc. **127,** 12192 (2005).
18. J. A. C. Lopes and A. A. H. Padua, J. Phys. Chem. B **110** , 3330 (2006).
19. A. Triolo, O. Russina, B. Fazio, R. Triolo, and E. D. Cola, Chem. Phys. Lett. **467** , 362 (2008).
20. P. K. Mandal, M. Sarkar, and A. Samanta, J. Phys. Chem. A **108,** 9048 (2004).
21. H. Jin, X. Li, M. Maroncelli, J. Phys. Chem. B **111,** 13473 (2007).

22. D. K. Sasmal, A. K. Mandal, T. Mondal, and K. Bhattacharyya, J. Phys. Chem. B. **115**, 7781 (2011).
23. A. Rahman, Phys. Rev. **136** , 405 (1964).
24. J. P. Hansen, I. R. McDonald, Theory of Simple Liquids, 2nd Ed., Academic Press, London, 1986.
25. J. Habasaki and K. L. Ngai, J. Non-Cryst. Solids **352,** 5170 (2006).
26. F. Faupel, W. Frank, M.-P. Macht, H. Mehrer, V. Naundorf, K. Ratzke, H. R. Schober, S. K. Sarma, and H. Teichler, Rev. Mod. Phys. **75** , 237 (2003).
27. D. Roy, N. Patel, S. Conte, and M. Maroncelli, J. Phys. Chem. B. **114,** 8410 (2010).
28. M. G. Del Popolo and G. A. Voth, J. Phys. Chem. B **108** , 1744 (2004).
29. J. Habasaki and K. L. Ngai, Phys. Chem. Chem. Phys. **9** , 4673 (2007).
30. J. Habasaki, K. L. Ngai, and Y. Hiwatari, J. Chem. Phys. **121**, 925 (2004).
31. C. Cramer, S. Bruckner, Y. Gao, and K. Funke, Phys. Chem. Chem. Phys. **4** , 3214 (2002).
32. K. Ueno and C. A. Angell, J. Phys. Chem. B **115** , 13994 (2011).
33. A. Muthukumar, J. Phys. A: Math. Gen. **14** , 2129 (1981).
34. J. Habasaki and Y. Hiwatari, Phys. Rev. E **62** , 8790 (2000).
35. M. P. Allen and D. J. Tildesley, Computer Simulations of Liquids, Oxford University Press, New York, 1987.
36. A. Aguado and P.A. Madden, J. Chem. Phys. **119** , 7471 (2003).
37. B. Peterson, J. Saykall, M. Mucha, and P. Jungwirth, J. Phys. Chem. B **109** , 10915 (2005).
38. P. Kumar and M. Maroncelli, J. Chem. Phys. **103** , 3038 (1995).
39. P. Jedlovszky and A. Idrissi, J. Chem. Phys. **129** , 164501 (2008).
40. R. Biswas and B. Bagchi, Acc. Chem. Res. **31,** 181 (1998).
41. A. S. Clarke and H. Jonsson, Phys. Rev. E. **47,** 3975 (1993).
42. E. Sim, A. Z. Patashinski, and M. A. Ratner, J. Chem. Phys. **109,** 7901 (1998).
43. S. Mahiuddin, Can. J. Chem. **74** , 760 (1996).
44. R. A. Wallace, J. Phys. Chem. **75** , 2687 (1971).
45. W. D. Williams, J. A. Ellard, and L. R. Dawson, J. Phys. Chem. **79,** 4652 (1957).
46. W. Kob, C. Donati, S. J. Plimpton, P. H. Poole, and S. C. Glotzer, Phys. Rev. Lett. **79**, 2827 (1997).

47. J. Habasaki and K. L. Ngai, J. Chem. Phys. **129** , 194501 (2008).
48. S. Bhattacharyya and B. Bagchi, Phys. Rev. Lett. **89** , 025504 (2002).
49. S. M. Bhattacharyya, B. Bagchi, and P. G. Wolynes, Proc. Natl. Acad. Sci. USA **105,** 16077 (2008).
50. S. M. Bhattacharyya, B. Bagchi, and P. G. Wolynes, J. Chem. Phys. **132**,104503 (2010).

Chapter 3

Rank Dependent Orientational Relaxation in an Ionic Liquid: An All-atom Simulation Study

3.1 Introduction

Modern day ionic liquids are those molten salts for which the liquid state is preserved even at ambient condition or near it. Frequently, these fused electrolytes are composed of organic cations with large alkyl chains and relatively smaller anions, and structural frustration coupled with entropy gain keep these systems molten at room temperature. These liquids possess several special solvent properties because of the presence of longer-ranged charge-charge interaction which varies as r_{ij}^{-1} ($u_{ij}(r_{ij}) \propto r_{ij}^{-1}$, r being the separation between the constituent ions) [1]. Negligible vapor pressure, high thermal stability and wide liquidous range are some of the manifests of this r_{ij}^{-1} interaction and have collectively made room temperature ionic liquids (RTILs) as alternative reaction media for chemical industry [2,3]. In some RTILs, cation possesses permanent electric dipole moment (eventhough accurate definition of dipole moment is somewhat difficult for charged species [4]) and in those cases additional interactions, such as, dipole-dipole ($\propto r_{ij}^{-3}$) and ion-dipole ($\propto r_{ij}^{-2}$) interactions, contribute to the complexities in structure and dynamics of these systems. Alkyl substituted imidazolium and pyridinium ionic liquids are examples of such 'dipolar' RTILs whose structure and dynamics have been investigated in some detail [5-18]. Here we consider 1-butyl-3-methylimidazolium hexafluorophosphate ([Bmim][PF_6]) for an all-atom simulation study of rotational motion of the cationic species, [Bmim]$^+$, at two different temperatures, and

subsequently understand the dynamical features in terms of temperature dependent viscosity and heterogeneity [5-6,19-23].

It is to be mentioned here that several simulation studies of [Bmim][PF_6] already exist which investigated various solvent aspects, ranging from determination of physicochemical quantities[24] and refinement of interaction potentials [25-28] to structural and dynamical properties [25-32]. However, temperature effects on orientational relaxation of this IL and its rank dependence [33-36] have not been investigated via atomistic simulations using no charge scaling. This is what has been attempted here where ion reorientation is analyzed in juxtaposition with ion translation and dynamic heterogeneity at different temperatures. In addition, our simulated radial distribution functions ($g(r)$), centre-of-mass diffusion coefficients, viscosity (η) values and non-Gaussian (α_2) parameters have been compared with the existing simulations and experiments (wherever available) to test the accuracy of the present simulations.

The organization of the rest of the chapter is as follows. A brief discussion on the force field and simulation methods employed in the present study is given in the next section. Section 3.2 provides a fidelity check of the present simulations where simulated structural and dynamical properties are compared against simulated results by other authors as well as those from suitable experiments. Subsequently, simulated results on orientational relaxation are presented in Section 3.3 where the rank dependence and heterogeneity effects are discussed. The chapter then ends with concluding remarks in Section 3.4.

3.2 Force Field and Method

Molecular dynamics simulations were performed using the DL_POLY 2.2 and MDynamix programs [37,38]. A schematic diagram of [Bmim][PF_6] along with the naming scheme for atoms is provided in Fig. 3.1.

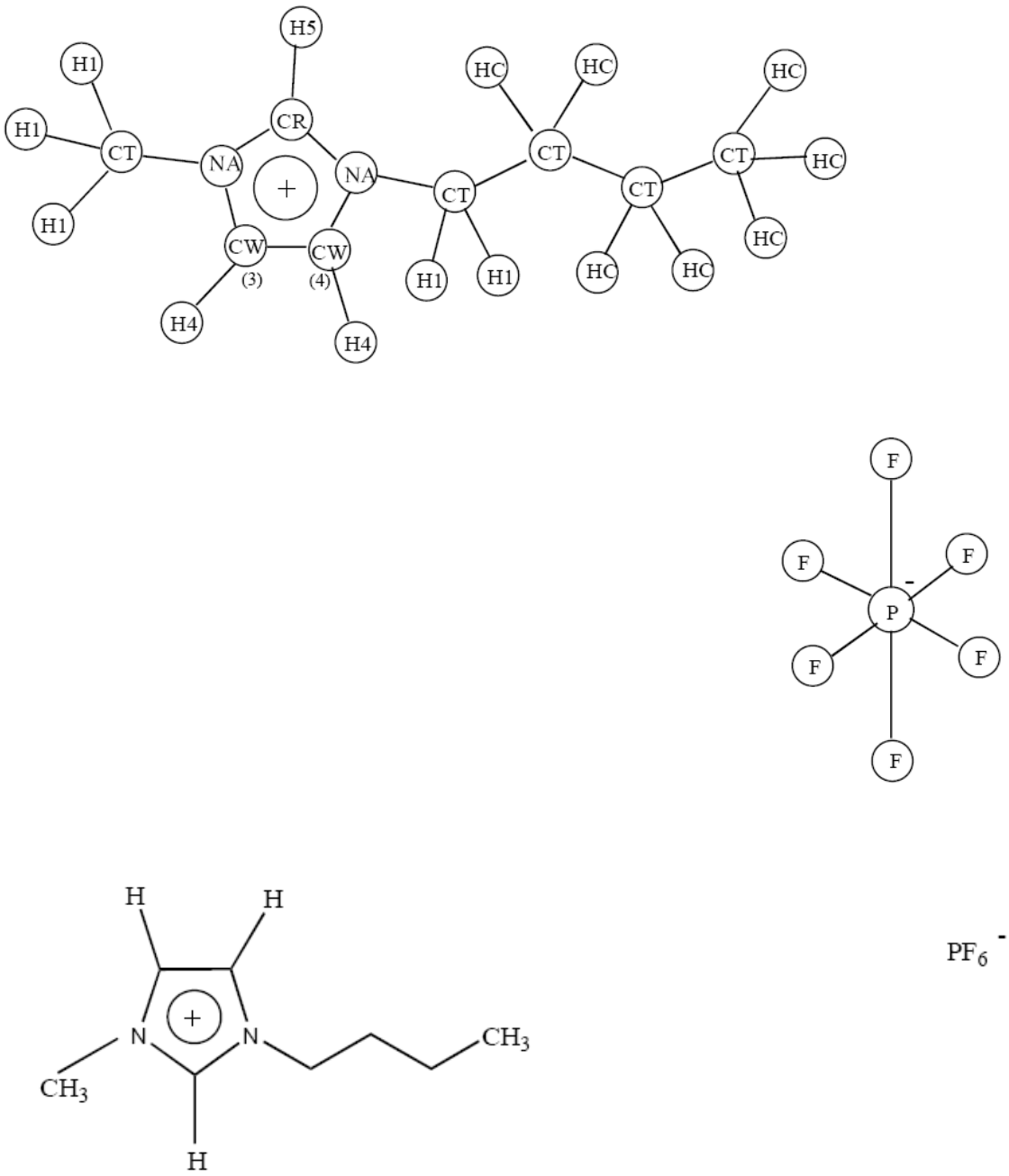

Figure. 3.1: Chemical Structure of [BMIM][PF_6] with AMBER force field atom types. Representations shown here are used in the text while discussing various simulated radial distribution functions.

In this work , we considered flexible molecules interacting by AMBER-type force field with the functional form [26,39].

$$V_{tot} = \sum_{bonds} k_b (r - r_0)^2 + \sum_{angles} k_\theta (\theta - \theta_0)^2 + \sum_{dihedrals} k_\chi [1 + \cos(n\chi - \delta)] + \sum_{i=1}^{N-1} \sum_{j>i}^{N} \left\{ \varepsilon_{ij} \left[\left(\frac{r_{\min,ij}}{r_{ij}} \right)^{12} - \left(\frac{r_{\min,ij}}{r_{ij}} \right)^{6} \right] + \frac{q_i q_j}{r_{ij}} \right\}, \quad (3.1)$$

where V_{tot} is the total potential energy of the system. Harmonic potentials governed bond length and bond angle about the normal values of r_0 and θ_0, and dihedral angles were modeled using a standard cosine series [26]. Lennard-Jones (LJ) parameters for unlike atoms, ε_{ij} and σ_{ij}, were obtained using the Lorentz-Berthelot combining rules [40], $\varepsilon_{ij} = \sqrt{\varepsilon_i \varepsilon_j}$ and $\sigma_{ij} = (\sigma_i + \sigma_j)/2$.

The van der Waals parameters for interaction between two atom types were taken from Ref. 26. The optimized geometry of isolated $[Bmim]^+$ and $[PF_6]^-$ were determined via ab-initio calculations at the HF/6-31+G(d) level of theory and setting the cation and anion charges at +1 and -1, respectively. The force constant of bonds and angles and the coefficients of torsions were taken from literature [26]. Partial atomic charges for $[Bmim]^+$ and $[PF_6]^-$ were also taken from Ref. 26. These force field parameters are summarized in Appendix B (Tables B1 – B5) and have been used without any modification. Relevant LJ parameters and partial charges for representing the solute, coumarin 153 (C153), in its ground state have been taken from Ref. 41 and summarized in Appendix B (Tables B6 and B7). The chemical structure of C153 alongwith the forcs field atom types are specified in Fig. B1 (Appendix B)

The simulation was performed in a cubic cell with standard periodic boundary condition at 1 atm. Pressure, and 298 K and 450 K, with $[Bmim]^+$ and $[PF_6]^-$ 128 each (a total of 4096 atoms) that were interacting via Eq. 3.1. Isothermal isobaric (NPT) ensemble was considered using the Nose-Hoover barostat and thermostat [42-45], with coupling constants of 2000 and 500 fs, respectively. Equations of motion were solved by the Verlet Leapfrog algorithm [40] with 1 fs time step. The cutoff radius was set to 16

Å which produced density at 298 K very close (but ~1.5% less) to that reported in measurements [46]. The Verlet Neighbour list had a shell width of 2.0 Å for both the temperatures. Electrostatic interactions were handled via the Ewald summation technique [40]. Equilibration was done first at 450 K and then brought down to 298 K via a step-down process with a step of 50 K and subsequent equilibration at each of the steps for a period of 2 ns. The production run was for 8 ns for both at 450 K and 298 K. The configurations of the system were saved every after 100 fs. Simulations in NPT ensemble were carried out using MDynaMix program and the structural and dynamical properties were calculated using TRANAL utility of the Program. Subsequently, we switched to DL_POLY 2.2 program where liquid viscosity was obtained via both NVT and NPT ensemble simulations. Fig. 3.2 provides a picture of the simulated system.

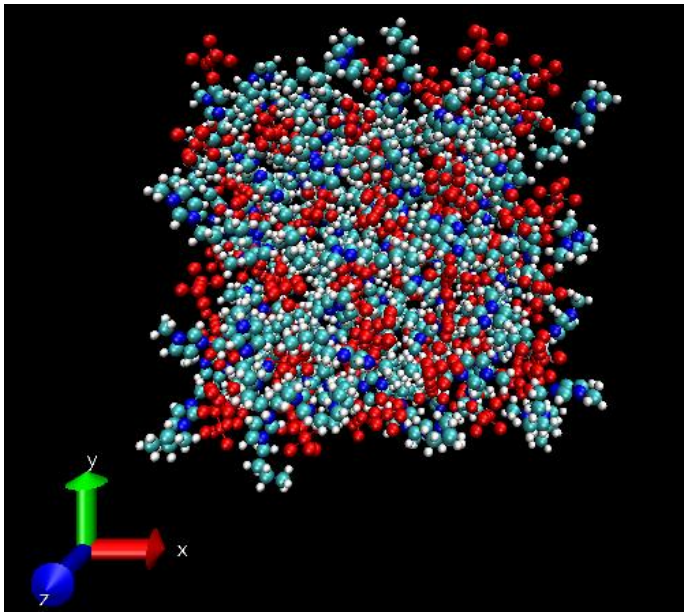

Figure. 3.2: Snapshot of the simulated system for [Bmim][PF_6] at 298 K. Red colors indicate the phosphorus and fluorine atoms of the anions . They are marked in red to separately identify from the cations. Nitrogens of the cation are marked in deep blue , carbons in cyan color and hydrogens as white spheres.

3.3 Present Simulations: Fidelity Check and New Results

3.3.1. Thermodynamic Quantities

Table 3.1 compares the densities obtained from our simulations at 298 K and 450 K with those from experiments [46,47] as well as from earlier simulations [25-29]. Evidently, simulated densities are in good agreement with the experimental data at these temperatures and also correlate well with those from other simulation works which had used somewhat different model and charge parameters while describing the IL, [Bmim][PF_6]. The simulated volume expansivity ($\alpha_P = V^{-1}(\partial V/\partial T)_P = \rho^{-1}(\partial \rho/\partial T)_P$) is found to be $6.06 \times 10^{-4} K^{-1}$ and is comparing well with the experimental result, $6.1126 \times 10^{-4} K^{-1}$ [47].

Table 3.1: Comparison of temperature dependent densities of [Bmim][PF_6] between present simulations and those from experiments and earlier simulations.

Temperature (K)	Our Simulation (gm/cc)	Experimental (gm/cc)		Simulations (gm/cc) Ref. 27		Simulations (gm/cc) Ref. 28	Simulations (gm/cc) Ref. 29
		Ref. 61	Ref. 24	United Atom (UA) Model	All-Atom (AA) Model	AA and charge scaling	AA
298	1.3498	1.3710	1.360	1.365	1.350	1.389	1.368
450	1.2242					1.248	

3.3.2. Structural Properties

Next we show in Fig. 3.3 the structural arrangement of the ions in solution phase at these temperatures via the simulated distance dependent radial distribution functions (rdfs, $g(r)$). The hydrogen marked as "H5" in Fig. 3.1 is the most acidic [48,49] and thus

expected to interact most strongly with the fluorine (F) atoms of the anion, $[PF_6]^-$. This is what has been observed in the present simulations (as by previous authors also [26]). Hydrogen atoms attached to the other two sp^2-hybridized ring carbons ("H4") do interact with $[PF_6]^-$ but with less probability than H5 for obvious reason (acidity difference). The same reason also leads to relatively less intimate interaction of H1 with $[PF_6]^-$ because they are connected to sp^3-hybridized carbons attached to the ring nitrogens as alkyl side chains. The interaction of $[PF_6]^-$ with the hydrogens ("HC") of the butyl chain is the least as suggested by the corresponding $g(r)$, indicating the anion locating around the imidazolium ring. This is natural as electrostatic interaction between opposite charges will force the anion to reside closer to the cation, allowing for preferential locations over the solid angle subjected to minimization of steric repulsions. Note that the peak of each of these rdfs at 450 K is uniformly lower than the corresponding $g(r)$ at 298 K and thus qualitatively very similar to the temperature effects on structure of simple liquids [1, 50]. This suggests that eventhough the longer-ranged electrostatic interactions regulate many physicochemical properties of ionic liquids, the spatial arrangement of the ions in the liquid state is still guided by the nearest neighbor repulsive interactions in these highly dense Coulomb fluids [16].

The possible spatial arrangements of ions reflected by various H-F rdfs discussed above is further supported by the simulated rdfs involving various carbons of $[Bmim]^+$ and the phosphorus of $[PF_6]^-$, shown in the lower panel of Fig. 3.3. A very intense "CR-P" $g(r)$ along with those involving "CW(3)-P" and "CW(4)-P" with decreasing intensity confirms uneven distribution of $[PF_6]^-$ around the imidazolium ring with preferential anion populations at the two ends of the axis bisecting the "CW(4)-CW(3)" bond through the carbon ("CR") attached to the most acidic hydrogen [25-29, 51-54]. An interplay between steric repulsion and site preferentiality is reflected via a smaller peak of "CW(4)-P" $g(r)$ than that of "CW(3)-P" $g(r)$. Temperature effects on these rdfs are also similar to that described already in connection with "H-F" rdfs presented in the upper panel of this figure, which indicate the order of preferentiality does not change upon raising the medium temperature.

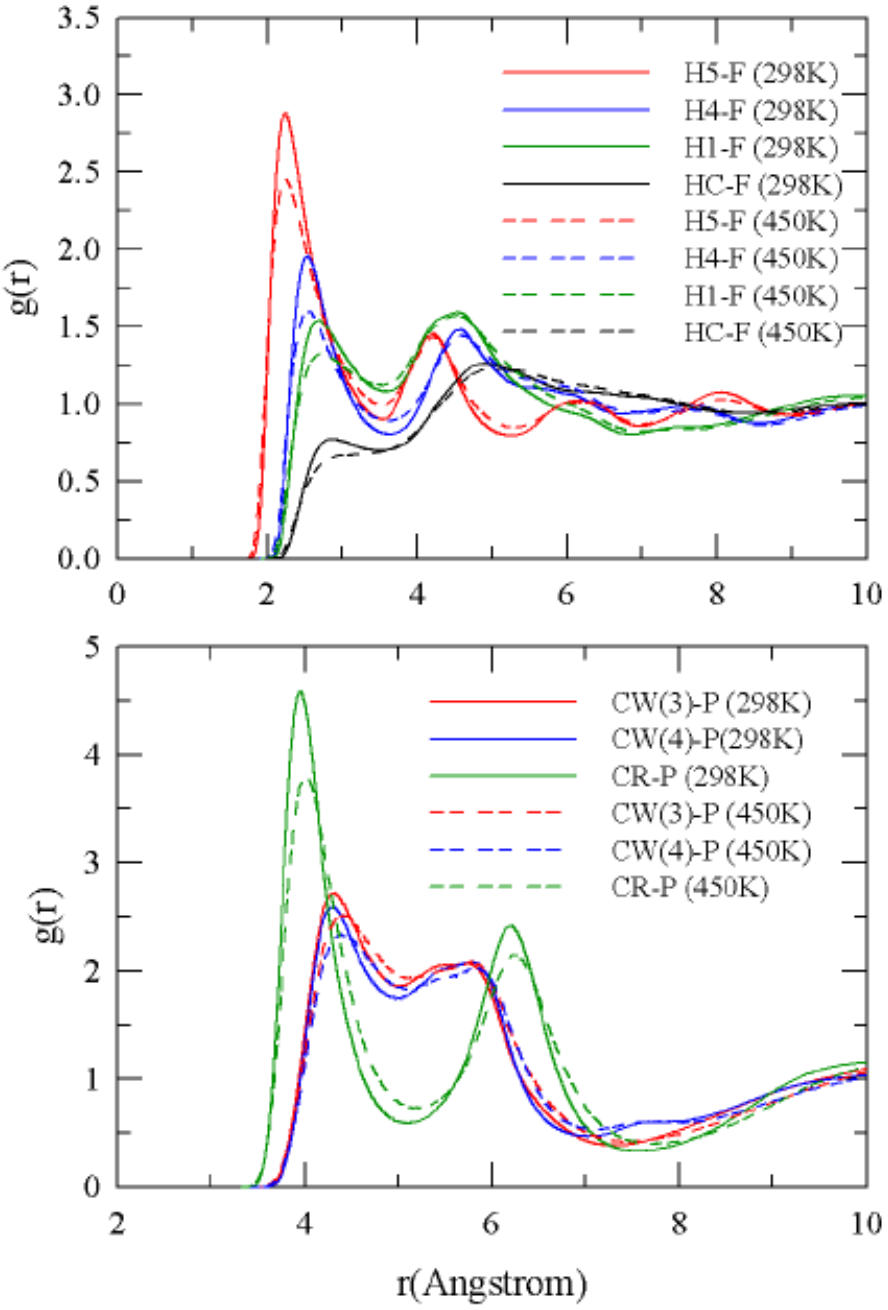

Figure. 3.3: Temperature dependent radial distribution functions (RDFs) between the cation and the anion.While the upper panel shows RDFs between various H-atoms of the cation and F-atom of the anion, the lower panel depicts those between various C-atoms of the cation and P-atom of the anion.

The basic correctness of the liquid structure predicted by the present simulations is further reexamined in Fig. 3.4 where we compare our simulated various "H-F" $g(r)$ with those from simulations described in Ref. 26. The agreement is near quantitative. Similar degree of agreement is also achieved for "C-P" rdfs when the results from the

present simulations are compared in Fig. 3.5 with those from Ref. 29. Note these comparisons are for 298 K and a similar comparison for 450 K could not be done because of non-availability of simulated results at this temperature from other researchers.

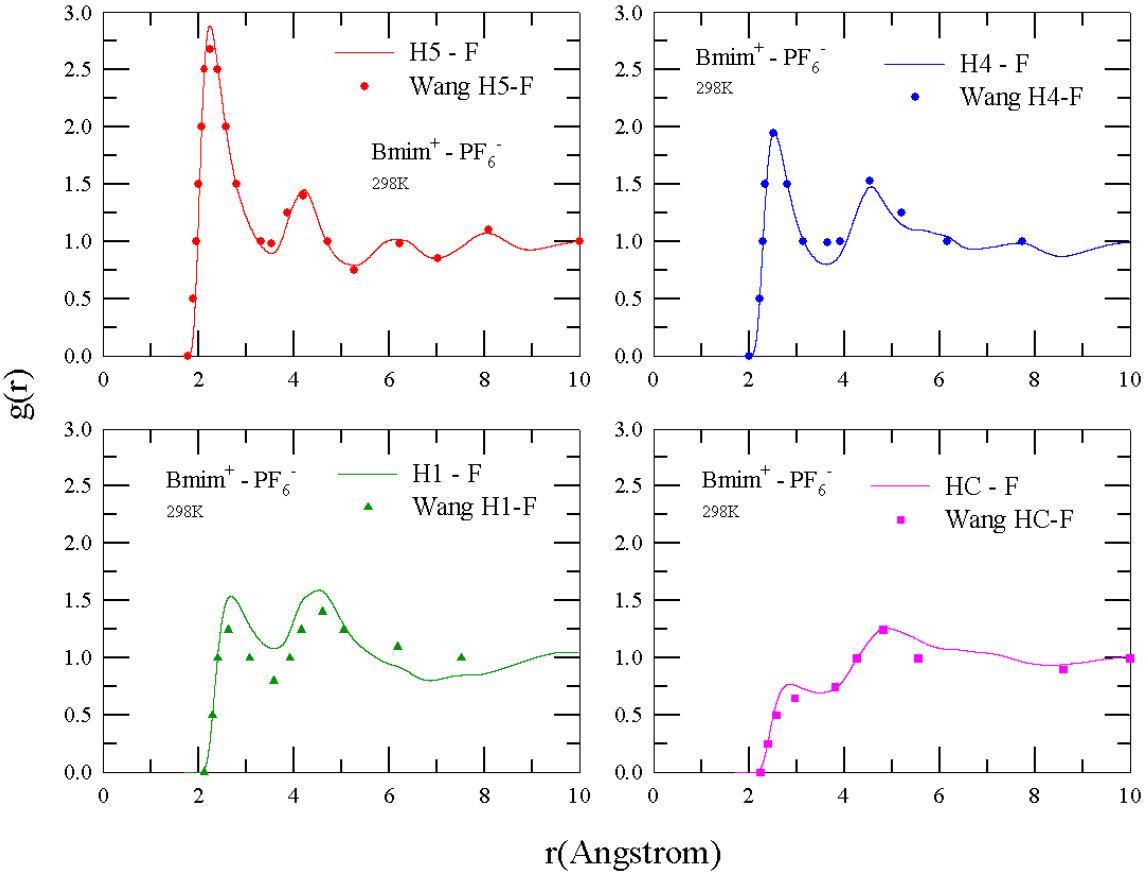

Figure. 3.4: Comparison of RDFs between the present simulations and those reported in Ref. 26. The comparison is made for the data obtained at 298 K. The RDFs are those between various cationic H-atoms and anionic F-atoms.

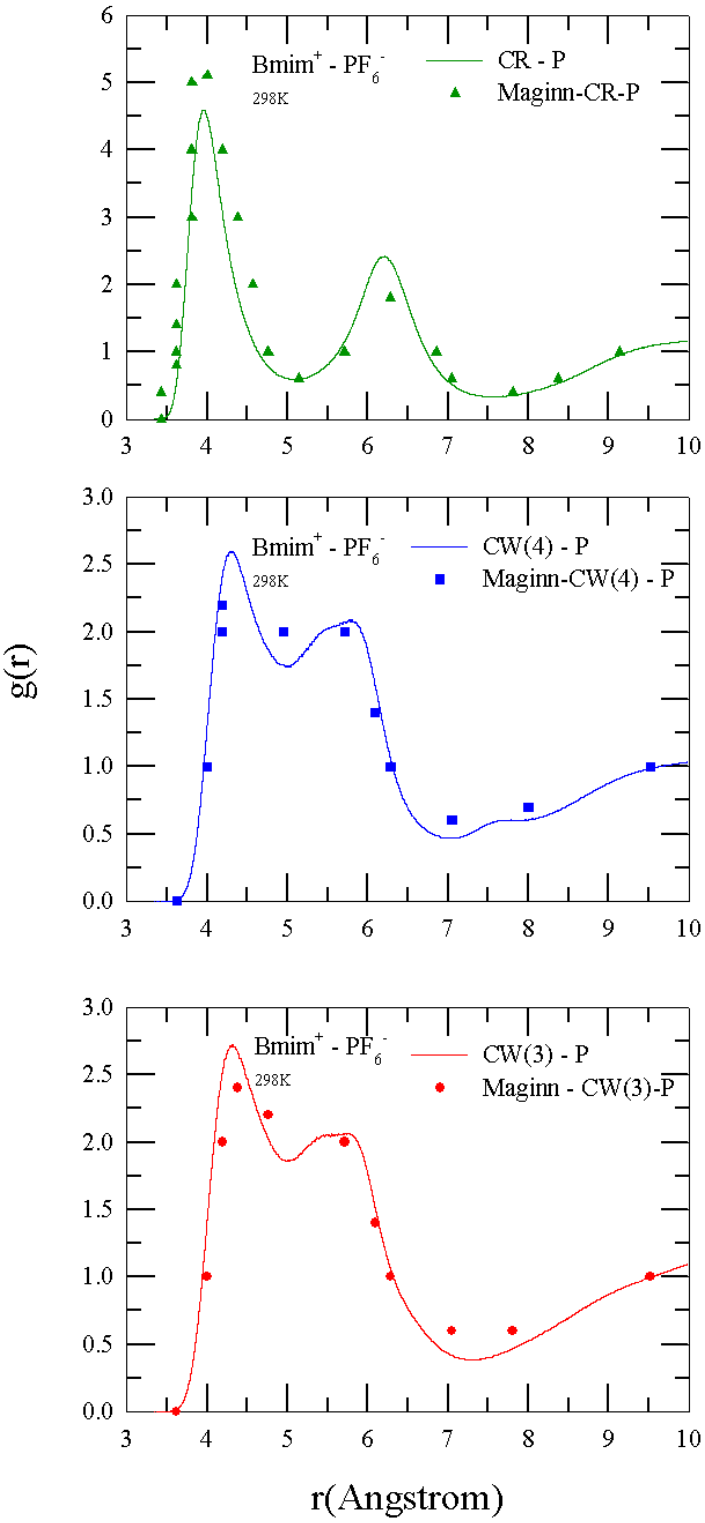

Figure. 3.5: The same as in Fig. 3.4 but now the RDFs are between various C-atoms of the cation and P-atom of the anion. Here the comparison is made against the simulated data reported in Ref. 29.

3.3.3. Diffusion Coefficient

The self-diffusion coefficient (D) of a particle moving in a fluid can be calculated from the simulated mean squared displacement (MSD) using the Einstein relation [1],

$$D = \left[\frac{1}{6t} \left(\left\langle \left| \Delta \vec{r}(t) \right|^2 \right\rangle \right) \right]_{t \to \infty} . \qquad (3.2)$$

The MSDs can be obtained from the simulated time-dependent centre-of-mass positional vectors ($\vec{r}_i^{\,c}(t)$) as follows [40,55],

$$\left\langle \left| \Delta \vec{r}(t) \right|^2 \right\rangle = \frac{1}{N} \left\langle \sum_{i=1}^{N} \left| \vec{r}_i^{\,c}(t) - \vec{r}_i^{\,c}(0) \right|^2 \right\rangle, \qquad (3.3)$$

where $\left\langle \left| \Delta \vec{r}(t) \right|^2 \right\rangle$ denotes the ensemble averaged MSD and $\vec{r}_i^{\,c}$ denotes the center-of-mass vector of particle *i*.

Simulated $\left\langle \left| \Delta \vec{r}(t) \right|^2 \right\rangle$ for $[Bmim]^+$ and $[PF_6]^-$ at both 298 K and 450 K are shown in Fig. 3.6. Note these simulated MSDs exhibit multiple time dependencies where $< | \Delta \vec{r}(t) |^2 \propto t^p$ with p = 2 (inertia dominated short time behavior), 1 (diffusion dominated long time behavior) and <1 (sub-diffusive behavior at intermediate times). This is typical of supercooled liquids [56] and ionic glasses [57], and has already been detected in earlier simulation studies of room temperature ionic liquids[58,59]. The new aspect here is that the temperature dependent MSDs reflect substantial shortening of the sub-diffusive time regime upon rise in temperature (~2- 40 ps at 298 K to ~3-10 ps at 450 K), signaling thermal energy induced cage breaking and more facile movement of the ions. This also suggests that departure from the Gaussian behavior of the MSD (which will be shown later) at intermediate time will be relatively less pronounced at higher temperature, indicating a definite role for the microscopic domain formation and the subsequent spatial heterogeneity (in addition to the temporal counter-part) to the "distributed kinetics" observed in solvation [9,10] and dielectric relaxation [11,12,60] measurements of this class of liquids. Note also that at both the temperatures, movement

of $[PF_6]^-$ is faster than that of the bulky $[Bmim]^+$ at the inertia dominated regime but becomes slower at the long-time limit. This has been seen earlier in simulations of model IL [58] and the observed long-time behavior is somewhat counter-intuitive (from size consideration [61]). The asymmetric shape of $[Bmim]^+$ and the delocalized nature of the charge distribution on it probably reduce the attractive strength of the collective potential created by the surrounding $[PF_6]^-$ as neighbors, inducing an easier anionic-cage breaking for the cation than the reverse (cationic-cage breaking) for the anion. This then leads to slightly higher diffusion coefficient for $[Bmim]^+$ than that of $[PF_6]^-$. Higher temperature forces the packing around $[Bmim]^+$ even less compact, allowing more facile movement of the cation than that of the anion. This explains higher degree of decoupling between the simulated MSDs of $[Bmim]^+$ and $[PF_6]^-$ at 450 K than at 298 K.

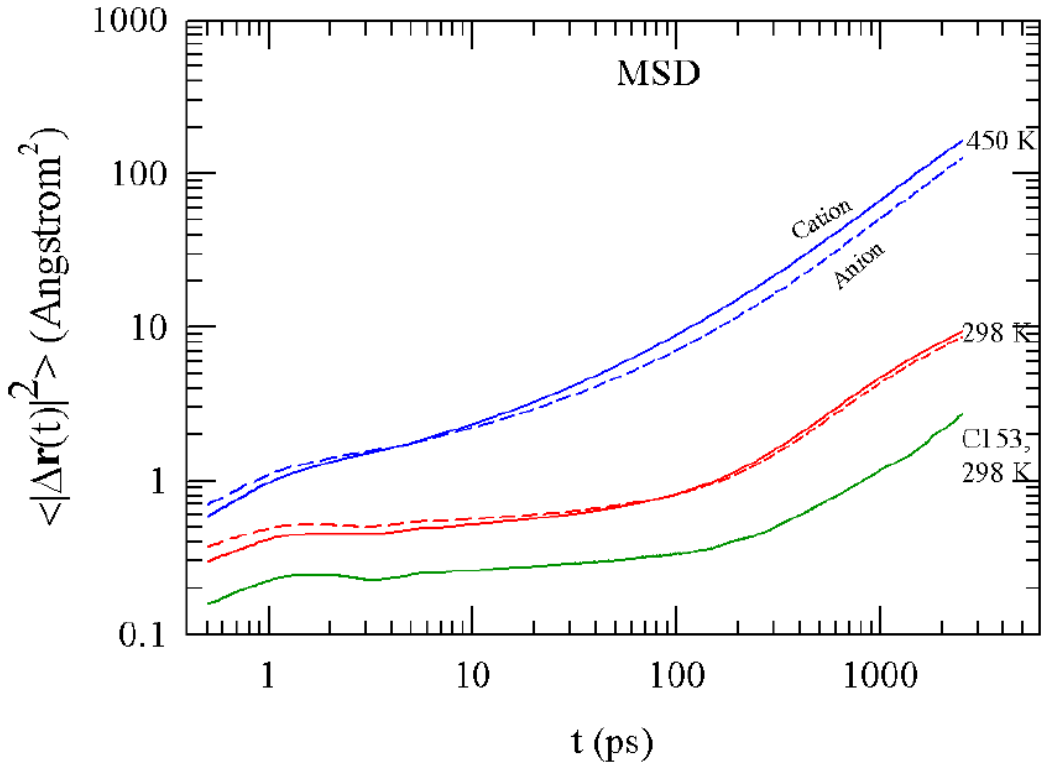

Figure. 3.6: Simulated mean squared displacements (MSDs) for cation, anion and a dissolved solute, C153. The dashed lines represent the MSDs for the anion at 298 K and 450 K.

The simulated MSD at 298 K for a well-known dipolar solvation probe, coumarin 153 (C153), is also presented in Fig. 3.6. A realistic charge distribution that produces ground state dipole moment 6.24 D has been considered for C153 [41, 62,63] and the MSD shown corresponds to that of a ground state solute. Interestingly, C153 also exhibits multiple

time-dependencies in its MSD, suggesting rattling of C153 in ionic cages. This is important for the following reasons. First, 3PEPS measurements of several ILs [13] using a dipolar solute have reported sub-hundred femtosecond solvation response of substantial magnitude, which has been very recently explained in terms of solute-IL binary collision [16]. Rattling of C153 in ionic cages provides a support to this collision model of ultrafast solvation response. Second, if the similarity in time dependencies of MSDs between the solute and the ions at 298 K is also extended between those at 450 K, one predicts that the ultrafast timescale will be lengthened and its amplitude shortened at 450 K. This is because of softening of the cage and decrease of the cage lifetime at higher temperature. This should be tested against suitable experiments.

The normalized velocity autocorrelation function ($C_V^N(t) = \langle \vec{V}(0).\vec{V}(t) \rangle / \langle \vec{V}(0).\vec{V}(0) \rangle$) for both the ions, simulated at 298 K and 450 K, are shown in Fig. 3.7. It is interesting to note that $C_V^N(t)$ in this ionic liquid, much like in uncharged model fluids at high density [1], exhibits negative minimum (because of back-scattering from the solvent cage) and decays completely within a few picoseconds. This suggests that repulsive inter-particle interaction dominates the nearest neighbor arrangements (packing effects) even for this ionic fluid because of its high density. It is also important to observe that the ionic cages, though minima occurring with reduced amplitudes at longer times, are intact even at a temperature ~170 K above its melting temperature (for [Bmim][PF_6], $T_m \approx 284$ K [64,65]). The reduction in minima amplitudes suggests cage-loosening upon rise in temperature which, in turn, shifts the minima at longer times via increasing the respective mean free paths. This is also in qualitative agreement with what has been observed for simple uncharged fluids [1]. All these similarities indicate that even-though the liquid state structure of [Bmim][PF_6] (and other alkylated ionic liquids as well) reflects a signature of charge-charge interaction via 'pre-peak' in the static structure factor [20,21], packing effects still regulate the nearest neighbor spatial arrangement in these highly dense coulomb fluids.

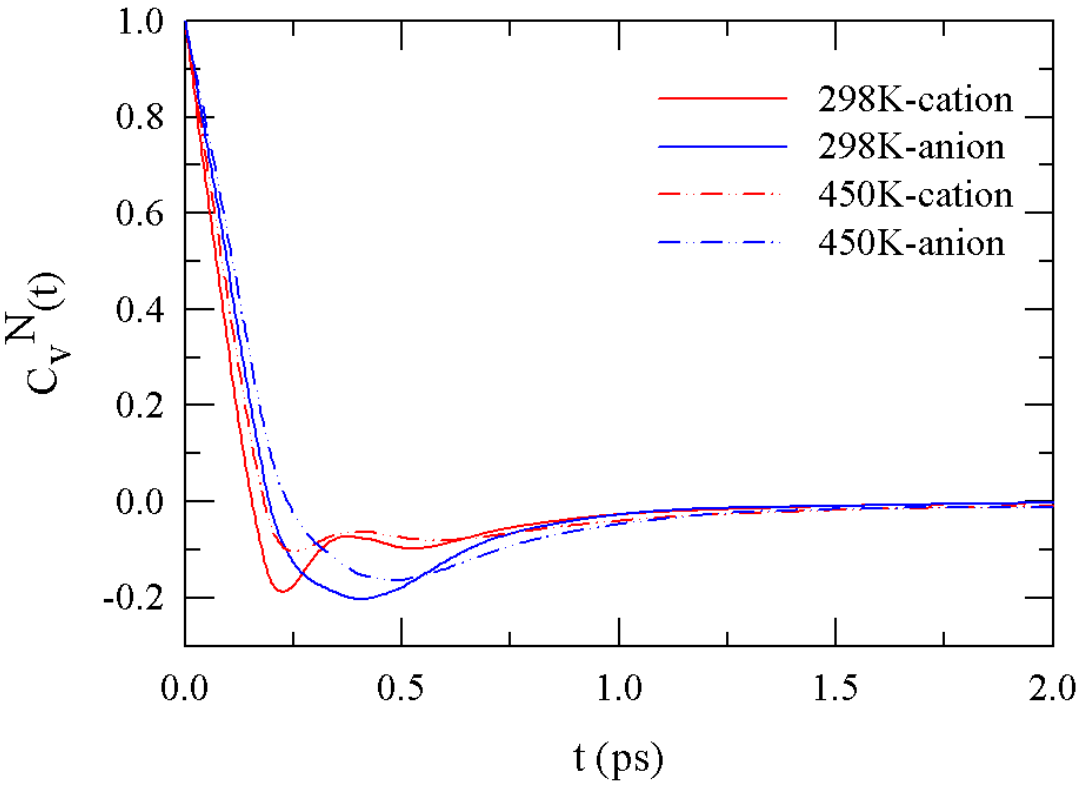

Figure. 3.7: Temperature dependent normalized velocity autocorrelation functions (VACF) for the cation and the anion. Solid lines denote the VACFs at 298 K, and the dashed-dot lines describe those at 450 K.

We next obtain centre-of-mass (translational) diffusion coefficients for $[Bmim]^+$ and $[PF_6]^-$ at 298 K and 450 K from the simulated $\left\langle \left|\Delta\vec{r}(t)\right|^2 \right\rangle$ (using Eq. 3.2) and $C_V^N(t)$ ($D = (k_B T/m)\int_0^\infty dt\, C_V^N(t)$) , and compare our results at 298 K with those from earlier simulations[26-29,31,66] and experiments [46.] Table 3.2 provides this comparison where simulation techniques and run-times are also mentioned for a better understanding of the tabulated results.

Table 3.2. Comparison of centre-of-mass diffusion coefficients at 298 K between our simulations, experiments and earlier simulations.

Authors	Ensemble type	D_{Bmim+} X 10^{-11} m^2/s	D_{PF6-} X 10^{-11} m^2/s	Model and Force Field
Huang & Wang (Ref. 26) 128 ion pairs No charge scaling	NVE followed by NPT Equilib. run = 200 ps. Production run = 100ps	1.20	1.00	All-atom model AMBER(some modifications)
Liu & Wang (Ref : 27) 128 ion pairs No charge scaling	NPT Equilib. run = 200ps Production run = 200ps	1.20	1.00	All-atom model AMBER(with some modifications)
Morrow & Maginn (Ref : 29) 300 ion pairs No charge scaling	NPT Equilib. run = 700 -1000ps Production run = 4ns	0.97±0.41	0.82±0.42	All-atom model CHARMM22
Maroncelli et. al (Ref : 58) 343 ion pairs No charge scaling	NPT (350 K) Equilib. run = 100ns Production run = 200ns	0.09	0.04	Coarse-grained 4-site model
Maroncelli et. al (Ref .66) 343 ion pairs charge scaling	NPT Equilib. run = 100ns Production run = 200ns	0.6	0.4	Coarse-grained 4-site model

Balasubramanium et. al (Ref : 28) 256 ion pairs No charge scaling	NPT followed by NVT Equilib. run = 8ns Production run = 4ns	0.158	0.085	All-atom model OPLS/AMBER
Balasubramanium et. al (Ref : 28) 256 ion pairs charge scaling	NPT followed by NVT Equilibration run = 8ns Production run = 4ns	0.67	0.47	All-atom model OPLS/AMBER
Our Simulations 128 ion pairs No charge scaling	NPT Equilib. run = 2ns Production run = 8ns	$0.71(\pm0.21)=\frac{1}{2}$ [$0.51^{a}(\pm0.26)+0.90^{b}(\pm0.17)$]	$0.45(\pm0.16)=\frac{1}{2}$ [$0.47^{a}(\pm0.12)+0.42^{b}(\pm0.20)$]	All-atom model (from Ref. 26)
Watanabe et. al (Ref : 46)	Technique used : PFG-Spin Echo NMR	0.68	0.4	

a) from MSD; b) from velocity auto-correlation function

Evidently, cation and anion diffusion coefficients from the present simulations ("Our Simulation") are in very good agreement with those from experiments [61]. Note also that *D* obtained from our simulated $\left\langle \left|\Delta\vec{r}(t)\right|^2 \right\rangle$ and $C_V^N(t)$ are in reasonable agreement with each other, providing further confidence to the present simulations. It is quite clear that both charge scaling of the ions and coarse graining of the force field affect the simulated diffusion coefficients. Interestingly, our simulated diffusion coefficients agree better with experiments than those reported in Ref. 26 although the same force field and ensemble as considered in the latter [26] have been employed in our simulations. Inadequate simulation run-time could be a possible reason behind such a difference [67].

At 450 K, we obtain D (in 10^{-11} m^2/s) for $[Bmim]^+$ as 10.75 ± 0.14 from $\left\langle |\Delta \vec{r}(t)|^2 \right\rangle$ and 11 ± 0.26 from $C_V^N(t)$ routes, the average of them being 10.87 ± 0.20. For $[PF_6]^-$ at this temperature, these values are 8.40 ± 0.20 and 10.60 ± 0.32, respectively, providing an average, 9.5 ± 0.26. These average D values are in reasonable agreement with the simulated values at 450 K reported in Ref. 28 (~15x10^{-11} m^2/s for $[Bmim]^+$ and ~10 x10^{-11} m^2/s for $[PF_6]^-$) which used a force field described in Ref. 25.

3.3.4. Viscosity

Subsequently, we simulate the shear viscosity coefficients (η) at 298 K and 450 K of [Bmim][PF_6] in order to investigate coupling between mass and momentum transports in this IL. This has been obtained from the simulated pressure autocorrelation function (PACF), $\left\langle P_{\alpha\beta}(t) P_{\alpha\beta}(0) \right\rangle$, via the Green-Kubo relation [1],

$$\eta = \frac{V}{k_B T} \int_0^\infty \left\langle P_{\alpha\beta}(t) P_{\alpha\beta}(0) \right\rangle dt, \qquad (3.4)$$

where, $\alpha, \beta = x, y, z$ and $P_{\alpha\beta}$ denotes the off-diagonal term of the pressure tensor

$$P_{\alpha\beta} = \frac{1}{V} \left(\sum_i \frac{p_{i\alpha} \, p_{i\beta}}{m_i} + \sum_i \sum_{j>i} r_{ij\alpha} f_{ij\beta} \right),$$

(3.5)

where $f_{ij\alpha}$ denotes the simulated force and m_i the mass of the i-th particle [50].

The computed viscosity coefficient (η) at 298 K from simulations using NPT ensemble has been found to be 266 ± 9.08 cP which compares well with the corresponding experimental value (261 cP). The decay of the pressure autocorrelation function at 298 K is shown in Fig. B2 (Appendix B) along with bi-exponential fits (upper panel). η from these fit parameters is found to be ~284 cP at 298 K which is close to that (266 ± 9.08 cP) obtained via numerical integration of simulated PACF using Eq. 3.4.

The computed η from bi-exponential fit to the simulated PACF is also presented as function of upper limit in the lower panel of Fig. B2 to show the required time-convergence. Note similar fast decay followed by strong fluctuations in PACF at short times as shown in the inset of Fig. B2 (upper panel) has also been observed in earlier simulation studies [58, 68,69]. At 450 K, we find η=21.67 $\pm$ 3.05 cP (NPT) and 27.14 $\pm$ 6.3 cP (NVT), the average being 24.40 $\pm$ 4.68 cP. This is also in reasonable agreement with the result (~16 cP) from non-equilibrium molecular dynamics simulations using all-atom force filed [70]. Note that the simulated η at 450 K cannot be compared directly with experiment because of the available experimental data [46] cover the temperature range, ~263 – 353 K. Decomposition temperature of alkyl imidazolium ILs is ~400 K [64,71] and this probably prohibits viscosity measurements of [Bmim][PF_6] at temperatures beyond 400 K. This caveat notwithstanding, these simulations assist in examining the heterogeneity aspect of a model ionic liquid mimicking the structure of [Bmim][PF_6] at a temperature as high as 450 K and make a comparison with that at room temperature. Moreover, simulations covering a broad temperature range assist in revealing the coupling between η and *D* via the application of hydrodynamic relation. For example, at 298 K where the simulated η matches very well with experiment, application of Stokes-Einstein relation with stick boundary condition and $\sigma_{[PF_6]^-}$ = 5.44 Å [46] produces $D_{[PF_6]^-} \approx 0.3$ x 10^{-11} m^2/s which is in fair agreement with both simulated and experimental values. At 450 K, however, similar exercise leads to $D_{[PF_6]^-} \approx 5$ x 10^{-11} m^2/s which is nearly half of the simulated diffusion coefficient for $[PF_6]^-$ at this temperature. This suggests a deviation from the conventional hydrodynamics although more data are required for a rigorous analysis of particle motion and its coupling to medium viscosity for these highly inhomogeneous liquids.

3.3.5. Temporal Heterogeneity

A further insight into the particle motion can be accessed via following the deviation of the self-part of the van Hove correlation function ($G_s(\vec{r},t)$) from the Gaussian distribution with respect to particle displacement, and a non-Gaussian

parameter, $\alpha_2(t)$ [6,66,72]. These quantities are related to temporal heterogeneity of the liquid. The time-dependent self-part of the van Hove correlation function is given as [1]

$$G_s(\vec{r},t) = \frac{1}{N}\left\langle \sum_{i=1}^{N} \delta\left(\vec{r}_i^{\,c}(t) - \vec{r}_i^{\,c}(0) - \vec{r}\right)\right\rangle, \qquad (3.6)$$

The non-Gaussian parameter is defined as follows [70]

$$\alpha_2(t) = \frac{3}{5}\frac{\left\langle \left|\Delta\vec{r}(t)\right|^4 \right\rangle}{\left\langle \left|\Delta\vec{r}(t)\right|^2 \right\rangle^2} - 1, \qquad (3.7)$$

with $\left\langle \left|\Delta\vec{r}(t)\right|^2 \right\rangle = \frac{1}{N}\left\langle \sum_{i=1}^{N} \left|\vec{r}_i^{\,c}(t) - \vec{r}_i^{\,c}(0)\right|^2 \right\rangle$. For homogeneous harmonic vibrations and in the cases of random walk, $G_s(\vec{r},t)$ is Gaussian and $\alpha_2(t) = 0$ [73]. For hot liquids, $\alpha_2(t) = 0$ for both at $t = 0$ and $t = \infty$ but $\alpha_2(t) = 0.2$ (a maximum) at intemediate times [73].

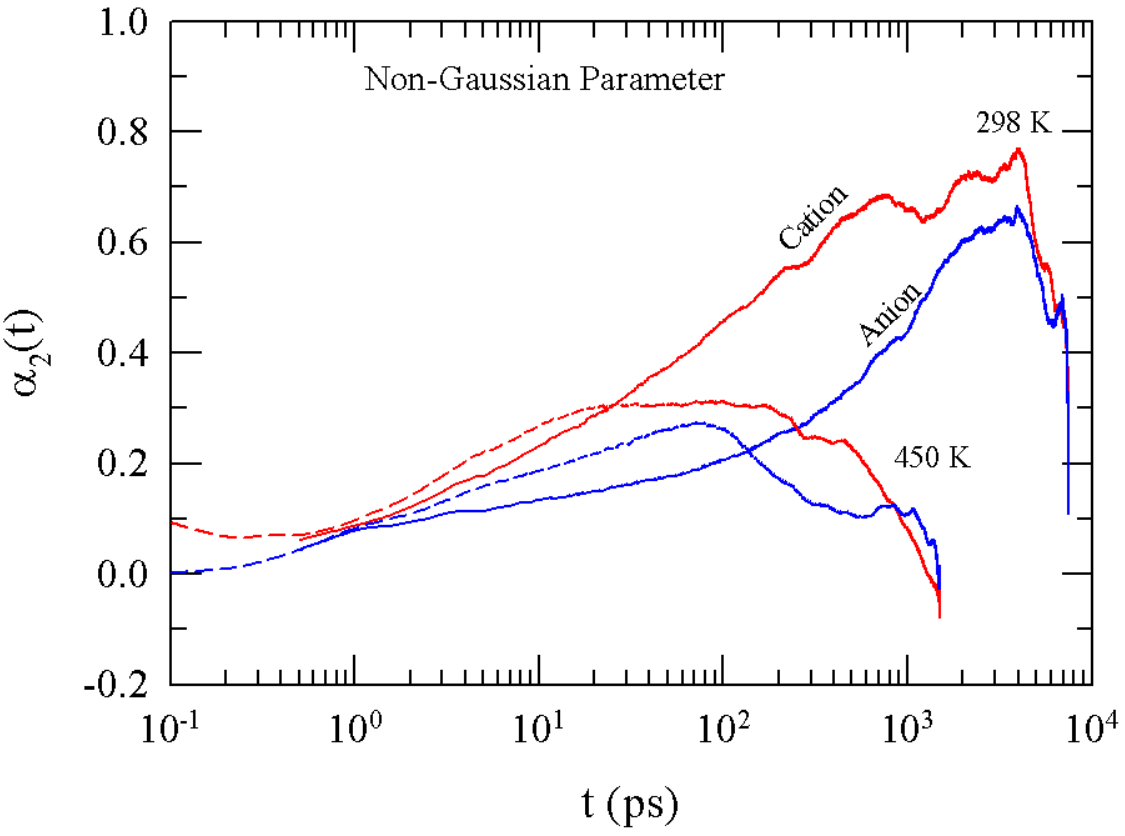

Figure. 3.8: Non-Gaussian parameter associated with cation and anion displacements at 298 K and 450 K for [Bmim][PF_6].

The simulated $\alpha_2(t)$ for both the ions at these two temperatures (298 K and 450 K) are presented in Fig. 3.8. Note $\alpha_2(t)$ for both the ions at lower temperature is not only showing larger peaks than those at the higher temperature but also the peaks are occuring at a much longer time (> 1ns). These results correlate well with earlier simulations of this IL performed using different model potentials [31,32]. In addition, qualititatively similar behaviour of $\alpha_2(t)$ has also been found in simulation studies [74] of [Emim][NO_3]. Large values of $\alpha_2(t)$ suggests strong presence of varying rates of both cationic and anionic motions, and their occurances at longer times means non-diffusive mechanism (such as particle jump) being operative even much after the onset of the diffusion timescale for this system. This is a signature of temporal heterogeneity. Interestingly, the simulated $\alpha_2(t)$ at 450 K exhibits significant temporal heterogeneity which can trigger departure from hydrodynamic relation in [Bmim][PF_6] even at a temperature ~170 K beyond its melting temperature where the liquid is expected to be spatially more homogeneous. However, we would like to mention here that temporal heterogeneity can exist even for much simpler systems [50] and thus presence of spatial heterogeneity (that is, microscopic domain formation) is not prerequisite for showing variation in motional rates.

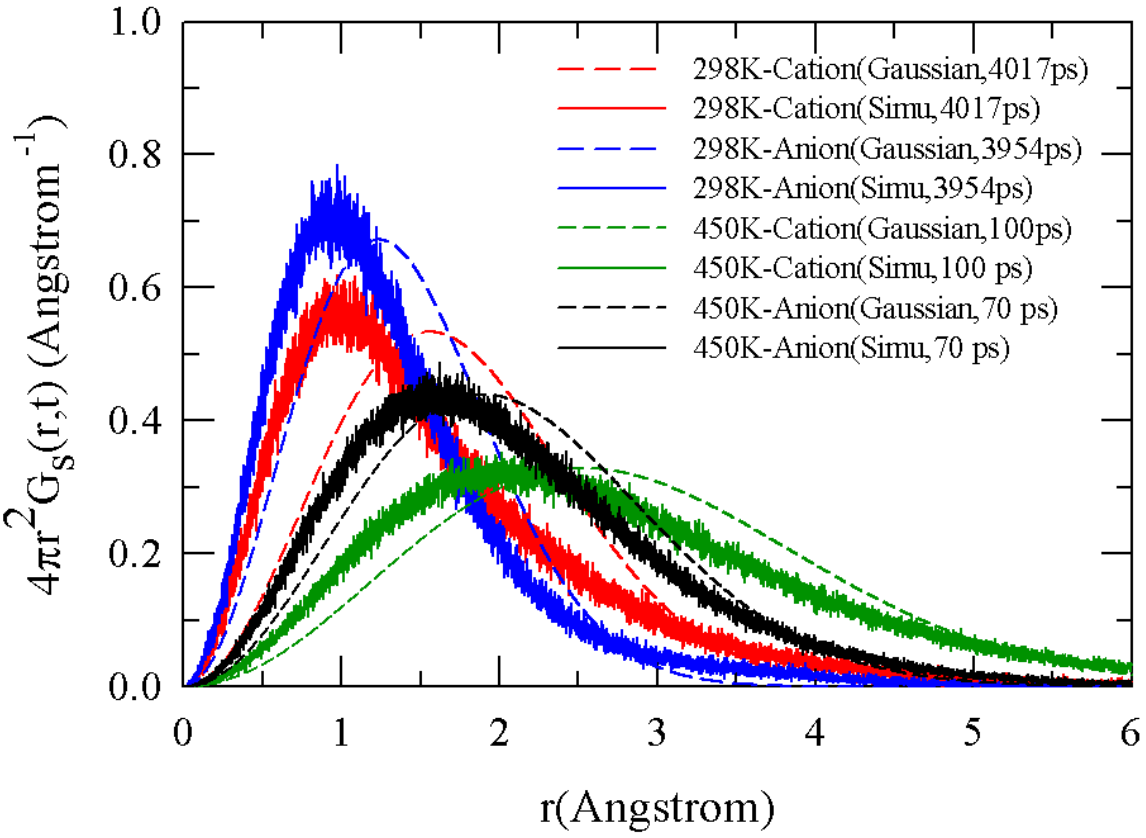

Figure. 3.9: Temperature dependence of the simulated self part of the van Hove correlation function for both the ions in [Bmim][PF_6]. Simulated functions correspond to the times at which the non-Gaussian parameters showed maxima. These times are mentioned in the accompanying legends. The dashed lines denote the calculations using Gaussian approximation at 298 K and 450 K for both the ions.

Fig. 3.9 depicts the simulated temperature dependent $G_s(\vec{r},t)$ for both the ions at times corresponding to the respective peaks. The predicted Gaussian behavior at those times from the relation, $G_s^0(r,t) = \left[3/2\pi\left\langle|\Delta\vec{r}(t)|^2\right\rangle\right]^{3/2} \exp\left(-3r^2/(2\left\langle|\Delta\vec{r}(t)|^2\right\rangle)\right)$, has also been shown in the same figure in order to reflect the extent of deviation from Gaussian behavior of the particle displacements. It is evident that $G_s(\vec{r},t)$ deviates from the Gaussian behavior at both the lower and higher temperatures and ion movements at lower temperature associate with relatively shorter amplitude displacements. Note the deviation is larger at the lower temperature, indicating increased heterogeneity at 298 K compared to that at 450 K. In addition, the cation $G_s(r,t)$ shows a longer tail suggesting

relatively large amplitude displacements are sustained for cation movements in this IL. This may be related to the difference in symmetry between $[Bmim]^+$ and $[PF_6]^-$.

3.4 Rank Dependence of Reorientational Time Correlation Function

The normalized reorientational time correlation function (RTCF) for the cationic species has been obtained as follows [1]

$$C_l(t) = \frac{\langle P_l[\vec{u}_i(t).\vec{u}_i(0)]\rangle}{\langle P_l[\vec{u}_i(0).\vec{u}_i(0)]\rangle}, \qquad (3.8)$$

where P_l denote the Legendre polynomial of rank l and $\vec{u}_i$ a unit vector parallel to the dipole axis of the cation, $[Bmim]^+$. The average reorientational correlation time ($\langle\tau_l\rangle$) is then obtained via time integration of $C_l(t)$ as follows: $\langle\tau_l\rangle = \int_0^\infty dt\, C_l(t)$. $\langle\tau_l\rangle$ is an important quantity as several experimental techniques are available to measure $\langle\tau_l\rangle$ with different l. For example, infrared absorption and dielectric relaxation measurements are associated with l =1, optical Kerr effect (OKE) and fluorescence anisotropy measurements deal with l =2. The measured $\langle\tau_l\rangle$ can then be used to reveal the rank dependence of reorientational motion of molecules or molecular species in a given liquid which subsequently assist in characterizing rotational motion of a species in a given system. If the angular diffusion of a spherical solute occurs through diffusive Brownian rotations (Debye rotation) then the ratio, $\langle\tau_1\rangle/\langle\tau_2\rangle$, approaches to 3, reflecting the validity of the $l(l+1)$ law [36,75]. Calculations of slow viscous liquid systems have revealed this ratio to be ~3 even at a temperature as low as 234 K [35] where the $l(l+1)$ law is expected to be violated. Since experimental and simulation studies indicate [Bmim][PF_6] to be heterogeneous, it is worth exploring the rank dependence of

RTCF in this IL. Fig. 3.10 depicts the simulated $C_l(t)$ at two different temperatures for both l =1 and l =2 where fit parameters and $\langle \tau_l \rangle$ are also shown for comparison.

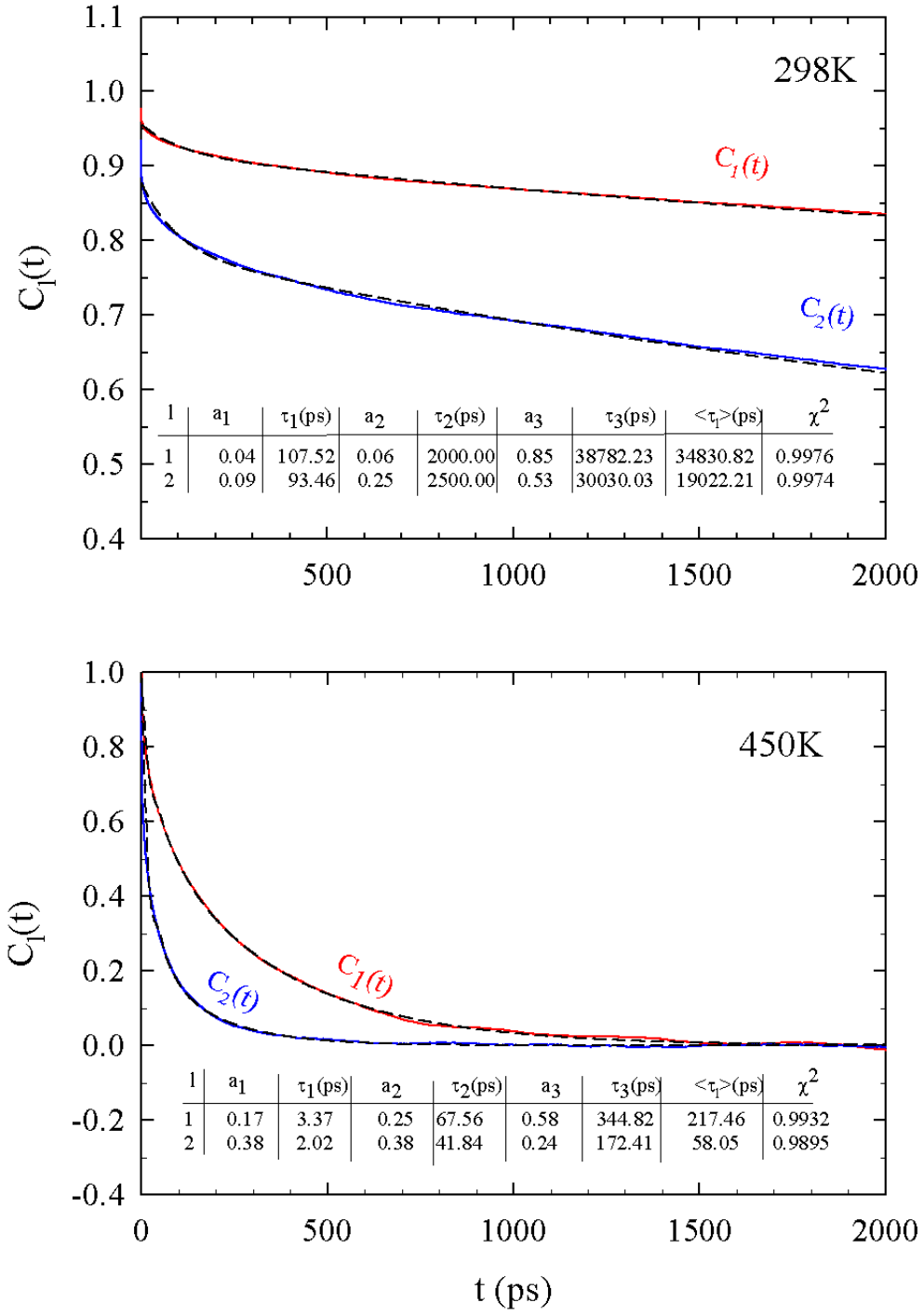

Figure. 3.10: Plot of simulated single particle reorientational correlation functions (RTCFs) of first and second ranks at 298 K (upper panel) and 450 K (lower panel) for the cation, $[Bmim]^+$. Corresponding fits (dashed lines) and fit parameters are also shown.

Note $C_l(t)$ at 298 K for both the ranks decay to only ~15-30% within the ~5 ns time-window, which suggests a presence of an extremely slow component in this RTCF. Fits to these incomplete decays produce three timescales, the faster one being ~100 ps with other slower ones in ~2-3 ns and 30-40 ns ranges. Eventhough these timescales cannot be considered as accurate because of incomplete decays, present simulations capture the qualitative trend correctly as $C_2(t)$ decays faster than $C_1(t)$. The strong multi-exponential (or non-exponential) nature of these decays is indicative of non-Markovian nature of the underlying dynamics and correlates well with the non-Debye behavior of the cation rotation reflected via Cole-Davidson or Cole-Cole description of the experimental dielectric relaxation (DR) data of this IL [60]. Note that although the time constant in 20-40 ns range does not have any counterpart in the relevant DR data, dipolar solute rotation in deep eutectic (acetamide + electrolyte) mixtures [76] and several ILs [77] has indicated presence of such a slow (or slower) timescale even at or near room temperature. In addition, the simulated incomplete $C_l(t)$ decays at 298 K leads to $\langle\tau_1\rangle/\langle\tau_2\rangle$ ~1.8 which is much lower than 3 and probably suggests break-down of the $l(l+1)$ law in presence of pronounced spatial heterogeneity [5] at this temperature. Interestingly, recent Kerr-effect spectroscopic and DR measurements [78] of ethylammonium nitrate (EAN) IL at $277 \le T(K) \le 338$ indicates this ratio between ~1.2-1.4, suggesting a break-down of the $l(l+1)$ law in microheterogeneous systems. Note $C_l(t)$ decays at 450 K (lower panel) are complete within ~2 ns, fit to tri-exponentials as those at 298 K but with much faster time constants. Here, $\langle\tau_1\rangle/\langle\tau_2\rangle$ ~ 3.75 showing a deviation from the complete validity of the $l(l+1)$ law for rotational diffusion. This correlates well with the simulated non-Gaussian parameter and deviation from the self part of the van Hove correlation function at 450 K shown in Figs. 3.8 and 3.9, respectively. We would like to mention here that time constants characterizing the $C_l(t)$ decays increase by ~5-10% modifying accordingly the $\langle\tau_1\rangle/\langle\tau_2\rangle$ value if the density is increased by ~2% by choosing a shorter cut-off distance, say, 14 Å. This result is in qualitative agreement with density dependence of solute rotation in

supercritical solvents [79] where the role of asymmetry in solute angular diffusion has also been discussed.

3.5 Conclusion

In summary, the comparison made in this chapter reveals that charge scaling and types of force fields used in simulations can affect predictions of transport quantities and their subsequent agreement to the experimental data. This correlates with results obtained in a recent simulation study [80] where a dependence of ion diffusion coefficient on both total charge of an ion and charge distribution within it has been reported. Diffusion coefficients obtained in the present simulation at 298 K agree well with those from experiments. Moreover, a good agreement has been observed between the simulated and experiments viscosity coefficients at 298 K, and between the present work and non-equilibrium simulations at 450 K. Simulated thermodynamic and structural properties also compare well with the existing simulated and/or experimental results, providing the confidence that the present approach can capture, at least semi-quantitatively, the structure and dynamics of the real ionic liquid. Reorientational relaxation studies reveal that the collective single particle orientational motions at 298 K are too slow to be completed within ~5 ns, and suggest strong departure from the Brownian diffusion for rotational motion. Rise in temperature reduces the heterogeneity but not to the extent which can ensure complete validity of the $l(l+1)$ law. These simulated results correlate well with recent experiments with EAN but do not provide accurate understanding of orientational relaxation in general. Further simulation studies at a few more temperatures involving this IL and others for which experimental results exist are therefore necessary for developing a better understanding of rotational relaxations in these ionic systems. This is indeed a challenging task given the difficulty in correctly representing ionic liquid molecules in bulk through an accurate polarizable force field.[81-85]

References :

1. J. P. Hansen and I. R. McDonald, Theory of Simple Liquids, 3rd ed. Academic, San Diego. (2006)
2. R. D. Rogers and K. R. Seddon, Ionic Liquids: Industrial Application for Green Chemistry (2002). ACS Symposium Series 818; American Chemical society, Washington DC.
3. P. Wasserscheid and T.Welton, Ionic Liquids in Synthesis. Wiley-VCH, New York. (2003)
4. M. N. Kobrak and N. Sandalow, Molten Salts XIV, Mantz, A., Trulove, P. (ed), Electrochemical Society, New Jersey. (2006)
5. A. Triolo, O. Russina, B. Fazio, R. Triolo, and E. D. Cola, Chem. Phys. Lett. **467**,362(2008).
6. Y. Wang and G. A. Voth, J. Am. Chem. Soc. **127**,12192(2005).
7. A. Samanta, J. Phys. Chem. Lett. **1**,1557(2010)
8. A. Samanta, J. Phys. Chem. B **110** ,13704 (2006).
9. S. Arzhantsev, H. Jin, G. A. Baker, and M. Maroncelli, J. Phys. Chem. B **111**,4978 (2007).
10. X.-X. Zhang, M. Liang, N. P. Ernsting, and M. Maroncelli, J. Phys. Chem. B **117**, 4291(2013).
11. D. A. Turton, J. Hunger, A. Stoppa, G. Hefter, A. Thoman, M. Walther, R. Buchner, and K. Wynne, J. Am. Chem. Soc. **131**, 11140 (2009).
12. M.-M. Huang, S. Bulut, I. Crossing, and H. Weingertner, J. Chem. Phys. **133**,101101(2010).
13. M. Muramatsu, Y. Nagasawa, and H. Miyasaka, J. Phys. Chem. A **115**, 3886 (2011).
14. H. K. Kashyap and R. Biswas, J. Phys. Chem. B **114** ,16811 (2010).
15. H. K. Kashyap and R. Biswas, J. Phys. Chem. B **114**,254 (2010).
16. S. Daschakraborty and R. Biswas, J. Chem. Phys. **137**,114501 (2012).
17. S. Daschakraborty and R. Biswas, Chem. Phys. Lett. **510**, 210 (2011).
18. S. Daschakraborty and R. Biswas, J. Phys. Chem. B **115**,4011(2011) .
19. A. Triolo, O. Russina, B. Fazio, G. B. Appetecchi, M. Carewska, and S. Passerini, J. Chem. Phys. **130**,164521 (2009).

20. C. S. Santos, N. S. Murthy, G. A. Baker, and Jr. E. W. Castner J. Chem. Phys. **134**,121101(2011).
21. H. K. Kashyap, C. S. Santos, H. V. R. Annapureddy, N. S. Murthy, C. J. Margulis, and Jr. E. W. Castner Faraday Discuss. **154**,133 (2012).
22. P. K. Mandal, M. Sarkar, and A. Samanta, J. Phys. Chem. A **108**, 9048 (2004).
23. D. K. Sasmal, A. K. Mandal, T. Mondal, and K. Bhattacharyya, J. Phys. Chem. B **115**,7781 (2011).
24. J. K. Shah , J. F. Brennecke, and E. J. Maginn, Green Chem. **4**,112 (2001).
25. J. N. C. Lopes, J. Deschamps, and A. A. H. Padua, **108** ,2038 (2004).
26. Z. Liu, S. Huang, W. Wang, J. Phys. Chem. B **108 ,**12978 (2004) .
27. Z. Liu, X. Wu, and W. Wang, Phys. Chem. Chem. Phys. **8**,1096 (2006).
28. B. L. Bhargava, S. Balasubramanian, J. Chem. Phys. **127**,114510 (2007) .
29. T. I. Morrow , E. J. Maginn, J. Phys. Chem. B **106**,12807 (2002).
30. C. J. Margulis, H. A. Stern, B. J. Berne, J. Phys. Chem. B **106**,12017 (2002).
31. S. S. Sarangi, W. Zhao, F. Muller-Plathe, S. Balasubramanian, ChemPhysChem **11**,2001 (2010).
32. Z. Hu, C. J. Margulis, Proc. Natl. Acad. Sci. USA **103**, 831 (2006).
33. J. G. Powles, J. Chem. Phys. **21**, 633 (1953).
34. P. Madden, D. Kivelson, Adv. Chem. Phys. **56**, 467(1984).
35. R. Biswas, B. Bagchi, J. Phys. Chem. **100** ,1238 (1996).
36. B. Bagchi, Molecular Relaxation in Liquids, Oxford, NY. (2012).
37. W. Smith, T. R. Forester, (eds.) in DL_POLY_2.2; CCLRC Daresbury Laboratory: Daresbury, UK. (2010).
38. A. P. Lyubartsev and A. Laaksonen, Comput. Phys. Commun. **128** ,565 (2000).
39. W. D. Cornell, P. Cieplak, C. I Bayly, I. R. Gould, K. M. Merz, D. M. Ferguson, D. C. Spellmeyer, T. Fox, J. W. Caldwell, and P. A. Kollman, J. Am. Chem. Soc. **117**, 5179 (1995).
40. M. P. Allen and D. J. Tildesley, Computer Simulations of Liquids, Oxford, NY. (1987).
41. P. V. Kumar and M. Maroncelli, J. Chem. Phys. **103**, 3038 (1995).
42. G. J. Martyna, M. E. Tuckerman, D. J. Tobias, and M. Klein, Mol. Phys. **87**,1117 (1996).
43. G. J. Martyna, M. Klein, and M. E. Tuckerman, J. Chem. Phys. **97**,2635 (1992).

44. S. Nose, J. Chem. Phys. **81** , 511 (1984).
45. W. G. Hoover, Phys. Rev. A **31** ,1695 (1985).
46. H. Tokuda, K. Hayamizu, K. Ishii, A. B. H. Susan, and M. Watanabe, J.Phys. Chem. B **108** , 16593 (2004).
47. Z. Y. Gu and J. F. Brennecke, J. Chem. Engg. Data **47** ,339 (2002).
48. T. L. Amyes, S. T. Diver, J. P. Richard, F. M. Rivas, and K. Toth, J. Am. Chem. Soc. **126** , 4366 (2004).
49. A. M. Fernandes, M. A. A. Rocha, M. G. Freire, I. M. Marrucho, J. A. P. Coutinho, and L. M. N. B. F. Santos, J. Phys. Chem. B **115** , 4033 (2011).
50. S. Daschakraborty and R. Biswas, J. Chem. Sci. **124 ,** 763 (2012).
51. K. Fumino, A. Wulf, and R. Ludwig, Angew. Chem. Int. Ed. **47**, 3830 (2008).
52. S. Men, K. R. J. Lovelock, and P. Licence, Phys. Chem. Chem. Phys. **13**,15244 (2011)
53. J. Thar, M. Brehm, A. P. Seitsonen, and B. Kirchner, J. Phys. Chem. B. **113** , 15129 (2009).
54. M. Brehm, H. Weber, A. S. Pensado, A. Stark, and B. Kirchner, Phys. Chem. Chem. Phys. **14** , 5030 (2012) .
55. T. Pal and R. Biswas, Chem. Phys. Lett. **517** ,180 (2011).
56. F. Faupel, W. Frank, M.-P. Macht, H. Mehrer, V. Naundorf, K. Ratzke, and H. R. Schober, et al, Rev. Mod. Phys. **75** , 237 (2003).
57. J. Habasaki, K. L. Ngai, J. Non-Cryst. Solids **352** , 5170 (2006).
58. D. Roy, N. Patel, S. Conte, and M. Maroncelli, J. Phys. Chem. B **114**,8410 (2010).
59. M. G. Del Popolo and G. A. Voth, J. Phys. Chem. B **108**, 1744 (2004) .
60. J. Hunger, A. Stoppa, S. Schrodle, G. Hefter, and R.Buchner, Chem. Phys. Chem. **10 ,** 723 (2009).
61. H. Tokuda, K. Hayamizu, K. Ishii, Md. A. B. H. Susan, and M. Watanabe, J.Phys. Chem. B **109** , 6103 (2005).
62. D. V. Matyushov, J. Chem. Phys. **122** , 044502 (2005).
63. N. Kometani, S. Arzhantsev, and M. Maroncelli, J. Phys. Chem. A **110** , 3405 (2006).
64. C. P. Fredlake, J. M. Crosthwaite, D. G. Hert, S. N. V. K. Aki, and J. F. Brennecke, J. Chem. Eng. Data **49** , 954 (2004) .

65. J. G. Huddleston, A. E. Visser, W. M. Reichert, H. D. Willauer, G. A. Broker, and R. D. Rogers, Green Chem. **3** , 156 (2001).
66. D. Roy, and M. Maroncelli, J. Phys. Chem. B **114**, 12629 (2010).
67. S. Gabl, C. Schroder, and O. Steinhauser, J. Chem. Phys. **137**, 094501 (2012).
68. T. Koddermann, R. Ludwig, and D. Paschek, ChemPhysChem **9** , 1851(2008).
69. B. L. Bhargava and S. Balasubramanian, J. Chem. Phys. **123**,144505 (2005).
70. J. Picalek and J. Kolafa, Mol. Simulation **35** , 685 (2009).
71. W. H. Awad, J. W. Gilman, M. Nyden, R. H. Harris, T. E. Sutto, J. Callahan, P. C. Truelove, H. C. Delong, and D. M. Fox, Thermochim. Acta, **409** , 3 (2004).
72. A. Rahman, Phys. Rev. **136** , 405 (1964).
73. F. Faupel, W. Frank, M.-P. Macht, H. Mehrer, V. Naundorf, K. Ratzke, and H. R. Schober, et. al. Rev. Mod. Phys. **75**, 237 (2003).
74. J. Habasaki, K. Ngai, J. Chem. Phys. **129** ,194501 (2008).
75. B. Bagchi, Annu. Rev. Phys. Chem. **40 ,** 115 (1989).
76. B. Guchhait, S. Daschakraborty, R. Biswas, J. Chem. Phys. **136** , 174503 (2012).
77. A. M. Funston, T. A. Fadeeva, J. F. Wishart, Jr. E. W. Castner, J. Phys. Chem. B. **111** , 4963 (2007).
78. D. A. Turton, T. Sonnleitner, A. Ortner, M. Walther, G. Hefter, R. Buchner, and K. Wynne, Faraday Discuss. **154** , 145 (2012).
79. N. Patel, R. Biswas, and M. Maroncelli, J. Phys. Chem. B **106** , 7096 (2002).
80. Y. Zhang and E. J. Maginn, J. Phys. Chem. B. **116** , 10036 (2012).
81. F. Dommert, K. Wendler, R. Berger, L. Delle Site, and C. Holm, ChemPhysChem **13**, 1625 (2012).
82. J. Schmidt, C. Krekeler, F. Dommert, Y. Zhao, R. Berger, L. Delle Site, and C. Holm, J. Phys. Chem. B. **114** , 6150 (2010) .
83. K. Wendler, S. Zahn, F. Dommert, R. Berger, C. Holm, B. Kirchner, L. Delle Site, J. Chem. Theory Comput. **7** , 3040 (2011).
84. K. Wendler, F. Dommert, Y. Zhao, R. Berger, C. Holm, L. Delle Site, Faraday Discuss. **154**, 111 (2012).
85. F. Dommert, J. Schmidt, C. Krekeler, Y. Y. Zhao, R. Berger, L. Delle Site, C. Holm, J. Mol. Liq. **152** , 2 (2010).

Chapter 4

Exploring Onsager-Glarum Relation in an Imidazolium Ionic Liquid: Insights from All-Atom Molecular Dynamics Simulations

4.1 Introduction

Orientational relaxation in liquids is an important dynamical event as it provides critical information on dynamical coupling between the rotating species and the medium. Various spectroscopic experiments measure orientational relaxation although each of the available experimental techniques does not probe the same component of the dynamical coupling. For example, rank dependence is a well-known characteristic of dipolar reorientation, and rank dependent reorientation time correlation function (RTCF) is what is relevant for studying orientational relaxation of dipolar liquids [1-5] and dipolar ILs.[6-12] The rank dependent relaxation time from RTCF can be connected to measured relaxation times via macro-micro relations[13,14] and can be related to collective single particle orientation via Stokes-Einstein-Debye (SED) Equation.[15-24] In fact, it is crucial to understand the rank dependence, as different experiments probe reorientation dynamics of different ranks ℓ.[25,26] For example, $\ell = 1$ is related to dielectric relaxation (DR) and infrared (IR) absorption measurements, while nuclear magnetic relaxation (NMR), depolarized light scattering (DLS), optical Kerr effect (OKE), and fluorescence anisotropy measurements associate with $\ell = 2$.

The DR measures the dynamical timescales originating from the rotational motion of the molecules in the collective ($k\sigma \to 0$) limit of solvent polarization modes. Onsager-Glarum (OG) relation provides a bridge between the timescales from the collective

response of the system and single particle rotation. The single particle Debye reorientation time of a rotating dipolar particle described by the Legendre polynomial of rank ℓ, $\tau_{\mathrm{rot}}^{\ell}$, can be connected to the SED relation as follows [16,17]

$$\tau_{rot}^{\ell} = \frac{6V_{eff}\eta}{\ell(\ell+1)k_B T} \quad , \tag{4.1}$$

where $V_{eff} = CfV$. Here V_{eff} is the effective hydrodynamic volume of the rotating dipolar species and is connected to V via C and f which are respectively the coupling parameter and shape factor. The shape factor is constant for a specific dipolar species under study and regulates the coupling with the medium. Rotations faster than the hydrodynamic predictions after considering the shape and coupling aspects are sometimes explained in terms of frictionless moves or angular jumps.[1,27-29] Faster dipolar solute rotations measured recently via dynamic fluorescence anisotropy experiments for (amide + electrolyte) deep eutectics much above glass transition temperature have been explained in terms of solute-medium decoupling induced by temporal heterogeneity of the medium.[30-33] Therefore, study of rank dependent RTCF is important to understand the effects of medium heterogeneity on orientational relaxation as well.

Debye relaxation time (τ_{D}) obtained from DR measurements is connected to $\tau_{\mathrm{rot}}^{\ell}$ via continuum theory as follows[34,35]

$$\tau_{rot}^{\ell} = \frac{n^2+2}{\varepsilon_0+2}\tau_D, \tag{4.2}$$

where n is the refractive index, and ε_0 the static dielectric constant of the medium. This expression is valid for weakly polar fluids. Subsequently, Glarum [36] modified this expression based on Onsager's [37] model of static dielectric constant,

$$\tau_{rot}^{\ell} = \frac{2\varepsilon_0+\varepsilon_\infty}{3\varepsilon_0}\tau_D, \tag{4.3}$$

which is valid for moderately polar fluids. This is known as the Onsager-Glarum (OG) relation. Here ε_∞ is the infinite-frequency dielectric constant. This is a limiting case of the Powles equation[38]

$$\tau_{rot}^{\ell} = \frac{2\varepsilon_0 + \varepsilon_\infty}{3\varepsilon_0}\left(\frac{\tau_D}{g}\right), \tag{4.4}$$

where g is the well-known Kirkwood's g factor.[39] This denotes a coupling factor which takes care of the local dipole-dipole correlations , and with $g = 1$ provides the OG relation. Kirkwood's g factor is related to an integration over the anisotropic part of the radial distribution function of the dipolar liquid molecules. Madden and Kivelson [40] showed that neither the Debye form nor the OG relation provides a correct description at large ε_0, and further modified the expression as follows,

$$\tau_{rot}^{\ell} = \frac{\beta\mu^2\rho_0}{3\varepsilon_0(\varepsilon_0 + 1)} g^{'}\tau_D \tag{4.5}$$

where $\beta = (k_B T)^{-1}$ and $g^{'}$ is the dynamic coupling parameter. k_B is the Boltzmann constant and T the temperature, μ the liquid dipole moment and ρ_0 the liquid density. Note that all these descriptions were based on continuum model picture of liquids and hence the molecular aspect of liquids was completely neglected. The first molecular level approach was formulated by Chandra and Bagchi which provided a microscopic expression that connected these two timescales for liquids that cover a large polarity range.[14, 34 , 41-43.]

Although macro-micro relation connecting the single particle rotation and Debye relaxation times has been derived and tested for liquids spanning large polarity range, no such relations have been formulated for systems that contain interactions longer ranged than dipole-dipole interaction. Even validity of the above relations has not been thoroughly examined for systems that are comprised of both dipole-dipole and ion-ion, and their cross interaction components. Ionic liquids are examples of liquid systems which possesses longer-ranged interactions in addition to dipole-dipole interaction. Interestingly, a recent simulation study has compared single-particle and collective motion and found that the Madden-Kivelson relation is fulfilled over a 100 ns simulation.[44] However, the validity of OG relation has not been explored. In this chapter attempts have been made to check the validity of OG relation in ionic liquids that possess at least one ion with permanent dipole moment.

We have performed simulations for a series of temperature, chosen to explore the role played by the longer-ranged interactions in connecting the two relaxation time constants. Subsequently, Sec 4.2 deals with the force field parameters used with a brief description of simulation details . Simulation results are provided in Sec 4.3 where the temperature dependence of rank-dependent orientational relaxation times are explored and discussed. Temperature dependent viscosity coefficients have also been simulated in order to investigate the coupling between the medium and relaxation rate. Kirkwood-Froehlich equation has been used to determine the g factor. Sec. 4.4 then provides a summary of the results presented in this chapter.

4.2 Methodology and Simulation Details

We performed classical molecular dynamics simulations using DL_POLY 2.2 [45] and MDynamix [46] packages and AMBER type force field [47,48] with the total potential energy having the following functional form:

$$V_{tot} = \sum_{bonds} k_b (r - r_0)^2 + \sum_{angles} k_\theta (\theta - \theta_0)^2 + \sum_{dihedrals} k_\chi [1 + \cos(n\chi - \delta)]$$

$$+ \sum_{i=1}^{N-1} \sum_{j>i}^{N} \left\{ \varepsilon_{ij} \left[\left(\frac{r_{min,ij}}{r_{ij}} \right)^{12} - \left(\frac{r_{min,ij}}{r_{ij}} \right)^{6} \right] + \frac{q_i q_j}{r_{ij}} \right\}. \qquad (4.6)$$

A fully flexible all-atom description was considered for both cations and anions with no charge scaling for a series of six different temperatures at 298, 350, 375, 400, 425 and 450 K. Since a detailed description of the methodology is given in the previous chapter, we provide here only a brief description. All the force-field parameters and Lennard-Jones (LJ) parameters for same atoms were taken from Ref. 47. The interactions between unlike LJ sites of two molecules were determined by the Lorentz-Berthelot combining rules. The simulated system consists of a cubic box of 128 ion pairs (comprising 4096 atoms) with periodic boundary condition employed. Long-range interactions were treated via Ewald summation technique. [49] The entire simulation was carried out in an isothermal isobaric ensemble (NPT) , with Nose-Hoover thermostat and barostat [50-53] having coupling constants of 500 and 2000 fs, respectively. The cut-off radius was set to 16 Å. Simulated IL structures and densities were compared against

the available data from literature. The box-lengths attained were 35.50 , 35.55 , 35.81 , 35.90 , 36.06 , 36.72 Å at 298, 350, 375, 400, 425 and 450 K, respectively. The configurations of the system were saved with an interval of 500 fs. Equilibration was initially done at 450 K and then brought down to 298 K via a step-down process with a step of 50 K, and subsequent equilibration at each of the steps for a period of 2 ns. The production run saved for 16 ns for all sets of temperature.

4.3 Results and Discussion

4.3.1 Reorientation Time Correlation Function

The single particle orientational motion of $[Bmim]^+$ molecules has been analyzed by calculating the normalized RTCF,[49]

$$C_\ell(t) = \frac{\langle P_\ell[\vec{u}_i(t).\vec{u}_i(0)]\rangle}{\langle P_\ell[\vec{u}_i(0).\vec{u}_i(0)]\rangle} \tag{4.7}$$

where P_ℓ denotes the Legendre polynomial of rank ℓ and $\vec{u}_i$ a unit vector parallel to the dipole axis of the cation, $[Bmim]^+$. The average reorientational correlation time, $\langle \tau^\ell \rangle$, is then obtained via time integration of $C_\ell(t)$ as follows: $\langle \tau^\ell \rangle = \int_0^\infty dt\, C_\ell(t)$. The Debye model predicts, $\frac{\langle \tau^{\ell=1} \rangle}{\langle \tau^{\ell=2} \rangle} = 3$. Any deviation from this value suggests non-Debye orientational moves, and long angular jumps may be involved in causing the deviations from Debye rotation. This behaviour reflects of a change in the mechanism of reorientation from consistently small random steps (Brownian rotation) to well-separated and sudden changes of orientation with relatively larger amplitude. Fig. 4.1. depicts the temperature dependence of simulated relaxation of $C_\ell(t)$ for $[Bmim]^+$. Subsequently, the simulated relaxations have been fitted to normalized tri -exponential functions of time, $C_\ell^{fit}(t) = \sum_{i=1}^{n} a_i \exp(-t/\tau_i)$ with $\sum_{i=1}^{n} a_i = 1$ and $a_i \geq 0$, to determine the amplitudes a_i and time constants τ_i. All the fit parameters for the simulated

RTCFs are summarized in Table 4.1. Average times obtained from the fits, $\left\langle \tau^{\ell} \right\rangle = \int_0^{\infty} C_{\ell}^{\,fit}(t)dt = \sum_i a_i \tau_i$, are also tabulated here. Surprisingly, the ratio of simulated rotational correlation times, $\frac{\left\langle \tau^{\ell=1} \right\rangle}{\left\langle \tau^{\ell=2} \right\rangle}$ is found to be ~3, suggesting the near validity of Debye rotations in these ILs at all the temperatures considered. It should, however, be noted here that this ratio depends on the time-interval employed for saving the simulation trajectories with effects from the size of the time-interval being the strongest at the lowest temperature. Therefore, larger simulations employing shorter time-interval are required to fully explore orientational relaxation in ILs, particularly at lower temperatures.

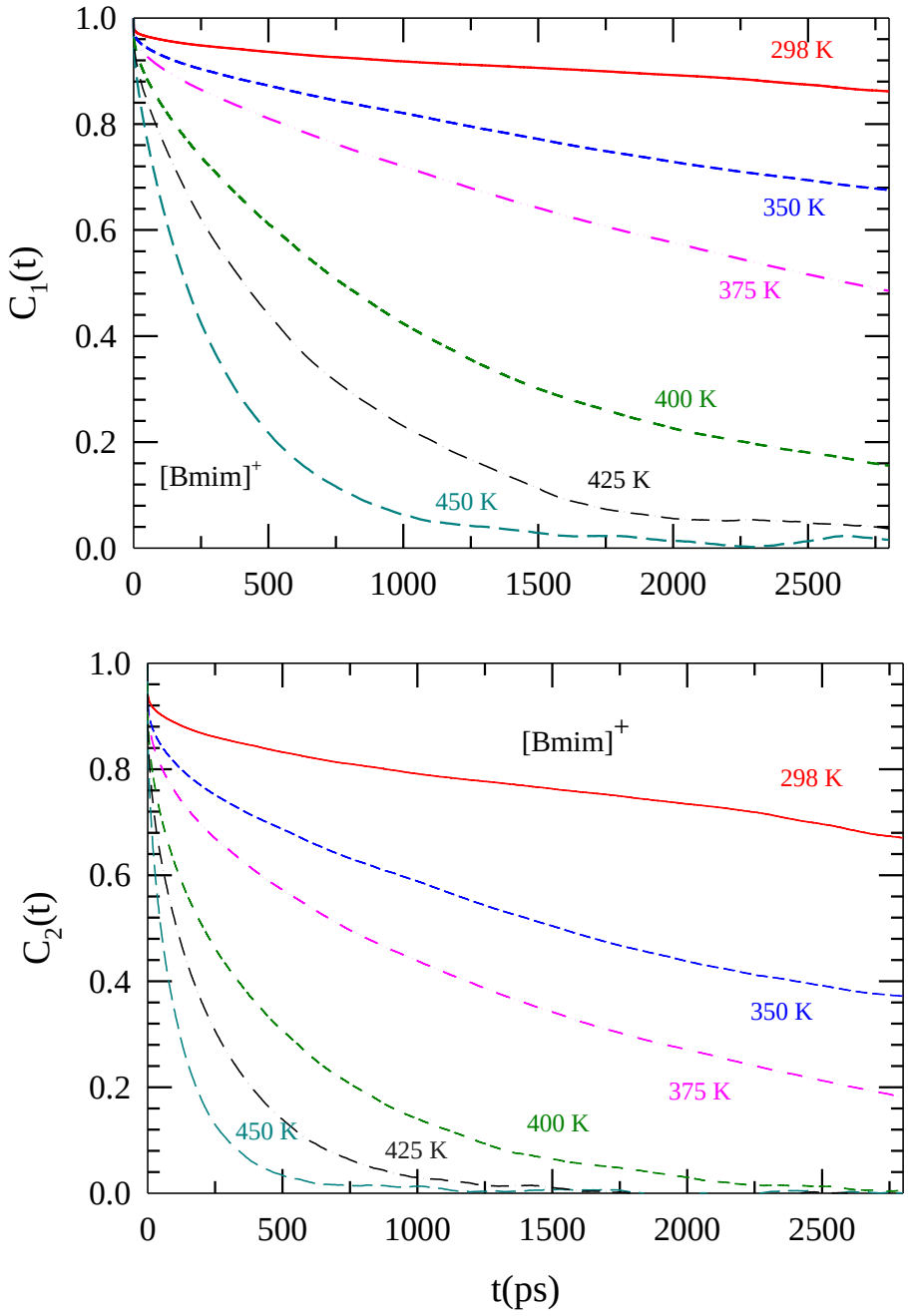

Figure. 4.1: Temperature dependent single-particle rotational time correlation functions of the cation for rank $\ell = 1$ (upper panel), and $\ell = 2$ (lower panel). Curves are color-coded and labelled.

Table 4.1. Tri-exponential fit parameters for the simulated rank dependent RTCF decays in [Bmim][PF_6] at six different temperatures.

Temp (K)	Rank	a_1	$\tau_1(ps)$	a_2	$\tau_2(ps)$	a_3	$\tau_3(ps)$	$\langle\tau\rangle(ps)$	χ^2	$\frac{\langle\tau^{\ell=1}\rangle}{\langle\tau^{\ell=2}\rangle}$
298	$\ell=1$	0.03	1.09	0.02	161.3	0.95	30220.6	28712.8	0.994	2.87
	$\ell=2$	0.08	1.07	0.06	158.7	0.86	11626.2	10008.0	0.995	
350	$\ell=1$	0.06	17.20	0.10	1250.0	0.84	11801.1	10038.9	0.999	2.77
	$\ell=2$	0.15	9.87	0.14	555.56	0.71	5000.0	3629.3	0.998	
375	$\ell=1$	0.06	8.10	0.05	322.58	0.89	5000.0	4466.6	0.999	3.08
	$\ell=2$	0.14	3.56	0.14	196.08	0.71	2000.0	1447.9	0.999	
400	$\ell=1$	0.05	1.71	0.06	51.84	0.89	1419.9	1266.9	0.999	2.90
	$\ell=2$	0.13	1.14	0.13	31.64	0.74	583.77	436.3	0.999	
425	$\ell=1$	0.08	5.14	0.10	200.0	0.82	777.65	658.1	0.999	3.02
	$\ell=2$	0.17	1.68	0.16	49.5	0.67	312.5	217.6	0.999	
450	$\ell=1$	0.06	1.50	0.05	16.2	0.89	357.2	318.8	0.999	2.98
	$\ell=2$	0.12	1.00	0.20	15.33	0.68	152.33	106.8	0.998	

We have obtained nearly complete decays of the RTCF at 400 , 425 and 450 K for both the ranks as illustrated in Fig. 4.2, at other temperatures ~ 10-30 % of the full decay is complete within the 4ns time window. Note these decays are characterised by an initial sub-picosecond component, followed by a second time constant of ~100 ps, this has been marked as one of the DR time scales at ~330 K.[18] Similar observations made by the solvation studies[54] in 1,3-dimethylimidazolium chloride using a dipolar probe at 425 K. Finally, the slowest ones fall the range of hundreds to nanoseconds order. However, this ~30-10 ns has been manifested in our previous study[9] as well as in relaxation timescales measured for (acetamide+electrolyte) deep eutectics[30-32,55] and in different kinds of ILs [56] at 298 K , but not reflected in the relevant DR data. [18] Simulated RTCF decays shown in Fig. 4.1 suggests presence of such a slow timescale.

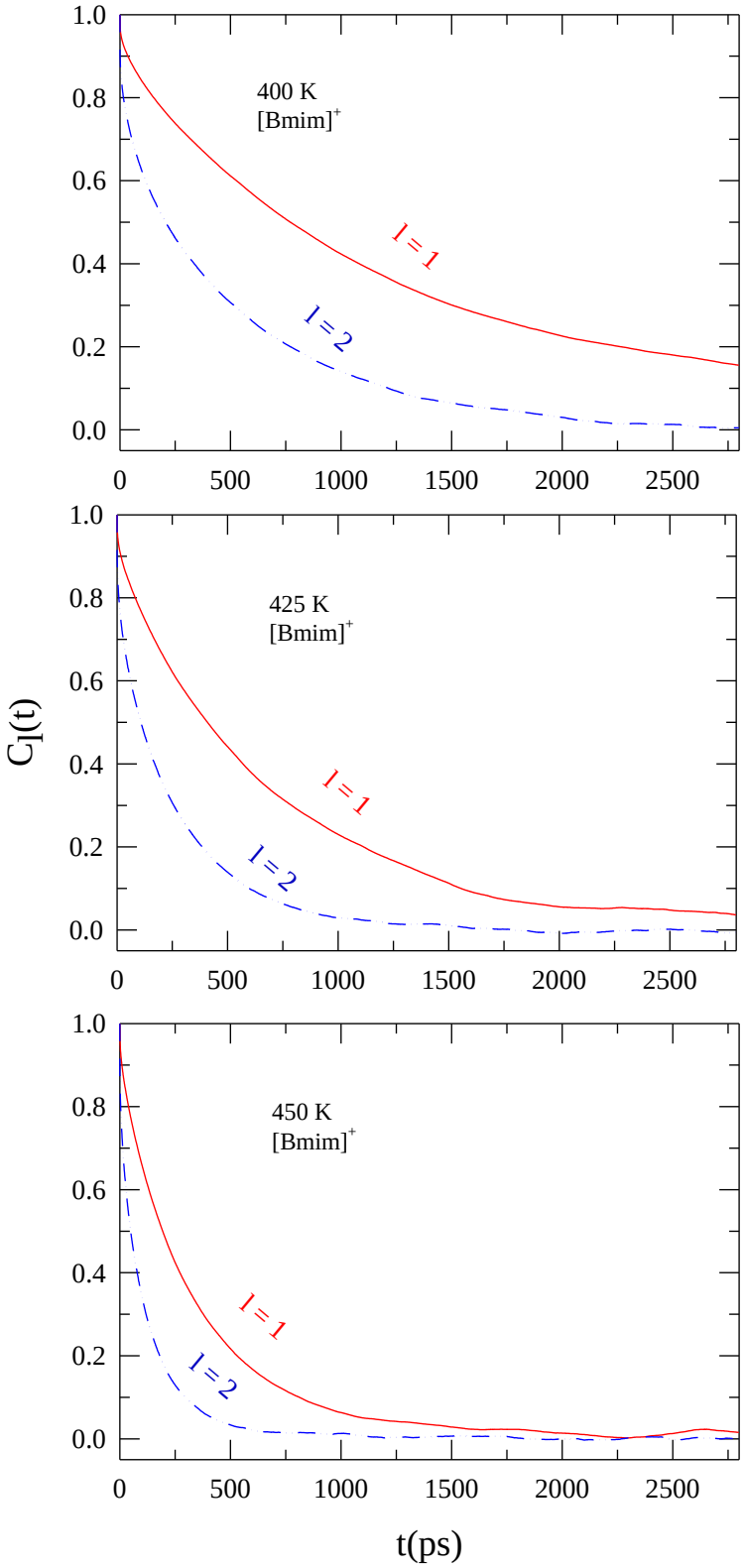

Figure. 4.2: Rank dependence of RTCF at three different temperatures.

When the inverse of the simulated rank-dependent relaxation times are plotted as a function of inverse-temperature (T^{-1}), an Arrhenius type of dependence emerges. This is show in Fig. 4.3. However, the observed linear decrease of relaxation times on T^{-1} does not necessarily suggest dipolar orientation in a homogeneous medium.

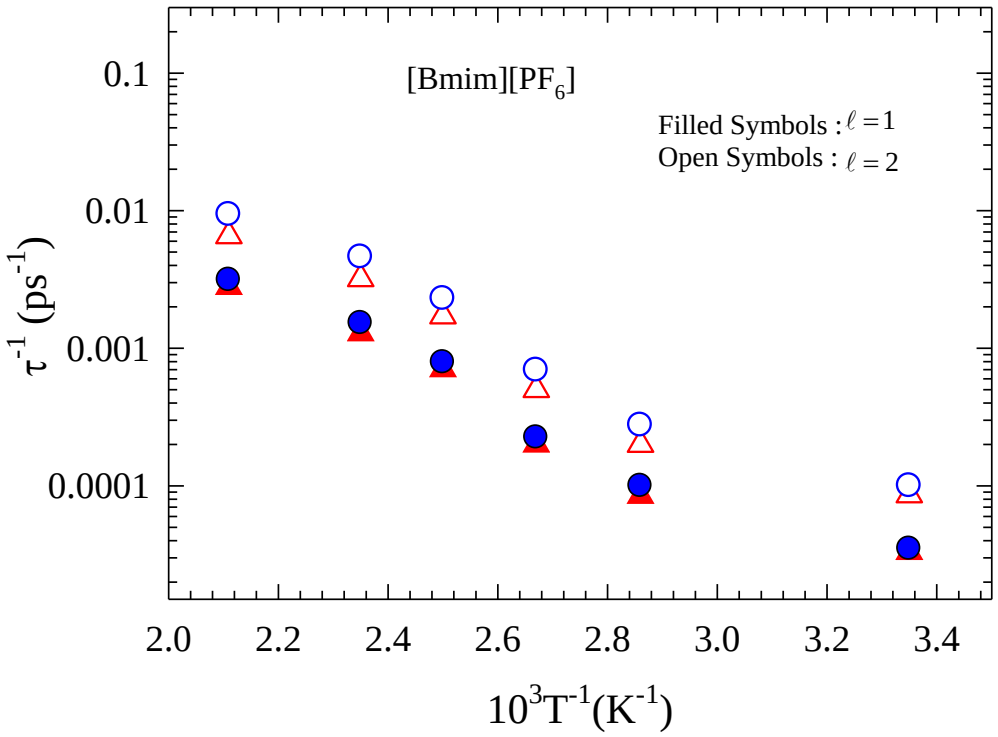

Figure. 4.3: Temperature dependence of the simulated rank-dependent orientational relaxation times. Triangles denote the slowest time constant τ_3 obtained from fits to the RTCFs, circles represent the average reorientational relaxation times $\langle\tau\rangle$.

4.3.2 Viscosity Coefficient

The shear viscosity η has been calculated from the equilibrium fluctuations of the pressure tensor $P_{\alpha\beta}$, by the well – known Green-Kubo correlation function [25,49]

$$\eta = \frac{V}{k_B T}\int_0^\infty \left\langle P_{\alpha\beta}(t)\, P_{\alpha\beta}(0)\right\rangle dt \qquad (4.8)$$

where $\langle P_{\alpha\beta}(t)P_{\alpha\beta}(0)\rangle$ is the pressure auto correlation function (PACF) and $\alpha\beta = x,y,z$ axis

$$P_{\alpha\beta} = \frac{1}{V}\left(\sum_i \frac{p_{i\alpha}\, p_{i\beta}}{m_i} + \sum_i \sum_{j>i} r_{ij\alpha} f_{ij\beta}\right) \qquad (4.9)$$

where $f_{ij\alpha}$ denotes the simulated force and m_i the mass and $p_{i\alpha}$ momentum of the *i*-th particle. The off – diagonal elements of the pressure tensor have been taken into account. As expected, the long time decay of the simulated pressure-autocorrelation function (PACF) is marked with large fluctuations. We have obtained η via time-integration of the bi-exponential fits to the simulated PACF by using Eq.(4.8), and obtained $\eta = 266 \pm 9.08$ cP at 298 K which agrees well with the experiments (261 cP). Note η may be also calculated via the Helfand – Einstein approach, but we chose to calculate via the pressure tensor form , since the pressure tensor can be readily obtained by using the DL_POLY 2.2 package.

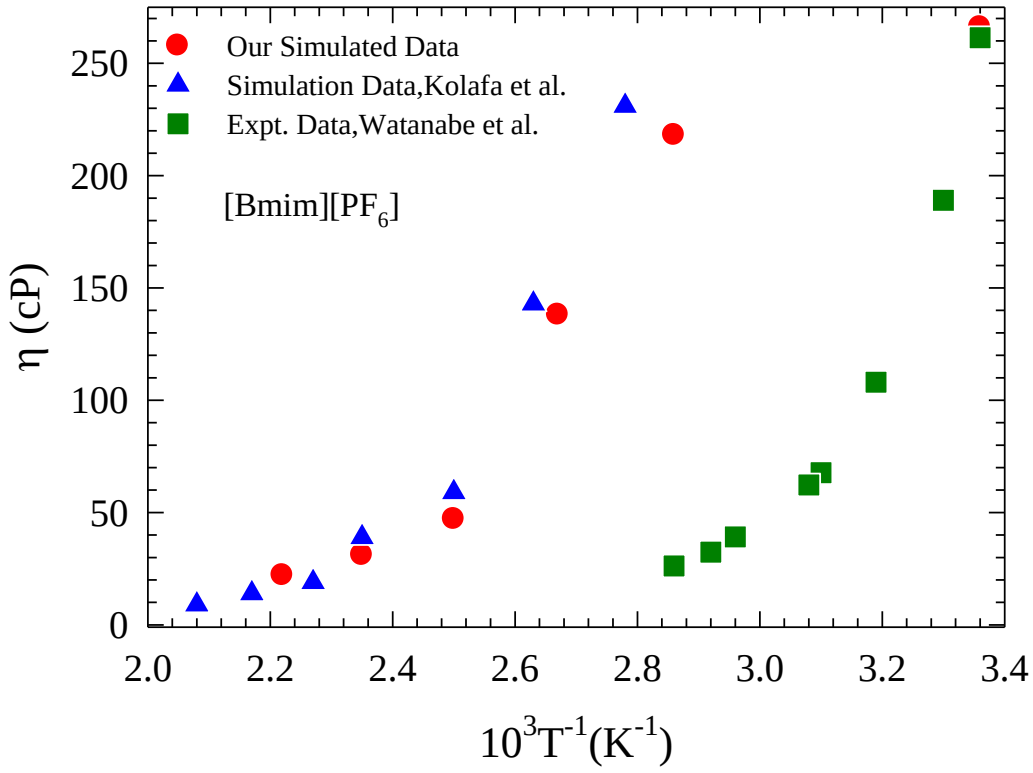

Figure. 4.4: Comparison of our simulated η for [Bmim][PF_6] at various temperatures with those from non-equilibrium MD simulations and experiments.

The reorientation motion of the dipolar species is coupled to medium viscosity. Fig. 4.4 compares η values obtained from our simulations at various temperatures with the existing non-equilibrium MD simulation predictions[57] and experimental results.[58,59] Note that experimental data are available for the temperature range 263 – 353 K. The decomposition temperature[30,60] for this IL being ~400 K may be a reason for non-availability of experimental viscosity beyond ~350 K. Fig. 4.5 shows the dependence of the calculated average reorientational times $\langle\tau\rangle$, on the temperature-scaled simulated viscosity, η/T, for this ionic liquid. $\langle\tau\rangle$ obtained for both the ranks are shown. If the SED relation is obeyed by the reorientational motion, a simple dependence of the form, $\langle\tau\rangle\alpha(\eta/T)^p$ with p =1, is expected to be observed. In contrast, simulated times for both the ranks indicate p ~1.43. Interestingly, experimentally measured viscosity dependent average solute rotational times[16] in ILs have been found to fit the SED relation with p =1.5. Such a deviation from p =1 indicates limited validity of hydrodynamics in describing rotational motions in ILs, and may suggest presence of non-Gaussian dynamics. When experimental DR data [18] for this IL at different temperatures are analyzed in the same manner, we obtain p ~1.13, and this is also shown in Fig. 4.5.

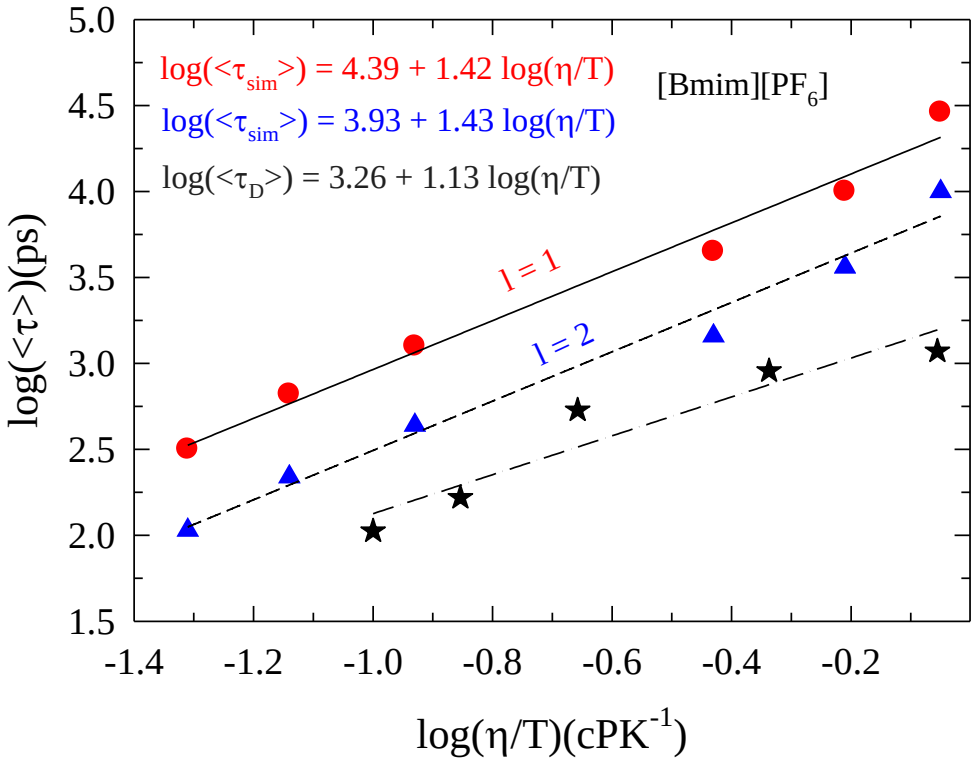

Figure. 4.5: Viscosity dependence of the average reorientational times for both the ranks (circles and triangles). Note viscosity is scaled by temperature and represented as η/T. Stars denote the slowest time constant of experimental DR data at a given temperature (Ref. 18). Lines through the simulated and experimental data represent fits of the following form, $\langle\tau\rangle \propto A\left(\frac{\eta}{T}\right)^{p}$. Fit parameters are shown inside the panel.

4.3.3 Testing the validity of the Onsager-Glarum relation: Collective and single particle rotation

In this section we explore the connection between the collective and single particle reorientation of dipolar species and test the validity of the Onsager-Glarum equation. Our analyses here are for T = 400, 425 and 450 K as relaxations of RTCF have been found to be complete in our simulations at these temperatures. As outlined in the beginning, we extracted the single particle reorientation time $\tau_{rot}^{\ell=1}$ from Eq 4.3 using the slowest time constant reported in the available DR measurements. Note here that at $T \geq 400$ K, experimental η are not available and thus simulated values at these temperatures have been used to determine the required relaxation times via viscosity scaling. Table 4.2 compares the OG times so obtained with those from simulations. Clearly, the simulated times are ~5-10 times larger than those from OG predictions at these temperatures, signalling an inability of the OG relation to predict collective reorientation for these complex liquids. Although a part of this failure may arise from the use of DR times from simple viscosity scaling, a role for short-range correlations present in these Coulomb fluids may not be neglected. Experiments and simulation studies have suggested that alkyl chains attached to cation in imidazolium ILs can give rise to nanoscale aggregation with charge ordering. [61-67] These correlations need to be considered, maybe via an effective Kirkwood g factor, in order to properly test the validity of OG relation.

Table 4.2. Comparison of single particle reorientation times between our simulations and those extracted from the Onsager-Glarum expression.

Temp (K)	$\tau_D(ps)$ [a]	$\tau_{rot}^{\ell=1}(ps)$	$\tau_{sim}^{\ell=1}(ps)$	$\chi = \frac{\tau_{sim}^{\ell=1}}{\tau_{rot}^{\ell=1}}$
400	154.2	115.7	1266.9	~11
425	101.7	76.3	658.1	~9
450	72.0	54.0	318.8	~6

[a] Dielectric relaxation times τ_D have been scaled by simulated viscosity using the simple η/τ method for all the temperatures , using the slowest relaxation time measured in DR experiments at 338.15 K as a reference (see Ref. 18 & 59). Static dielectric constant $\varepsilon_0 = 13.0$ and the infinite-frequency dielectric constant, $\varepsilon_\infty = 3.27$ measured at 338.15 K have been used in the OG relation for calculations of reorientation times at $T \geq 400$ K.

For highly associated liquids, like alcohols and water, the g factor is highly deviated from unity due to the strong H-bonding. Interestingly, g factor has been considered as a useful index in qualitatively undertanding the impact on short-range structural correlations in highly dense polar protic liquids.[68] In case of water, application of OG equation along with $g = 3$ produces $\tau_{rot}^{\ell=1} = 0.23\tau_D$.[69] Ab-initio calculations[70] have been performed to estimate the contribution of orientation polarization to the static dielectric constant for various ILs. It has been found that the elimination of short range specific interactions, like H-bonding in water, leads to an increase in net dipole moment compared to that in the gas phase of the molecule due to the parallel alignment of the molecules. Anti-parallel configuration of dipolar molecules in liquid phase has been conjectured on the basis of average lower dipole moment of molecules in liquid phase than in gas phase.[71]

In ILs therefore, it is unlikely that g will be unity as charge-charge and hydrophobic interactions produce extra correlations. Simulation runs over 100 ns for $[Bmim]^+$ with different anions have reflected a variation in the estimated g factor which remained always much less than unity.[72] However, at a larger distance (beyond 25 Å) simulations report a value of ~ 0.82 for the g-factor in $[Bmim][BF_4]$, ~ 0.84 for $[Bmim][PF_6]$.[44,71,72] Intuitively, one would expect that the charge-ordered structure in ILs should give rise to single particle relaxation shielding the collective effects. A very recent dielectric relaxation study on polymerized imidazolium-based ILs has shown that, for ILs having $\varepsilon_0 \leq 30$, anti-parallel arrangement is preferred producing $g \approx 0.1$ for $[Bmim][NTf_2]$.[73] This anti-parallel alignment of the same dipolar ions may substantially reduce the collective average dipole moment of the system. This may in turn produce g values much less than unity.

There are two approaches for calculating the Kirkwood g factor :

(i) Madden and Kivelson (MK) method[71,72] where the difference in the values of average squared total molecular dipole moment from the mean square of the dipole moment of the single molecules acting at short range was termed as Kirkwood - g factor,

(ii) Kirkwood-Froehlich (KF) equation (Eq. 4.10),[74,75]which has been found to be sufficiently good to relate ε_0 and g even for ILs, [73] where g was calculated to be ~ 0.5-0.8.[76] Such a g-value is reasonable and agrees semi-quantitatively with MK prediction. The KF equation is given by

$$\frac{(\varepsilon_0 - \varepsilon_\infty)(2\varepsilon_0 + \varepsilon_\infty)}{3\varepsilon_0} = \frac{4\pi\mu^2 g\rho}{3k_B T}\left[\frac{(\varepsilon_\infty + 2)}{3}\right]^2 \qquad (4.10)$$

The determination of exact dipole moment of $[Bmim]^+$ molecule is a bit tricky and different works suggest different values.[18,76-80] We used this expression to compare between calculated Kirkwood - g factors using two different dipole moment values in Table 4.3. We have also listed the Kirkwood - g factor , from the Powles Eqn. assuming that the $\tau_{sim}^{\ell=1} = \tau_{rot}^{\ell=1}$, which determines g ~ 0.10-0.20.

Table 4.3. A comparison among g-factors estimated from various methods

Temp (K)	$\tau_D(ps)$	$\tau_{sim}^{\ell=1} = \tau_{rot}^{\ell=1}(ps)$ at $\chi = 1$	Kirkwood factor g Powles Eqn.	g from Kirkwood-Froehlich Eqn. using $\mu = 2.15D$[78]	g from Kirkwood-Froehlich Eqn. using $\mu = 4.4D$[77]
400	154.2	1266.9	0.10	3.27	0.75
425	101.7	658.1	0.12	3.14	0.75
450	72.0	318.8	0.17	2.89	0.63

4.3.4 Hydrodynamic explanation : Effective volume of the rotating dipolar ion

The Stokes-Einstein-Debye is one of the simplest route to connect the rotational correlation time $\tau_{rot}^{\ell=1}$ of the dipolar species with the viscosity η of the surrounding medium . To facilitate a qualitative understanding , we calculated the effective volumes from both the single particle rotational times obtained from our simulation and that extracted from the OG equation. The effective volumes and coupling parameter as deduced from $\tau_{sim}^{\ell=1}$ and $\tau_{rot}^{\ell=1}$ are given in Table 4.4 and designated as $V_{eff}^{\ sim}$, f_{sim} and $V_{eff}^{\ OG}$, f_{OG} respectively.

Table 4.4. Hydrodynamic coupling factor for the dipolar cation $[Bmim]^+$, as derived from Stokes-Einstein-Debye equation , using the simulated single particle reorientation

time and the time obtained from OG relation . Note molecular volume of $[Bmim]^+$, $V = 311.6\,\text{Å}^3$

Temp (K)	$\tau_{sim}^{\ell=1}(ps)$	Coupling parameter f_{sim}	$V_{eff}^{\ sim} = Vf_{sim}$	$\tau_{rot}^{\ell=1}(ps)$	Coupling parameter f_{OG}	$V_{eff}^{\ OG} = Vf_{OG}$
400	1266.9	0.16	49.8	115.7	0.015	4.7
425	658.1	0.13	40.5	76.3	0.015	4.7
450	318.8	0.10	31.2	54.0	0.017	5.3

For both the cases we have found that the effective volume is much less than cation molecular volume V . More precisely, $V_{eff}^{\ sim}$ is only ~16 % of V (sub-slip condition) , while $V_{eff}^{\ OG}$ is ~1% of V [18] (perfect-slip condition , where $f_{OG} \sim 0$). This is somewhat counter-intuitive given the results reported in Ref. 20.

4.4 Conclusion

In conclusion, the present study suggests that the presence of ion-ion and ion-dipole interactions in addition to dipole-dipole interaction can have profound effects on reorientational dynamics of dipolar ions in ILs, and use of the Onsager-Glarum equation may not be valid. The present studies highlights several insufficiencies which may arise due to (i) small system size (ii) correct selection of cut-off radius (iii) incomplete decay of RTCF near room temperature (iv) smaller run time. A much longer simulation run (>100ns) might lead to better results as it would provide better equilibration and statistical averaging. Approximate method used for obtaining dielectric relaxation time may also be source for the failure of the OG relation here. Extensive computer simulations are therefore required for a better understanding of the connection between the single and collective reorientation dynamics in dipolar ILs.

References :

1. D. Laage and J. T. Hynes,Science **311**, 832 (2006).
2. S. Ravichandran and B. Bagchi, J. Phys. Chem.,**98**, 2729 (1994).
3. A. Rahman, J. Chem. Phys. **55**, 3336 (1971).
4. L. Saiz, E. Guàrdia, and J.-A. Padró, J. Chem. Phys. **113**, 2814 (2000).
5. R. Biswas and B. Bagchi, J. Phys. Chem. **100**,1238(1996).
6. D. Roy, N. Patel, S. Conte, and M Maroncelli, J. Phys. Chem. B, **114**, 8410(2010).
7. C. G. Hanke , S. L. Price and R. M. Lynden-Bell , Mol. Phys. **99**,801 (2001).
8. Y. Shim, and H. J. Kim, J. Phys. Chem. B, **112**, 11028 (2008).
9. T. Pal and R. Biswas, Theor. Chem. Acc. **132**,1348 (2013).
10. H. Liu and E. Maginn , J. Chem. Phys,**135**,124507 (2011).
11. H. V. R. Annapureddy, Z. Hu, J. Xia, and C. J. Margulis, J. Phys. Chem. B,**112**,1770 (2008).
12. W. Zhao ,F. Leroy , B. Heggen , S. Zahn , B. Kirchner , S. Balasubramanian , and F. Muller-Plathe , J. Am. Chem.. Soc, **131** , 15825 (2009).
13. C. J. F. Bottcher, P. Bordewijk, Theory of Electric Polarization, 2nd ed.; Elsevier: Amsterdam, Vol. 2.(1978).
14. A. Chandra and B. Bagchi, J. Chem. Phys **94**, 3152 (1990).
15. T. Koddermann, R. Ludwig, D. Paschek, Chem. Phys. Chem. **9**,1851(2008).
16. H. Jin, G. A. Baker, S. Arzhantsev, J. Dong, and M Maroncelli , J. Phys. Chem. B, **111**, 7291 (2007).
17. M. L. Horng, J. A. Gardecki, and M. Maroncelli , J. Phys. Chem. A, **101**, 1030 (1997).
18. J. Hunger, A. Stoppa, S. Schrödle, G. Hefter, and R. Buchner, Chem. Phys. Chem **10**, 723 (2009).
19. J. Hunger , S. Niedermayer , and R. Buchner , J. Phys. Chem. B, **114** , 13617 (2010).
20. M.-M. Huang, S. Bulut, I. Krossing, and H. Weingärtner, J. Chem. Phys. **133**, 101101 (2010).

21. H. Shirota , A. M. Funston ,J. F. Wishart , and E. W. Castner , J. Chem. Phys. **122**, 184512(2005).
22. S. Daschakraborty and R. Biswas , J. Chem. Phys. **138**, 204502 (2013).
23. B. Guchhait, H. A. R. Gazi, H. K. Kashyap and R. Biswas, J. Phys. Chem. B. **114**, 5066(2010).
24. T. Pal and R. Biswas, Chem. Phys. Lett. **517**, 180(2011).
25. J. P. Hansen, I. R. McDonald, Theory of Simple Liquids, 3rd ed. Academic, San Diego. (2006).
26. S. Taraphder, J. Chem. Phys. **109**,4948 (1998).
27. J. Hunger , T. Sonnleitner , L. Liu, R. Buchner , M. Bonn, and H. J. Bakker , J. Phys. Chem. Lett. **3**,3034 (2012).
28. I. Ohmine and H. Tanaka, Chem. Rev. **93**, 2545(1993).
29. J. E. Anderson Faraday Symp. Chem. Soc. **6**, 82(1972).
30. B. Guchhait, S. Das, S. Daschakraborty and R. Biswas, J. Chem. Phys. **140**, 104514 (2014).
31. B. Guchhait, H. A. R. Gazi, H. K. Kashyap, and R. Biswas, J. Phys. Chem. B **114**, 5066 (2010).
32. B. Guchhait, S. S. Daschakraborty and R. Biswas, J. Chem. Phys. **136**, 174503 (2012).
33. T. Pal and R. Biswas, Chem. Phys. Lett. **517**, 180 (2011).
34. B. Bagchi and A. Chandra , Adv. Chem. Phys. **80**,1(1991).
35. J. Deutch, J. Faraday Symp. Chem. Soc. **11**, 26 (1977).
36. S. H. Glarum, J. Chem. Phys. **33**, 1371 (1960).
37. L. Onsager , J. Am. Chem. Soc. ,**58**,1486(1936).
38. J. G. Powles, J. Chem. Phys. **21**, 633 (1953).
39. J. G. Kirkwood, J. Chem. Phys. **7**, 911 (1939).
40. P. Madden and D. Kivelson, Adv. Chem. Phys. **56**, 467 (1984).
41. A. Chandra and B. Bagchi, J. Chem. Phys **90**, 1832 (1989).
42. B. Bagchi and A. Chandra, Phys. Rev. Lett. **64**, 455 (1990).
43. B. Bagchi and A. Chandra, J. Chem. Phys. **93**, 1955 (1990).
44. C. Schroder , C. Wakai , H. Weingartner, and O. Steinhauser , J. Chem. Phys. , **126** , 084511 (2007).

45. W. Smith, T. R. Forester, (eds.) (2010) in DL_POLY_2.2; CCLRC Daresbury Laboratory: Daresbury, UK.
46. A. P. Lyubartsev, A. Laaksonen, Comput. Phys. Commun. **128**,565(2000).
47. Z. Liu, S. Huang, and W. Wang, J. Phys. Chem. B. **108**, 12978 (2004).
48. W. D. Cornell, P. Cieplak, C. I. Bayly, I. R. Gould, K. M. Merz, D. M. Ferguson, D. C. Spellmeyer, T. Fox, J. W. Caldwell, P. A. Kollman, J. Am. Chem. Soc. **117**, 5179(1995).
49. M. P. Allen and D. J. Tildesley, Computer Simulations of Liquids (Oxford University Press, New York, 1987).
50. S. Nose, J. Chem. Phys. **81**, 511 (1984).
51. W. G. Hoover, Phys. Rev. A **31**, 1695 (1985).
52. G. J. Martyna, M. E. Tuckerman, D. J. Tobias, and M. Klein, Mol. Phys. **87**, 1117 (1996).
53. G. J. Martyna, M. Klein, and M. E. Tuckerman, J. Chem. Phys. **97**, 2635 (1992).
54. B. L. Bhargava, and S. Balasubramanian , J. Chem. Phys,**123**,144505 (2005).
55. A. Das, S. Das, and R. Biswas, Chem. Phys. Lett. **581**, 47 (2013).
56. A. M. Funston, T. A. Fadeeva, J. F. Wishart, E. W. Castner, Jr. J. Phys. Chem. B. **111**,4963(2007).
57. J. Picalek, J. Kolafa, Mol. Simulation **35**,685(2009).
58. H. Tokuda, K. Hayamizu, K. Ishii, A. B. H. Susan, M. Watanabe, J.Phys. Chem. B **108**,16593(2004).
59. W. Li , Z. Zhang, B. Han, S. Hu, Y. Xie, and G. Yang , J.Phys. Chem. B,**111**,6452(2007).
60. W. H. Awad, J. W. Gilman, M. Nyden, R. H. Harris, T. E. Sutto, J. Callahan, P. C. Truelove, H. C. Delong, D. M. Fox, Thermochim. Acta, **409**,3(2004).
61. A. Triolo, O. Russina, B. Fazio, R. Triolo, E. D. Cola, Chem. Phys. Lett. **467**,362(2008).
62. C. S. Santos, N. S. Murthy, G. A. Baker, E. W. Castner Jr. J. Chem. Phys. **134**,121101 (2011).
63. H. K. Kashyap, C. S. Santos, H. V. R. Annapureddy, N. S. Murthy, C. J. Margulis, E. W. Castner Jr. Faraday Discuss. **154**,133(2012).
64. S. M. Urahata and M. C. Ribeiro, J. Chem. Phys. **120**, 1855 (2004).

65. Y. Wang and G. A. Voth, J. Am. Chem. Soc. **127**, 12192 (2005).
66. J. N. A. Canongia Lopes and A. A. H. Pádua, J. Phys. Chem. B **110**, 3330 (2006).
67. M. G. Del Popolo and G. A. Voth ,J. Phys. Chem. B , **108**,1744 (2004).
68. G. Oster and J. G. Kirkwood,J. Chem. Phys. ,**11**,175(1943).
69. B. Bagchi , Molecular Relaxation In Liquids, Oxford University Press (2012).
70. E. I. Izgorodina , M. Forsyth and D. R. MacFarlane , Phys. Chem. Chem. Phys. ,**11**,2452 (2009).
71. C. Schroder , J. Chem. Phys. **135**, 024502 (2011).
72. C. Schroder , T. Rudas, and O. Steinhauser , J. Chem. Phys. **125**, 244506 (2006).
73. U. H. Choi, A. Mittal, T. L. Price, Jr. , H. W. Gibson , J. Runt , and R. H. Colby ,Macromolecules **46**,1175 (2013).
74. A. Y. Zasetsky , S. V. Petelina , A. K. Lyaschchenko and A. S. Lileev , J. Chem. Phys., **133**,134502 (2010).
75. H. Weingärtner, H. Nadolny, A. Oleinikova, and R. Ludwig, J. Chem.Phys. **120**, 11692 (2004).
76. H. Jin, B. O'Hare , J. Dong , S. Arzhantsev , G. A. Baker , J. F. Wishart , A. J. Benesi and M. Maroncelli, J. Phys. Chem. B. **112**,81 (2008).
77. H. Kashyap , and R. Biswas , J. Phys. Chem. B,**114**,16811 (2010).
78. B. L. Bhargava, and S. Balasubramanian , J. Phys. Chem. B,**111**,4477 (2007).
79. J. Hunger, A. Stoppa, R. Buchner, and G. Hefter, J Phys. Chem. B,**112**,12913 (2008).
80. C. Schroder , J. Hunger, A. Stoppa, R. Buchner, and O. Steinhauser , J. Chem. Phys. **129**,184501 (2008).

Chapter 5

Slow Solvation in Ionic Liquids: Connections to Non-Gaussian Moves and Multi-point Correlations

5.1 Introduction

'Slow solvation' here refers to the slowest of the multiple solvation timescales reported by time-dependent Stokes shift (TDFSS) measurements of neat room temperature ionic liquids (RTILs) employing fluorescent dipolar solutes.[1-3] The slow solvation timescale, which is often in nanosecond regime, has also been predicted recently by a semi-molecular theory that envisions relaxation of translational ion dynamic structure factor as origin for this nanosecond component in such media.[4] This and other previous theoretical works[5-10] have suggested that translational ion dynamic structure factor contributes only ~10-15% to the measured total solvation response and regulates the slow late stage solvation. However, simple diffusion at the single particle level cannot be responsible for the nanosecond solvation component as the diffusive timescale predicted by hydrodynamics is much longer than the observed timescale. For example, hydrodynamic calculations using stick boundary condition produce an ion diffusion timescale (time required to diffuse over one ion diameter, σ_+ or σ_-) of ~100 ns for 1-butyl-3-methylimidazolium hexafluorophosphate ([Bmim][PF_6]) at 300 K. This is nearly ~100 times longer than the slowest time constant reported[1] for this IL at this temperature. In addition, the predicted single particle reorientation time for the dipolar cation $[Bmim]^+$ is ~40 times slower than the slowest solvation time constant at this temperature for this IL.[11] It is therefore evident that mechanism other than simple

diffusion is operating which makes the late stage solvation much faster than that predicted by the hydrodynamics. Exploration of this microscopic mechanism is the central theme of the present chapter. We have considered here [Bmim][PF_6] as a representative example where attempts have been made to connect the slow solvation time at room temperature to the simulated translational non-Gaussian parameters[12-15] and four point, time-dependent density correlation functions[16-18] for this IL.

Interestingly, the aspect of slow solvation in ILs was first reported in a systematic study[19] that involved temperature dependent measurements of dynamic fluorescence Stokes shift and anisotropy of coumarin 153 (C153) in two alkylpyrrolidinium and two alkylammonium ILs in the temperature range, T ~278-353 K. While multi-exponential fits to dynamic Stokes shift data indicated presence of the slowest timescale in ~0.4-1 ns range for alkylpyrrolidinium and in ~4-9 ns for alkylammonium ILs at ~300 K, similar exercise with data measured at lower temperatures had revealed a timescale ~2-4 times slower than that at ~300 K. Even longer timescale in the range of ~100 ns for reorientational dynamics of C153 in these ILs was observed, and interpreted in terms of reorganization of long-lived local structures (domains) surrounding the dissolved solute.[19] Coherent quasi-elastic neutron scattering (QENS) measurements at the collective wavevector for an IL, 1-octyl-3-methylimidazolium chloride (C8mimCl), indeed suggested presence of such a slow timescale for domain relaxation.[20] Incoherent QENS measurements with [Bmim][PF_6] at ~300 K reported a sub-nanosecond α-relaxation process possibly due to butyl group relaxation along with an indication of a much slower dynamics.[21] Subsequent neutron scattering[22] and broadband dielectric spectroscopic (BDS) measurements[23] attributed this sub-nanosecond relaxation to diffusive dynamics. Note relaxation processes with characteristic time slower than sub-nanosecond at ~300 K for this IL have not been detected by these scattering measurements[21,22] because of their inability to probe the relevant spatial and temporal scales involved in such slow dynamics.

However, depolarized light scattering (DLS) measurements, which probe the second rank ($\ell = 2$) collective orientational relaxation of the dipolar species, reported cation

reorientation time in the nanosecond regime[24] for [Bmim][PF_6] at T ~300. This reorientation timescale is qualitatively similar to the simulated first rank ($\ell = 1$) reorientation time for $[Bmim]^+$ at room temperature.[25] In addition, the above DLS study also revealed a similarity between the times required for cation reorientation and electric modulus relaxation, and provided a qualitative estimate for the mean jump length that might be associated with ion conductivity. Further measurements using a combination of BDS and pulsed field gradient nuclear magnetic resonance (PFGNMR) on a series of imidazolium ionic liquids possessing a common anion, bis(trifluoromethylsulfonyl)imide ($[(CF_3SO_2)_2N]^-$ abbreviated as TFSI) suggested that the mean jump length for $[Bmim]^+$ would be within ~40-50% of the cation diameter.[26] Note that even though the mean jump lengths provided by these analyses are only rough estimates and the approximations involved in extracting them from experimental data can be debated, these studies do highlight the importance of jump movements for ion diffusion in ILs. This is an important aspect as this mechanism can make the slow solvation timescales 'faster' than hydrodynamic predictions in ILs through diffusion-viscosity ($D - \eta$) decoupling even at room temperature – a feature characteristic of deeply supercooled liquids near glass transition temperature (T_g).[27] Note such a $D - \eta$ decoupling has recently been observed also for (amide + electrolyte) deep eutectics[28-31] at temperatures much above T_g of the melts. In fact, this slow nanosecond solvation component reported by dynamic fluorescence Stokes shift measurements is expected to leave a signature in the structural dynamics measured via neutron scattering experiments as both the measurements are coupled to medium density fluctuations. Indeed, heterogeneous relaxation dynamics measured via neutron spin echo (NSE) technique at the nearest neighbour length scale (ionic correlation) reports[32] a slow nano-second timescale for [Omim][TFSI] (Omim, 1-octyl-3-methylimidazolium) at ~300 K which is strikingly similar to the long-time solvation time constant reported recently[33] for this IL at room temperature. Note that this slow nanosecond timescale observed in NSE measurements has been attributed to ion diffusion, and also detected for ILs, [Omim][PF_6] and [Omim][Cl] at room temperature. Simulation study of solvation dynamics of C153 in [Bmim][BF_4] that include polarization forces via Drude charges report ~1.3 ns as time constant for the long-time decay of the simulated total response[34] which corroborates well with the slowest (~0.8 ns) of the multiple time constants

reported in a very recent experimental study.[3] Interestingly, such a slow relaxation dynamics has neither been observed in the simulated solvation response for C153 in model [Bmim][PF_6][35] nor detected in a recent microsecond length simulations of C153 solvation in 1-ethyl-3-methyl imidazolium tetrafluoroborate ([Emim][BF_4]).[36]

In this chapter we have performed molecular dynamics simulation studies of four point density time correlation function and new non-Gaussian parameter (denoted by γ in the next section) for [Bmim][PF_6] at ~300 K and 450 K using all-atom potential for the IL with no charge scaling. As the principal aim of this work is to explore the inter-relationship between the dynamic heterogeneity (DH) timescale and slow solvation in IL, we have also followed solvation energy relaxation of C153 in [Bmim][PF_6] at these temperatures. Realistic charge distribution for the solute (C153) has been used along with all-atom potential for IL for the solvation studies performed here. Simulated new non-Gaussian parameter peaks at a time different from that exhibited by the conventional non-Gaussian parameter (denoted by α_2 in the next section) at these temperatures, indicating DH persists over a much longer timescale than that suggested by the corresponding α_2. DH revealed by the four point correlation function exhibits temperature sensitivity and the corresponding particle overlap function becomes faster upon increasing temperature. Interestingly, the timescales reported by the simulated γ correlate well with the slow solvation timescale in this IL. The slow solvation of the simulated response at these temperatures are characterised by time constants much *faster* than that predicted by the hydrodynamics, suggesting presence of non-Brownian moves, such as, jumps. Dynamical correlation lengths obtained from four-point correlation functions appear to span about an ion diameter at these temperatures. The simulated single particle displacement distribution develops bimodality at a time coinciding with the peak of γ, indicating a change in the particle motion characteristics at longer time. In addition, simulated displacement distribution suggests jump motion with jump length similar to the estimates provided by experiments with ILs containing $[Bmim]^+$ cation.

5.2 Theoretical Background and Simulation Details

5.2.1. Simulation Details

Molecular dynamics simulations were performed by using the MDynamix programs.[37] As detailed previously,[13] AMBER-type force field[38] describes the interacting flexible molecular ions with the following expression for the total interaction potential energy:[39]

$$V_{tot} = \sum_{bonds} k_b (r - r_0)^2 + \sum_{angles} k_\theta (\theta - \theta_0)^2 + \sum_{dihedrals} k_\chi [1 + \cos(n\chi - \delta)]$$

$$+ \sum_{i=1}^{N-1} \sum_{j>i}^{N} \left\{ \varepsilon_{ij} \left[\left(\frac{r_{min,ij}}{r_{ij}} \right)^{12} - \left(\frac{r_{min,ij}}{r_{ij}} \right)^{6} \right] + \frac{q_i q_j}{r_{ij}} \right\}. \qquad (5.1)$$

A more detailed description of each term in Eq. 5.1 and implementation of the force field is already given elsewhere[13,39] and thus not repeated here. Lennard-Jones (LJ) parameters for interaction between same type of atoms were taken from Ref. 39 and Lorentz-Berthelot combining rules[40] were employed to determine the LJ parameters (σ_{ij} and ε_{ij}) for interaction between different types of atoms. In addition, partial atomic charges for $[Bmim]^+$ and $[PF_6]^-$ were also used as described in Ref. 39. Relevant LJ parameters and partial charges for C153 in its ground state were taken from Ref. 41. However, this model for C153, though reproduces experimental ground state dipole moment, provides a rigid description of the solute which was realized in our simulations via SHAKE algorithm.

Quantities related to DH of neat IL were obtained via simulations of 128 ion pairs (a total of 4096 atoms) interacting via Eq. 5.1 in a cubic cell with the standard periodic boundary condition at 298 K and 450 K having pressure set at 1 atm. Isothermal isobaric (NPT) ensemble was considered using the Nose-Hoover[42-45] barostat and thermostat, with coupling constants of 2000 and 500 fs, respectively. The Verlet neighbour list had a shell width of 2 Å for both the temperatures considered. Ewald summation technique was employed to treat the electrostatic interactions. Verlet Leapfrog algorithm[40] with 1 fs time step was used to solve the equation of motion. The

cut-off radius was set to 16 Å which produced an IL density at 298 K within 1.5% of the experimental density.[46] Our simulated density (1.224 gm/cc) at 450 K matched well with the existing all-atom simulation result (1.248 gm/cc).[47] Equilibration was first performed at 450 K and then brought down to 298 K via a step down process with a step of 50 K with equilibration at each of the step for a period of 2 ns. A 100 ns simulation run was then performed of which the last 80 ns was treated as the production run. Analyses of the simulated data were performed by employing codes developed at home. Note that structural properties obtained from such simulations agreed well[13] with the available data simulated by others.[39]

Simulations of solvation dynamics were then performed for systems with a single C153 molecule dissolved in 128 ion pairs at 298 K and 450 K. Effects of system size on solvation energy relaxation was investigated via simulations of a single C153 immersed in 256 ion pairs at 298 K and ambient pressure. Note that several earlier simulation studies reported weak-to-moderate (~10-20%) system size dependence of IL transport properties.[48-54] The effects of solute mobility on its own rate of solvation[8,55-60] at ambient condition (298 K and 1 atm. pressure) was subsequently investigated via carrying out simulations with single C153 in 128 ions pairs – in one case by allowing C153 to rotate and translate (but bonds held rigid) and eliminating these solute motions in the other.

5.2.2. Data Analyses: Relevant Expressions and Theoretical Background

As already mentioned, the primary check for the presence of dynamic heterogeneity was carried out via the conventional translational non-Gaussian parameter (α_2) and a new non-Gaussian parameter (γ). These quantities were determined from the simulated mean squared displacements (MSDs) of $[Bmim]^+$ and $[PF_6]^-$ by using the following expressions:[14,15]

$$\alpha_2(t) = \frac{3\langle \delta r^4(t) \rangle}{5\langle \delta r^2(t) \rangle^2} - 1, \qquad (5.2)$$

where $\langle \delta r^2(t) \rangle = \left\langle N^{-1} \sum_{i=1}^{N} |\Delta \mathbf{r}_i(0,t)|^2 \right\rangle$ and $\langle \delta r^4(t) \rangle = \left\langle N^{-1} \sum_{i=1}^{N} |\Delta \mathbf{r}_i(0,t)|^4 \right\rangle$ with δr signifying the distance over which a particle moved in time t (single particle displacement). $\Delta \mathbf{r}_i(0,t) = \mathbf{r}_i(t) - \mathbf{r}_i(0)$ denotes the displacement vector for the i-th particle in a system comprised of N particles. Note that although the peak position of $\alpha_2(t)$ is commonly accepted as a rough estimate for the maximum DH timescale,[61] a much slower timescale associated with DH may also exist.[62-63] This additional 'slower' DH timescale can be accessed via a new non-Gaussian parameter (γ) and four-point density-time correlation function. $\gamma(t)$ has the following form:[14]

$$\gamma(t) = \frac{1}{3} \langle \delta r^2(t) \rangle \left\langle \frac{1}{\delta r^2(t)} \right\rangle - 1, \qquad (5.3)$$

where the average of inverse square of δr is defined as,

$$\left\langle \frac{1}{\delta r^2(t)} \right\rangle = \left\langle \frac{1}{N} \sum_{i=1}^{N} \frac{1}{|\Delta \mathbf{r}_i(0,t)|^2} \right\rangle. \qquad (5.4)$$

Note here that while $\gamma(t)$ is strongly influenced by the particles which move less ('slow' particles) through the term $\langle 1/\delta r^2 \rangle$, $\alpha_2(t)$ derives contributions mainly from those which travel more distance than expected from a Gaussian distribution of particle displacements. Naturally therefore, simultaneous analyses of $\alpha_2(t)$ and $\gamma(t)$ provide information of particles with different relaxation rates.

The distribution of δr further quantifies the DH signatures which can be obtained from the self part of the van Hove correlation function, $G_s(\delta r, t)$:[14,15,61,65]

$$P[\log_{10}(\delta r); t) = \ln(10) 4\pi \delta r^3 G_s(\delta r, t). \qquad (5.5)$$

For a $G_s(\delta r, t)$ possessing Gaussian distribution of δr (that is, diffusive motion for a tagged particle at all times), $P[\log_{10}(\delta r); t]$ becomes independent of time with a peak height[14] ~2.13. Deviations from this height suggest non-Gaussian $G_s(\delta r, t)$ with fluctuations in local mobility of particles rendering heterogeneity in dynamics. High

temperature removes this heterogeneity via making 'local' particle mobilities identical to each other.

Four point, time dependent, density correlation function provides an avenue to explore the local mobility fluctuations and the spatial correlations among particles with similar mobility via tracking the local liquid density at two space points, each at two different times. Two point density correlation functions, for example, the self intermediate scattering function,[66] $F_s(k,t) = \langle \rho_s(k,t)\rho_s(-k,0) \rangle$, cannot follow this simultaneous time evolution of local liquid densities and thus fails to detect emergence of any spatially correlated mobile domains in a given system. The four-point density correlation function, $G_4(\mathbf{r},t)$, is defined as[67]

$$G_4(\mathbf{r},t) = \langle \rho(0,0)\rho(0,t)\rho(\mathbf{r},0)\rho(\mathbf{r},t) \rangle - \langle \rho(0,0)\rho(0,t) \rangle \langle \rho(\mathbf{r},0)\rho(\mathbf{r},t) \rangle , \qquad (5.6)$$

where $\rho(\mathbf{r},t)$ denotes time dependent density at a position $\mathbf{r}$. $G_4(\mathbf{r},t)$ measures the probability of occurrence of an event (for example, density decorrelation) at $\mathbf{r}$ over a specified time interval, given that a similar event is also taking place simultaneously at the origin. A dynamic correlation length, $\xi(t)$, emerges due to these simultaneous occurrences of cooperative dynamical events at two space points and can be evaluated from the four point dynamical susceptibility, $\chi_4(t)$, defined as the volume integral of $G_4(\mathbf{r},t)$. Information similar to that provided by $G_4(\mathbf{r},t)$ can also be accessed by analyzing the variance of the fluctuation of the self-intermediate scattering function, $F_s(k,t)$, as follows:[67-71]

$$\chi_4(\mathbf{k},t) = N\left[\left\langle \left(N^{-1} \sum_i \cos\mathbf{k} \cdot [\mathbf{r}_i(t) - \mathbf{r}_i(0)] \right)^2 \right\rangle - \left\langle N^{-1} \sum_i \cos\mathbf{k} \cdot [\mathbf{r}_i(t) - \mathbf{r}_i(0)] \right\rangle^2 \right], \quad (5.7)$$

where $F_s(k,t) = N^{-1} \sum_i \langle \cos\mathbf{k} \cdot [\mathbf{r}_i(t) - \mathbf{r}_i(0)] \rangle$. We have used Eq. 5.7 to calculate $\chi_4(t)$ at a given wavenumber from the simulated particle positions, $\mathbf{r}_i(t)$.

The dynamic correlation length, $\xi(t)$, can be estimated via analyzing a four-point correlation involving the overlap function, $Q(\mathbf{k},t)$, as follows:[70-73]

$$S_4(k,t) = N^{-1} \langle Q(\mathbf{k},t)Q(-\mathbf{k},t) \rangle , \qquad (5.8)$$

where $$Q(\mathbf{k},t) = \sum_{i=1}^{N} W_i(a,t)\exp[i\mathbf{k}\cdot\mathbf{r}_i(0)], \quad (5.9)$$

Note that the overlap function avoids a singularity arising from evaluation of density at the same position demanded by Eq. 5.6 for a system of extremely slow relaxing N particles, and this is performed via a Heaviside step function for distance criterion as follows: $W_i(a,t) = \Theta(a - |r_i(t) - r_i(0)|)$ with $a = 0.3\sigma$, σ being the diameter of the particle of interest.[18,72] It has been shown earlier[18] that the relaxation profile, $Q(t) = N^{-1}\left\langle \sum_i^N W_i(a,t) \right\rangle$, with $a = 0.3\sigma$ closely follows the relaxation of $F_s(k,t)$ at the nearest neighbour wavenumber ($k\sigma = 2\pi$). In the limit of small wavenumbers, the four-point overlap correlation function, $S_4(k,t)$, is related to $\xi(t)$ via the Ornstein-Zernike relation[18,72,74-75]

$$\frac{S_4(k,t)}{\chi_4(k \to 0,t)} = \frac{1}{1+[k\xi(t)]^p}. \quad (5.10)$$

In this work we have obtained $S_4(k,t)$ from the radial distribution function ($g(r)$) as follows:[18]

$$S_4(k,t) = 4\pi\rho[Q(t)/N]^2 \int_0^\infty dr\, r^2 \frac{\sin kr}{kr} g(r), \quad (5.11)$$

In addition, $\chi_4(k \to 0,t) = S_4(k \to 0,t) = 4\pi\rho[Q(t)/N]^2 \int_0^\infty dr\ r^2 g(r)$. Following previous studies[18,74,75] we have set $p = 2$ and determined $\xi(t)$ in the present work, although there are examples[71] where different values for this exponent have been used for the same purpose. Also note that thermal decomposition of [Bmim][PF_6] begins at ~400 K[76,77] and therefore our simulations at 450 K should be treated as a study performed to facilitate a qualitative comparison of DH aspects at two widely different temperatures.

5.3 Results and Discussion

In this section we will first present our simulation results at 298 K and 450 K on DH of neat IL ([Bmim][PF_6]) via exploring the non-Gaussian and new non-Gaussian parameters, single particle displacement distributions, overlap functions and four-point density correlation functions. Then, a connection of the DH timescales provided by these simulation studies is made to the slow solvation timescales reported by time dependent fluorescence Stokes shift measurements and molecular dynamics simulations. Subsequently, these DH timescales of for neat IL are compared with our own simulation results on temperature dependent solvation dynamics of C153 in [Bmim][PF_6] at 298 K and 450 K. This ensures uniformity in comparison between the DH timescales of neat IL and slow solvation timescale in it – both obtained from the same in-house simulations. This provides better validity to the proposed connections between them.

5.3.1 Temperature Dependent Dynamic Heterogeneity in Neat [Bmim][PF_6] and the Associated Timescales: Simulation Results

5.3.1.1 Non-Gaussian and New Non-Gaussian Parameters: Signature of Slower Moves

Fig. 5.1 presents a comparison between $\alpha_2(t)$ and $\gamma(t)$ for the cation ($[Bmim]^+$) and anion ($[PF_6]^-$) of neat IL simulated at 298 K and 450 K. For both the ions, these diagnostic functions exhibit non-monotonic time-dependence with peaks for $\alpha_2(t)$ occurring at times (τ_{NG}) shorter than those (τ_{NNG}) for $\gamma(t)$ at these temperatures. This means that the DH in this IL at a given temperature sustains over a timescale much longer than that suggested by τ_{NG} (peak time of α_2), and some ions can remain slower for a much longer duration extending up to the timescale provided by τ_{NNG} (peak time of γ). In addition, at 450 K both the profiles broaden with peak positions shifted towards shorter times with substantial reduction in the peak values (with respect to those at 298 K). These results, in part, are qualitatively similar to those observed earlier

in simulation studies of model super-cooled liquids[14,15,61] and ILs.[78-80] $\tau_{NG} < \tau_{NNG}$ because $\alpha_2(t)$ is dominated by ions possessing δr larger than expected from a Gaussian distribution of displacements whereas $\gamma(t)$ is dictated by those ions possessing δr shorter than expected from a Gaussian distribution. These results suggest presence of ions with widely different mobilities – a criterion for systems that exhibit DH. In addition, τ_{NG} and τ_{NNG} indicate timescales during which the deviation from Gaussian behaviour of δr would be the strongest due to the ions executing larger and shorter displacements respectively than predicted by the Gaussian distribution.

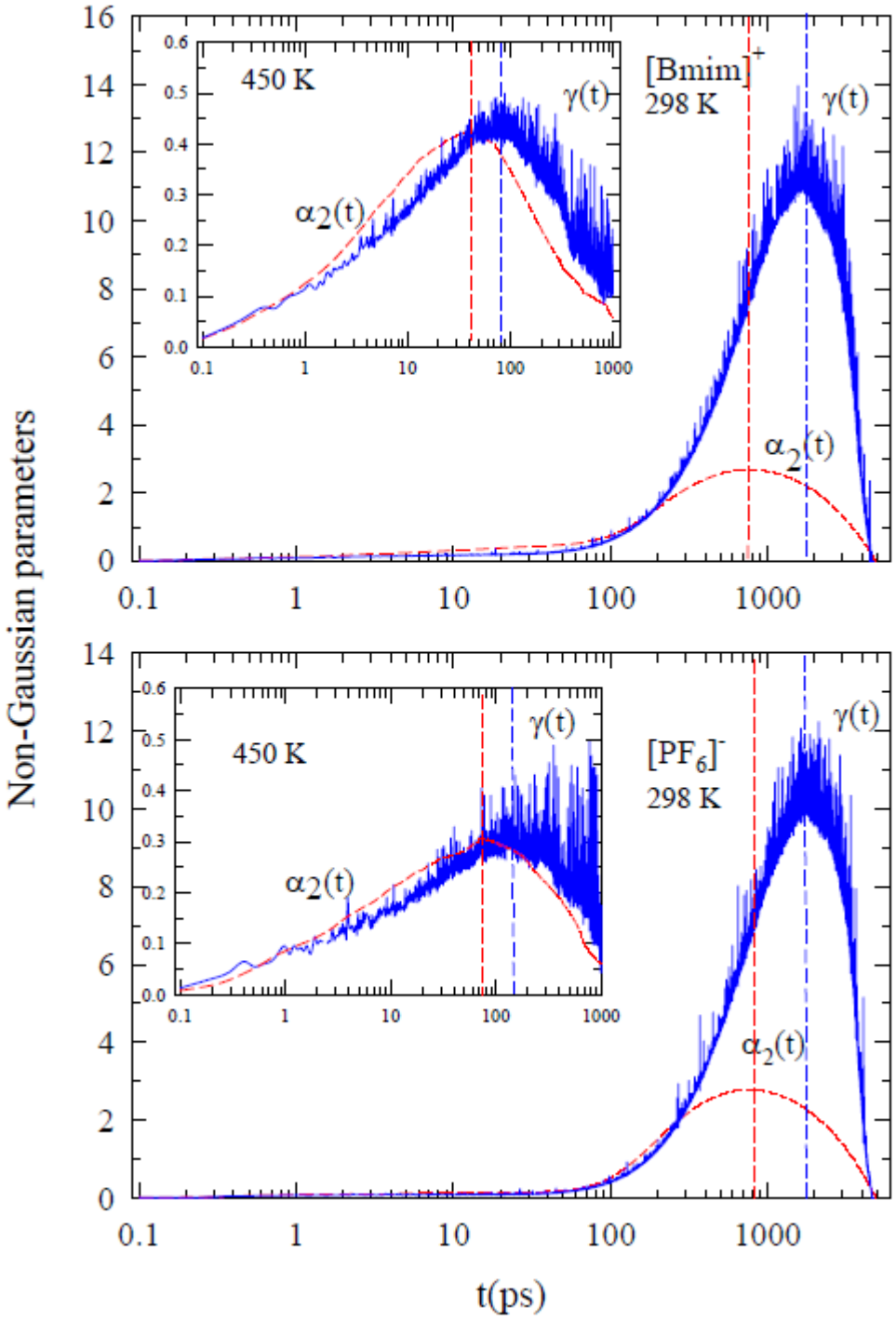

Figure. 5.1: Comparison between the simulated non-Gaussian and new non-Gaussian parameters, $\alpha_2(t)$ and $\gamma(t)$ respectively, for $[Bmim]^+$ (upper panel) and $[PF_6]^-$ (lower panel) at 298 K and 450 K. While the broken lines denote $\alpha_2(t)$, solid lines represent $\gamma(t)$. Vertical broken lines indicate peak times for the non-Gaussian parameter (τ_{NG}) and the new non-Gaussian parameter (τ_{NNG}).

Table 5.1: Comparison between temperature dependent τ_{NNG} and τ_{α} for $[Bmim]^+$ and $[PF_6]^-$

Ion	τ_{α} (ns)[a]		τ_{NNG} (ns)[b]	
	298 K	450 K	298 K	450 K
$[Bmim]^+$	1.90	0.05	1.70	0.08
$[PF_6]_-$	2.10	0.07	1.73	0.15

a) τ_{α} are assumed to be given by $\tau_{1/e}$ where $\tau_{1/e}$ denotes the time at which the corresponding normalized self dynamic structure factor at the nearest neighbour wavenumber ($F_s(k\sigma \to 2\pi, t)$ has relaxed to a value of $1/e$.

b) represents a time at which the new non-Gaussian parameter, $\gamma(t)$, attains a peak.

Note that increasing IL temperature from 298 K to 450 K not only lowers substantially the peak values of α_2 and γ, but also bring the peak values and times of these NG parameters closer to each other. This is due to temperature-induced 'homogenization' of displacement distribution (δr), reducing the mobility difference between 'mobile' and 'immobile' ions at higher temperature and subsequently making the IL dynamically less heterogeneous. Another important aspect is that τ_{NNG} for these ions at these temperatures coincide well with the $1/e$ time ($\tau_{1/e}$) of $F_s(k\sigma, t)$ decay with $k\sigma = 2\pi$ which is often identified[15] with the α-relaxation timescale (τ_{α}) of the system. Table 5.1 compares τ_{NNG} to the corresponding $\tau_{1/e}$. Note in this table that τ_{NNG} at these temperatures for $[PF_6]^-$ are somewhat longer than those for $[Bmim]^+$. Similar trend for τ_{NG} is also evident in Fig. 5.1. This is due to relatively slower diffusion[13] of $[PF_6]^-$ than $[Bmim]^+$.

5.3.1.2 Displacement (δr) Distribution: Bimodality, Ion Hopping and Connection to Slow Solvation

Fig. 5.2 depicts the probability distributions of the logarithm of single particle displacements at various times, $P[\log_{10}(\delta r); t]$, for both $[Bmim]^+$ and $[PF_6]^-$ at 298 K and 450 K, as a function of logarithm of single particle displacements, $\log_{10}(\delta r)$. As discussed in the previous section, Eq. 5.5 has been used to obtain $P[\log_{10}(\delta r); t]$ at several representative times across the full time-window of $\alpha_2(t)$ and $\gamma(t)$ shown in Fig. 5.1. Interestingly, the distribution moves to larger distances for longer times with time-dependent peak-height, and none of the distributions, even those at 450 K, attain a peak-height of 2.13. This indicates marked deviations of the underlying δr distributions from the Gaussian behaviour. Note that $P[\log_{10}(\delta r); t]$ for both cation and anion at 298 K remain single-peaked (with reduced height though) until $t < \tau_{NG}$ but starts growing a shoulder at $t \geq \tau_{NG}$. This shoulder for cation at 298 K finally develops into a separate peak in the timescale of τ_{NNG}, producing a full bimodal distribution of δr. Such a bimodality suggests existence of two dynamically different sets of populations – in one ions undergoing small displacements ('immobile' ions) while in the other ions executing large displacements ('mobile' ions) via hopping.[64] Such a bimodality in δr distribution is a hallmark of particle motions in supercooled model neat liquids[15] and binary mixtures,[14] and has also been observed for polymer colloids close to gelation.[61,65] In contrast, $P[\log_{10}(\delta r); t]$ for anion at this temperature shows only the shoulder at $t \geq \tau_{NG}$ and never blossoms into a full-fledged bimodal distribution. Ion-size may be one of the reasons for $P[\log_{10}(\delta r); t]$ being different at long time for cation and anion as simulations on model systems[14,65] have already reported size dependent displacement distributions and DH.

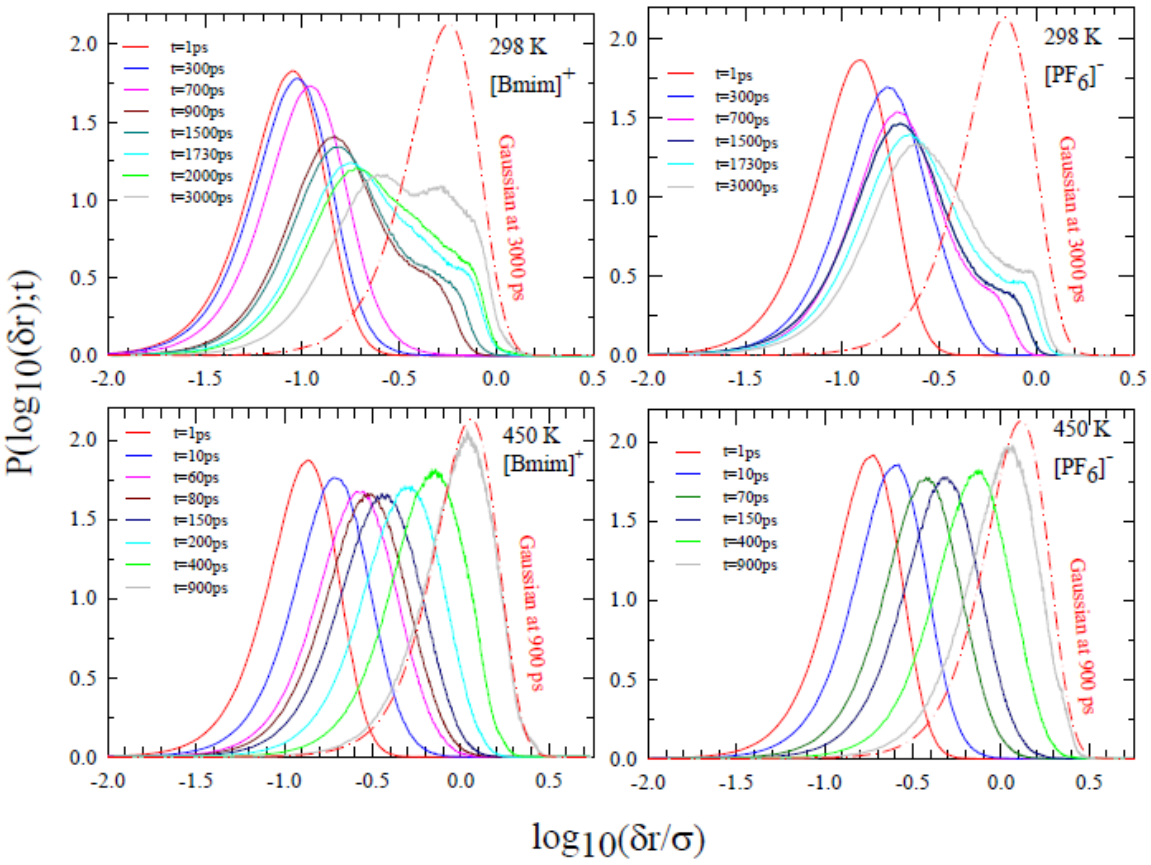

Figure. 5.2: Simulated single particle displacement distributions at 298 K (upper panel) and 450 K (lower panel) for $[Bmim]^+$ and $[PF_6]^-$ at different times. These times represent various time-points across the α and γ curves shown in Fig. 5.1. Gaussian distributions at the respective longest times (dashed-dot lines) are also shown for comparison. Note distributions of the logarithm of the simulated displacements (obtained by Eq. 5.5) are shown as a function of logarithm of displacements.

The distributions at 450 K, as already mentioned, only shifts with time never showing any shoulder growing at the large δr wing of the long time distribution. However, for both ions, peak-height of the distribution initially decreases and then gradually increases with time. The extent of loss and recovery of peak-height is more pronounced for $[Bmim]^+$ than that for $[PF_6]^-$. Therefore, $P[\log_{10}(\delta r); t]$ are different for $[Bmim]^+$ and $[PF_6]^-$ at 450 K also although the difference at this temperature is reflected through an aspect different from that at 298 K. Note the δr coverage of $P[\log_{10}(\delta r); t]$ in the first 700 ps at 298 K ranges from ~2% to ~30% of ion diameter for $[Bmim]^+$ and ~2% to ~80% of $[PF_6]^-$. Interestingly, dynamic Stokes shift measurements using C153[33] at ~293 K indicate ~80% of the solvation energy relaxation being complete within this

timescale. The length-scale of ion displacement involved in solvation energy relaxation of an excited polar dye in this IL at this temperature would, therefore, be about a half to full ion diameter ($\sim 0.5\sigma$ to 1.0σ). This length-scale agrees qualitatively with prediction from a previous simulation study involving a model IL mimicking [Bmim][PF_6] which reports[35] ion adjustments over a distance of $\sim 0.3\sigma$ are sufficient to make the solvation energy relaxation complete. More importantly, at 298 K and at 3ns, the second peak of $P[\log_{10}(\delta r); t]$ for $[Bmim]^+$ corresponds to $\delta r \sim 0.5\sigma$ which is in close agreement with the jump-length ($\sim 0.4 - 0.5\sigma$) for the cation estimated from combined BDS and PFGNMR measurements.[26] In fact, ion hopping at 298 K starts emerging at the timescale of τ_{NG} (~0.7-0.8 ns) – a time at which ~80% of the solvation is complete and the mechanism for relaxation at long time has taken over. At this stage with time the jump population increases and the participation of ions to solvation energy relaxation via hopping intensifies. Consequently, the long-time solvation component decouples from the viscosity and relaxes at a rate much faster than that predicted by the hydrodynamics. This is how the slow long-time solvation component in RTIL becomes 'faster' than hydrodynamic prediction due to DH. The DH effects would be much reduced at 450 K as partitioning of ions into two groups of differing mobilities vanishes shortening the timescales of τ_{NG} and τ_{NNG}. This makes the relaxation of long-time solvation component at higher temperatures much faster and dynamically less heterogeneous.

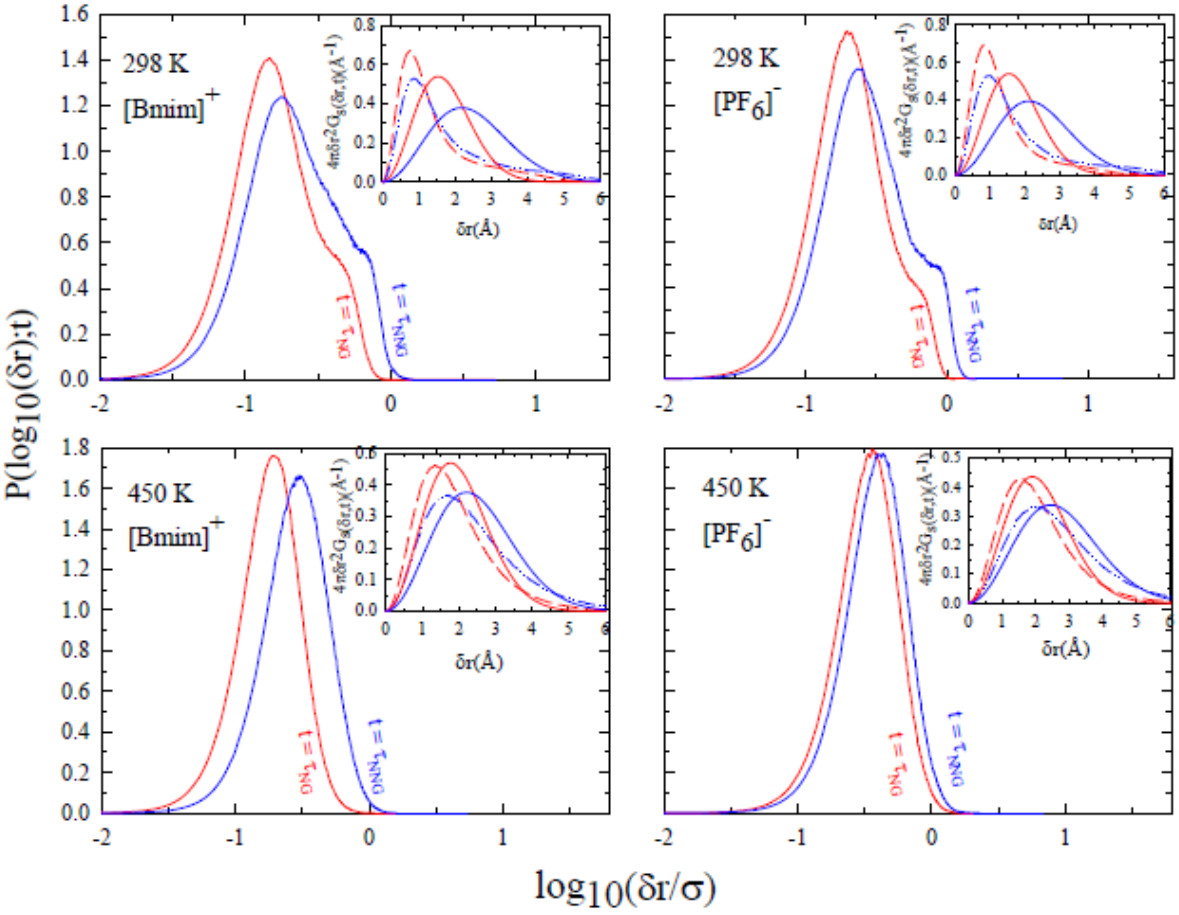

Figure. 5.3: Comparison between displacement distributions at τ_{NG} and τ_{NNG} for $[Bmim]^+$ and $[PF_6]^-$ at 298 K (upper panel) and 450 K (lower panel). Insets show the corresponding comparison between the self part of the simulated van Hove correlation functions at τ_{NG} (dashed lines) and τ_{NNG} (dashed-dot lines). Solid lines in the insets represent the Gaussian distributions at these times.

Fig. 5.3 explores the relative contributions of ion jumps in the displacement distributions at τ_{NG} and τ_{NNG} and the associated deviations of the simulated $G_s(\delta r, t)$ from being Gaussian at these two temperatures. As $\tau_{NNG} \approx 3\tau_{NG}$, $P[\log_{10}(\delta r); t]$ at $t = \tau_{NNG}$ samples larger δr and incorporates increased ion jumps although the extents of these increments are not large. A comparison of the underlying $G_s(\delta r, t)$ in the respective insets reflects that the deviation from being Gaussian is larger at τ_{NNG} than at τ_{NG}, and also more pronounced at 298 K than at 450 K. In addition, this comparison

indicates the domination of slow ion movements at these DH timescales and significant suppression of the medium length-scale displacements ($\delta r \sim 0.2 - 0.5\sigma$). Larger displacements at longer DH timescale strengthen the presence of nanosecond solvation component as these adjustments can contribute to spectral shifts leading to solvation energy relaxation at the late to very late stage of solvation. However, the contribution of these larger jumps at longer times could be tiny and would require for detection an improved signal-to-noise ratio along with measurements in a longer time window in relevant experiments. In fact, dynamic fluorescence measurements employing such improved experimental conditions[19] have already confirmed presence of nanosecond solvation component in various ILs at ~300 K.

5.3.1.3 Overlap Function and Self Dynamic Structure Factor: Inherent Slow Timescales

As results presented above suggest tiny centre-of-mass displacements of ions are linked to a major part of the solvation energy relaxation in IL, it is only natural to explore the timescales associated with $Q(t)$ as it tracks ion density fluctuations over a small length-scale (0.3σ). Such a length-scale of density fluctuations introduces similarity between relaxations of $F_s(k\sigma \to 2\pi, t)$ and $Q(t)$,[18,71] and constructs a kinship among timescales associated with these and solvation energy relaxations. Fig. 5.4 shows the relaxation profiles of $Q(t)$ for $[Bmim]^+$ and $[PF_6]^-$ at two different temperatures, and compares with the corresponding decays of $F_s(k\sigma \to 2\pi, t)$. Evidently, relaxation behaviours are similar for both the self dynamic structure factor and overlap function spreading over a few nanoseconds, although the decay of the latter is always slower than that of the former. This difference is quantified by a comparison of $1/e$ decay times summarized in Table C1 (Appendix C)[81] which indicates a trend of $1/e$ time for $Q(t)$ being ~1.5 times larger than that of $F_s(k\sigma \to 2\pi, t)$ for both the ions at these two temperatures. Noting of this difference is important because $\chi_4(t)$ can be calculated equivalently from fluctuations of either of the quantities ($Q(t)$ and $F_s(k\sigma, t)$) and, in such a case, $\xi(t)$ estimated via these two different routes may differ. However, that will not pose any

barrier to generate a qualitative understanding of 'slow' dynamics in terms of dynamic correlation length, if at all exists, because the present work focuses on exploring the underlying motion of the ions pertaining to the nanosecond component of the solvation energy relaxation in ILs.

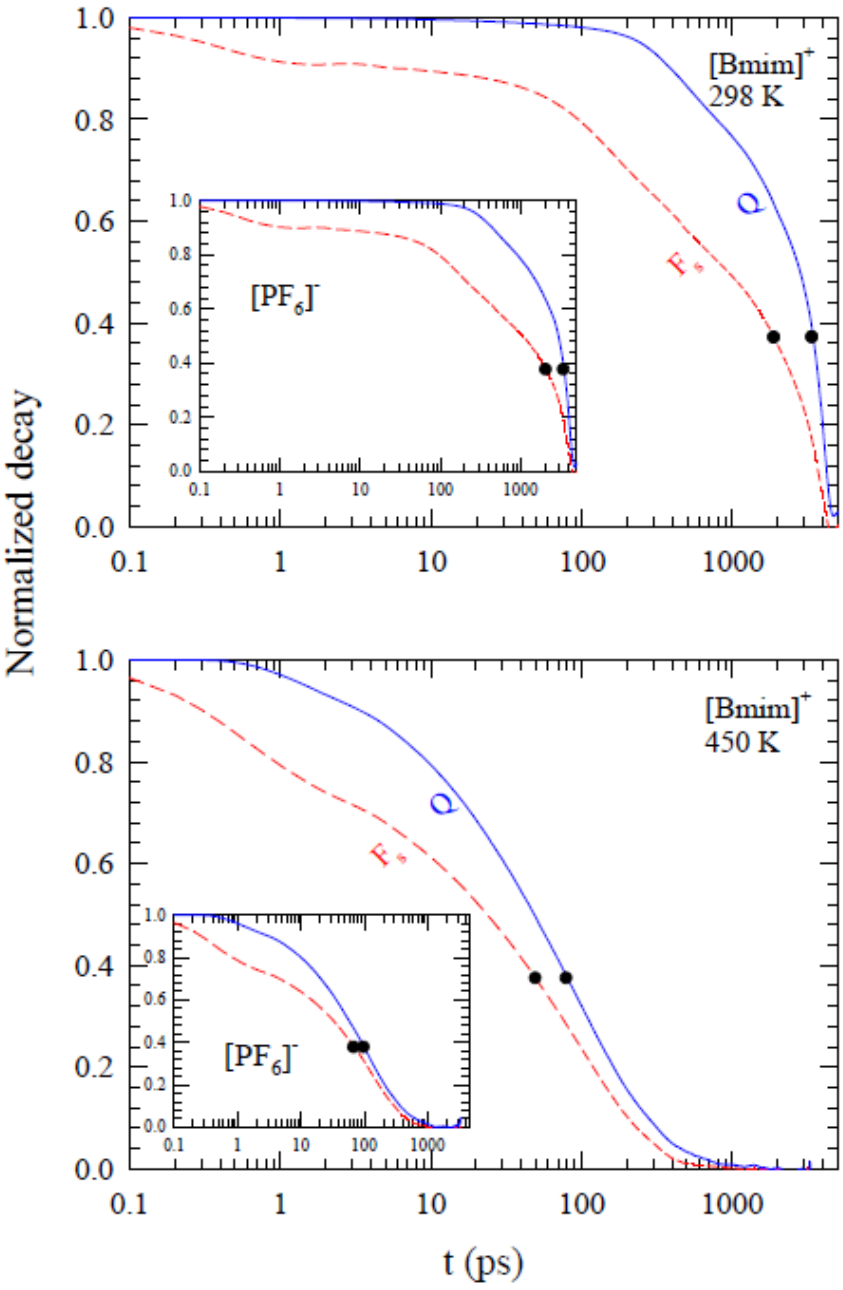

Figure. 5.4: Comparison between normalized decays of self dynamic structure factor at the nearest neighbour wavenumber ($F_s(k\sigma \rightarrow 2\pi, t)$) and overlap function ($Q(t)$) at 298 K (upper panel) and 450 K (lower panel) for $[Bmim]^+$ and $[PF_6]^-$. Bullet on each of the curves in these panels and insets denotes $1/e$ decay point and the time corresponding to this point represent

$1/e$ decay time, $\tau_{1/e}$. Note $\tau_{1/e}$ values for $Q(t)$ curves (solid lines) are always larger than those for $F_s(k\sigma \to 2\pi, t)$ curves (dashed lines). In addition, $\tau_{1/e}^{F_s} \approx \tau_\alpha$ (assumed).

Our best fits of $Q(t)$ and $F_s(k\sigma \to 2\pi, t)$ decays at 298 K correspond to (Gaussian + 2-exponentials) descriptions with timescales roughly in 200 fs (~5%), 50 ps (~10%) and 2 ns, suggesting complex relaxation processes that include rattling in a cage, followed by cage breaking and structural reorganization. At 450 K, however, $Q(t)$ decays require a stretched exponential for the entire time domain with the corresponding $F_s(k\sigma \to 2\pi, t)$ fitting to a combination of a fast exponential and a slow stretched one, producing a time constant of ~100 ps with β (stretching exponent) in 0.6-0.8 range. Representative fits are shown in Fig. C2 (Appendix C)[81] and our repeated attempts did not produce any better descriptions of these simulated decays. Interestingly, the slow timescales associated with these relaxation functions at 298 K and 450 K (~2 ns and ~100 ps, respectively) are quite similar to τ_{NNG} for these systems. This further highlights the link between the centre-of-mass density fluctuations and DH timescales, supporting the natural inheritance of a slow nanosecond solvation component in ILs at or around room temperature.

5.3.1.4 Four-Point Dynamic Susceptibility and Correlation Length: Time- and Length-scales of Correlated Ion Motions

The existence of a DH timescale in the nanosecond regime is further investigated in Fig. 5.5 where the simulated four-point dynamic susceptibility, $\chi_4(k,t)$, is shown as a function of time for both cation and anion at 298 K and 450 K. Eq. 5.7 has been used to obtain $\chi_4(k,t)$ shown here and correspond to the nearest neighbour wavenumber, $k\sigma = 2\pi$. Simulated $\chi_4(k,t)$ for both cation and anion at these temperatures exhibit non-monotonic time dependence with a peak at a certain time (t_4^{max}). Note that upon raising temperature the amplitude of $\chi_4(k,t)$ decreases with concomitant shift of t_4^{max} to lower time. The observed non-monotonic behaviour is a characteristic of $\chi_4(k,t)$ for

systems possessing DH and has been observed earlier for a variety of systems, ranging from super-cooled model liquids and their mixtures,[15,18,67,71,82] to polydispersed sytems,[83,84] colloidal gels[85] and confined systems in random media.[86,87] Several of these studies[15,18,67,71,82] have also revealed similar temperature effects on $\chi_4(k,t)$. Since the correlation of the fluctuations in $F_s(k,t)$ is what $\chi_4(k,t)$ measures, the non-monotonic behaviour reflects time dependence of correlations between a pair of particles (or trajectories) that grows with time in the beginning and then decays after showing a maximum at t_4^{max}. Previous studies involving super-cooled model liquids have indicated t_4^{max} to be in the timescale of τ_α. For $[Bmim]^+$ and $[PF_6]^-$ in the present case, t_4^{max} occurs at ~3-4 ns at 298 K, and at ~100-200 ps at 450 K. Interestingly, these timescales are comparable to the $1/e$ times of $Q(t)$ relaxation, reflecting a kinship between four-point DH timescale and slow density relxation. These times, being ~2- 3 times longer than the corresponding τ_α and τ_{NNG}, support the emergence of a nanosecond or even slower component in the solvation energy relaxation in RTILs.

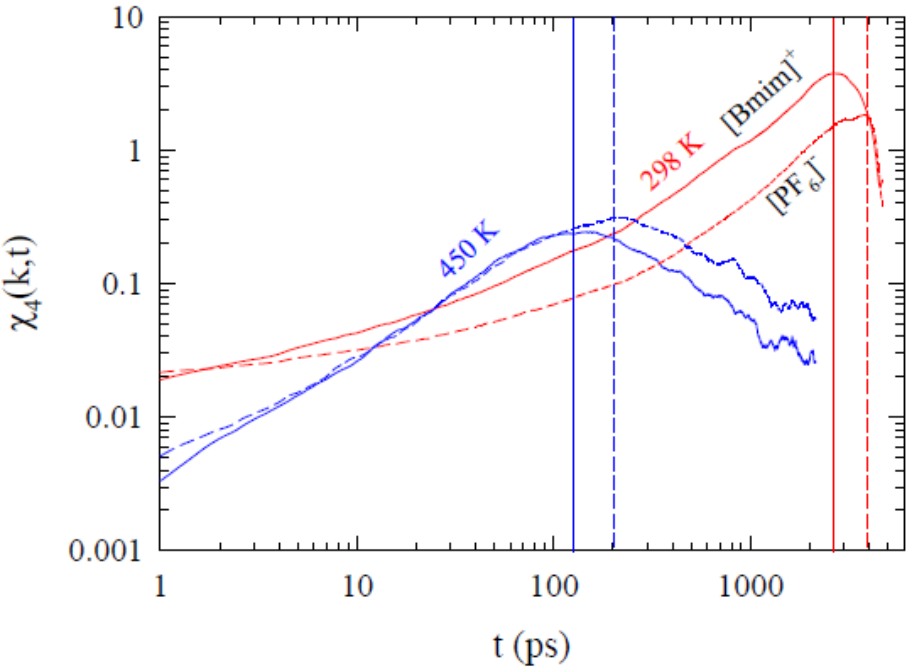

Figure. 5.5: Comparison between the simulated four-point dynamic susceptibilities, $\chi_4(k,t)$ evaluated at the nearest neighbour wavenumber, for $[Bmim]^+$ (solid lines) and $[PF_6]^-$ (dashed lines) at 298 K and 450 K. Vertical lines denote the peak times, t_4^{max}, of the respective $\chi_4(k,t)$ curves. The values for the nearest neighbour wavenumbers are 1.15 $Å^{-1}$ for $[Bmim]^+$ and 1.10 $Å^{-1}$ for $[PF_6]^-$. Note the extent of total dynamic correlation (reflected by the $\chi_4(k,t)$ amplitudes) at 298 K is much larger than that at 450 K.

We have already related the slow solvation time constant (~1 ns) in the measured Stokes shift dynamics of [Bmim][PF_6] at ~300 K to the corresponding τ_{NNG} (~ 2 ns). Simulations at ~300 K using C153 as a solute in [Bmim][BF_4][34] and model [Bmim][PF_6][35] have also revealed the slow solvation time constant to be ~1 ns. Such a comparison at 450 K is not viable due to the non-availability of experimental results at this high temperature. However, qualitative comparison can be made with the existing simulation studies of solvation dynamics in ILs at temperatures higher than 300 K. For example, simulations at 350 K of C153 solvation in model [Bmim][PF_6] report a slow time constant of ~80 ps which is in the timescale of τ_{NNG} (~100 ps) at 450 K found here. Similar studies with a dipolar solute probe in 1,3-dimethylimidazolium chloride ([Dmim][Cl]) at 425 K[88] have observed a slow long time component with time constant of ~70 ps. This slow time constant has been found to be somewhat shorter (~10-15 ps) in the simulated solvent relaxation at 450 K in response to oxidation of a model ion by one unit in [Dmim][PF_6].[89] At 400 K, the long-time tail of the time dependent solvation friction simulated for an ion-pair (IP) solute in 1-ethyl-3-methylimidazolium chloride ([Emim][Cl])[90] has been found to decay with a time constant of ~100 ps. These simulation data, therefore, collectively provide support to the proposition that slower solvation rate at long-time in ILs is indeed connected to the DH timescales revealed by τ_{NNG} and t_4^{max}, and originates naturally from the complex non-hydrodynamic movements of the constituent ions.

Next we estimate the dynamic correlation lengths, $\xi(t)$, at t_4^{max} of the simulated $\chi_4(k\sigma = 2\pi, t)$ at 298 K and 450 K by using Eq. 5.10 in order to provide a sense of length-scales associated with the correlated motions at these temperatures. This assumes importance particularly in the discussion of slow dynamics as larger ξ is believed to be connected to longer timescale[18,67,71,82] and vice-versa. Fig. 5.6 presents the normalized $S_4(k, t_4^{max})$ for $[Bmim]^+$ and $[PF_6]^-$ from simulations and the associated fits satisfying Eq. 5.10 at these two temperatures. Note that the values of ξ corresponding to the peak of χ_4 at the nearest neighbour wavenumber is ~9 Å at 298 K and ~7 Å at 450 K for these ions.

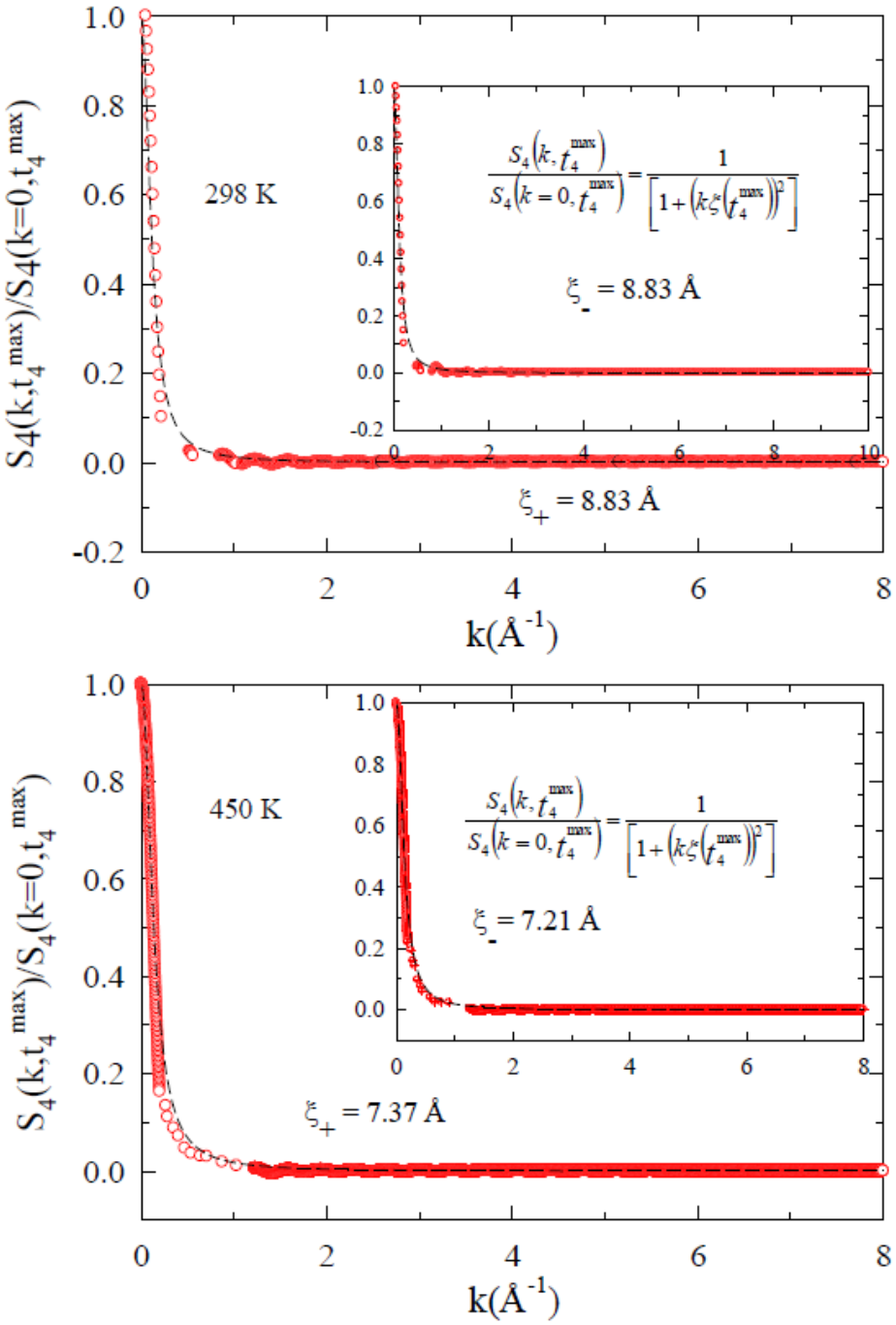

Figure. 5.6: Estimation of dynamic correlation lengths for $[Bmim]^+$ (ξ_+) and $[PF_6]^-$ (ξ_-) at 298 K (upper panel) and 450 K (lower panel). Circles represent simulated data (after removing oscillations) and the dashed lines going through them denote fits through them. ξ_+ and ξ_- obtained from fits and the fit expressions are shown inside the insets. While the main panels correspond to $[Bmim]^+$, insets represent $[PF_6]^-$.

Keeping in mind the system size dependence and ensemble sensitivity of ξ (and other associated approximations),[67] these length-scales of approximately one ion diameter should serve only as a rough estimate that are probably involved in producing the slower solvation timescale in ILs. These estimates, however, follow the expected qualitative trend as ξ decreases upon increasing temperature, suggesting reduction of dynamic heterogeneity length-scale at higher temperature with concomitant shortening of the peak heterogeneity timescale. At temperatures lower than ~300 K, this length-scale (correlating slowly moving particles) may further grow and produce even slower cooperative dynamics. This may explain the presence of slower dynamics with timescale in tens of nanoseconds in the time-resolved fluorescence measurements[19] of several ILs at temperatures below 300 K.

5.3.2 Temperature Dependent Solvation Response in [Bmim][PF_6]: Reflection of DH Timescales in Simulated Slow Solvation

Fig. 5.7 presents solvation response functions simulated using NPT ensemble for C153 in [Bmim][PF_6] at 298 K and 450 K along with the tri-exponential fits. The relevant fit parameters are summarized in Table 2.

Table 5.2: Tri-exponential fit parameters required to describe the simulated total solvation response functions, $S(t)$, for C153 in [Bmim][PF_6] at 298 K and 450 K

$S(t)$ [a]	a_1	τ_1 (ps)	a_2	τ_2 (ps)	a_3	τ_3 (ns)	$\langle\tau_s\rangle$ (ns)
298 K	0.66	0.22	0.07	89	0.27	11.34	3.1
450 K	0.80	0.22	0.09	4	0.11	0.07	0.01

a) Total $S(t)$ contains contributions from both cation and anion.

Note the solvation response functions shown here are the normalized equilibrium fluctuating energy autocorrelation functions defined as,[35] $C(t) = \langle \delta\Delta E_{sol}(t)\delta\Delta E_{sol}(0)\rangle \Big/ \langle |\delta\Delta E_{sol}(0)|^2 \rangle$, with $\langle\ \rangle$ denoting averaging over solvent configurations with solute either in the ground ('0') or in the excited ('1') states. This, under the assumption of solvent response being linear to solute perturbation,[91-93] is equivalent to the non-equilibrium solvation response function, $S(t) = \left[\Delta\bar{E}_{sol}(t) - \Delta\bar{E}_{sol}(\infty)\right] \Big/ \left[\Delta\bar{E}_{sol}(0) - \Delta\bar{E}_{sol}(\infty)\right]$. $\Delta\bar{E}_{sol}(t)$ here represents the solvation energy averaged over non-equilibrium trajectories and is given by the difference (Δ) in the time-dependent solute-solvent interaction energies (U_x, x =1 and 0) as follows, $\Delta E_{sol}(t) = U_1(t) - U_0(t)$. $\delta\Delta E_{sol}(t) = \Delta E_{sol}(t) - \langle \Delta E_{sol} \rangle$. In the present simulations, the equilibrium solvent configurations in presence of the solute in its ground state have been used in calculating the interaction energy between the excited solute and the solvent molecules. The simulated decays have started from 100 fs as the relevant solvent trajectories were saved after employing the same time interval. The decays shown here represent the relaxations of total solvation energy at these temperatures due to interaction of the solute with both the ions, $[Bmim]^+$ and $[PF_6]^-$. The average solvation times ($\langle \tau_s \rangle$) have been obtained from fitted amplitudes (a_i) and time constants (τ_i) as follows, $\langle \tau_s \rangle = \sum_i a_i \tau_i$, with $\sum_i a_i = 1$.

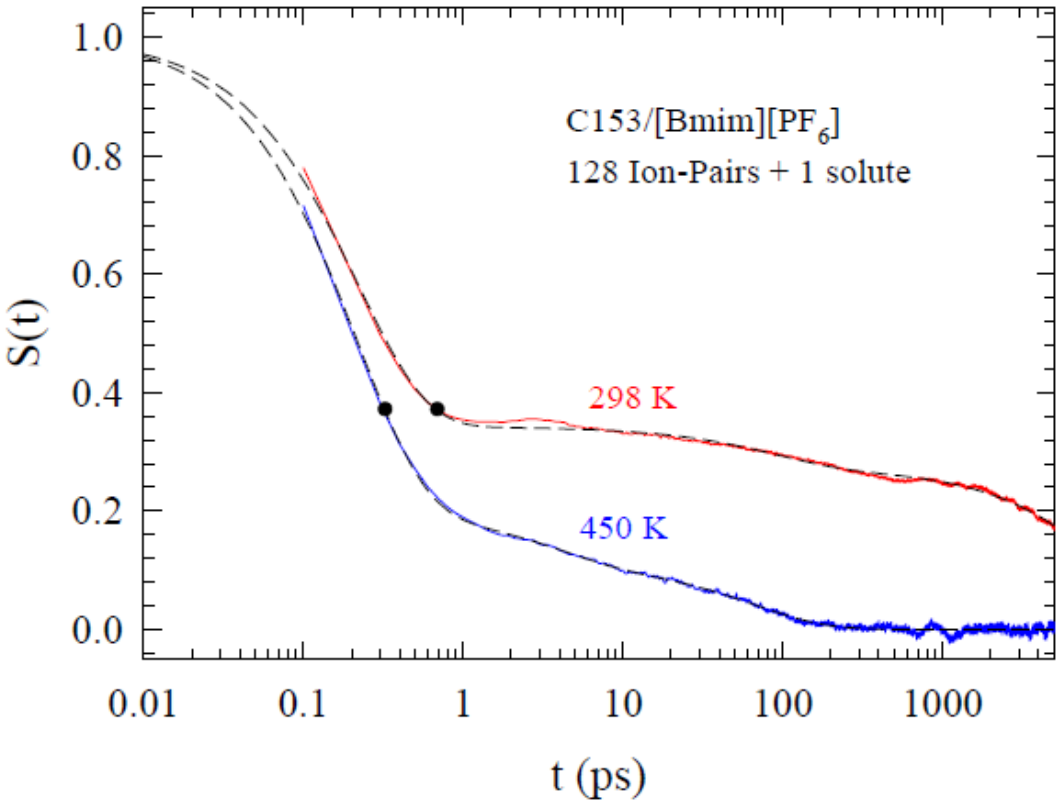

Figure. 5.7: Comparison of total solvation response function, $S(t)$, in [Bmim][PF_6] at 298 K and 450 K, simulated using single C153 dissolved in 128 pairs of $[Bmim]^+$ and $[PF_6]^-$. Tri-exponential fits through the simulated curves are shown by dashed lines. Bullets represent the $1/e$ decay points.

It is evident from Fig. 5.7 that the simulated response at 298 K spreads over sub-picosecond to nanosecond regime and is much slower than that at 450 K. Note in Table 5.2 that $\langle \tau_s \rangle$ at 298 K is slower by a factor of ~400 than that at 450 K. This is in good agreement with the temperature dependence of $\langle \tau_s \rangle$ observed earlier[35] in simulations of solvation dynamics in model [Bmim][PF_6]. This factor of ~400 arises almost entirely from the temperature effects on the slowest solvation component since $(a_3 \tau_3)_{298K} / (a_3 \tau_3)_{450K} \approx 400$. In addition, both the simulated decays are characterized by a dominating (~70-80%) ultrafast component with a time constant of ~200 fs which does not show any temperature dependence. This temperature insensitivity of the

ultrafast time constant has also been found in earlier simulations.[35] However, such a large amplitude (~70%) for the ultrafast component with C153 solvation in [Bmim][PF_6] around room temperature has neither been observed in simulations[35,94] nor in measurements that detect complete response.[95] These simulations[35,94] indicate ultrafast Gaussian time constant in ~200-300 fs range but with varying amplitudes – ~10% in one study[94] and ~45% in the other.[35] In comparison, complete dynamic Stokes shift measurements of C153 in [Bmim][PF_6] at ~293 K[95] report an ultrafast component with amplitude of ~25-40% that decays with a time constant of ~200-300 fs. Three pulse photon echo peak shift (3PEPS) measurements[96] using oxazine 4 in [Bmim][PF_6] have revealed an ultrafast time constant of ~150 ps, which a subsequent theoretical work[9] have argued to arise from solvation energy relaxation due to solute-IL non-dipolar interactions, contributing ~90% to the total calculated response function. Therefore, the ultrafast time constant found in the present simulations are in good agreement with the existing experimental[95] and simulation results.[35,94] Interestingly, several simulation studies carried out previously have reported sub-picosecond ultrafast component of ~70-80% in [Dmim][Cl] at 425 K,[88] in [Dmim][PF_6] at 450 K,[89] and in [Emim][PF_6] and [Emim][Cl] in the temperature range 350-500 K.[97] All these results probably suggest that an ultrafast component with amplitude of ~70-80% as found here is not quite unlikely in simulations of ILs that contain alkylimidazolium cations.

A new and more intriguing aspect in Fig. 5.7 is the emergence of a slow solvation component (~30%) with a time constant of ~10 ns at 298 K. Such a slow timescale has not been observed before in both experiments and simulations although several early dynamic Stokes shift measurements (performed using ~50 ps temporal resolution)[98-101] have indicated presence of a time constant in ~1- 4 ns range that accounts for ~30-70% of the total solvation response. Interestingly, a slow time constant of ~2.5 ns with ~20% amplitude emerges for [Bmim][PF_6] when the full solvation response from complete measurements is forced to fit to a four-exponential function of time (see Fig. C3, Appendix C[81]). Interestingly, such a slow time constant is indeed supported by DH timescales, τ_{NNG} and t_4^{max}, which are in the 2 - 4 ns regime. At 450 K, the slowest solvation time constant (~70 ps) also corroborates well with the values of τ_{NNG} (~80-150 ps) and t_4^{max}(~100-200 ps) for these ions. Moreover, previous simulations have

suggested a slow time constant of ~70 ps for solvation dynamics in [Dmim][Cl] at 425 K,[88] and predicted a time constant of ~100 ps for the long-time decay of solvation friction in [Emim][Cl] at 400 K.[90] All these similarities between DH timescales and long-time solvation rates appear to strongly support the conjecture that slower solvation in an IL is sustained by its own DH timescales and thus its occurrence is only natural.

We would, however, would like to mention here that the slowest time constant (~11 ns) at 298 K is ~3 times slower than the slowest of the t_4^{max} values for these ions (~4 ns for $[PF_6]^-$) at this temperature. This discrepancy may arise from a variety of reasons that include (i) inaccuracy in the description of IL interaction potential, (ii) insufficiency in system size and simulation run-time[48] and (iii) influence of solute on IL dynamics. The first of the reasons may have a limited validity as the interaction potential for IL used here has been found earlier[13] to produce IL viscosity and ion diffusion coefficients at ~298 K that agree well to those from experiments. Effects of system size and run-time on solvation energy relaxation have been investigated after considering 128 and 256 ion pairs (plus one C153 molecule in each case) in NPT ensemble at 298 K and allowing a production run of 30 ns. Results shown in Fig. C4 (Appendix C)[81] suggest a weak dependence on system size but indicates a stronger effect of run-time on the slower component of the solvation energy relaxation. More specifically, tri-exponential fits to these 30 ns data suggest these response are composed of a dominating (~80%) ultrafast component with ~200 fs time constant, and two slower components (~10% each) with time constants in ~20-30 ps and ~ 0.5-1 ns regime. Note here that a relatively shorter run-time produces a slow solvation time constant comparable to that reported in experiments[95] and differs significantly from the long time rate predicted by the 100 ns simulation (see Fig. 5.7). This discrepancy stresses once more on the importance of performing simulations of larger systems with longer duration[48] for obtaining correct descriptions of collective dynamics as envisaged here. A comparison between solvation responses obtained from our representative simulations (results not shown) with and without solute motions (both translation and rotation) indicates somewhat slower relaxation for dynamically frozen solute, a result in qualitative agreement with earlier theoretical prediction[55] and subsequent simulation observation.[35] Unfortunately, modification of heterogeneity timescales of neat IL due to the presence of a solute has not been investigated yet and thus it is not certain whether the numerical difference

between τ_{NNG} and t_4^{max}(~2 - 4 ns) , and the slowest solvation timescale (~11 ns) can be attributed to the solute's influence on ion displacement distribution particularly at longer times. This warrants further study.

5.4 Conclusion

In brief, the present chapter conjectures that the slow nanosecond solvation component in ILs originates from the dynamic heterogeneity of these media, and thus viscosity decoupling of long-time solvation rate is natural. Our simulated single ion displacement distribution for $[Bmim]^+$ suggests ion hopping in the timescale of structural relaxation, and the hopping length-scale ($\sim 0.5\sigma_+$) has been found to agree well with the relevant experimental estimate. Simulated peak times of the four-point dynamic susceptibility exhibit a close resemblance to the $1/e$ times associated with the relaxations of overlap function, and are almost doubly slower than the DH timescales produced by the slow moving ions. The four-point DH timescales are in 2-4 ns regime at room temperature and thus support the emergence of a nanosecond or even slower solvation component in RTILs. The estimated maximum dynamic correlation length has been found to be about one ion diameter ($\sim 1.0\sigma$) which exhibits correct temperature dependence, suggesting presence of larger correlation length at lower temperature forcing IL dynamics to be much slower. The simulated solvation response at 298 K for $[Bmim][PF_6]$ reports a 10 ns solvation component of ~30% amplitude which has not been observed before. This has been explained in terms of four-point DH timescales of the ions constituting the IL at that temperature. At 450 K, the long-time solvation rate agree well with the previous simulation results at similar temperature for ILs possessing alkylimidazolium cations, and corroborates well with the corresponding DH timescales.

Although this is a first study exploring the connection between the DH timescales of a neat IL and the solvation rate for a dissolved dipolar probe in the same IL, there exist several simulations that investigated DH of neat IL at different temperatures via following the non-Gaussian behaviour of van Hove correlation function. However, there exists no study that has examined the modification of DH in presence of a solute.

Electrostatic interaction between solute and ions is expected to elongate further the slow DH timescales (for example, τ_{NNG} and t_4^{max}) arising from ion displacements that are smaller than the Gaussian estimates. Consequently, simulated slow solvation timescale would show improved agreements with τ_{NNG} and t_4^{max}. In addition, the role of orientational DH should also be investigated as slow rotation of a dipolar ion (in this case the cation) can have important bearing on the timescale of fluorescence spectral shifts. It is intriguing that no experiments have so far reported slow solvation timescales at room temperature that is as long as 10 ns. The difficulty for detecting such a slow component in dynamic Stokes shift measurements may be associated with a very low signal-to-noise ratio at long-time. Therefore, the debate whether the predicted 10 ns solvation component in ILs is a simulation artifact or it really exists and can be detected in suitable measurements need be resolved. Composition dependence of dynamic heterogeneity in binary mixtures of ILs with common dipolar solvents would be interesting as it would provide a window to observe how slow timescales becomes faster upon successive addition of dipolar solvent in an IL. Results from our initial simulation study of aqueous binary mixtures of 1-octyl-3-methyl-imidazolium tetrafluoroborate is presented in Addendum I (end of the thesis) suggest dramatic effects of added solvent on heterogeneity timescales. It would be interesting to explore how spatial heterogeneity and dynamic correlation length in IL grows upon successive lowering of temperature from ~300 K down to a temperature a few percent above its T_g and how relaxation dynamics responds to the associated changes. Temperature transferability of interaction potential for IL molecules coupled with the necessity of simulating very large systems for significantly longer duration makes such a study highly non-trivial. However, increasing availability of extremely fast computing facilities in conjunction with controlled approximations on the temperature dependence of interaction potential may enable one to study this challenging problem and help building, at least, a qualitatively correct understanding of interconnection between structure and dynamics of these Coulomb fluids.

References:

1. A. Samanta, J. Phys. Chem. B **110**, 13704 (2006).
2. X.-X. Zhang, M. Liang, J. Hunger, R. Buchner, and M. Maroncelli, J. Phys. Chem. B. **117**, 15356 (2013).
3. M. Liang, X.-X. Zhang, A. Kaintz, N. P. Ernsting, and M. Maroncelli, J. Phys. Chem. B. **118**, 1340 (2014).
4. S. Daschakraborty and R. Biswas, J. Phys. Chem. B. **118**, 1327 (2014).
5. H. K. Kashyap and R. Biswas, J. Phys. Chem. B. **112**, 12431 (2008).
6. H. K. Kashyap and R. Biswas, J. Phys. Chem. B. **114**, 254 (2010).
7. H. K. Kashyap and R. Biswas, J. Phys. Chem. B. **114**, 16811 (2010).
8. S. Daschakraborty, T. Pal, and R. Biswas, J. Chem. Phys. **139**, 164503 (2013).
9. S. Daschakraborty and R. Biswas, J. Chem. Phys. **137**, 114501 (2012).
10. S. Daschakraborty and R. Biswas, J. Phys. Chem. B. **115**, 4011 (2011).
11. S. Daschakraborty and R. Biswas, J. Chem. Phys. **140**, 014504 (2014).
12. A. Rahman, Phys. Rev. **136**, 405 (1964).
13. T. Pal and R. Biswas, Theor. Chem. Acc. **132**,1348 (2013)
14. E. Flenner and G. Szamel, Phys. Rev. E. **72**, 011205 (2005).
15. K. Kim and S. Saito, J. Chem. Phys. **133**, 044511 (2010).
16. C. Dasgupta, A. V. Indrani, S. Ramaswamy, and M. K. Phani, Europhys. Lett. **15**, 307, (1991); [Addendum: Europhys. Lett. **15**, 467, (1991)].
17. S. C. Glotzer, J. Non-Cryst. Solids, **274**, 342 (2000).
18. N. Lacevic, F. W. Starr, T. B. Schroder, and S. C. Glotzer, J. Chem. Phys. **119**, 7372 (2003).
19. A. M. Funston, T. A. Fadeeva, J. F. Wishart, and E. W. Castner, Jr., J. Phys. Chem. B. **111**, 4963 (2007).
20. O. Yamamuro, T. Yamada, M. Kofu, M. Nakakoshi, and M. Nagao, J. Chem. Phys. **135**, 054508 (2011).
21. A. Triolo, O. Russina, V. Arrighi, F. Juranyi, S. Janssen, and C. M. Gordon, J. Chem. Phys. **119**, 8549 (2003).
22. A. Triolo, O. Russina, C. Hardacre, M. Nieuwenhuyzen, M. A. Gonzalez, and H. Grimm, J. Phys. Chem. B **109**, 22061 (2005).
23. A. Rivera and E. A. Rossler, Phys. Rev. B **73**, 212201 (2006).

24. A. Rivera, A. Brodin, A. Pugachev, and E. A. Rossler, J. Chem. Phys. **126**, 114503 (2007).
25. T. I. Morrow and E. J. Maginn, J. Phys. Chem. B **106**, 12807 (2002).
26. J. R. Sangoro, C. Iacob, S. Naumov, R. Valiullin, H. Rexhausen, J. Hunger, R. Buchner, V. Strehmel, J. Kärger, and F. Kremer, Soft Matter **7**, 1678 (2011).
27. M. D. Ediger, Annu. Rev. Phys. Chem. **51**, 99 (2000).
28. B. Guchhait, S. Das, S. Daschakraborty, and R. Biswas, J. Chem. Phys. **140**, 104514 (2014).
29. B. Guchhait, S. Daschakraborty, and R. Biswas, J. Chem. Phys. **136**, 174503 (2012).
30. (a) A. Das, S. Das, and R. Biswas, Chem. Phys. Lett. **581**, 47 (2013); (b) T. Pal and R. Biswas, Chem. Phys. Lett. **517**, 180 (2011).
31. B. Guchhait, H. A. R. Gazi, H. K. Kashyap, and R. Biswas, J. Phys. Chem. B **114**, 5066 (2010).
32. M. Kofu, M. Nagao, T. Ueki, Y. Kitazawa, Y. Nakamura, S. Sawamura, M. Watanabe, and O. Yamamuro, J. Phys. Chem. B **117**, 2773 (2013).
33. X.-X. Zhang, M. Liang, N. P. Ernsting, and M. Maroncelli, J. Phys. Chem. B. **117**, 4291 (2013).
34. M. Schmollngruber, C. Schröder, and O. Steinhauser, J. Chem. Phys. **138**, 204504 (2013).
35. D. Roy and M. Maroncelli, J. Phys. Chem. B. **116**, 5951 (2012).
36. Z. L. Terranova and S. A. Corcelli, J. Phys. Chem. B. **117**, 15659 (2013).
37. A. P. Lyubartsev and A. Laaksonen, Comput. Phys. Commun. **128**, 565 (2000).
38. W. D. Cornell, P. Cieplak, C. I. Bayly, I. R. Gould, K. M. Merz, D. M. Ferguson, D. C. Spellmeyer, T. Fox, J. W. Caldwell, and P. A. Kollman, J. Am. Chem. Soc. **117**, 5179 (1995).
39. Z. Liu, S. Huang, and W. Wang, J. Phys. Chem. B. **108**, 12978 (2004).
40. M. P. Allen and D. J. Tildesley, *Computer Simulations of Liquids* (Oxford University Press, New York, 1987).
41. P. V. Kumar and M. Maroncelli, J. Chem. Phys. **103**, 3038 (1995).
42. S. Nose, J. Chem. Phys. **81**, 511 (1984).
43. W. G. Hoover, Phys. Rev. A **31**, 1695 (1985).

44. G. J. Martyna, M. E. Tuckerman, D. J. Tobias, and M. Klein, Mol. Phys. **87**, 1117 (1996).
45. G. J. Martyna, M. Klein, and M. E. Tuckerman, J. Chem. Phys. **97**, 2635 (1992).
46. H. Tokuda, K. Hayamizu, K. Ishii, A. B. H. Susan, and M. Watanabe, J. Phys. Chem. B **108**, 16593 (2004).
47. Z. Liu, S. Huang, and W. Wang, Phys. Chem. Chem. Phys. **8**, 1096 (2006).
48. S. Gabl, C. Schröder, and O. Steinhauser, J. Chem. Phys. **137**, 094501 (2012).
49. Z. Hu and C. J. Margulis, J. Phys. Chem. B **111**, 4705 (2007).
50. C. Rey-Castro and L. F. Vega, J. Phys. Chem. B **110**, 14426 (2006).
51. J. Pićalek and J. Kolafa, J. Mol. Liq. **134**, 29 (2007).
52. A. Bagno, F. D'Amico, and G. Saielli, J. Mol. Liq. **131-132**, 17 (2007).
53. D. Roy, N. Patel, S. Conte, and M. Maroncelli, J. Phys. Chem. B **114**, 8410 (2010).
54. O. Borodin, J. Phys. Chem. B **113**, 11463 (2009).
55. H. K. Kashyap and R. Biswas, Ind. J. Chem. 49A, 685, 2010.
56. B. Bagchi and R. Biswas, Adv. Chem. Phys. **109**, 207 (1999).
57. R. Biswas and B. Bagchi, J. Phys. Chem. **100**, 1238 (1996).
58. B. Bagchi, D. W. Oxtoby, and G. R. Fleming, Chem. Phys. **86**, 257 (1984).
59. P. V. Kumar and M. Maroncelli, J. Chem. Phys. 103, 3038 (1995).
60. M. Sajadi, M. Weinberger, H.-A. Wagenknecht, and N. P. Ernsting, Phys. Chem. Chem. Phys. **13**, 17768 (2011).
61. D. R. Reichman, E. Rabani, and P. L. Geissler, J. Phys. Chem. B **109**, 14654 (2005).
62. G. Szamel and E. Flenner, Europhys. Lett. **67**, 779 (2004).
63. E. Flenner and G. Szamel, Phys. Rev. E **70**, 052501 (2004).
64. J.-P. Hansen, Physica A **201**, 138 (1993).
65. A. M. Puertas, M. Fuchs, and M. E. Cates, J. Chem. Phys. **121**, 2813 (2004).
66. J. P. Hansen and I. R. McDonald, *Theory of Simple Liquids* 3rd ed. (Academic, London, 2006).
67. C. Toninelli, M. Wyart, L. Berthier, G. Biroli, and J.-P. Bouchaud, Phys. Rev. E **71**, 041505 (2005).
68. C. Bennemann, C. Donati, J. Baschnagel, and S. C. Glotzer, Nature **399**, 246 (1999).

69. S. C. Glotzer, V. N. Novikov, and T. B. Schrøder, J. Chem. Phys. **112**, 509 (2000).
70. N. Lacevic, F. W. Starr, T. B. Schrøder, V. N. Novikov, and S. C. Glotzer, Phys. Rev. E **66**, 030101(R) (2002).
71. K. Kim and S. Saito, J. Chem. Phys. **138**, 12A506 (2013).
72. S. Franz and G. Parisi, J. Phys.: Condens. Matter **12**, 6335 (2000).
73. C. Donati, S. Franz, G. Parisi, and S. C. Glotzer, J. Non-Cryst. Solids **307**, 215 (2002).
74. L. Berthier, Phys. Rev. E **69**, 020201(R) (2004).
75. R. Yamamoto and A. Onuki, Phys. Rev. E **58**, 3515 (1998).
76. C. P. Fredlake, J. M. Crosthwaite, D. G. Hert, S. N. V. K. Aki, and J. F. Brennecke, J. Chem. Eng. Data **49**, 954 (2004).
77. W. H. Awad, J. W. Jilman, M. Nyden, R. H. Harris, T. E. Sutto, J. Callahan, P. C. Truelove, H. C. Delong, and D. M. Fox, Thermochim Acta **409**, 3 (2004).
78. J. Habasaki and K. Ngai, J. Chem. Phys. **129**,194501(2008).
79. S. S. Sarangi, W. Zhao, F. Muller-Plathe, and S. Balasubramanian, ChemPhysChem **11**, 2001 (2010).
80. Z. Hu and C. J. Margulis, Proc. Natl. Acad. Sci. USA **103**, 831 (2006).
81. See Appendix C containing a comparison of $1/e$ times for $Q(t)$ and $F_s(k\sigma \to 2\pi, t)$ decays, Fits to these decays, tri- and tetra-exponential fits to measured complete solvation response for [Bmim][PF_6] at ~293 K and the relevant fit parameters,and figure showing system size and run-time dependence of $S(t)$.
82. G. Szamel and E. Flenner, Phys. Rev. E **74**, 021507 (2006).
83. S. E. Abraham and B. Bagchi, Phys. Rev. E **78**, 051501 (2008).
84. T. Kawasaki and H. Tanaka, J. Chem. Phys. J. Phys.: Condens. Matter **23**, 194121 (2011).
85. T. Abete, A. de Candia, E. Del Gado, A. Fierro, and A. Coniglio, Phys. Rev. Lett. **98**, 088301 (2007).
86. K. Kim, K. Miyazaki, and S. Saito, Europhys. Lett. **88**, 36002 (2009).
87. K. Kim, K. Miyazaki, and S. Saito, J. Phys.: Condens. Matter **23**, 234123 (2011).

88. B. L. Bhargava and S. Balasubramanian, J. Chem. Phys. **123**, 144505 (2005).
89. I. Streeter, R. M. Lynden-Bell, and R. G. Compton, J. Phys. Chem. C **112**, 14538 (2008).
90. Y. Shim, M. Y. Choi, and J. H. Kim, J. Chem. Phys. **122**, 044511 (2005).
91. M. Maroncelli and G. R. Fleming, J. Chem. Phys. **89**, 5044 (1988).
92. A. E. Carter and J. T. Hynes, J. Chem. Phys. **94**, 5961 (1991).
93. B. B. Laird and W. H. Thompson, J. Chem. Phys. **126**, 211104 (2007).
94. M. N. Kobrak, J. Chem. Phys. **125**, 064502 **(2006**).
95. X.-X. Zhang, M. Liang, N. P. Ernsting, and M. Maroncelli, J. Phys. Chem. B. **117**, 4291 (2013).
96. M. Muramatsu, Y. Nagasawa, and H. Miyasaka, J. Phys. Chem. A **115**, 3886 (2011).
97. Y. Shim, J. Duan, M. Y. Choi, and H. J. Kim, J. Chem. Phys. **119**, 6411 (2003).
98. R. Karmakar and A. Samanta, J. Phys. Chem. A. **106**, 4447 (2002).
99. R. Karmakar and A. Samanta, J. Phys. Chem. A. **106**, 6670 (2002).
100. R. Karmakar and A. Samanta, J. Phys. Chem. A. **107**, 7340 (2003).
101. S. Saha, P. K. Mandal, and A. Samanta, Phys. Chem. Chem. Phys. **6**, 3106 (2004).

Chapter 6

Stokes Shift Dynamics in (Non-Dipolar Ionic Liquid + Dipolar Solvent) Binary Mixtures: A Semi-Molecular Theory

6.1 Introduction

Solvent reorganization dynamics is more complex in room-temperature ionic liquids (RTILs)[1-6] than in common dipolar solvents. In RTILs, longer-ranged ion-ion , ion-dipole and dipole-dipole interactions contribute to the medium dynamics and heterogeneous structure.[7-13] This heterogeneity in liquid structure profoundly influences the course and time-scales of solvation energy relaxation for a dissolved dye in RTILs.[3,14,15] The interrelationship between dynamic solvent response and reaction rate[16-18] has been one of the reasons for fuelling extensive study of Stokes shift dynamics in RTILs in the last ten years or so. However an intense debate regarding the origin of the ultrafast solvation in ILs is still continuing.[6,19,20] Binary mixtures of alkylimidazolium ILs with dipolar solvents have also been studied employing time-resolved fluorescence experiments [21-25], theory [26,27] and computer simulations.[28] Such binary mixtures are important for chemical reactions as solvent control (via dynamic and static effects) on reaction rate can be tuned rather easily through composition variation. However, the existing dynamic Stokes shift studies of (IL + dipolar solvent) binary mixtures involve only dipolar ILs, and no such measurements or simulations are available for (non-dipolar IL + dipolar solvent) binary mixtures. Recently, some preliminary results on composition dependence of probe lifetime in binary mixtures of a phosphonium IL with methanol have been reported.[29] In such a scenario, we focus on developing a semi-

molecular theory for studying solvation energy relaxation of a dissolved dipolar solute in (non-dipolar IL + common dipolar solvent) binary mixtures. For the proposed study, we have considered binary mixture of trihexyltetradecyl phosphonium chloride ($[P_{14,666}][Cl]$) and methanol (MeOH) as a representative system given in Fig 6.1. The dipolar solute used here is the well-known solvation probe, coumarin 153 (C153). This study will serve the two following purposes. First, predicted dynamics will help understanding the role played by added dipolar solvent molecules in modifying the reorganization dynamics of a non-dipolar IL. A comparison with the existing theoretical results for (dipolar IL + dipolar solvent) binary mixtures may then reveal the microscopic reasons behind the qualitatively different solvation response measured for neat dipolar and non-dipolar ILs. Second, predicted results may stimulate dynamic Stokes shift measurements for these mixtures and help gaining further understanding of the role of dipolar solvents in regulating the dynamic solvation response in systems possessing charge-charge interaction.

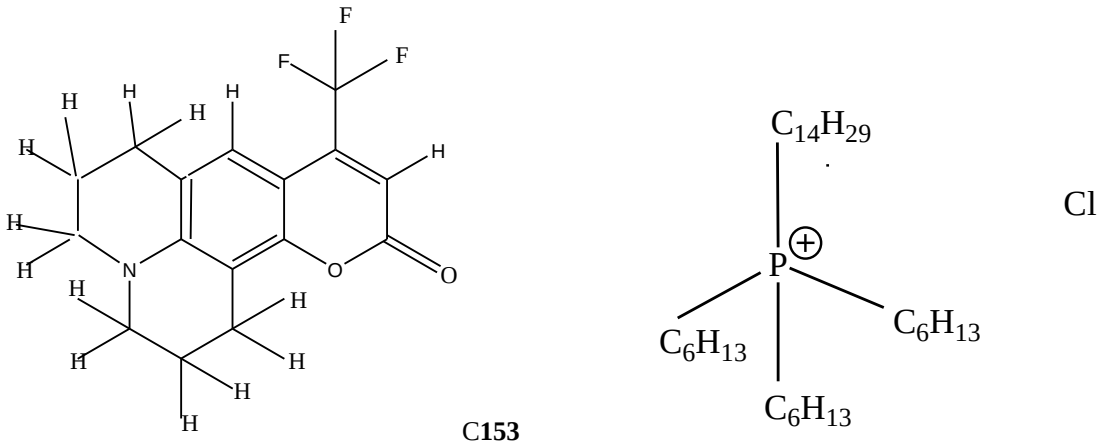

Figure 6.1. A schematic diagram of dipolar probe , Coumarin 153 (C153) and Ionic Liquid trihexyl(tetradecyl)phosphonium chloride $[P_{14,666}][Cl]$

We have already developed a semi-molecular theory for studying solvation energy relaxation for a dipolar solute in binary mixtures of imidazolium ILs with conventional

dipolar solvents and found good agreement with the relevant experimental results.[26-27] In this theory, dipolar interaction between the solute and added solvent molecules, and that between solute and dipolar ion of the IL have been counted in addition to the solute-ion dipole-ion interaction. The difference from earlier mixture work for ($[P_{14,666}][Cl]$ + MeOH) binary mixture is the absence of solute-IL dipole-dipole interaction. Therefore, the dynamic shift for binary mixtures of (non-dipolar IL + dipolar solvent) is assumed to be determined by the other two interactions. However, the dipole-dipole solute-IL interaction can still be introduced in the calculations for (non-dipolar IL + dipolar solvent) binary mixtures if the presence of ion-pairs (IPs) and their interaction with dipolar solute are accounted for.[5] Following earlier prescription,[26-27] we have performed here two sets of calculations : (i) separate medium (SM) calculations and (ii) effective medium (EM) calculations. As before, SM accounts for interactions between the same species in the binary mixture and neglects completely the cross interactions between the mixture components. EM, on the other hand, incorporates the IP interaction contribution into the calculated total dynamics effectively via combining with the added dipolar solvents.

Our previous theoretical studies on pure phosphonium ILs[5] have shown that solute-ion (dipole-ion) interaction accounts for ~75% of the measured dynamic Stokes shift, and the rest arises from solute-IP (dipole-dipole) interaction. Interestingly, formation of IP in ILs has been reflected in various studies,[31-33] and for non-dipolar ILs, ~30% of their molar concentration has been found to remain associated[31-33] as IPs. The contribution to dynamics of the IPs for non-dipolar ILs would be non-negligible, and for binary mixtures with dipolar solvent, such a contribution combined with that from added solvent would be substantial. One can in fact expect the dominance of solute-medium dipolar interaction even in IL-rich region for this binary mixture, making it qualitatively comparable to the findings for (dipolar IL + dipolar solvent) binary mixtures. However, the slower solvation timescale would still be governed by the centre-of-mass movements of the ions present in such mixtures.[34] The effects of IL volume on the composition dependent dynamic shift magnitude have been explored, and a non-monotonic composition dependence predicted. This is opposite to what has been found recently for binary mixtures containing imidazolium ILs.[22,27]

6.2 Theory and Calculation Details

6.2.1 Separate Medium (SM) Treatment

Here we follow closely the earlier prescription[26,27,34] for deriving an approximate microscopic expression for the fluctuating total solvation energy for a mobile dipolar solute in a (non-dipolar IL + dipolar solvent) binary mixture using the classical density functional theory. In this approach first the interaction part of the free energy functional is expressed in terms of position ($\mathbf{r}$) dependent ion densities (from IL), position and orientation ($\mathbf{\Omega}$)dependent added dipolar solvent density, and position and orientation dependent dipolar solute density.[35-37] The condition that the functional derivative of this free energy functional with respect to the solute density would be zero at equilibrium provides the expression for the average solvation energy.[35,38] Subsequent extension to time-domain then provides the following expression for the time dependent fluctuating solvation energy:[35]

$$\delta E_{total}(r,\Omega;t) = -k_B T\rho_s(r,\Omega;t)\left[\int dr' d\Omega' c_{sp}(r,\Omega;r',\Omega')\delta\rho_p(r',\Omega';t) + \sum_{\alpha=1}^{2}\int dr' c_{s\alpha}(r,\Omega;r')\delta n_\alpha(r';t)\right]$$
$$= \delta E_{sp}(\mathbf{r},\mathbf{\Omega},t) + \delta E_{si}(\mathbf{r},\mathbf{\Omega},t), \qquad (6.1)$$

where $\delta\rho_p(\mathbf{r},\mathbf{\Omega},t)$ denote the position, orientation and time dependent density of the dipolar solvent molecules added in the mixture, $\delta n_\alpha(\mathbf{r},t)$ the position and time dependent density of the ion of species α (cation or anion), and $\rho_s(\mathbf{r},\mathbf{\Omega},t)$ the dipolar solute density. $c_{sp}(\mathbf{r},\mathbf{\Omega})$ and $c_{s\alpha}(\mathbf{r},\mathbf{\Omega})$ represent the position and orientation dependent static direct correlation functions between the dipolar solute and the added dipolar solvent molecules, and between the dipolar solute and non-polar charged ions dissociated from IL, respectively. k_BT is the Boltzmann constant times the absolute temperature. Note while writing Eq. 6.1 the non-dipolar IL is assumed to be fully dissociated in the binary mixture, and the solute concentration extremely dilute ($\rho_s \to 0$). The dipole-dipole (δE_{sd}) and dipole-ion (δE_{si}) interaction contributions to total solvation energy are given by

$$\delta E_{sp}(\mathbf{r},\mathbf{\Omega},t) = -k_B T\rho_s(\mathbf{r},\mathbf{\Omega},t)\int d\mathbf{r}'\, d\mathbf{\Omega}'\, c_{sp}(\mathbf{r},\mathbf{\Omega};\mathbf{r}',\mathbf{\Omega}')\,\delta\rho_p(\mathbf{r}',\mathbf{\Omega}',t), \qquad (6.2)$$

and

$$\delta E_{si}(\mathbf{r},\mathbf{\Omega},\mathrm{t}) = -\,\mathrm{k_B}T\rho_s(r,\Omega,\mathrm{t})\sum_{\alpha=1}^{2}\int d\mathbf{r}'\, c_{s\alpha}(\mathbf{r},\mathbf{\Omega};\mathbf{r}')\,\delta \mathrm{n}_{\alpha}(\mathbf{r}',\mathrm{t}). \qquad (6.3)$$

Note Eq. 6.1 does not contain the contribution from interaction between dipolar solute and dipolar IL ions and thus differs from the equivalent expression derived for a dipolar solute in (dipolar IL + dipolar solvent) mixture.[27]

The total (fluctuating) solvation energy auto-correlation function then takes the following form

$$\left\langle \delta \mathrm{E}_{\mathrm{total}}(\mathrm{t})\delta \mathrm{E}_{\mathrm{total}}(\mathrm{t}')\right\rangle = <\delta \mathrm{E}_{\mathrm{sp}}(\mathrm{t})\delta \mathrm{E}_{\mathrm{sp}}(\mathrm{t}')> + <\delta \mathrm{E}_{\mathrm{si}}(\mathrm{t})\delta \mathrm{E}_{\mathrm{si}}(\mathrm{t}')> = \mathrm{C}_{\mathrm{sp}}(\mathrm{t}) + \mathrm{C}_{\mathrm{si}}(\mathrm{t}) = \mathrm{C}_{\mathrm{E}}(\mathrm{t})$$

, (6.4)

Eq. 6.4 has been obtained after assuming that cross-correlation between dipole-dipole and dipole-ion interaction contributions does not survive because of the density fluctuation timescales involved with them are widely different. Such an approximation, although not expected to work for systems with longer-ranged interactions where ion and dipole density fluctuations are adiabatically coupled, has been found to provide semi-quantitative description of experimental Stokes shift dynamics for neat ILs[5,6,30,39] and (dipolar IL + dipolar solvent) binary mixtures,[27] and slow dielectric relaxation time constants[40] measured for several neat imidazolium ILs

Subsequently, the normalized total solvation energy autocorrelation function is written as,

$$\mathrm{S}_{\mathrm{E}}(\mathrm{t}) = \frac{\mathrm{C}_{\mathrm{E}}(\mathrm{t})}{\mathrm{C}_{\mathrm{E}}(0)} = \frac{\mathrm{C}_{\mathrm{sp}}(\mathrm{t}=0)\mathrm{S}_{\mathrm{sp}}(\mathrm{t})}{\mathrm{C}_{\mathrm{sp}}(\mathrm{t}=0)+\mathrm{C}_{\mathrm{si}}(\mathrm{t}=0)} + \frac{\mathrm{C}_{\mathrm{si}}(\mathrm{t}=0)\mathrm{S}_{\mathrm{si}}(\mathrm{t})}{\mathrm{C}_{\mathrm{sp}}(\mathrm{t}=0)+\mathrm{C}_{\mathrm{si}}(\mathrm{t}=0)}, \qquad (6.5)$$

where $\mathrm{S}_{\mathrm{sp}}(\mathrm{t}) = \mathrm{C}_{\mathrm{sp}}(\mathrm{t})/\mathrm{C}_{\mathrm{sp}}(\mathrm{t}=0)$ and $\mathrm{S}_{\mathrm{si}}(\mathrm{t}) = \mathrm{C}_{\mathrm{si}}(\mathrm{t})/\mathrm{C}_{\mathrm{si}}(\mathrm{t}=0)$. As before, the total dynamic Stokes shift is predicted as,[26-27]

$$\sqrt{\mathrm{C}_{\mathrm{E}}(\mathrm{t}=0)} = \sqrt{\mathrm{C}_{\mathrm{sp}}(\mathrm{t}=0)} + \sqrt{\mathrm{C}_{\mathrm{si}}(\mathrm{t}=0)}\,. \qquad (6.6)$$

The microscopic expressions for the individual (normalized) solvation energy autocorrelation function are given as follows[27]

$$S_{sp}(t) = \frac{C_{sp}(t)}{C_{sp}(t=0)} = \frac{A\int_0^\infty dk k^2 S^{10}_{solute}(k,t)\left|c^{10}_{sp}(k)\right|^2 S^{10}_{p}(k,t) + 2A\int_0^\infty dk k^2 S^{11}_{solute}(k,t)\left|c^{11}_{sp}(k)\right|^2 S^{11}_{p}(k,t)}{A\int_0^\infty dk k^2 S^{10}_{solute}(k)\left|c^{10}_{sp}(k)\right|^2 S^{10}_{p}(k) + 2A\int_0^\infty dk k^2 S^{11}_{solute}(k)\left|c^{11}_{sp}(k)\right|^2 S^{11}_{p}(k)}, \quad (6.7)$$

And

$$S_{si}(t) = \frac{C_{si}(t)}{C_{si}(t=0)} = \frac{B\sum_{\alpha,\beta}\sqrt{n^0_\alpha n^0_\beta}\int_0^\infty dk k^2 S^{10}_{solute}(k,t) c^{10}_{s\alpha}(k) c^{10}_{s\beta}(-k) S^{ion}_{\alpha\beta}(k,t)}{B\sum_{\alpha,\beta}\sqrt{n^0_\alpha n^0_\beta}\int_0^\infty dk k^2 S^{10}_{solute}(k) c^{10}_{s\alpha}(k) c^{10}_{s\beta}(-k) S^{ion}_{\alpha\beta}(k)}, \quad (6.8)$$

where $A = 2\rho^0_d k_B T/(2\pi)^2$ and $B = 2(k_B T/2\pi)^2$.

Note $c^{lm}_{sp}(k)$ (l,m=1,0 or 1,1) in Eq. 6.7 denotes the Fourier transform of the (*l*,*m*) component of the static direct correlation functions between the solute and added dipolar solvent molecules, and have been obtained from the mean spherical approximation (MSA) theory.[41] $S^{lm}_p(k,t)$ denotes the orientational dynamic structure factor of the added dipolar solvent, and has been obtained by using the experimental dielectric relaxation data ($\varepsilon(\omega)$) in an approximate method employed earlier for predicting Stokes shift dynamics in neat dipolar solvents,[35,42-44] ILs,[45-47] and (dipolar IL + dipolar solvent) binary mixtures.[36,37] The relevant microscopic expressions are given below:[35]

$$S^{10}_p(k,t) = \frac{1}{4\pi 3Y}\left[1 - \frac{1}{\varepsilon_L(k)}\right] L^{-1}[z + \Sigma_{10}(k,\omega)]^{-1}, \quad (6.9)$$

and, $$S^{11}_p(k,t) = \frac{1}{4\pi 3Y}[\varepsilon_T(k) - 1] L^{-1}[z + \Sigma_{11}(k,\omega)]^{-1}, \quad (6.10)$$

where $3Y = (4\pi/3k_B T)\mu^2\rho_p$ with μ and ρ_p being the dipole moment and density of the added dipolar solvent. $[1 - \varepsilon^{-1}_L(k)] = 3Y f^{-1}_{110}(k)$, and $[\varepsilon_T(k) - 1] = 3Y f^{-1}_{111}(k)$ with $f_{llm}(k) = 1 - (\rho_p/4\pi)(-1)^m c(llm,k)$. L^{-1} represents Laplace inversion.

The wavenumber and frequency (ω) dependent generalized rate of the medium polarization relaxation, $\Sigma_{lm}(k,\omega)$, contains two frictional kernels - rotational ($\Gamma_R(k,\omega)$) and translational ($\Gamma_T(k,\omega)$). $\Gamma_R(k,\omega)$ has been obtained from experimental $\varepsilon(\omega)$ of neat dipolar solvent, and $\Gamma_T(k,\omega)$ from solution viscosity (η) via approximate relations.[27,35] The solute dynamic structure factor, $S_{solute}^{lm}(k,t)$, has been calculated by using the relation [27,35]

$$S_{solute}^{lm}(k,t) = \frac{1}{4\pi}\exp\left[-\left(l(l+1)D_R^s + k^2 D_T^s\right)t\right], \tag{6.11}$$

where D_R^s and D_T^s are the rotational and translational diffusion coefficients of the solute, determined via hydrodynamics using the stick boundary condition and η. $c_{s\alpha}^{10}(k)$, the longitudinal component of the wave number dependent static structural correlations between the dipolar solute and an ion of type α, is given by[27]

$$c_{s\alpha}^{10}(k) = -\sqrt{\frac{4\pi}{3}}\left(\frac{4\pi i\mu_1 q_\alpha}{k_B T\varepsilon_0 k}\right)\frac{\sin(kr_c)}{kr_c}, \tag{6.12}$$

where μ_1 is the excited state dipole-moment of the dissolved dipolar solute, q_α the charge on α^{th} type ion, and r_c the distance of the closest approach between the solute dipole and the ionic species. Diffusive form for $S_{\alpha\beta}^{ion}(k,t)$ has been used and the relevant details are provided in Ref. 30.

If now one allows for an additional contribution to total fluctuating solvation energy due to dipole-dipole interaction between the dipolar solute and dipolar IPs (from IL),[5,31-33] the expression for $\delta E_{total}(t)$ becomes

$$\begin{aligned}\Delta E_{total}(\mathbf{r},\boldsymbol{\Omega};t) &= -k_B T\rho_s(\mathbf{r},\boldsymbol{\Omega};t)\left[\begin{array}{l}\int d\mathbf{r}'d\boldsymbol{\Omega}' c_{sp}(\mathbf{r},\boldsymbol{\Omega};\mathbf{r}',\boldsymbol{\Omega}')\delta\rho_p(\mathbf{r}',\boldsymbol{\Omega}';t)\\ +\int d\mathbf{r}'d\boldsymbol{\Omega}' c_{sip}(\mathbf{r},\boldsymbol{\Omega};\mathbf{r}',\boldsymbol{\Omega}')\delta\rho_{ip}(\mathbf{r}',\boldsymbol{\Omega}';t) + \sum_{\alpha=1}^{2}\int dr' c_{s\alpha}(\mathbf{r},\boldsymbol{\Omega};\mathbf{r}')\delta n_\alpha(\mathbf{r}';t)\end{array}\right]\\ &= \delta E_{sp}(\mathbf{r},\boldsymbol{\Omega};t) + \delta E_{sip}(\mathbf{r},\boldsymbol{\Omega};t) + \delta E_{si}(\mathbf{r},\boldsymbol{\Omega};t),\end{aligned} \tag{6.13}$$

where $\delta\rho_{ip}$ denotes the fluctuating IP density and c_{sip} the static orientational correlation function between the dipolar solute and IPs. $\delta E_{sip}(\mathbf{r}, \mathbf{\Omega}, t)$ This has been obtained by following the method used for determining c_{sp} but with using proper number density and dipole moment for IPs. Employing once again the argument of widely different density fluctuation timescales for different species, the following expression for the normalized total response function has been derived

$$S_E(t) = \frac{C_E(t)}{C_E(0)} = \frac{C_{sp}(t=0)S_{sp}(t)}{C_{sp}(t=0)+C_{si}(t=0)+C_{sip}(t=0)} + \frac{C_{sip}(t=0)S_{sip}(t)}{C_{sp}(t=0)+C_{si}(t=0)+C_{sip}(t=0)}$$

$$+ \frac{C_{si}(t=0)S_{si}(t)}{C_{sp}(t=0)+C_{si}(t=0)+C_{sip}(t=0)}, \qquad (6.14)$$

with $S_{sip}(t) = C_{sip}(t)/C_{sip}(t=0)$, and $C_{sip}(t) = \langle \delta E_{sip}(t)\delta E_{sip}(t=0) \rangle$. The total dynamic Stokes shift can then be evaluated as

$$\sqrt{C_E(t=0)} = \sqrt{C_{sp}(t=0)} + \sqrt{C_{si}(t=0)} + \sqrt{C_{sip}(t=0)}. \qquad (6.15)$$

Since $S_{sip}(t)$ is arising from dipole-dipole interaction, its calculation procedure remains the same as detailed for $S_{sp}(t)$.

In the absence of any experimental data, $\varepsilon(\omega)$ required for the calculations of $\Gamma_R(k,\omega)$ have been approximated as a single Debye relaxation process with time constant (τ_D) obtained via viscosity scaling of a reference τ_D. For solutions with $x_{IL} > 0$, the slowest time constant reported in experimental dielectric relaxation measurements of [Hmim][BF_4] at ~298 K[49] has been used as a reference for τ_D. Such a choice of reference IL is motivated by the fact that [Hmim][BF_4] is an IL with longest alkyl chain for which experimental $\varepsilon(\omega)$ are known. As done earlier,[5,34] a dipole moment of ~5 D has been assigned for IPs in [$P_{14,666}$][Cl], and subsequently used in MSA[41] for estimating the required static dielectric constant (ε_0). This estimated ε_0 then disperses to square of the refractive index, $n_D^2 = 2$, via a Debye relaxation time scaled by medium viscosity. Required number densities have been calculated as per the mixture

composition and supplied for obtaining the static correlations and structure factors. However, viscosity coefficients for neat systems have been used in SM calculations for all mixture compositions.

6.2.2 Effective Medium (EM) Treatment

The EM calculations for (non-dipolar IL + dipolar solvent) are motivated by the possible presence of IPs in such mixtures and their effects on Stokes shift dynamics. For deriving the necessary expressions we closely follow what we have already done for EM calculations on (dipolar IL + dipolar solvent) binary mixtures.[27] The EM treatment provides the following expression for normalized solvation response function[27]

$$S_E^{eff}(t) = \frac{C_E^{eff}(t)}{C_E^{eff}(0)} = \frac{C_{sd}^{eff}(t=0)S_{sd}^{eff}(t)}{C_{sd}^{eff}(t=0)+C_{si}^{eff}(t=0)} + \frac{C_{si}^{eff}(t=0)S_{si}^{eff}(t)}{C_{sd}^{eff}(t=0)+C_{si}^{eff}(t=0)}, \quad (6.16)$$

where $S_{sd}^{eff}(t)$ represent the effective dipole-dipole interaction contribution to total solvation energy due to the presence of both added dipolar solvent molecules and IPs. In such a treatment, the total dynamic shift can be calculated as, $\sqrt{C_E^{eff}(0)} = \sqrt{C_{sd}^{eff}(t=0)} + \sqrt{C_{si}^{eff}(t=0)}$. Considering presence of ~30% undissociated IL molecules in neat ILs, the effective diameter and dipole moment have been approximated as follows:

$$\sigma_{eff}^3 = (1-x_{IL})\sigma_p^3 + 0.3x_{IL}\sigma_{IL}^3, \quad (6.17)$$

and

$$M_{eff} = (1-x_{IL})M_P + 0.3x_{IL}M_{IL,} \quad (6.18)$$

where M_p denotes the molar mass of the added dipolar solvent and M_{IL} that of IL. For methanol, σ_{MeOH} may be equated to its collision diameter. σ_{IL} can be estimated from the ionic radii, $\sigma_{IL}^3 = \sigma_+^3 + \sigma_-^3$. Details regarding the calculations of effective reduced number density of various species are provided in the Appendix D.[48]

For ([$P_{14,666}$][Cl] + MeOH) binary mixtures, no mole-fraction dependent experimentally measured $\varepsilon(\omega)$ exists and thus calculations of effective medium dynamic structure

factor (necessary for estimation of $S_{sd}^{eff}(t)$) requires approximate method. We have obtained x_{IL} dependent ε_0 for this binary mixture by using the fit of composition dependent ε_0 measured for ([Bmim][BF_4] +H_2O) binary mixtures at ~300 K[21] and scaling the fit values by ε_0 of methanol (ε_0~32.6).[50] The estimated ε_0 then disperses to n_D^2 via a single Debye relaxation. We assume n_D^2 =2 for mixtures with $x_{IL} > 0$, and use the corresponding experimental value for neat meathanol.[50] We have estimated the required τ_Ds from the hydrodynamics by using experimental viscosity[29] of ([$P_{14,666}$][Cl] + MeOH) binary mixtures (approximating the effective dipolar species as a spherical rotor obeying the stick boundary condtion)[51] although such an attempt have led to vary large time constants (~5-20 ns) at the IL-rich region. At $x_{IL} = 1.0$, the slowest time constant obtained in experimental $\varepsilon(\omega)$ for [Hmim][BF_4][49] has been used as reference. Note the absence of suitable experimental results has forced this approximate method to obtain the necessary input parameters, and hence the predicted results are amenable to further refinement and correction. However, the theoretical framework remains valid and provides a base to analyze Stokes shift dynamics in systems as complex as binary mixtures of non-dipolar ILs with common dipolar solvents.

6.3 Numerical Results and Discussion

In this section first we present numerical results on composition dependent dynamic Stokes shift for C153 in ([$P_{14,666}$][Cl] + MeOH) binary mixtures from EM and SM calculations at 298 K. Subsequently, predicted results on solvation response function at various compositions for this binary mixture have been presented and discussed. Note composition dependent effective dipole moment values required for EM calculations have been obtained from Cavell's equation[52,53] by using the estimated composition dependent ε_0 values. In both SM and EM calculations an excited state dipole moment, μ_1 = 14 D[54] for C153 has been used.

An important aspect that warrants a brief discussion is the dipole moment for methanol (μ_{MeOH}) that should be used in the SM calculations of Stokes shift dynamics of this

mixture. If gas phase value μ_{MeOH}=1.7 D[55] is used, SM predicts a dynamic shift of 385 cm^{-1} for C153 in neat methanol. Use of simulated dipole moment, μ_{MeOH}=2.8 D,[56] for liquid methanol produces a dynamic shift of 865 cm^{-1}, which is larger than above but still smaller by a factor of ~2.7 than that (2370 cm^{-1}) observed in experiments.[54] Interestingly, if μ_{MeOH}= 4.5 D is used, SM predicts a shift of 2311 cm^{-1} and agrees better with experiments. This observation is similar to what has been noticed earlier[27] for solvent dipole moment dependence of dynamic Stokes shift magnitude of C153-like solute in water, and appears to reflect the inadequacy of a simple theory to describe dynamic Stokes shifts in hydrogen-bonded liquids. However, we have used μ_{MeOH}=2.8 D in our all SM calculations presented here because this value for methanol is supported by both simulations[56] and experiments.[57] Moreover, the focus here is on qualitative prediction of composition dependent Stokes shift dynamics in binary mixtures of a non-dipolar IL with a conventional polar solvent where quantitative comparison for a specific system becomes meaningless in the absence of any experimental results. Note here that as before[27] the SM-predicted solvation dynamics has been found to be insensitive to the value of dipole moment used in the calculations. Diameters for methanol,[44] phosphonium cation,[58] chloride anion[58] and C153[54] used are respectively as follows: 4.1 Å, 10.68 Å, 4.18 Å and 7.8 Å. Other parameters required for calculations of shift and dynamics are summarized in Tables D1 and D2 (Appendix D).[48]

Another important issue is the wavenumber ($k\sigma$) range chosen for calculating the dipole-ion (solute-ion) interaction contribution to the total Stokes shift dynamics. Our earlier study on phosphonium ILs[5] have revealed that for a dipolar solute in these non-dipolar solvents solvation energy relaxation corresponding to the nearest neighbour ($k\sigma \to 2\pi$) solvent modes possesses a timescale comparable to that reported in experiments. Following this observation we have incorporated contributions only from solvent modes with wavenumbers ranging from $k\sigma = 1$ to $k\sigma = 2\pi$ for determining the dipole-ion contribution, C_{si}. For the dipole-dipole contributions, however, the full wavenumber regime has been considered.

6.3.1 Composition Dependent Dynamic Stokes Shift: Comparison Between SM and EM Predictions

Fig. 6.2 presents the x_{IL} dependent total dynamic shift ($\Delta\nu^{t}_{tot}$) for C153 in ([$P_{14,666}$][Cl] + MeOH) binary mixture at 298 K and contributing pieces obtained from EM and SM calculations. For comparison, experimental shifts for C153 in neat methanol (x_{IL}=0)[54] and neat IL (x_{IL}=1)[59,60] are also shown along with the predicted total shifts, $\Delta\nu^{t}_{tot}$. Note that both SM and EM predictions for neat IL at 298 K are agreeing well with the experimental shifts of 1760 cm^{-1} at 331 K[60] and 1500 cm^{-1} at 343 K,[59] although for reasons already discussed predicted shift for neat methanol is much lower than that in experiments. Interestingly, both EM and SM predict linear increase of $\Delta\nu^{t}_{tot}$ with x_{IL} for mixtures in the composition range $0.2 < x_{IL} \leq 1$. This is counter-intuitive in the sense that increase of x_{IL} in ([$P_{14,666}$][Cl] + MeOH) binary mixture should lower the average dielectric constant (ε_0) of the resultant solution which, in turn, is expected to decrease the magnitude of the total dynamic Stokes shift. Such a behaviour of Stokes shift from polarity (represented loosely by ε_0) consideration is indeed observed for the dipole-dipole contribution, $\Delta\nu^{t}_{sd}$, shown in the middle panel of this figure.

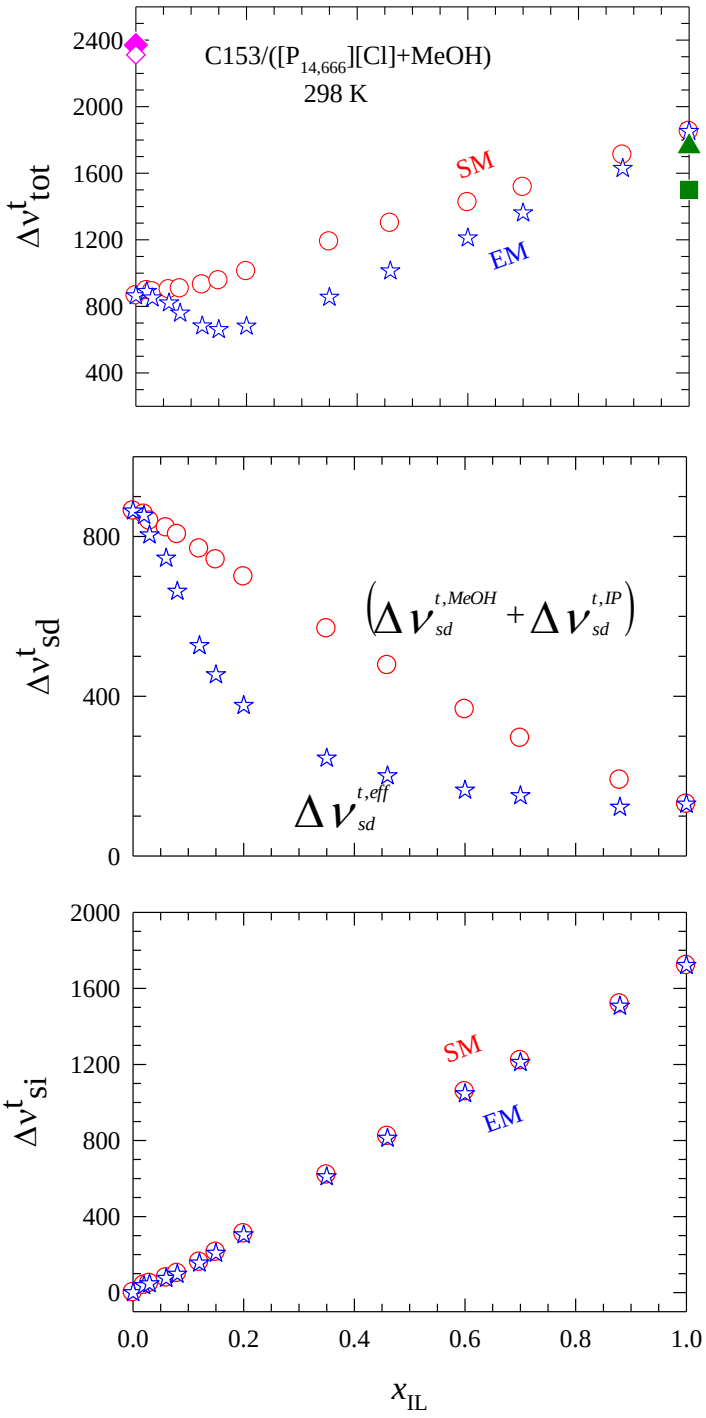

Figure. 6.2: Mixture composition dependence of dynamic Stokes shift magnitudes predicted by separate medium (SM) and effective medium (EM) calculations for C153 in ([$P_{14,666}$][Cl] + MeOH) binary mixture at 298 K. Predicted total shift ($\Delta\nu^t_{tot}$, upper panel), dipole-dipole interaction contribution ($\Delta\nu^t_{sd}$, middle panel) and dipole-ion interaction contribution ($\Delta\nu^t_{si}$, lower panel) are shown as a function of IL mole fraction, x_{IL}. Stars denote EM predictions and circles SM calculations. Filled symbols at x_{IL}=0 and 1 denote the dynamic shift magnitudes

observed in the corresponding measurements. Open diamond at x_{IL}=0 represents the calculated dynamic shift using 4.5 D as dipole moment for methanol.

While SM prediction for $\Delta\nu^{t}_{sd}$ includes contributions from both solute-methanol and solute-IP dipole-dipole interaction contributions and exhibits linear decrease with x_{IL} for the entire composition range, EM-predicted $\Delta\nu^{t}_{sd}$ depicts a non-ideal dependence and decreases with x_{IL}. In contrast, EM- and SM-predicted dipole-ion interaction contributions, $\Delta\nu^{t}_{si}$, exhibit a near-linear increase with x_{IL}. This is shown in the lower panel of Fig. 6.2. A close examination of shift values summarized in Tables D3 and D4 (Appendix D)[48] reveals that $\Delta\nu^{t}_{si}$ grows more steeply than $\Delta\nu^{t}_{sd}$ decreases with x_{IL} for mixtures with $x_{IL} > 0.2$ and is thus responsible for the over-all increase of total shift with x_{IL}. Note such a linear increase of $\Delta\nu^{t}_{si}$ with x_{IL} is predicted because the current theory assumes complete dissociation of IL in the mixture at all compositions and thus increase of ion concentration upon each successive addition of IL. Complete dissociation of IL may not take place in real mixtures and therefore the predicted increase of $\Delta\nu^{t}_{tot}$ with x_{IL} should be tested against experiments.

Next we turn our attention to the EM-predicted decrease of $\Delta\nu^{t}_{tot}$ with x_{IL} for the mole fraction range, $0 < x_{IL} \leq 0.2$. Note that the composition dependence of $\Delta\nu^{t}_{tot}$ predicted here for ([$P_{14,666}$][Cl] + MeOH) binary mixture is qualitatively different from what has been observed in experiments for binary mixtures of imidazolium IL (an example of dipolar IL) with water[21] and acetonitrile.[22] In addition, systematic incorporation of IL volume through effective number densities in EM calculations[27] was found to reproduce the experimentally observed x_{IL} independence of observed shift in these (dipolar IL + dipolar solvent) binary mixtures. Similar exercise here, however, has led EM-predictions to depict a non-monotonic x_{IL} dependence where $\Delta\nu^{t}_{tot}$ initially decreases with x_{IL} and then increases as IL is gradually added to the ([$P_{14,666}$][Cl] + MeOH) mixture. Since $\Delta\nu^{t}_{tot}$ in EM is determined by the effective solute-IL dipole-dipole and dipole-ion interaction contributions, we examine in Fig. 6.3 the wavenumber ($k\sigma$)

dependence of the corresponding solute-IL static direct correlation functions, c_{sd} and $c_{s\alpha}$ at a few representative IL mole fractions.

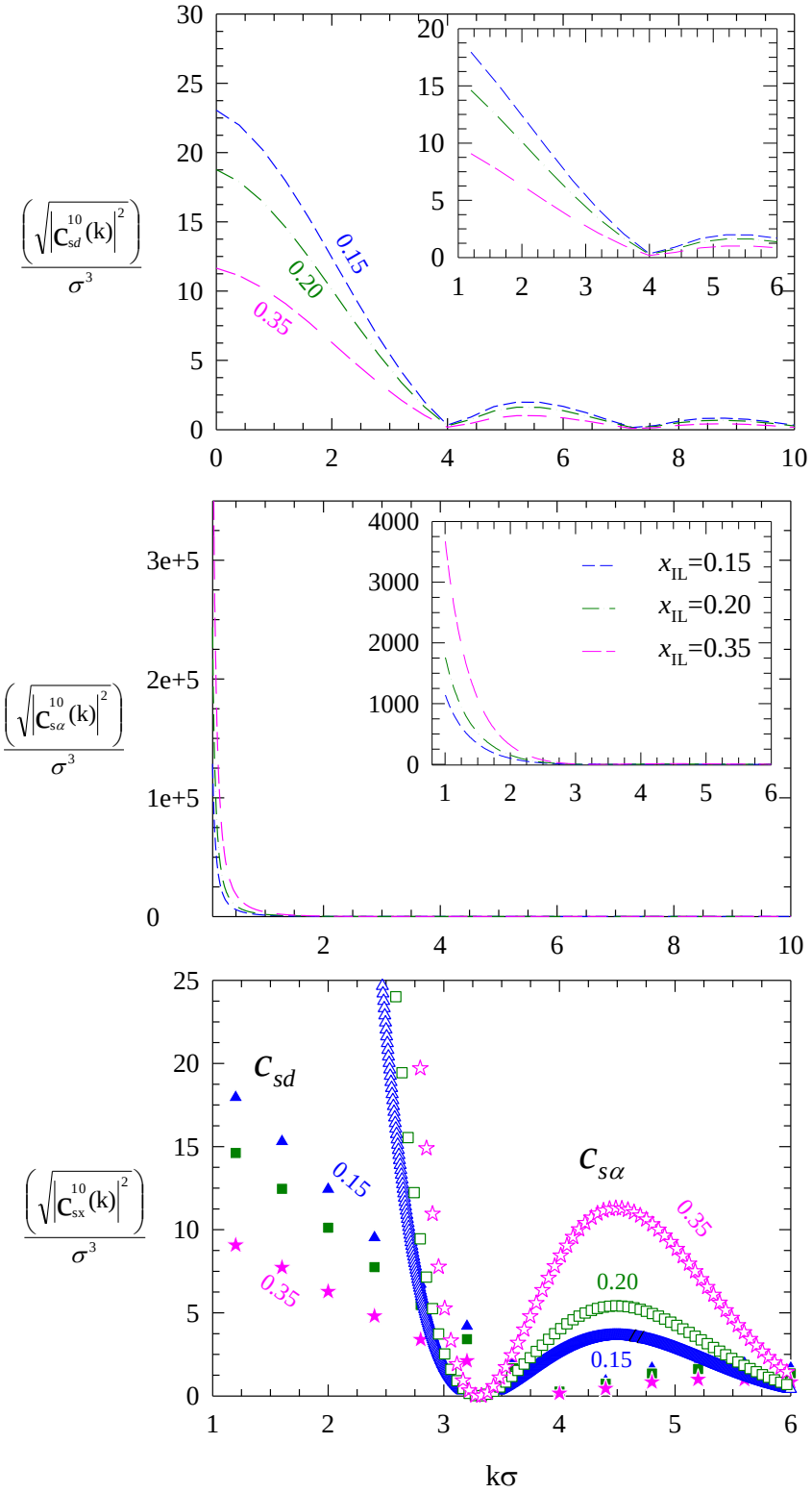

Figure. 6.3: Wavenumber dependent solute-IL dipole-dipole and dipole-ion static direct correlations at a few representative IL mole fractions of ([$P_{14,666}$][Cl] + MeOH) binary mixture at 298 K. While the longitudinal component of the dipole-dipole static correlations (c_{sd}^{10}) are

shown in the upper panel, the dipole-ion ($c_{s\alpha}^{10}$) correlations are shown in the middle panel, and a comparison between the two are presented in the lower panel. The curves are color-coded and represent the x_{IL} values for which the correlations are shown.

The longitudinal component (dominant part) of the wavenumber dependent dipole-dipole static correlation function, $c_{sd}^{10}(k)$, shown in the upper panel, clearly indicates decrease of static correlations at all wavenumbers with increase of x_{IL} in the mixture. This is due to the decrease of effective dipole number density with x_{IL} (see Table D1)[48] in the mixture which, in turn, decreases the dipole-dipole interaction contribution. In contrast, the dipole-ion static correlations, $c_{s\alpha}^{10}(k)$ shown in the middle panel, exhibit an increase with x_{IL} at all wavenumbers due to the increase of effective ion number density (Table D1).[48] This is more clearly shown in the bottom panel where these static correlations are directly compared for the wavenumber range relevant for the dipole-ion contribution. This explains the increase of dipole-ion interaction contribution to the total shift with x_{IL}. This in conjunction with density terms in the prefactors of working expression (see Eq. 6.8) and static ion structure factor ($S_{\alpha\beta}^{ion}(k)$), and the complex wavenumber dependence of the latter[30] enables the dipole-ion interaction contribution($\Delta\nu_{si}^{t}$) to remain lower than the effective dipole-dipole contribution ($\Delta\nu_{sd}^{t,eff}$) up to a certain IL mole fraction and then increase with x_{IL}. This is the reason for the domination of $\Delta\nu_{si}^{t}$ over $\Delta\nu_{sd}^{t}$ after a certain x_{IL} reflected in the individual shift values tabulated in Tables D3 and D4.[48]

6.3.2 Stokes Shift Dynamics: Composition Dependence

For SM calculations, the solvation response function is constructed as follows

$$S(t) = (1 - x_{IL})S_{sp}(t) + x_{IL}[0.3S_{sip}(t) + 0.7S_{si}(t)]. \qquad (6.19)$$

Since methanol is one of the components of the mixture under study, $S_{sp}(t)$ represents contribution to the total relaxation from due to the interaction between the dipolar solute

and methanol molecules. Use of Eq. 6.19 instead of Eq. (6.14) for predicting x_{IL} dependent solvation response function is rather ad-hoc but motivated by the following considerations. First, previous use[27] of such an expression for binary mixtures of imidazolium ILs with water and acetonitrile has led to semi-quantitative predictions of experimental Stokes shift dynamics. Second, Eq. 6.19 allows one to avoid the unphysical excessive domination of the slow relaxation due to $S_{si}(t)$ over the entire course of solvation energy relaxation. In fact, experimental Stokes shift dynamics of electrolyte solutions[61] suggests $S_{si}(t)$ should contribute only to the late stage of the solvation, and Eq. 6.19 derives support from this observation. Third, calculation of response functions by this way provides an opportunity to study how dipolar solvent dynamics is being increasingly replaced by the IL dynamics upon successive increase of x_{IL} in such a mixture. Note the assumption that the IL component of the total solvation response is composed of 70% contribution from the solute-ion interaction and 30% from the solute-IP interaction is based on our earlier analyses[5] of dynamic Stokes shift magnitudes in several phosphonium ILs.

For EM calculations, the working expression for the solvation response function is given by[27]

$$S(t) = (1 - 0.7x_{IL})S_{sd}^{eff}(t) + S_{si}^{eff}(t). \qquad (6.20)$$

Subsequently, the calculated x_{IL} dependent solvation response functions are fitted to a sum of multi-exponential functions of time, $S^{fit}(t) = \sum_{i=1}^{n} a_i \exp(-t/\tau_i)$ with $\sum_{i=1}^{n} a_i = 1$ and $a_i \geq 0$, where a_i denotes the amplitude of the i-th component and τ_i the associated time constant. The average solvation times are then obtained from fits as follows, $\langle \tau_{solv} \rangle = \sum_i a_i \tau_i$.

Fig. 6.4 displays the SM-predicted solvation response functions for C153 in ($[P_{14,666}][Cl]$ + MeOH) binary mixture at several IL mole fractions covering the range, $0 \leq x_{IL} \leq 1.0$. Parameters obtained from multi-exponential fits to these calculated

decays are summarized in Table D5 (see Appendix D). Note that the calculated S(t) for neat methanol (that is, at x_{IL}=0) is somewhat different from earlier prediction[44] as the present calculations have used solvent static structure factor directly from the MSA rather than employing the simulated one.[62] In addition, data in Table D5[48] suggest that the predicted average solvation time ($\langle \tau_{solv} \rangle$) for neat methanol is faster than what is reported in experiments.[54] However, we do not make any attempt here to obtain better agreement with experiments for neat methanol as the main focus of the present calculations is to explore the qualitative trend of the x_{IL} dependent solvation dynamics in this binary mixture.

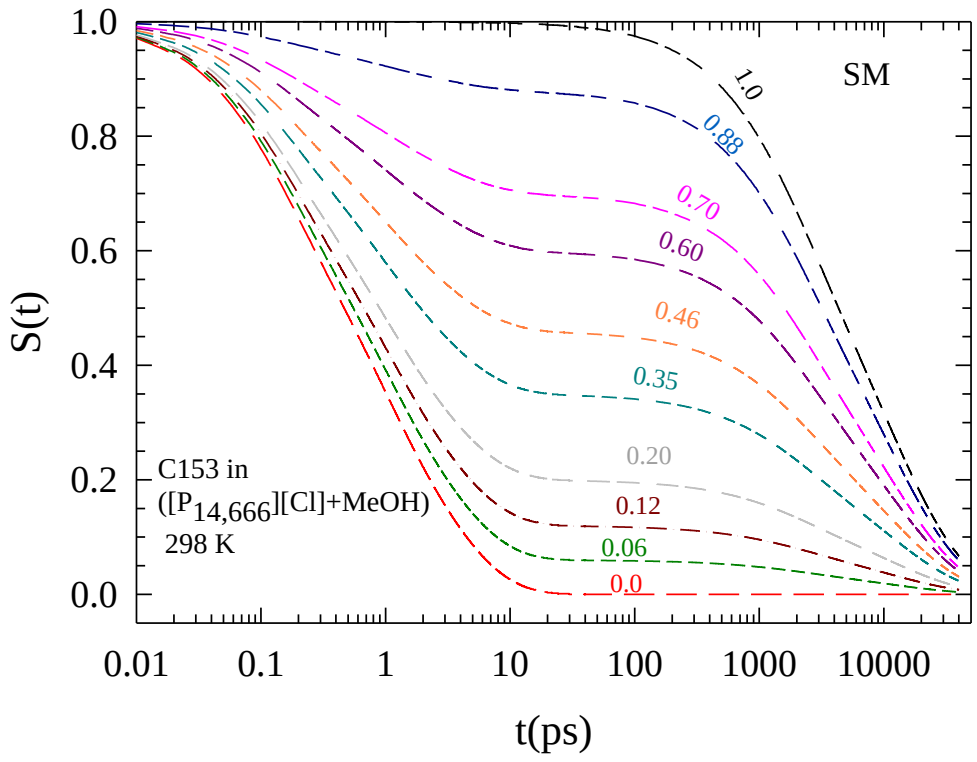

Figure. 6.4: SM-predicted solvation response functions as a function of time at various IL mole fractions for C153 in ([$P_{14,666}$][Cl] + MeOH) binary mixture at 298 K. Response functions calculated for neat systems (that is, x_{IL}=0 and 1) are also shown for comparison. Numerics tagged to curves denote the IL mole fractions.

Fig. 6.4 clearly demonstrates the existence of sub-picosecond and nanosecond solvation timescales in the predicted solvation response even for mixture with IL concentration as large as x_{IL}~0.9. Indeed, fitted data (Table D5) indicate ~10-30% of the initial solvation response for this binary mixture occurs with a time constant of ~150-300 fs which is very similar to the ultrafast response for several neat imidazolium ILs detected in recent experiments.[3] This ultrafast component in the SM-predictions for binary mixture originates from methanol response and disappears naturally at x_{IL}=1. In fact, the predicted picosecond timescale, which has also been found in experiments with neat methanol, can be linked to methanol response as this one is absent at x_{IL}=1 in both experiments[59,60] and theory. For mixtures with $x_{IL} > 0$, an extremely slow timescale of ~10-20 ns has been predicted. Interestingly, such a long timescale has not been reported in dynamic Stokes shift experiments with non-dipolar phosphonium ILs,[59,60] although experiments with several ILs at lower temperature[63] and a very recent simulation study of solvation dynamics of C153 in an IL at room temperature[15] have indicated presence of a similar slow timescale. The typical ~1-2 ns solvation timescale reported in dynamic Stokes shift measurements using C153 in non-dipolar phosphonium IL[59,60] starts appearing in the SM calculations for mixtures with $x_{IL} \geq 0.1$. However, the predicted value of $\langle \tau_{solv} \rangle$ for the neat IL is almost twice as large as that reported in experiments[59,60] and this is because of the substantial contribution (~40%) of the ~20 ns component in the predicted dynamics.

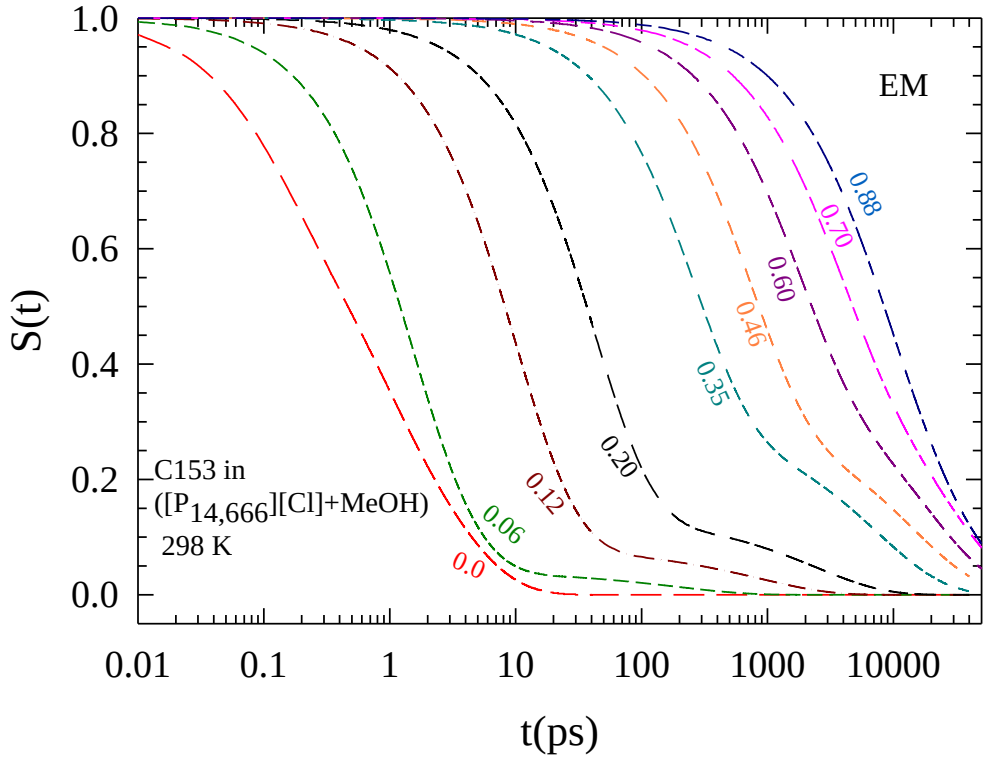

Figure. 6.5: EM-predicted solvation response functions for the binary mixture under study. The calculated response functions are tagged with x_{IL} values.

The EM-predicted solvation response functions at several IL mole fractions for this binary mixture are shown in Fig. 6.5. EM-predicted solvation response functions for these binary mixtures can be adequately described by tri-exponential functions of time, and parameters from such fits are summarized in Table D6 (Appendix D).[48] Data in this table indicate that EM-predicted dynamics is faster than that from SM calculations for mixtures with $x_{IL} \leq 0.35$. Beyond this IL mole fraction, SM-predicted response functions decay faster than EM-predictions. In addition, the sub-picosecond component disappears rather quickly and the fastest solvation component at $x_{IL} \geq 0.6$ becomes even slower than that predicted for the neat IL. These observations are summarized in Fig. 6.6 where the EM- and SM-predicted average solvation times ($\langle \tau_{solv} \rangle$), the fastest and the slowest solvation time constants (τ_f and τ_s) are shown as a function of x_{IL}.

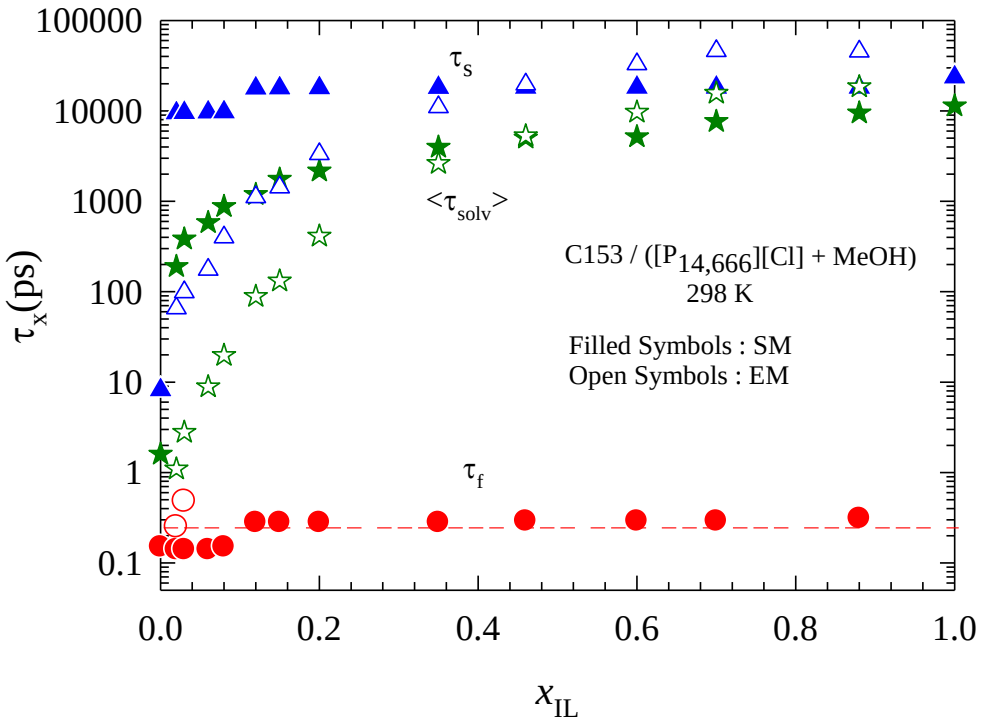

Figure. 6.6: Comparison between the SM- and EM-predicted various solvation times for C153 in ([$P_{14,666}$][Cl] + MeOH) binary mixture at 298 K. While $\langle \tau_{solv} \rangle$ denote the average solvation times obtained from SM (filled symbols) and EM (open symbols) calculations, τ_f and τ_s represent the fastest and the slowest times constants obtained from fits of the SM and EM predicted solvation response functions. The broken line acts as a guide to the eye.

Clearly, the qualitative trend for the x_{IL} dependence of $\langle \tau_{solv} \rangle$ is similar for both the model calculations although τ_s from EM shows stronger mixture composition dependence than those from the SM calculations. In the absence of any experimental results on solvation dynamics and dielectric relaxation for this mixture, it is not certain how x_{IL} dependence of these time constants should appear. However, it may be conjectured that the near absence of sub-picosecond timescale in EM predictions and cross-over of the slowest timescales between EM and SM predictions at certain mixture composition might have arisen from the approximate method employed for determining τ_D which were subsequently used for calculating the dipole-dipole component of the total solvation response. Use of proper experimental dielectric relaxation data will lead to better predictions because such data for binary mixtures of imidazolium ILs with

water and acetonitrile have been found to provide a semi-quantitative theoretical description[27] of the corresponding dynamic Stokes shift measurements.

6.4 Conclusion

A semi-molecular theory for studying Stokes shift dynamics of a dissolved dipolar solute in binary mixtures of (non-dipolar ionic liquid + common dipolar solvent) has been developed here. Subsequently, the theory is applied to predict IL mole fraction dependent dynamic Stokes shift magnitude and solvation energy relaxation for C153 in binary mixtures with methanol of a non-dipolar ionic liquid, $[P_{14,666}][Cl]$. In the absence of suitable experimental results for such binary mixtures, many input parameters necessary for calculations have been obtained via approximate methods. The theory predicts strong mixture composition dependence for both dynamic Stokes shift magnitude and average solvation time. The increase of dynamic shift with IL mole fraction is opposite to the trend expected on polarity (ε_0) consideration, and stresses the importance of solute-IL dipole-ion interaction. Interestingly, the predicted composition dependence of average solvation time is similar to what has been observed for (imidazolium IL + dipolar solvent) binary mixtures[27] but the same (composition dependence) for dynamic shift has been found to be qualitatively different. However, non-availability of dynamic Stokes shift measurements has restricted direct comparison between theory and experiments, leaving out the ambit of testing the performance of the theory developed and performing subsequent refinement over it. Such a caveat notwithstanding, this is a first theory that provides a semi-molecular framework for understanding Stokes shift dynamics in binary mixtures of non-dipolar ionic liquids with common dipolar solvents in terms of measured dielectric relaxation data. This, in turn, provides an opportunity for examining the relationship between the frequency dependent dielectric relaxation of and time-dependent solvation response in these complex binary mixtures possessing ion-ion interactions.

Apart from carrying out the necessary refinement of this theory after suitable experimental results are made available, a few interesting studies can be performed with such mixtures. For example, investigation of various heterogeneity timescales[15] and

their relationship to solvation timescales may be quite insightful as it provides an independent check of qualitative correctness of the predicted solvation timescales. A theoretical study of dielectric relaxation of these mixtures can provide information about the role of ion-dipole interaction and spatial heterogeneity[40] in dictating the dielectric relaxation timescales in such complex mixtures. It would also be interesting to explore the degree of decoupling between the solution viscosity and average relaxation rates of solute-centered dynamics in these binary mixtures along the line of what has been done for deep eutectics.[64-68] All these proposed studies are necessary for generating microscopic understanding of how longer-ranged interactions influences solute-medium coupling in mixtures containing electrolytes, and highlight the reasons for ILs to be qualitatively different (if at all) from common dipolar solvents.

References:

1. A. Samanta, J. Phys. Chem. B , **110**, 13704 (2006).
2. A. Samanta, J. Phys. Chem. Lett. **1**, 1557 (2010).
3. X.-X. Zhang, M. Liang, N. P. Ernsting, and M. Maroncelli, J. Phys. Chem. B **117**, 4291(2013).
4. S. Arzhantsev, H. Jin, N. Ito,and M. Maroncelli , Chem. Phys. Lett. **417**, 524 (2006).
5. H. K. Kashyap and R. Biswas , J. Phys. Chem. B , **114**, 254, (2010).
6. S. Daschakraborty and R. Biswas, J. Chem. Phys. **137**, 114501 (2012).
7. E. W. Castner Jr., C. J. Margulis, M. Maroncelli, and J. F. Wishart, Annu. Rev. Phys. Chem. **62**, 85 (2011).
8. A. Triolo, O. Russina, B. Fazio, G. B. Appetecchi, M. Carewska, and S. Passerini, J. Chem. Phys. **130**,164521, (2009).
9. Y. Wang and G. A. Voth, J. Phys. Chem. B **110,** 18601 (2006)
10. J. N. C. Lopes, M. F. C. Gomes, and A. A. H. Padua, J. Phys. Chem. B **110**, 16816(2006).
11. S. S. Sarangi, W. Zhao, F. Muller-Plathe, S. Balasubramanian, ChemPhysChem **11**,2001 (2010).
12. T. Pal and R. Biswas, Theor. Chem. Acc., **132**, 1348 (2013).
13. O. Russina, B. Fazio, C. Schmidt and A. Triolo, Phys. Chem. Chem. Phys., **13**, 12067 (2011).
14. M. Kofu, M. Nagao, T. Ueki, Y. Kitazawa, Y. Nakamura, S. Sawamura, M. Watanabe, and O. Yamamuro, J. Phys. Chem. B **117**, 2773 (2013).
15. T. Pal and R. Biswas , J. Chem. Phys. submitted, (2014).
16. J. T. Hynes , Annu. Rev. Phys. Chem. **36**, 573 (1985).
17. R. F. Grote and J. T. Hynes, J. Chem. Phys. **73**, 2715 (1980).
18. T. Pradhan and R. Biswas , J. Phys. Chem. A , **111**,11524 (2007).
19. M. Muramatsu, Y. Nagasawa and H. Miyasaka, J. Phys. Chem. A **115**, 3886 (2011)
20. M. Maroncelli, X.-X. Zhang, M. Liang, D. Roy, and N. P. Ernsting, Faraday Discuss. Chem. Soc. **154**, 409 (2012).
21. X.-X. Zhang , M. Liang , J. Hunger , R. Buchner and M. Maroncelli J. Phys. Chem. B **117**,15356 (2013).

22. M. Liang, X. –X. Zhang, A. Kaintz, N. P. Ernsting, and M. Maroncelli, J. Phys. Chem. B , **118**,1340 (2014).
23. S. Sarkar, R. Pramanik, C. Ghatak, P. Setua, and N. Sarkar J. Phys. Chem. B, **114**, 2779 (2010).
24. S. K. Das, P. K. Sahu, M. Sarkar, J. Fluoresc., **2**, 1217 (2013).
25. K. A. Fletcher and S. Pandey, J. Phys. Chem. B. **107**,13532 (2003).
26. S. Daschakraborty and R. Biswas, J. Phys. Chem. B, **115**, 4011 (2011).
27. S. Daschakraborty and R. Biswas, J. Phys. Chem. B, **118**, 1327 (2014).
28. H. V. R. Annapureddy, Z. Hu, J. Xia, and C. J. Margulis, J. Phys. Chem. B, **112**, 1770 (2008).
29. M. Heitz, private communication.
30. H. K. Kashyap and R. Biswas, J. Phys. Chem. B **114** , 16811 (2010) .
31. K. J. Fraser, E. I. Izgorodina, M. Forsyth, J. L. Scott, and D. R. MacFarlane, Chem. Commun., **37**, 3817 (2007).
32. H. Tokuda, S. Tsuzuki, M. A. B. H. Susan, K. Hayamizu, and M. Watanabe J. Phys. Chem. B **110**, 19593 (2006).
33. H. Tokuda, S. Tsuzuki, K. Hayamizu, and M. Watanabe, J. Phys. Chem. B **109,** 16474 (2005).
34. H. K. Kashyap and R. Biswas, Indian. J. Chem. **49A**, (2010), 685.
35. B. Bagchi and R. Biswas, Adv. Chem. Phys. **109**, 207 (1999).
36. R. Biswas and B. Bagchi, J. Phys. Chem. **100**, 1238 (1996).
37. H. K. Kashyap, T. Pradhan, and R. Biswas, J. Chem. Phys. **125**, 174506 (2006).
38. B. Bagchi and A. Chandra, Adv. Chem. Phys. , **80**, 1 (1991).
39. S. Daschakraborty, T. Pal, and R. Biswas, J. Chem. Phys. **139**, 164503 (2013).
40. S. Daschakraborty and R. Biswas, J. Chem. Phys. **140**, 014504 (2014).
41. G. C. Gray, and K. E. Gubbins, Theory of Molecular Fluids; Clarendon: Oxford, U.K., 1984; Vol. I.
42. B. Bagchi and S. Roy, J. Chem. Phys. **98**, 1310 (1993).
43. B. Bagchi and S. Roy, J. Chem. Phys. **99**, 9938 (1993).
44. R. Biswas, N. Nandi, and B. Bagchi, J. Phys. Chem. B **101**, 2968 (1997).
45. H. K. Kashyap and R. Biswas, J. Phys. Chem. B **112**, 12431 (2008).

46. S. Daschakraborty and R. Biswas, Chem. Phys. Lett. **545**, 54 (2012).
47. S. Daschakraborty and R. Biswas, Chem. Phys. Lett. **510**, 202 (2011).
48. See Appendix D for the calculations of effective number densities , tables containing density, viscosity and dielectric relaxation parameters, composition dependent EM- and SM-predicted dynamic Stokes shift values, and tables summarizing fit parameters describing x_{IL} dependent solvation response functions obtained via SM and EM calculations.
49. J. Hunger, A. Stoppa, S. Schrodle, G. Hefter, and R. Buchner, ChemPhysChem **10**, 723 (2009).
50. J. T. Kindt and C. A. Schmuttenmaer, J. Phys. Chem. **100**, 10373 (1996).
51. A. Das, R. Biswas, and J. Chakrabarti, Chem. Phys. Lett. **558**, 36 (2013).
52. E. A. S. Cavell, P. C. Knight and M. A. Seikh, J. Chem. Soc., *Faraday Trans.* **67**, 2225 (1971).
53. J. Hunger , A. Stoppa and R. Buchner , J. Phys. Chem. B., **112**,12913 (2008).
54. M. L. Horng, J. A. Gardecki , A. Papazyan and M. Maroncelli, J. Phys. Chem. **99**, 17311 (1995).
55. J. A. Riddick , W. B. Bunger and T. K. Sakano. *Organic Solvents* ; Wiley: New York, 1986.
56. L. X. Dang and T. M. Chang, J. Chem. Phys. **119**, 9851 (2003).
57. McClellan, A.L. Tables of Experimental Dipole Moments; W.H. Freeman: San Francisco,1963, Vol. 1; Rahara Enterprises: El Cerrito, CA, 1974, Vol. 2; Rahara Enterprises: El Cerrito, CA, 1989, Vol. 3.)
58. H. Jin, G. A. Baker, S. Arzhantsev, J. Dong, and M. Maroncelli , J. Phys. Chem. B **111**,7291 (2007).
59. N. Ito, S. Arzhantsev, M. Heitz, and M. Maroncelli, J. Phys. Chem. B **108**, 5771 (2004).
60. S. Arzhantsev, N. Ito, M. Heitz, and M. Maroncelli, Chem. Phys. Lett. **381**, 278 (2003).
61. C. F. Chapman and M. Maroncelli, J. Phys. Chem. **95**, 9095 (1991).
62. F. O. Raineri, H. Resat and H. L. Friedman, J. Chem. Phys. **70**, 2946 (1979).
63. A. M. Funston, T. A. Fadeeva, J. F. Wishart, and E. W. Castner, Jr., J. Phys. Chem. B **111**, 4963 (2007).

64. B. Guchhait, S. Das, S. Daschakraborty and R. Biswas, J. Chem. Phys. **140**, 014514 (2014).
65. B. Guchhait, H. A. R. Gazi, H. K. Kashyap, and R. Biswas, J. Phys. Chem. B 114, 5066, (2010).
66. B. Guchhait, S. Daschakraborty, and R. Biswas, J. Chem. Phys. **136**, 174503 (2012).
67. A. Das, S. Das, and R. Biswas, Chem. Phys. Lett. **581**, 47 (2013).
68. T. Pal and R. Biswas, Chem. Phys. Lett. **517**, 180 (2011).

Chapter 7

7.1 Concluding Remarks and Future Problems

To summarize, the present Thesis provides a simulation study on the complex dynamics of systems that contain, in addition to other interactions, charge-charge and charge-dipole interactions, and attempts to explain the observed anomalies in terms of temporal heterogeneity. The systems considered are (amide+ electrolyte) deep eutectics and ionic liquids which represent two different classes of solvents. Methodologies used for studying dynamics in supercooled liquids have been employed to explore the signatures of dynamical (temporal) heterogeneities in these systems. Subsequently, temporal heterogeneity aspect in binary mixtures of ionic liquids with small molecular solvents has been investigated. Results obtained from our simulations have been compared with either experiments or simulations from other authors wherever possible. A semi-molecular theory has been developed for studying composition dependence of Stokes shift dynamics in binary mixtures of non-dipolar ionic liquids with conventional molecular solvents. This later study is expected to motivate suitable experimental and simulation studies. These are required not only for generating a comprehensive understanding of dynamics of these complex liquid systems but also for sustaining the symbiosis among theory, experiments and computer simulations.

Since conclusions are provided at the end of each chapter presented in the Thesis, we refrain from providing concluding remarks separately. Instead, we discuss here a few important problems that are connected to the works described here and may be studied in the near future. These problems, once studied, are expected to shed new lights on the heterogeneity aspect of ionic liquids, and its impact on liquid dynamics.

7.1.1 Investigation of particle spatial and temporal correlations in (IL+dipolar solvent) binary mixtures

Investigation of liquid structure using small angle x-ray scattering [1] (SAXS) , small angle neutron scattering [2] (SANS) and neutron-spin echo [3,4] (NSE) techniques in ionic liquids (ILs) have showed the presence of considerable scattering from a low-*Q* peak. It is known that with increase in alkyl chain length the packing of the bulky alkyl groups becomes more compact, separated by a charged matrix of polar heads and counter ions. It would be interesting to explore the relation between the rearrangement timescales of these alkyl (nonpolar) and charged (polar) domains and those in solvation energy relaxation. This idea has already been tested in Chapter 5 through dynamic heterogeneity in neat ILs and can be expanded further to address similar issues in binary mixtures of ILs with molecular solvents. We have already performed a simulation study of binary mixtures with 1-octyl-3-methylimidazolium tetrafluoroborate [Omim][BF_4] and H_2O [5] (for preliminary results , See Addendum I) . In the IL-rich region, it is more likely to show signatures of pronounced dynamic heterogeneity accessed via new non-gaussian parameter[6], single particle displacements[7] , and help understanding the role of spatial and dynamical correlations via multi-point correlation functions.[6,8,9]

7.1.2 Cluster size and life-time distributions in (IL+water) binary mixtures

Another interesting problem is the determination of cluster size and lifetime in neat IL and their binary mixtures with either another IL or a molecular solvent. This can be done via simple monitoring of the spatial correlations between two particles by tracking their mobility fluctuations (i) mobile particles that breaks out of the cage and (ii) immobile particles which show rattling in a cage. This process of making and breaking of cages can be accessed by monitoring a cage correlation function[10] and give information regarding formation of cluster and cluster size distribution.[11] A study on the effects of molecular solvent on IL cluster distribution and stability time (lifetime) would be an important contribution for understanding the solvation timescales in such binary mixtures.

7.1.3 Orientational jump dynamics in (IL + solvent) binary mixtures

Dielectric relaxation (DR) and femto-second infrared (fs-IR) studies[12] have suggested non-diffusive rotational motions in protic ionic liquids are associated with large angle jumps reminiscent of liquid water.[13,14] The Debye-rule of diffusive rotational moves producing $\frac{\tau^{\ell}}{\tau^{\ell+1}} = \frac{\ell(\ell+2)}{\ell}$ completely fails even in aprotic ionic liquids. [15] A detailed study therefore may help to understand the factors that influence the jump motions and the impact of molecular solvent on such non-Brownian moves.

7.1.4 Potential energy landscape view of Ionic Liquids

Understanding the non-Gaussian moves or hop mechanism of mobile particle, and collective motion of the immobile particles which remains correlated over time and several length scales, encourages discussion in terms of potential energy landscape. [16-22] At lower temperatures, the liquid gets trapped in the deepest accessible energy basin. The non – exponential nature of relaxation processes arises from the average of varying timescales for the fast and slow moving ions. At low temperatures, particles in the local energy minima are separated by large energy barrier heights relative to $k_B T$. The dynamical processes can be interpreted as transitions between adjacent local minima. Investigating the same involves appropriate selection of order parameter depending on the desired property under study. For understanding mass transport, potential energy is considered as a function of the atomic configurations, while the rotational geometry can be analysed by torsional energy profile. The interplay between translational and rotational order parameters will help understand the onset of decoupling of diffusion from medium viscosity in these liquids.

7.1.5 Alkyl chain length and anion dependence of Stokes shift Dynamics in ILs

High quality experimental results are now available on both Stokes shift dynamics and dielectric relaxation in ILs that vary in alkyl chain-length attached to the cation, and counter ions that balance the over-all charge. Interestingly, semi-molecular theories have been developed and found to successfully describe the experimental Stokes shift dynamics.[23-25]

Recent measurements of complete solvation response function for imidazolium , pyrrolidinium , ethyl ammonium and sulfonium room-temperature ionic liquids with different anions have revealed a biphasic decay.[26,27] The fast relaxation has been attributed to inertial ion translations and the slower ones linked to structural relaxations. Semi-molecular theory that accounts for the ion size can be extended to investigate the anion size effects on solvation response for a series of ILs that differ only in counter ions. Available dielectric relaxation (DR) data[28,29] can be used, as done earlier,[30] for the necessary theoretical calculations. A direct comparison between theoretical results and measurements would reveal the translation contribution of the ions to the total solvation energy relaxation for an excited dye dissolved in such a medium. Likewise, one can suitably use the existing semi-molecular theory to explore the alkyl chain-length dependence of dynamic solvation response in ILs as good quality experimental DR data[31] for some of the systems are already available. All-atom simulations should be performed to cross-examine the theoretical predictions on these dependences.

Likewise, the effects of alkyl chain-length on solvation response in (IL+polar solvent) binary mixtures may be studied by employing both theory and simulations. For example, the existing semi-molecular theory[32] for studying Stokes shift dynamics in (IL + polar solvent) binary mixtures can be employed to first predict the dependence on alkyl chain-length and then simulate the same by employing realistic interaction potential. Note complete measurements of Stokes shift dynamics have been reported for such binary mixtures[33,34] but they are done for ILs with fixed alkyl chain-length. With more experimental data on similar mixtures are expected to be made available soon, and

a theoretical and/or simulation study will only help better understanding of these complex systems.

The above are only a few representative problems that are connected to the central theme of the present thesis. A careful study of them via all-atom simulations and theory may provide semi-quantitative understanding of microscopic mechanisms that are responsible for producing multiple timescales in solvation energy relaxations, and medium decoupling. In addition, these studies are expected to shed light on the role of temporal heterogeneity in setting up the slow relaxation timescales in these systems. With the increasing availability of better computational resources and high quality experimental data, the ground is well prepared for constructing a symbiosis among theory, experiments and simulations. We look forward to such an exciting development.

References:

1. Triolo, O. Russina, B. Fazio, R. Triolo, and E. D. Cola, Chem. Phys. Lett. **467**,362(2008).
2. C. Hardacre, J. D. Holbrey, C. L. Mullan, T. G. A. Youngs, and D. T. Bowron, J. Chem. Phys. **133**, 074510 (2010).
3. O. Yamamuro, T. Yamada, M. Kofu, M. Nakakoshi, and M. Nagao, J. Chem. Phys. **135**, 054508 (2011).
4. M. Kofu, M. Nagao, T. Ueki, Y. Kitazawa, Y. Nakamura, S. Sawamura, M. Watanabe, and O. Yamamuro, J. Phys. Chem. B **117**, 2773 (2013).
5. H. Shirota, and R. Biswas , J. Phys. Chem. B, **116**, 13765 (2012).
6. K. Kim and S. Saito, J. Chem. Phys. **133**, 044511 (2010).
7. E. Flenner and G. Szamel, Phys. Rev. E. **72**, 011205 (2005).
8. C. Toninelli, M. Wyart, L. Berthier, G. Biroli, and J.-P. Bouchaud, Phys. Rev. E **71**, 041505 (2005).
9. N. Lacevic, F. W. Starr, T. B. Schroder, and S. C. Glotzer, J. Chem. Phys. **119**, 7372 (2003).
10. T. I. Morrow and E. J. Maginn , J. Phys. Chem. B , **106**, 12807(2002).
11. S. C. Glotzer, J. Non-Cryst. Solids, **274**, 342 (2000).
12. J. Hunger, T. Sonnleitner, L. Liu, R. Buchner, M. Bonn, and H. J. Bakker , J. Phys. Chem. Lett., **3**, 3034(2012).
13. D. Laage and J. T. Hynes, *Science* **311**, 832 (2006).
14. I. Ohmine, H. Tanaka, Chem. Rev. **93**, 2545(1993).
15. Y. Shim , and H. J. Kim, J. Phys. Chem. B,**112**,11028(2008).
16. D. Chakrabarti and B. Bagchi , Phys. Rev. Lett. **96**, 187801 (2006).
17. A. Heuer, J. Phys.: Condens. Matter **20** , 373101 (2008).
18. S. Sastry, P. G. Debenedetti and F. H. Stillinger , Nature , **393** , 554 (1998).
19. M. D. Ediger and P Harrowell , J. Chem. Phys. , **137**, 080901 (2012).
20. D. Chakrabarti and B. Bagchi , Proc. Natl. Acad. Sci., **103**, 7217 (2006).
21. P. G. Debenedetti and F. H. Stillinger , Nature , **410** , 259 (2001).

22. J. N. C. Lopes, K. Shimizu, A. A. H. Padua, Y. Umebayashi, S. Fukuda, K. Fujii, and S. Ishiguro, J. Phys. Chem. B, **112**, 9449 (2008).
23. H. K. Kashyap and R. Biswas , J. Phys. Chem. B , **114**, 254, (2010).
24. H. K. Kashyap and R. Biswas , J. Phys. Chem. B , **114**, 16811, (2010).
25. S. Daschakraborty and R. Biswas, J. Phys. Chem. B, **115**, 4011 (2011).
26. X.-X. Zhang, M. Liang, N. P. Ernsting, and M. Maroncelli, J. Phys. Chem. B **117**, 4291(2013).
27. S. Arzhantsev , H. Jin , G. A. Baker , and M. Maroncelli , J. Phys. Chem. B , **111** , 4978 (2007).
28. J. Hunger, A. Stoppa, S. Schrödle, G. Hefter, and R. Buchner, Chem. Phys. Chem **10**, 723 (2009).
29. A. Stoppa , J. Hunger , R. Buchner , G. Hefter , A. Thoman, and H. Helm , J. Phys. Chem. B. Lett. **112** , 4854 (2008).
30. S. Daschakraborty, T. Pal, and R. Biswas, J. Chem. Phys. **139**, 164503 (2013).
31. H. Weingartner, P. Sasisanker, C. Daguenet, P. J. Dyson, I. Krossing, J. M. Slattery, and T. Schubert , J. Phys. Chem. B **111**, 4775 (2007).
32. S. Daschakraborty and R. Biswas , J. Phys. Chem. B.,**118**,1327 (2014).
33. M. Liang, X.-X. Zhang, A. Kaintz, N. P. Ernsting, and M. Maroncelli, J. Phys. Chem. B. **118**, 1340 (2014).
34. X.-X. Zhang, M. Liang, J. Hunger, R. Buchner, and M. Maroncelli, J. Phys. Chem. B. **117**, 15356 (2013).

Appendix A

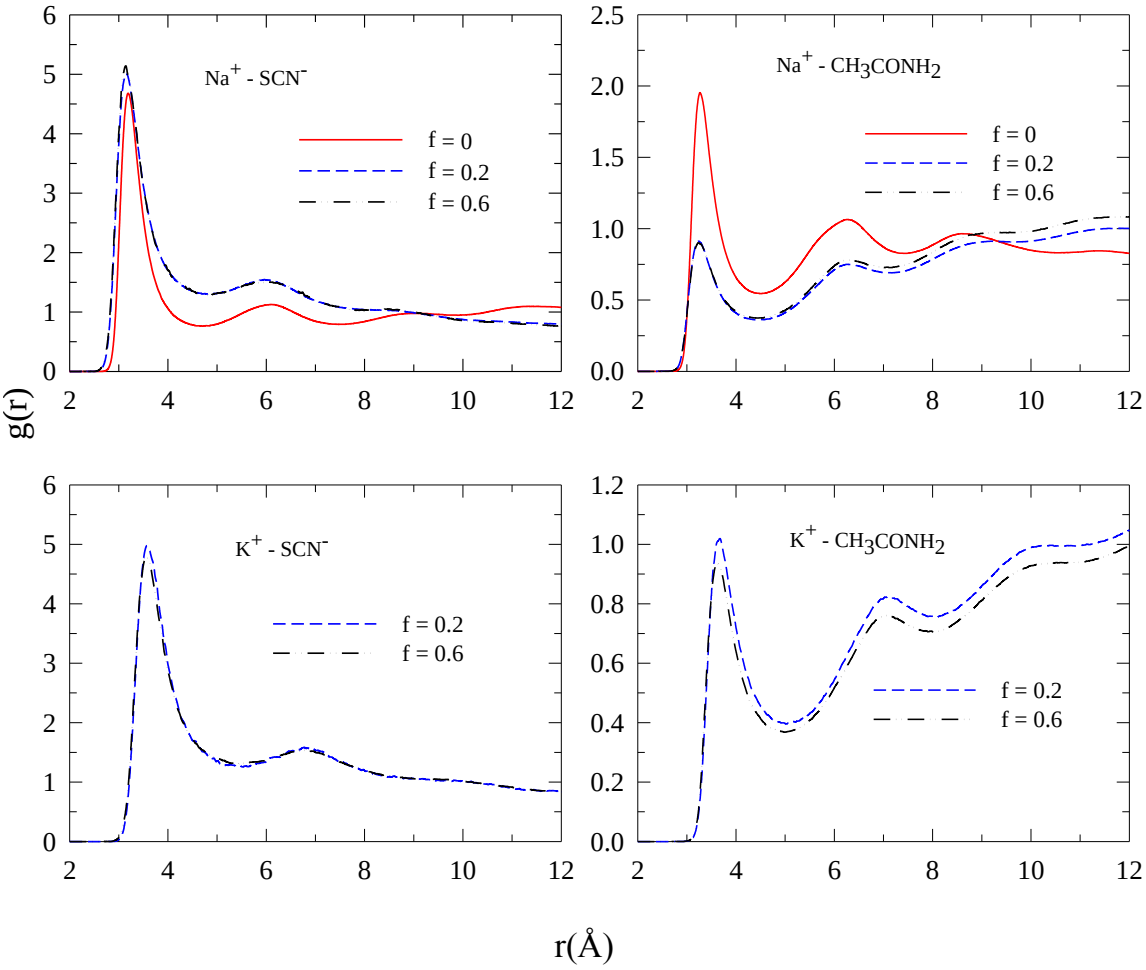

Figure. A1: Cross RDFs for the melt under study at 318 K. The representations are indicated in each panel.

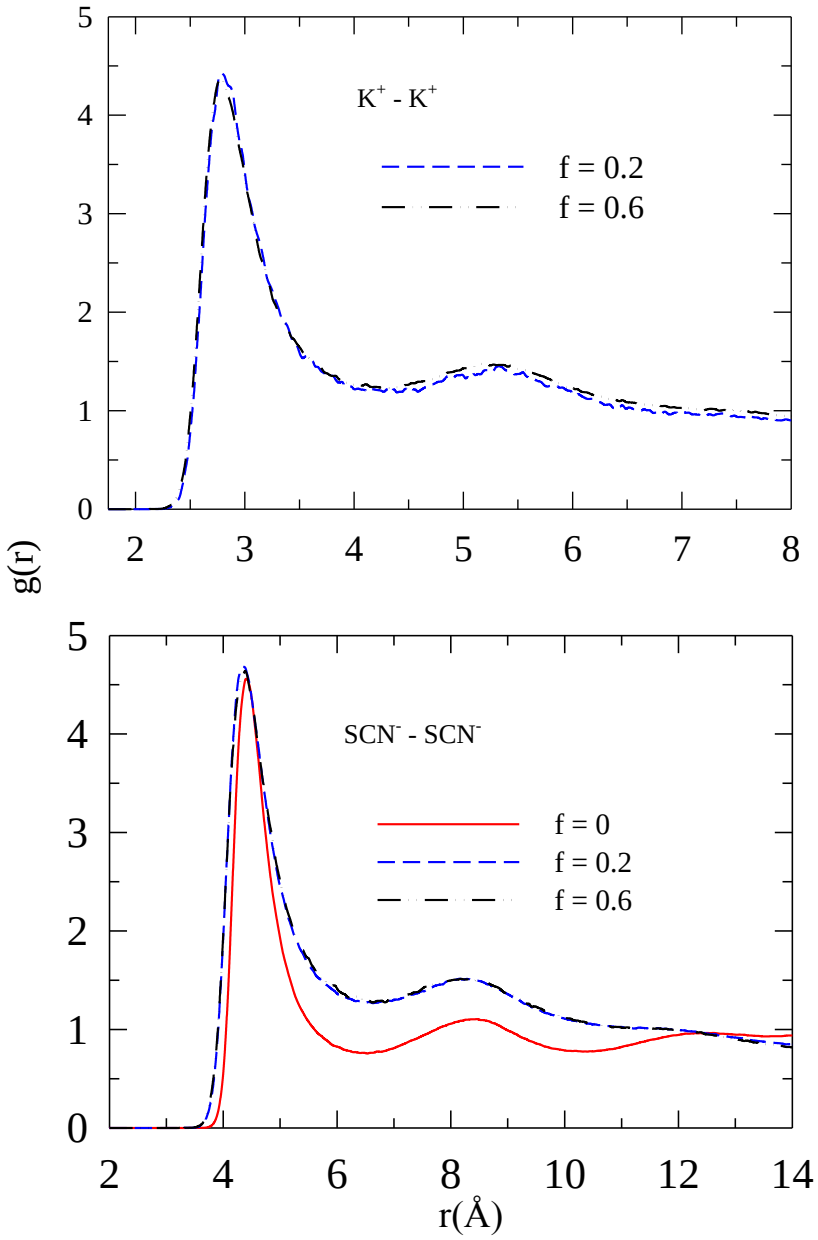

Figure. A2: $g(r)$ for $K^+ - K^+$, $SCN^- - SCN^-$ ions.

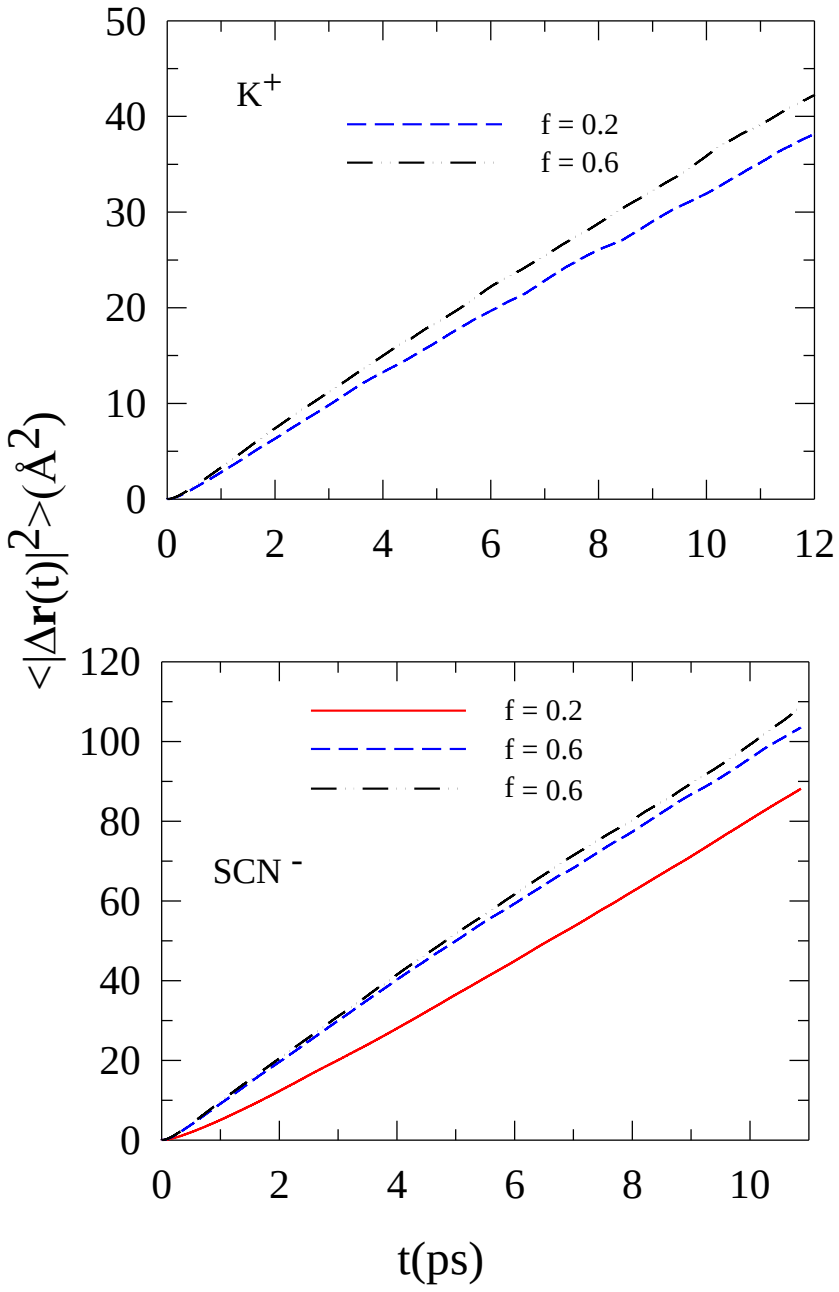

Figure. A3: Composition dependent MSDs for potassium cation and thiocyanates anion.

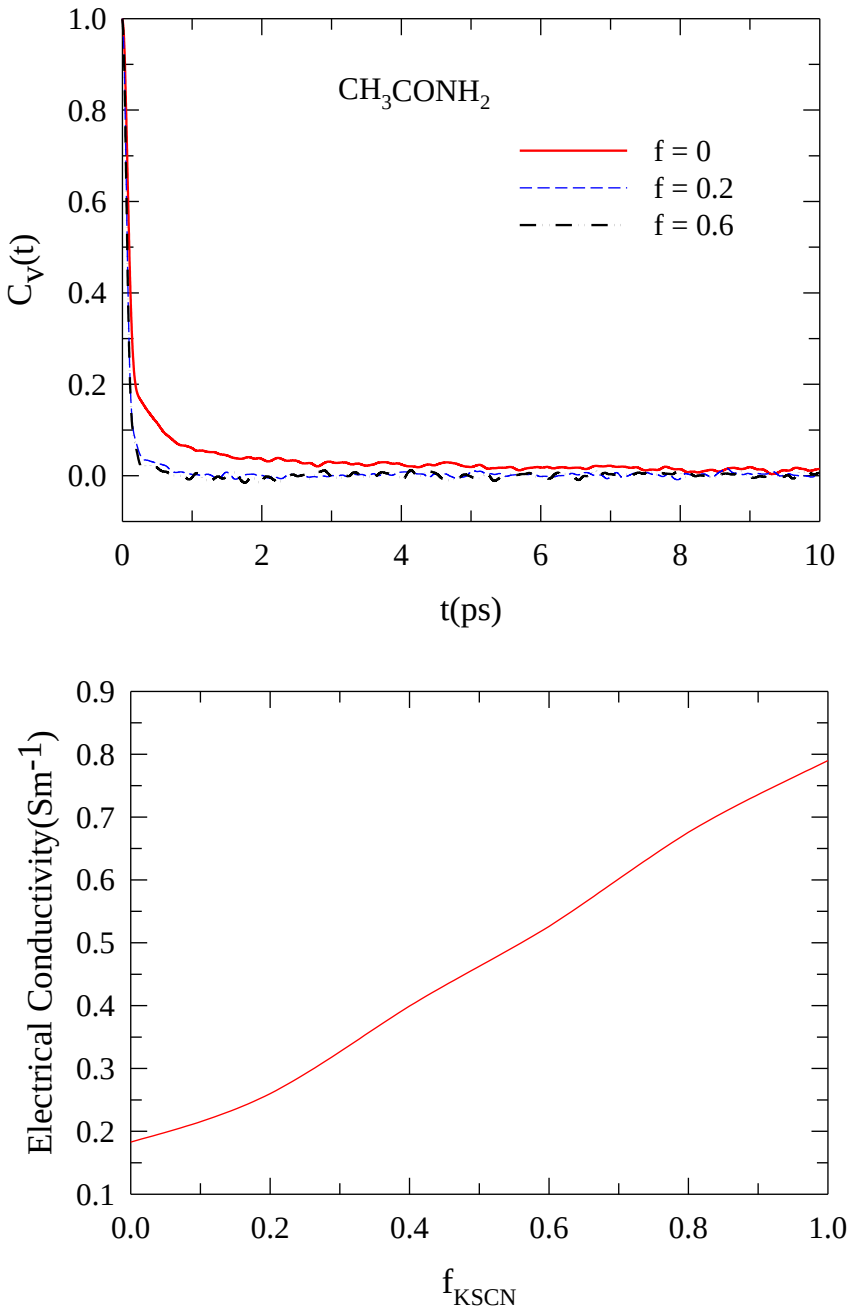

Figure. A4: Effects of mixture composition on the velocity autocorrelation function (VACF) of acetamide molecules (upper panel) in the melt under study at 318 K. Note this is a representative figure. Lower panel shows composition dependent electrical conductivity measured (Ref. 43) for this melt at this temperature.

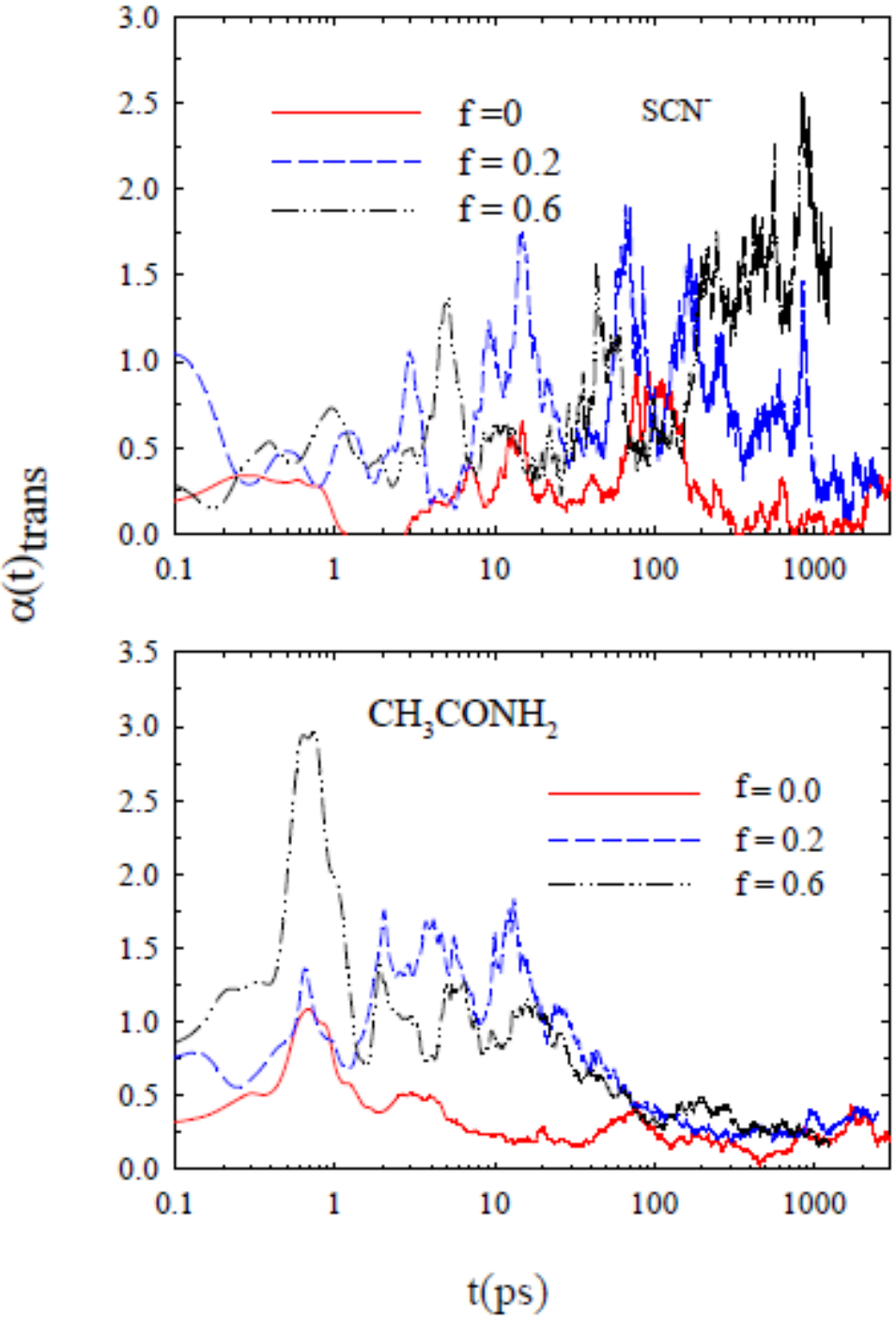

Figure. A5: Mixture composition dependent $\alpha(t)$s for SCN^- and acetamide particles. Note $\alpha(t)$ for SCN^- at $f = 0.6$ has not decayed to zero even after ~2ns, indicating extremely sluggish dynamics and requirements for a much longer simulation run.

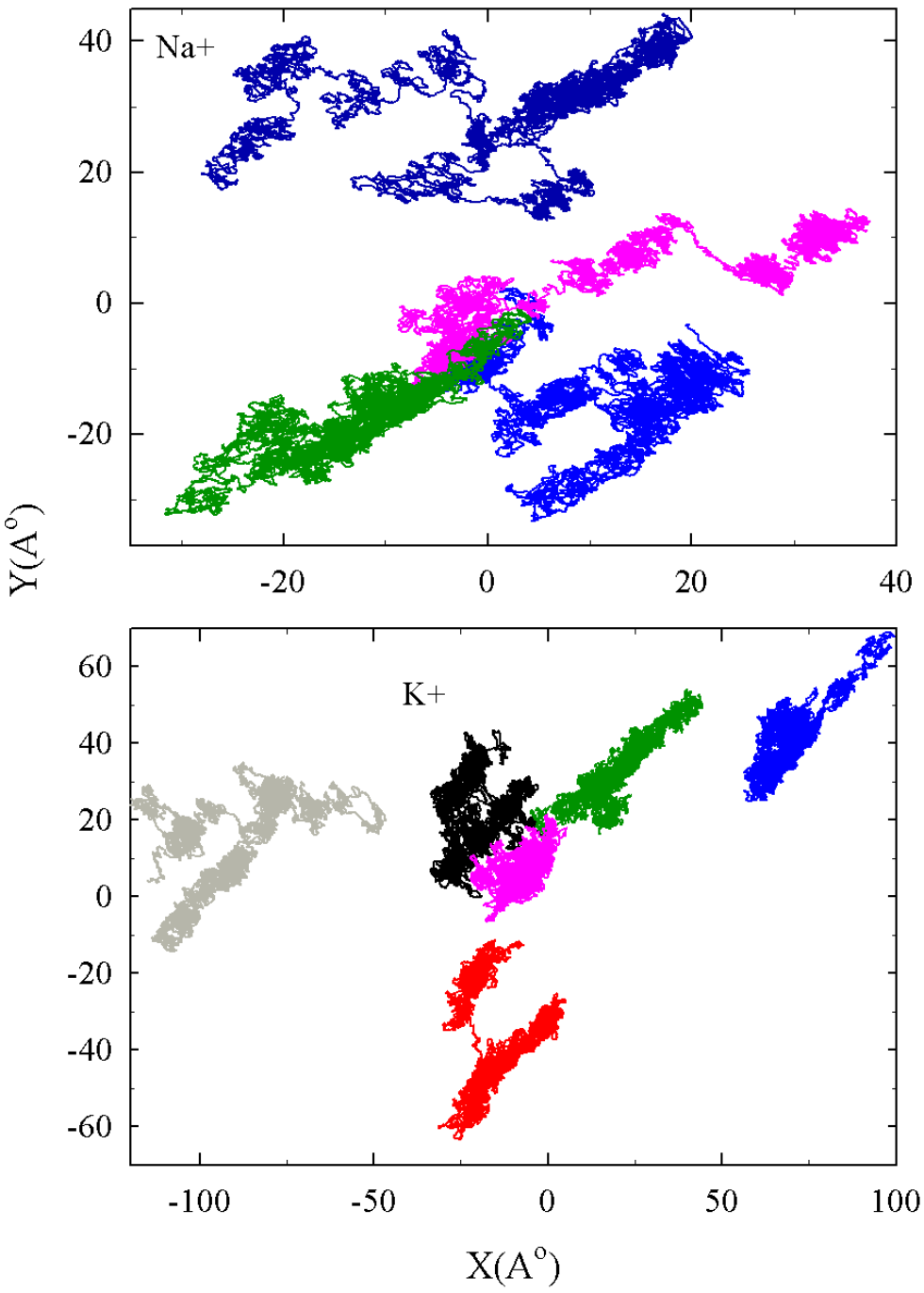

Figure. A6: A plot of projected 1 ns trajectories of the centre-of-mass motions of some arbitrarily selected Na^+ and K^+ ions in the melt at $f = 0.2$. T(K) = 318. Colors represent different trajectories.

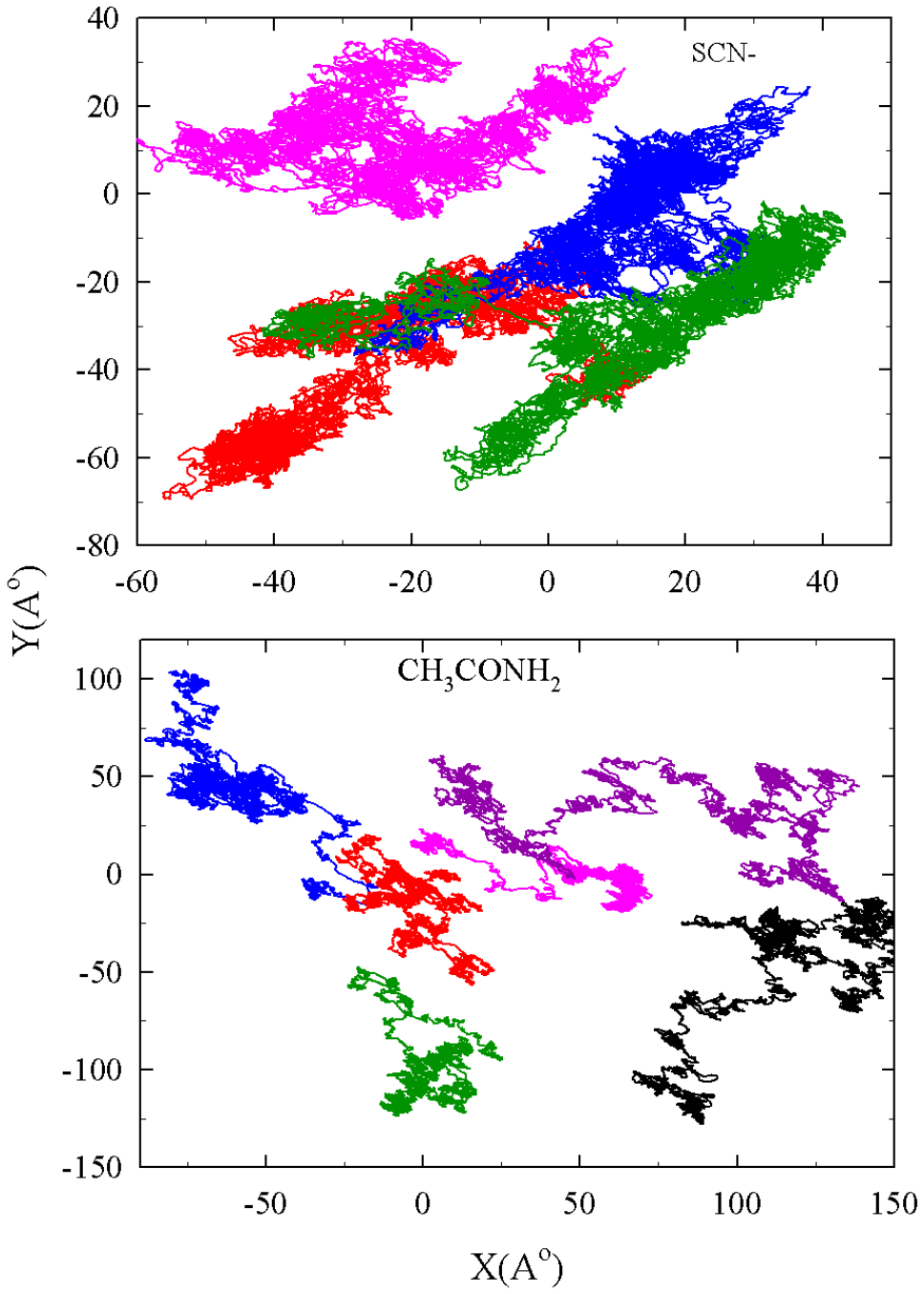

Figure. A7: A plot of projected 1 ns trajectories of the centre-of-mass motions of some arbitrarily selected SCN^- and solvent particles in the melt at $f = 0.2$. T(K) = 318. Colors represent different trajectories.

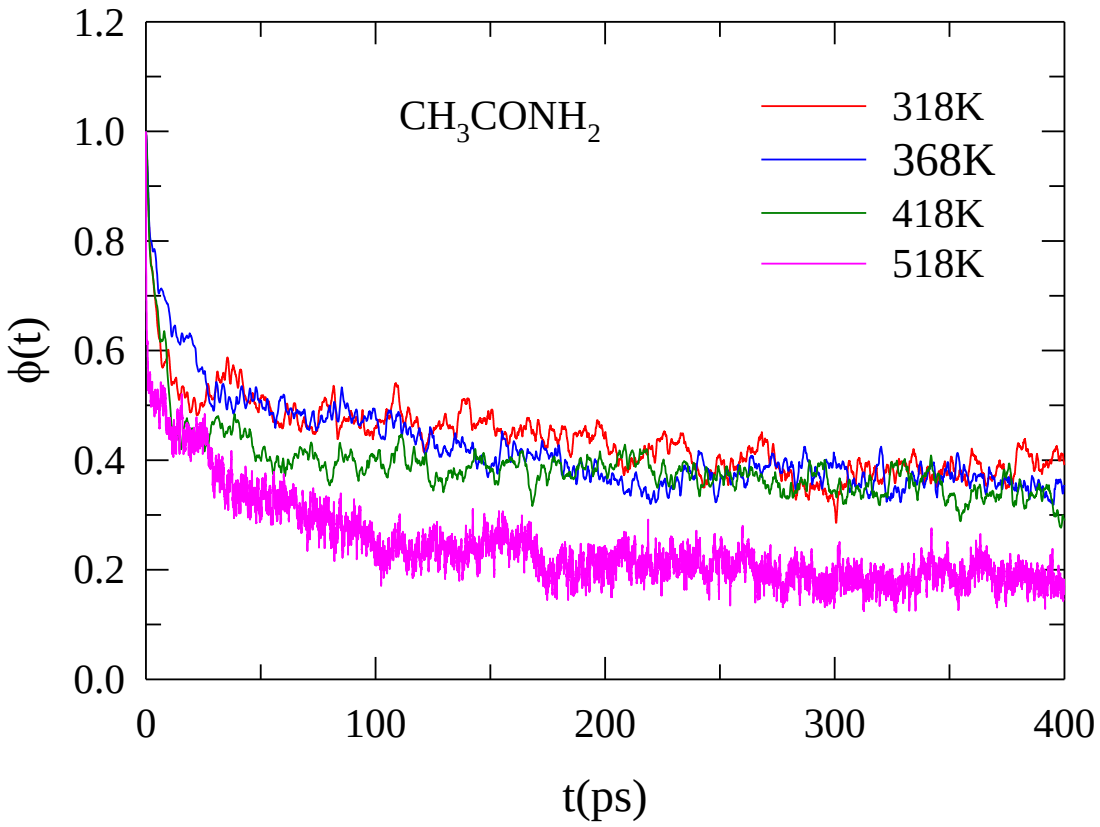

Figure. A8: Temperature dependent decay of collective dipole moment autocorrelation function for acetamide in the melt under study at $f = 0$. Curves are color-coded and described inside the panel.

Appendix B

Table B1 : LJ Parameters for $[Bmim]^+$ and $[PF_6]^-$

ATOM	ε_{ii} (kJ/mol)	σ_{ii} (Å)
CR	0.3598	3.4
NA	0.7113	3.25
CW	0.3598	3.4
H4	0.0628	2.511
H5	0.0628	1.782
CT	0.4577	3.4
H1	0.0657	2.471
HC	0.0657	2.65
P	0.8368	3.742
F	0.2552	3.118

Table B2 : Partial charges on each atom of $[Bmim]^+$ and $[PF_6]^-$

ATOM	q_i (e)
CR	-0.0055
NA(m)	0.0596
NA(a)	0.0682
CW(m)	-0.1426
CW(a)	-0.2183
H5	0.2258
H4(m)	0.234
H4(a)	0.2633
CT(m)	-0.0846
H1	0.1085
CT(a1)	-0.0153
H1	0.0796
CT(a2)	0.0107
HC	0.0204
CT(a3)	0.0309
HC	0.0157
CT(a4)	-0.0713
HC	0.0294
P	0.7562
F	-0.2927

Table B3 : Bond force constant for $[Bmim]^+$ and $[PF_6]^-$

BONDS	r_0(Å)	K_b (kJ mol^{-1} $Å^2$)
CT-CT	1.526	1297
CT-H1	1.08	1423
CW-H4	1.07	1611
CR-H5	1.07	1590
CR-NA	1.325	1674
CW-NA	1.378	1506
CT-NA	1.472	1172
CW-CW	1.343	1715
CT-HC	1.09	1423
P-F	1.6	795

Table B4 : Angle force constant for $[Bmim]^+$ and $[PF_6]^-$

ANGLES	θ_0 (deg)	K_θ (kJ mol^{-1} rad^2)
CT-CT-CT	109.5	167
CT-CT-H1	109.5	159
CT-CT-HC	109.5	155
CT-CT-NA	112.5	293
H1-CT-H1	109.5	146
HC-CT-HC	109.5	142
H1-CT-NA	109.5	230
CW-NA-CT	125.7	209
CR-NA-CT	126.3	209
CW-CW-NA	107.1	502
CR-NA-CW	108	502
NA-CR-NA	109.9	502
H4-CW-NA	122.1	126
H5-CR-NA	125.7	126
CW-CW-H4	130.7	126
F-P-F	90	335

Table B5 : Torsion force constant for $[Bmim]^+$ and $[PF_6]^-$

TORSIONS	δ (deg)	Kχ/2(kJ/mol)	n
Proper torsions			
NA-CR-NA-CW	180	50.21	2
NA-CR-NA-CT	180	8.368	2
H5-CR-NA-CW	180	6.276	2
H5-CR-NA-CT	180	6.276	2
CW-CW-NA-CR	180	50.21	2
CW-CW-NA-CT	180	8.368	2
H4-CW-NA-CR	180	8.368	2
H4-CW-NA-CT	180	6.276	2
NA-CW-CW-H4	180	6.276	2
NA-CW-CW-NA	180	50.21	2
H4-CW-CW-H4	180	6.276	2
CT-CT-CT-H1	0	0.669	3
CT-CT-CT-CT	0	1.046	3
CT-CT-CT-HC	0	0.669	3
NA-CT-CT-CT	0	1.046	3
NA-CT-CT-HC	0	0.669	3
H1-CT-CT-HC	0	0.628	3
HC-CT-CT-HC	0	0.628	3
H1-CT-NA-CW	0	1.021	3
H1-CT-NA-CR	0	0.686	3
CT-CT-NA-CW	0	-0.745	1
CT-CT-NA-CR	0	-0.987	1
Improper torsions			
NA-NA-CR-H5	180	4.602	2
CW-NA-CW-H4	180	4.602	2
CR-CW-NA-CT	180	8.368	2

Table B6 : LJ Parameters for C153

ATOM	σ (Å)	ε (kJ/mol)
C	3.5	0.335
N	3.25	0.7118
O	2.96	0.8796
F	2.8	0.4389
H	2.5	0.2093

Table B7 : Ground state charges on the atoms of C153 used in simulation. See Fig. B2 for atom identity.

ATOM	q_i (e)
CT	0.171
CA	-0.19
CT	0.052
CT	-0.03
CA	0.08
CA	-0.2
CA	0.221
CO	0.374
CM	-0.098
HC	-0.003
HC	0.015
HC	0.018
HA	0.066
HA	0.111
CA	0.243
CT	0.061
CT	0.169
CT	-0.032
HC	0.015
HC	-0.002
HC	0.02
HC	0.021
HC	0.013
CA	-0.195
HC	0.011
HC	0.013
HC	0.018
HC	0.025
NT	-0.379
OS	-0.243
O	-0.287
CT	0.641
CM	-0.017
F	-0.227
F	-0.227
F	-0.229

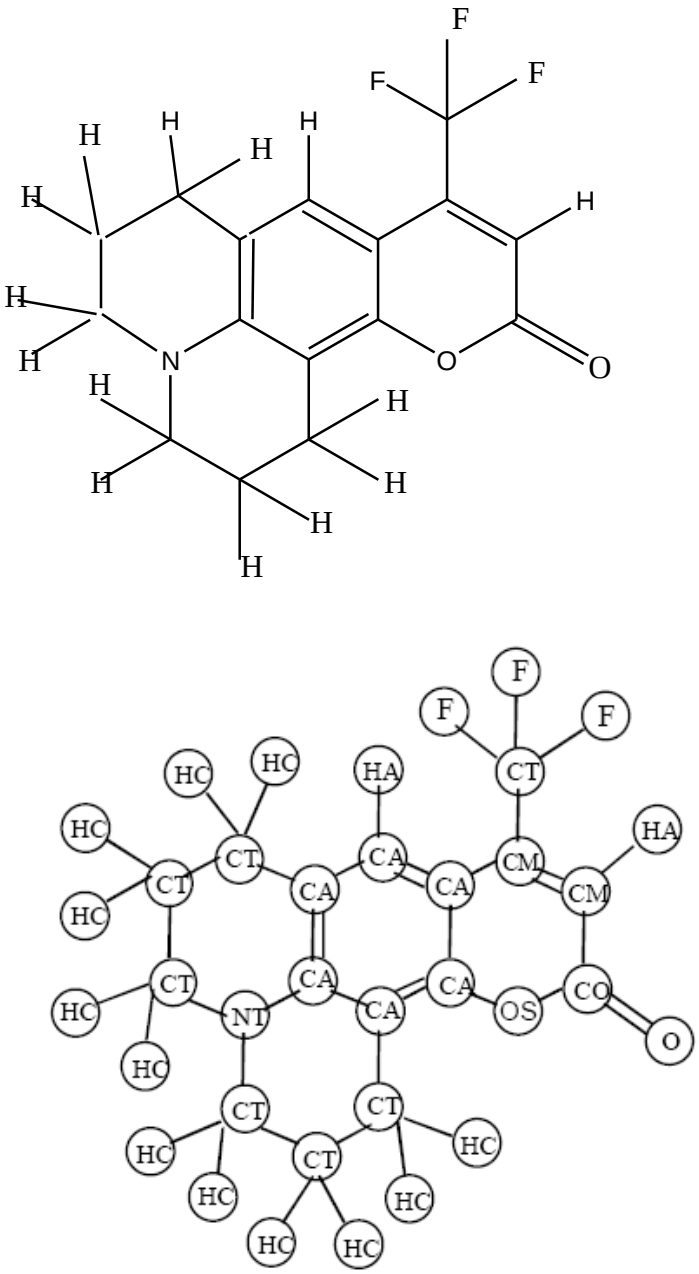

Figure B1 : Chemical structure of the solute , Coumarin 153 (C153) with OPLS force-field atom types

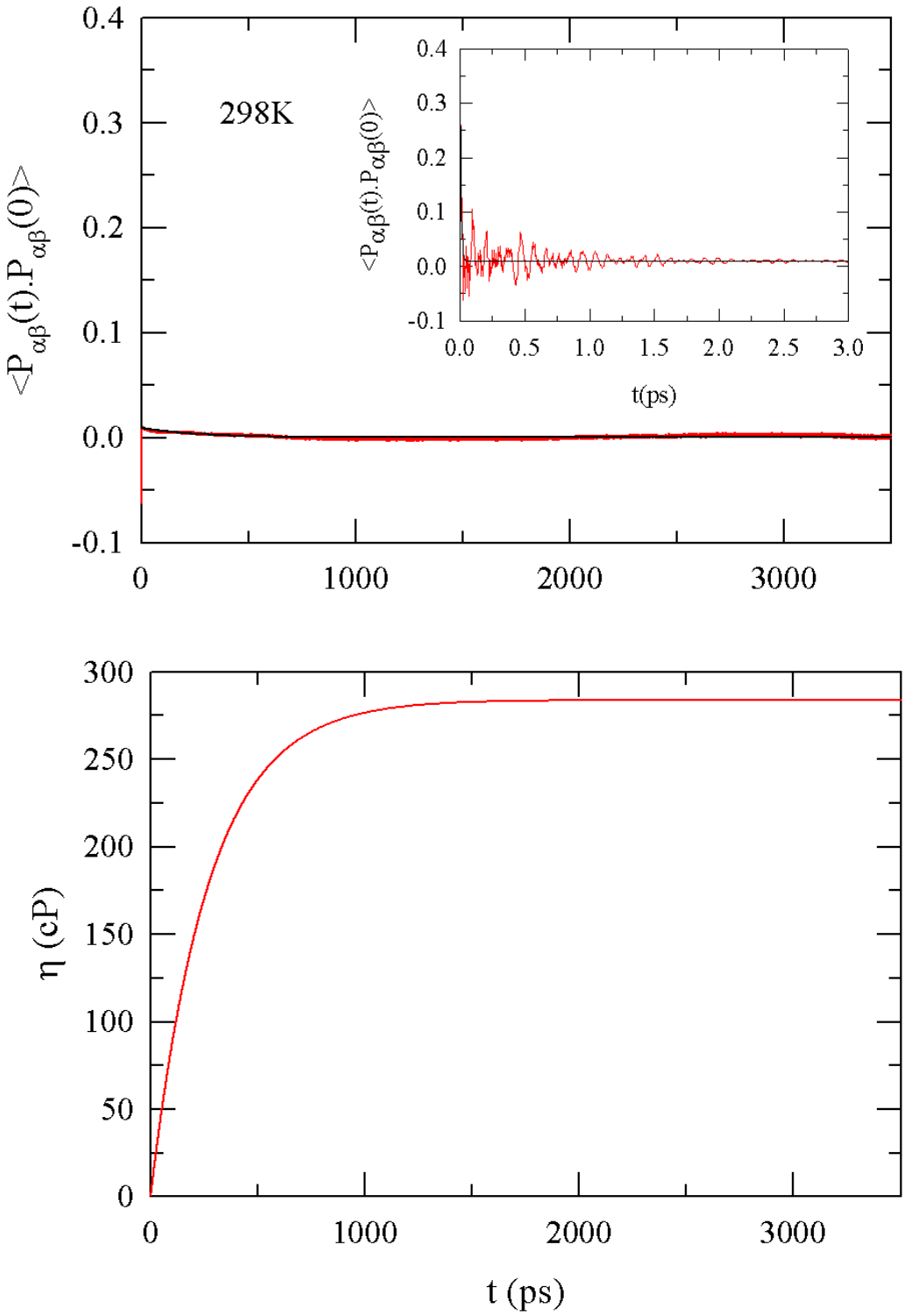

Figure B2: The decay of the pressure autocorrelation function at 298 K is shown in this figure along with bi-exponential fits (upper panel). The computed η from bi-exponential fit to the simulated PACF is also presented as function of upper limit in the lower panel to show the required time-convergence. Strong fluctuations in PACF at short times as shown in the inset of the upper panel.

Appendix C

Table C1: Comparison of temperature dependent $1/e$ decay times between $F_s(k\sigma \to 2\pi, t)$ and $Q(t)$ for $[Bmim]^+$ and $[PF_6]^-$.

T (K)	Ion	τ_α (ns)[a]	$\tau_{1/e}^{Q}$ (ns)[b]
298	$[Bmim]^+$	1.9	3.4
	$[PF_6]^-$	2.1	3.5
450	$[Bmim]^+$	0.05	0.08
	$[PF_6]^-$	0.07	0.10

a) τ_α is assumed to be equal to the time at which normalized $F_s(k\sigma \to 2\pi, t)$ has relaxed to a value of $1/e$. That is, $\tau_\alpha \approx \tau_{1/e}^{F_s}$

b) $\tau_{1/e}^{Q}$ represents a time at which normalized $Q(t)$ relaxes to a value of $1/e$.

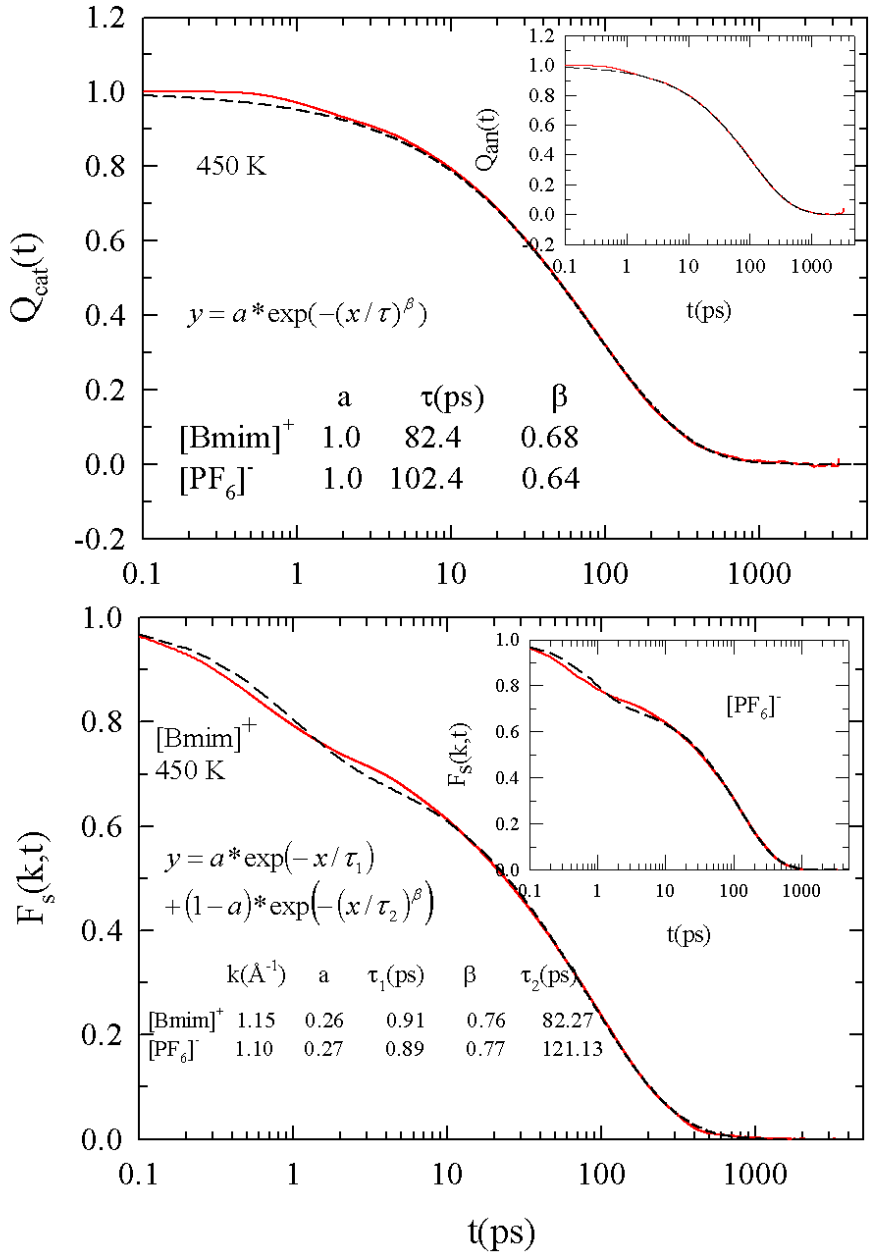

Figure. C2: Normalized decays of overlap function, Q(t) (upper panel), and self dynamic structure factor at the nearest neighbour wavenumber, $F_s(k,t)$ (lower panel) at 450 K and their fits for $[Bmim]^+$ and [PF6]-. Fit parameters are shown inside the panels. $Q_{cat}(t)$ denotes relaxation of overlap function for $[Bmim]^+$ and $Q_{an}(t)$ for $[PF_6]^-$.

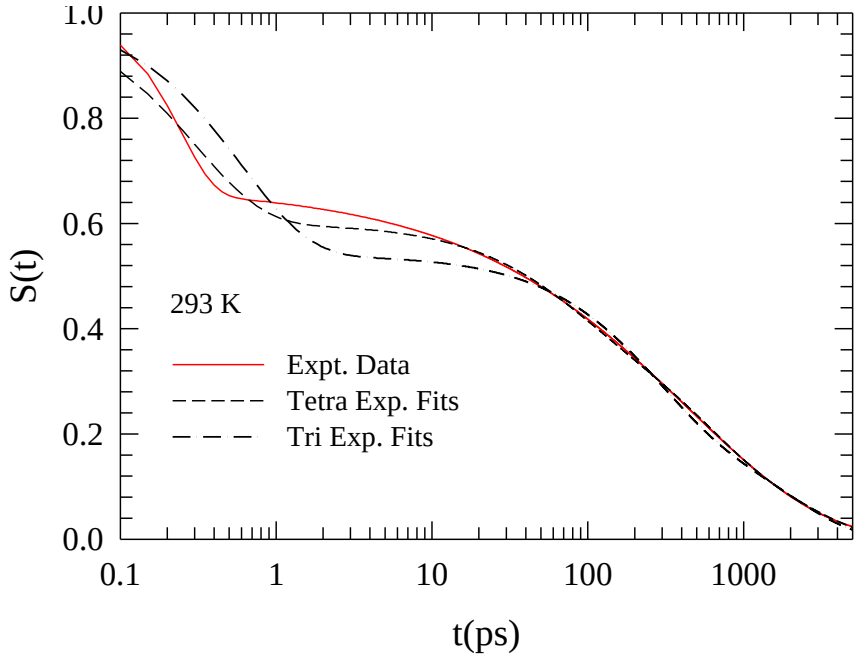

Figure. C3 Experimental solvation response function obtained using C153 in [Bmim][PF_6] in complete measurements at ~293 K and multi-exponential fits through it. Note the experimental response is represented by a (Gaussian + stretched exponential) fit as described in the original paper. In the table below, fit parameters are summarized for a comparison.

Data	a_1	τ_1(ps)	a_2	τ_2(ps)	a_3	τ_3(ps)	a_4	τ_4(ns)	β
Our Simulations at 298 K	0.66	0.22	0.07	89			0.27	11.34	1
Expts at ~293 K; **4**-Exp. fits	0.4	0.31	0.17	68	0.25	488	0.18	2.41	1
Expts at ~293 K; **3**-Exp. fits	0.46	0.61			0.31	252	0.23	1.96	1
Expts at ~293 K; Gaussian + Stretched Exp. fits	0.33	0.24[a]			0.67	450			0.5

a) For this fit, $\tau_1 = \sqrt{2}/\omega_G$, $\omega_G = 5.8\,\text{ps}^{-1}$. Experimental data considered here are from M. Maroncelli and co-workers, J. Phys. Chem. B **117**, 4291 (2013).

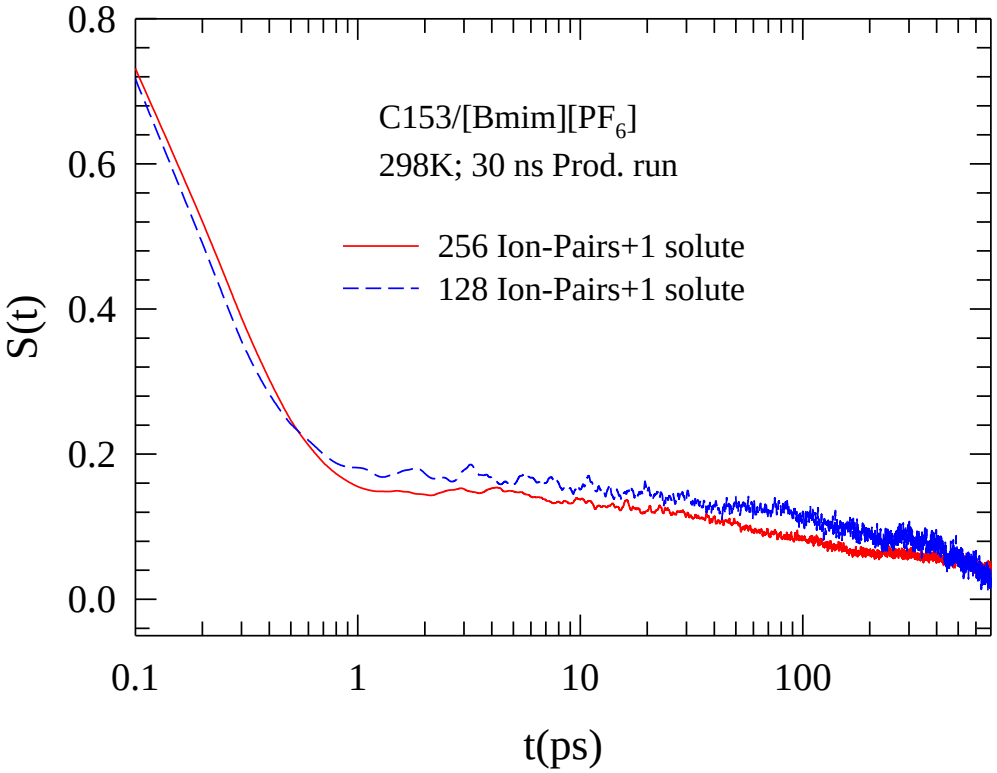

Figure. C4: System size dependence of total solvation response function for C153 in [Bmim][PF_6]. While the blue curve denotes the response function obtained using one C153 molecule in 128 ion pairs, the red curve represents the same obtained using 256 ion pairs. Both curves fit to tri-exponential functions of time. Fit parameters are as follows. For 256 ion pairs: $a_1 = 0.84$, $\tau_1(ps) = 0.23$, $a_2 = 0.07$, $\tau_2(ps) = 30$, $a_3 = 0.09$ and $\tau_3(ps) = 900$; For 128 ion pairs: $a_1 = 0.83$, $\tau_1(ps) = 0.21$, $a_2 = 0.04$, $\tau_2(ps) = 21$, $a_3 = 13$ and $\tau_3(ps) = 556$.

Appendix D

Calculations of number densities and size required for EM calculations of Stokes shift dynamics of C153 in C153 in ([$P_{14,666}$][Cl] + MeOH) binary mixture at 298 K.

For a binary mixture containing x_{IL} mole-fraction of [$P_{14,666}$][Cl] , 30% of its molar concentration has been attributed to ion-pair formation , and $(1-x_{IL})$ of Methanol .The description for effective dipolar component is given by effective molar mass M_{eff} and effective collision diameter σ_{eff} , details of which has already been discussed in text. The mole-fraction weighted total molar mass and total collision diameter of the binary mixture is given by :

$$M_{tot} = x_{IL} M_{IL} + (1-x_{IL}) M_{MeOH} \qquad (D.1)$$

$$\sigma_{tot}^3 = x_{IL}\,\sigma_{IL}^3 + (1-x_{IL})\,\sigma_{MeOH}^3 , \qquad (D.2)$$

where the effective volume of the Ionic liquid molecule is the summation of the volume of the cation and the volume of the anion ,

$$\sigma_{IL}^3 = \sigma_{+}^3 + \sigma_{-}^3 \quad . \qquad (D.3)$$

If the measured experimental density is ρ, then the total number density of the mixture is

$$\rho_N = \frac{\rho N_A}{M_{tot}} . \qquad (D.4)$$

To make the above quantity dimensionless, we multiply it by the mole-fraction weighted total volume of the particles in the binary mixture σ_{tot}^3 , to give the reduced number density

$$\rho_N^* = \frac{\rho N_A}{M_{tot}} \sigma_{tot}^3 \quad . \qquad \text{(D.5)}$$

Now we exemplify this as ,

the reduced number density of the dipolar methanol species

$$\rho_d^* = (1 - x_{IL}) \rho_N^* \ , \qquad \text{(D.6)}$$

reduced number density of the dipolar Ion-pairs in ILs

$$\rho_{IP}^* = 0.3 x_{IL} \rho_N^* \ , \qquad \text{(D.7)}$$

and the reduced number density of the ionic species in ILs

$$\rho_i^* = 2 * 0.7 x_{IL} \rho_N^* \quad . \qquad \text{(D.8)}$$

The total reduced number density of the dipolar species in the binary mixture is

$$\rho_D^* = \rho_d^* + \rho_{IP}^* = (1 - x_{IL}) \rho_N^* + 0.3 x_{IL} \rho_N^* = (1 - 0.7 x_{IL}) \rho_N^* . \qquad \text{(D.9)}$$

Now , if the effective diameter of the dipolar species is

$$\sigma_{eff}^3 = (1 - x_{IL}) \sigma_{MeOH}^3 + 0.3 x_{IL} \sigma_{IL}^3 \ , \qquad \text{(D.10)}$$

and the effective diameter of the ionic species is $\sigma_{eff,i}^3 = \frac{1}{2} \sigma_{IL}^3$. $\qquad$ (D.11)

Hence , the number density of the effective dipolar species $\rho_N^d = \frac{\rho_D^*}{\sigma_{eff}^3}$, $\qquad$ (D.12)

and the number density of the ionic species is , $\rho_N^i = \frac{\rho_i^*}{\sigma_{eff,i}^3}$. $\qquad$ (D.13)

Table D1: IL mole fraction dependent mass density (ρ), number density of dipolar species (ρ_N^d), number density of ionic species (ρ_N^i), viscosity (η),effective dipole moment (μ_{eff}) and dielectric relaxation time (τ_D) required by the EM calculations for the binary mixture of ([$P_{14,666}$][Cl] + MeOH) at 298 K.

x_{IL}	$\rho(g.cm^{-3})$	$\rho_N^d(cm^{-3})$ $\times 10^{-21}$	$\rho_N^i(cm^{-3})$ $\times 10^{-21}$	$\eta(cP)$	μ_{eff} (D)	τ_D (ps)
0.00	0.7862	14.8	0	0.340	2.8	48.0
0.02	0.8091	14.3	0.05	0.988	2.8	2.3
0.03	0.8264	14.1	0.07	1.70	2.7	4.1
0.06	0.8392	12.8	0.15	3.08	2.7	8.4
0.08	0.8510	12.0	0.21	5.79	2.6	16.8
0.12	0.8638	10.6	0.32	14.3	2.4	47.3
0.15	0.8650	9.6	0.41	19.1	2.3	68.9
0.20	0.8750	8.3	0.55	40.3	2.2	164.9
0.35	0.8840	5.5	0.99	150.0	2.0	834.4
0.46	0.8877	4.1	1.31	342.0	2.0	2267.1
0.60	0.8905	2.9	1.73	600.0	2.0	4805.8
0.70	0.8932	2.3	2.02	1040.0	2.1	9348.2
0.88	0.8928	1.5	2.55	1670.0	2.1	17971.7
1.00	0.9073	1.1	2.90	1746.0	2.1	4499.7

Table D2: IL mole-fraction dependent static dielectric constant (ε_0), dielectric constant at infinite frequency (ε_∞), amplitude of the dispersion step (S_j) employed in the EM-calculations for the binary mixture of ([$P_{14,666}$][Cl] + MeOH) at 298 K.

.

x_{IL}	ε_0	ε_∞	S_j
0.00	32.63	2.10	30.53
0.02	29.63	2.10	27.53
0.03	27.67	2.10	25.57
0.06	22.76	2.10	20.66
0.08	20.17	2.10	18.07
0.12	16.20	2.10	14.10
0.15	14.03	2.10	11.93
0.20	11.48	2.10	9.38
0.35	7.95	2.10	5.85
0.46	6.95	2.10	4.85
0.60	6.23	2.18	4.05
0.70	5.85	2.18	3.67
0.88	5.30	2.18	3.12
1.00	5.00	2.18	2.82

Table D3: SM-predicted total shifts and individual interaction contributions at various IL mole fractions for C153 in ([$P_{14,666}$][Cl] + MeOH) binary mixture at 298 K.

x_{IL}	Solute-MeOH dipole-dipole contribution $\Delta\nu_{sd}^{t,MeOH}$ (cm^{-1})	Solute-IP (IL) dipole-dipole contribution $\Delta\nu_{sd}^{t,IP}$ (cm^{-1})	Solute-IL Ion-dipole Contribution $\Delta\nu_{si}^{t}$ (cm^{-1})	Total $\Delta\nu_{tot}^{t}$ (cm^{-1})
0.00	864	0	0	864
0.02	843	13	39	895
0.03	824	15	49	888
0.06	800	22	78	900
0.08	780	25	101	906
0.12	738	31	160	929
0.15	707	35	212	954
0.20	658	41	310	1009
0.35	512	57	619	1188
0.46	409	68	822	1299
0.60	284	83	1057	1424
0.70	201	94	1220	1515
0.88	75	115	1519	1709
1.00	0	130	1721	1851

Table D4: EM-predicted composition dependence of dynamic Stokes shift for C153 in ([$P_{14,666}$][Cl] + MeOH) binary mixture at 298 K.

x_{IL}	Solute-dipole Effective dipole contribution $\Delta\nu_{sd}^{t,eff}$ (cm^{-1})	Ion-dipole Contribution $\Delta\nu_{si}^{t,eff}$ (cm^{-1})	Total $\Delta\nu_{tot}^{t,eff}$ (cm^{-1})
0.00	864	0	864
0.02	853	37	890
0.03	804	47	851
0.06	746	75	821
0.08	663	97	760
0.12	527	156	683
0.15	454	207	661
0.20	377	304	681
0.35	245	610	855
0.46	201	812	1013
0.60	165	1046	1211
0.70	151	1211	1362
0.88	122	1507	1629
1.00	130	1721	1851

Table D5: Fit parameters required to describe the SM-predicted solvation response functions at various IL mole fractions for C153 in ([$P_{14,666}$][Cl] + MeOH) binary mixture at 298 K.

S(t) x_{IL}	a_1	τ_1 (ps)	a_2	τ_2 (ps)	a_3	τ_3 (ps)	a_4	τ_4 (ps)	$\langle \tau_{solv} \rangle$ (ps)
0.00	0.35	0.15	0.37	1.00	0.26	3.94	0.02	8.19	1.6
0.02	0.34	0.14	0.37	1.00	0.27	4.29	0.02	9454.9	190.7
0.03	0.34	0.14	0.37	1.01	0.25	4.35	0.04	9554.6	383.7
0.06	0.34	0.14	0.37	1.10	0.23	4.64	0.06	9678.1	582.2
0.08	0.34	0.15	0.37	1.18	0.2	4.93	0.09	9728.9	877.1
0.12	0.49	0.28	0.39	3.05	0.06	2070.5	0.06	17792.3	1193.1
0.15	0.47	0.28	0.37	3.05	0.07	2125.6	0.09	17884.2	1759.6
0.20	0.45	0.28	0.35	3.06	0.09	2181.1	0.11	17957.9	2172.9
0.35	0.36	0.28	0.28	3.07	0.16	2253.1	0.20	18093.7	3980.2
0.46	0.30	0.29	0.24	3.08	0.21	2276.3	0.25	18131.3	5011.7
0.60	0.23	0.29	0.17	3.12	0.28	2293.6	0.25	18159.3	5182.6
0.70	0.17	0.29	0.13	3.15	0.32	2301.7	0.38	18172.5	7642.6
0.88	0.07	0.31	0.05	3.44	0.41	2312.2	0.47	18189.3	9497.2
1.00	0.31	1596.5	0.33	7253.9	0.36	23576.2			11376.1

Table D6 : Fit parameters required to describe the EM-predicted solvation response functions at various IL mole fractions for C153 in ($[P_{14,666}][Cl]$ + MeOH) binary mixture at 298 K.

S(t) x_{IL}	a_1	τ_1 (ps)	a_2	τ_2 (ps)	a_3	τ_3 (ps)	$\langle \tau_{solv} \rangle$ (ps)
0.02	0.57	0.25	0.42	0.72	0.01	65.79	1.1
0.03	0.57	0.48	0.41	1.34	0.02	99.00	2.8
0.06	0.58	1.17	0.38	3.10	0.04	175.44	8.9
0.08	0.59	2.53	0.37	6.20	0.04	400.00	19.8
0.12	0.65	8.43	0.28	20.41	0.07	1111.11	88.9
0.15	0.69	13.78	0.23	33.33	0.08	1428.57	131.5
0.20	0.75	38.46	0.14	125.00	0.11	3333.33	413.0
0.35	0.70	250.0	0.10	2500.0	0.20	11003.5	2625.7
0.46	0.66	666.67	0.11	3333.3	0.23	19634.8	5322.7
0.60	0.60	1666.7	0.20	10764.3	0.20	32843.9	9721.7
0.70	0.52	3333.3	0.26	14872.1	0.22	46044.8	15729.9
0.88	0.29	5000.0	0.48	13869.6	0.23	45390.59	18547.2

Addendum I

Composition Dependence of Dynamic Heterogeneity in Binary Mixtures of 1-octyl-3-methylimidazolium Tetrafluoroborate with Water: Initial Simulation Results

I. Introduction

Here we present initial results of our molecular dynamics simulation study of binary mixtures of 1-octyl-3-methylimidazolium tetrafluoroborate ([Omim][BF_4]) and water (H_2O). We have considered five different mixture compositions at 298 K. Composition dependence of dynamic heterogeneity in ([Omim][BF_4] + H_2O) is the primary focus in this work. Microscopic phase segregation and domain formation in ILs is a well-discussed aspect. [1-7] Some ILs are known to be hygroscopic,[8,9] and the miscibility of an IL with water is determined by the hydrophilicity of halides present in an ILs as counter ions.[9-11] Addition of water in a given IL changes viscosity which strongly influences the ion translation and rotation in binary mixtures.[7,12-15] Tiime dependent fluorescence studies[16] report the dramatic changes in interaction between ions in presence of water via showing faster relaxation dynamics. Temporal heterogeneity and its connection to mass transport for neat ILs has been investigated in a few study.[19-21] In this study we focus on how a strongly polar small molecular solvent, such as water, influences the dynamic heterogeneity of a neat IL.

II. Computational Details

Molecular dynamics simulations of mixtures of 3-site rigid SPC/E water and 42-site flexible [Omim][BF_4] were performed using Mdynamix package [20] at 298 K. The mole-fractions of IL investigated were f = 0.0, 0.2, 0.4, 0.6, 1.0. The number of ion-pairs used in the system and their respective box-lengths are given in Table Ad.1. The chemical structures of the cation and anion of IL alongwith the force field atom types are shown in Fig. Ad.1.

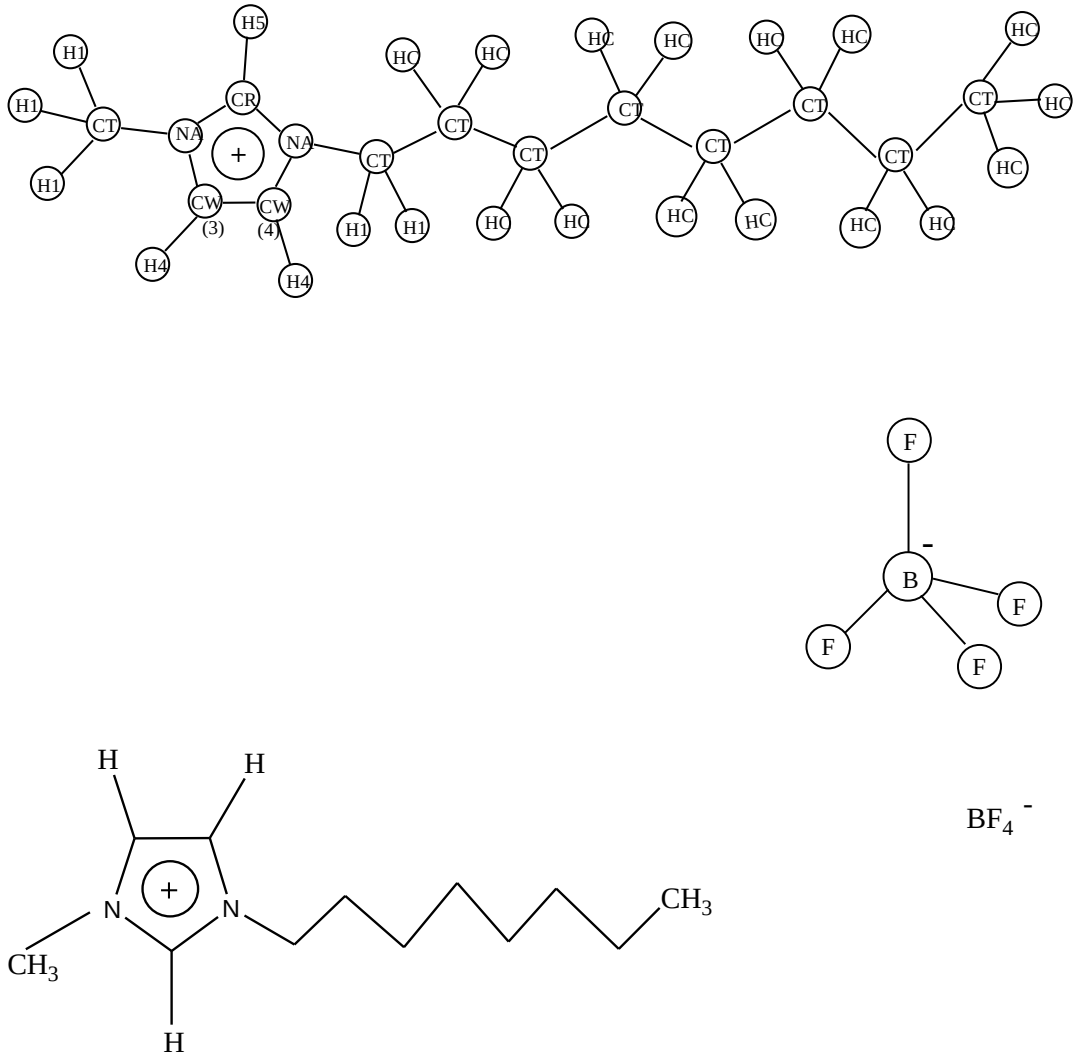

Figure Ad.1. Chemical structure of [Omim][BF_4]

All the atoms interacted via AMBER-type [21,22] force field as already mentioned in various chapters of the Thesis. The functional form for the total potential energy is given by

$$V_{tot} = \sum_{bonds} k_b (r - r_0)^2 + \sum_{angles} k_\theta (\theta - \theta_0)^2 + \sum_{dihedrals} k_\chi [1 + \cos(n\chi - \delta)] + \sum_{i=1}^{N-1} \sum_{j>i}^{N} \left\{ \varepsilon_{ij} \left[\left(\frac{r_{min,ij}}{r_{ij}} \right)^{12} - \left(\frac{r_{min,ij}}{r_{ij}} \right)^{6} \right] + \frac{q_i q_j}{r_{ij}} \right\}, \quad \text{(Ad.1)}$$

Simulations were carried out in a cubic box having periodic boundary conditions. The minimum energy geometry of the $[Omim]^+$ and $[BF_4]^-$ was determined by performing the ab-initio calculations at the HF/6-31+G(d) level of theory and setting the cation and anion charges at +1 and -1, respectively. The partial atomic charges and van der Waals parameters ε_i and σ_i were taken from Ref. 22 . Those were used for obtaining the interaction between two different atom types via the Lorentz-Berthelot combination rules [23], $\varepsilon_{ij} = \sqrt{\varepsilon_i \varepsilon_j}$ and $\sigma_{ij} = (\sigma_i + \sigma_j)/2$. For water , the well-known SPC/E model developed by Berendsen et al. [24] was used . Simulations were performed in a cannonical ensemble using the Nose-Hoover thermostat, [25,26] with coupling constant of 200 fs. Verlet Leapfrog algorithm [23] with 2 fs time step was used to solve classical equations of motion. Electrostatic interactions were handled via the Ewald summation technique.[23] The system was equilibrated for 10 ns at 298 K and the production run of 40ns trajectory was saved at a time gap of 100fs . Prior to NVT run the system was initially equilibrated in NPT ensemble. Subsequently, it was cooled down in step-wise process from 450 K to generate the minimum energy configuration at 298 K . This pre-equilibrated stable configuration was utilized for the final NVT run. This protocol was followed for all compositions studied.

Table Ad.1 : System sizes for different mixture compositions

f	Nos. Of water molecules	Nos. Of $[Omim]^+$ molecules	Nos. Of $[BF_4]^-$ molecules	Simulation cell (X,Y,Z) Å
0.0	256	0	0	19.75,19.75,19.75
0.2	204	52	52	30.29,30.29,30.29
0.4	154	102	102	36.09,36.09,36.09
0.6	102	154	154	40.86,40.86,40.86
1.0	0	128	128	38.01,38.01,38.01

III. Results and Discussion

Diffusion coefficient

Fig. Ad.2 displays the simulated mean square displacement [23] (MSD) curves for water and both the ions in ([Omim][BF_4] + H_2O) mixture at various compositions. Subsequently, translational diffusion coefficients have been calculated from these simulated MSDs. At short times , the dynamics is guided by the inertial motions, followed by intermediate sub-diffusive terrain, and finally a linear diffusive regime appears where particle motions undergo diffusive translation. Diffusion coefficients have been calculated from this linear part of the curve. Note the sub-diffusive region suggests particle rattling in a cage formed by neighbours. As concentration of water increases in the mixture, the extent of the plateau decreases. Understandably, the plateau region is the most pronounced for the neat IL ($f = 1.0$) as shown in the middle panel. Attenuated total reflectance (ATR) and transmission IR spectroscopic studies [9] have revealed the presence of strong H-bonding between water and two $[BF_4]^-$. Similarly, interaction between the most acidic H-atom (H5) on the imidazolium ring with the oxygen atom of water molecule has been substantiated by comparative study of preferential location of polar solvents [6] in ILs . Thus, water acts as a lubricating agent via screening the Coulomb interactions between oppositely charged ions, enhancing diffusion of ions.

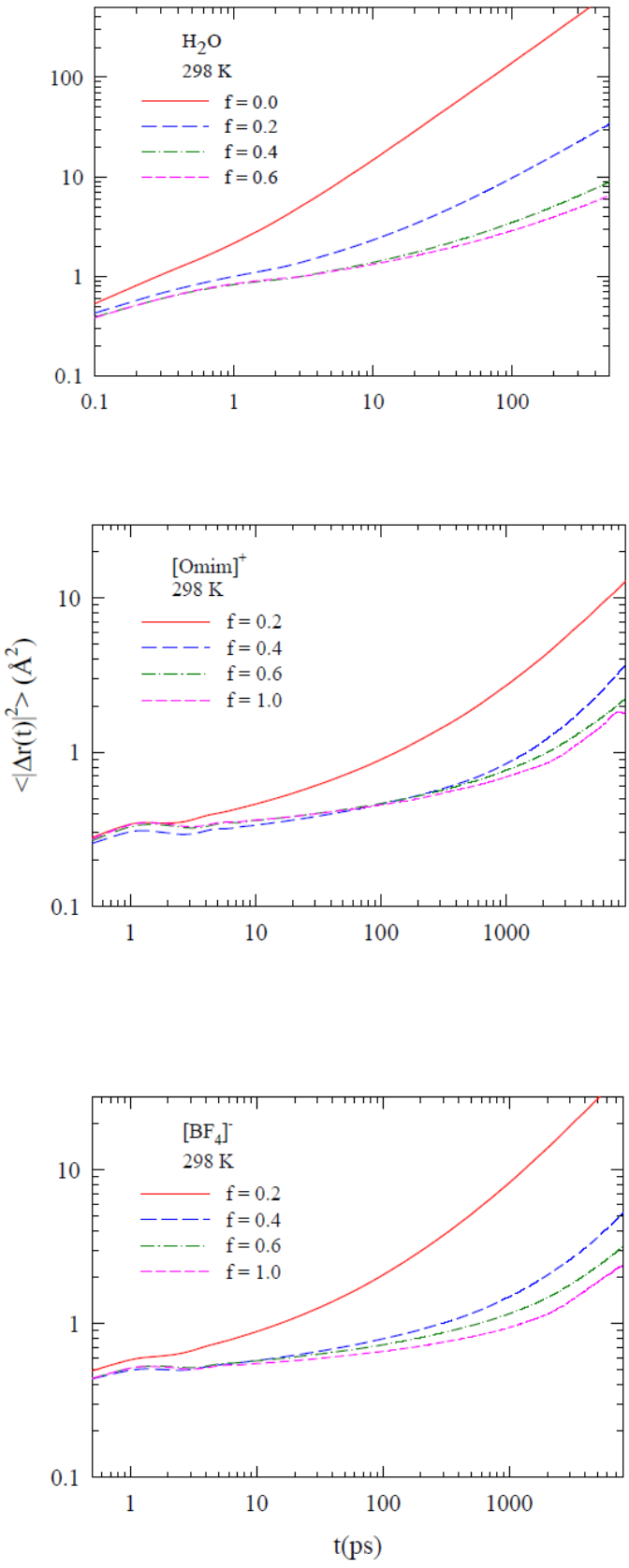

Figure Ad.2. Composition dependence study of simulated MSDs for water (upper panel) , cation (middle panel), and anion(lower panel) at 298 K .

Non-Gaussian and New Non-Gaussian parameter :

We follow our earlier prescription for studying dynamic heterogeneity via calculating the non-Gaussian (NG) and new non-Gaussian (NNG) parameters defined respectively by $\alpha_2(t)$ and $\gamma(t)$.[27-30] Necessary expressions for calculating these quantities from the simulated particle displacements are already given in chapter 5 of the thesis. The timescales associated with the peaks of these parameters are denoted by τ_{NG} and τ_{NNG}. These peaks indicate particles of different mobilities reflecting the presence of DH. Fig. Ad.3 illustrates the DH for the pure components at 298 K . In case of H_2O both the parameters are not much separated in peak-times. In addition, $\alpha_2(t) \approx 0.2$, which reflects homogeneous medium as in hot liquids. For the IL, however, we notice that τ_{NG} and τ_{NNG} for the anion occurs at shorter timescales than those for the cation. Fig. Ad.4 depicts the composition dependence of the $\alpha_2(t)$ for the three components in the binary mixture. As IL concentration increases, the peak-time, τ_{NG}, shifts toward longer timescale. This may be attributed to the increase in medium viscosity upon addition of IL in the mixture which makes every particle slow. Composition dependence of the simulated $\gamma(t)$ is shown in Fig. Ad.5. Note here that for all the three components, $\tau_{NNG} > \tau_{NG}$. Noise seen in these curves can be filtered out via better averaging if we carry out longer simulation runs. Even with such a lacuna, the difference between these timescales cannot be missed, signalling presence of inherent slow timescales for all the species. These slow timescales are expected to be reflected in other dynamical studies, for example, in time-resolved fluorescence Stokes shift dynamics measurements. These predictions should be tested in experiments.

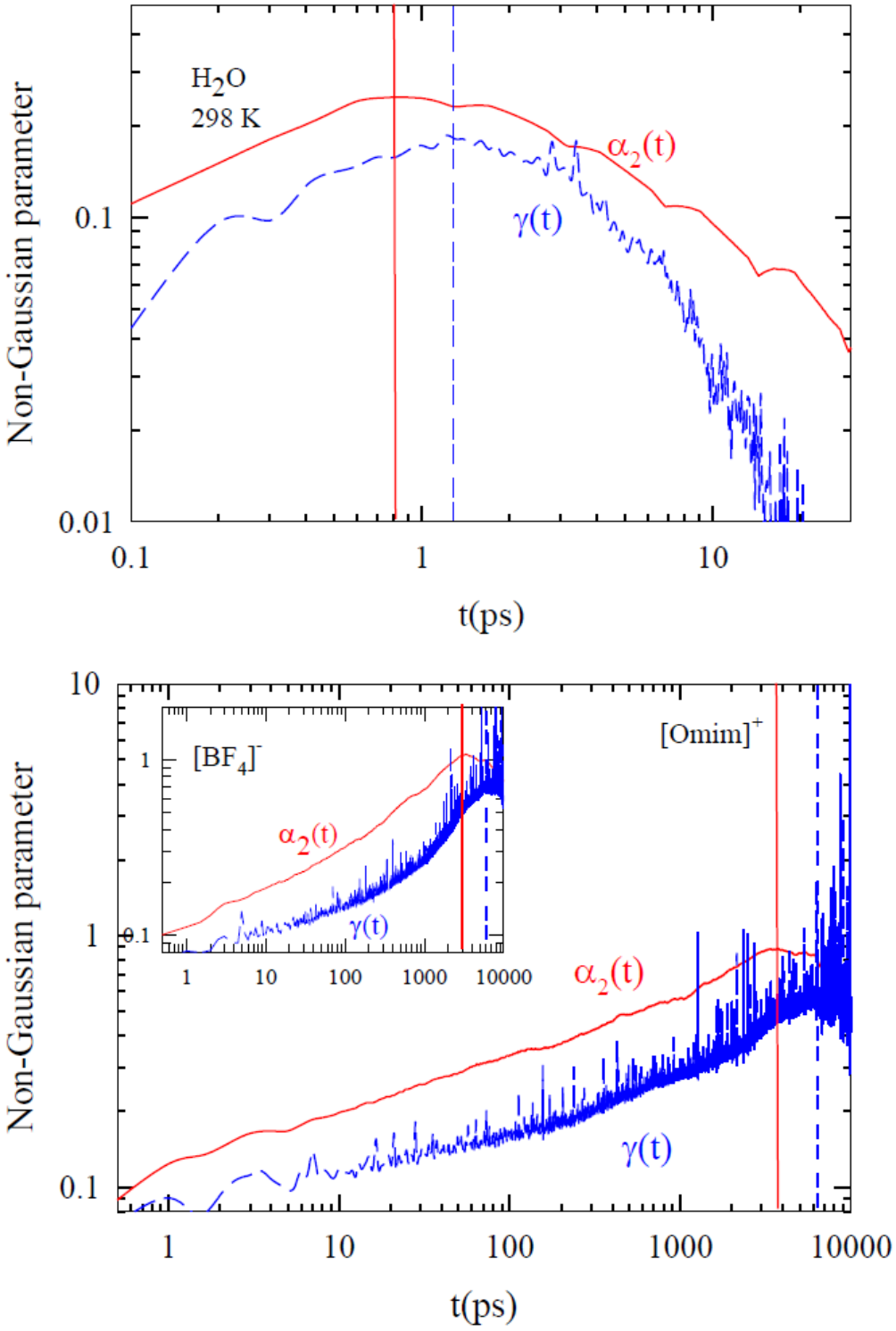

Figure Ad.3. Comparison between the simulated NG and NNG parameters, $\alpha_2(t)$ and $\gamma(t)$ respectively, for H_2O(upper panel) and $[Omim]^+$ (lower panel) with $[BF_4]^-$ provided inset at 298 K. While the solid lines denote $\alpha_2(t)$, dashed lines represent $\gamma(t)$. Vertical lines indicate peak times for the NG parameter and the NNG parameter .

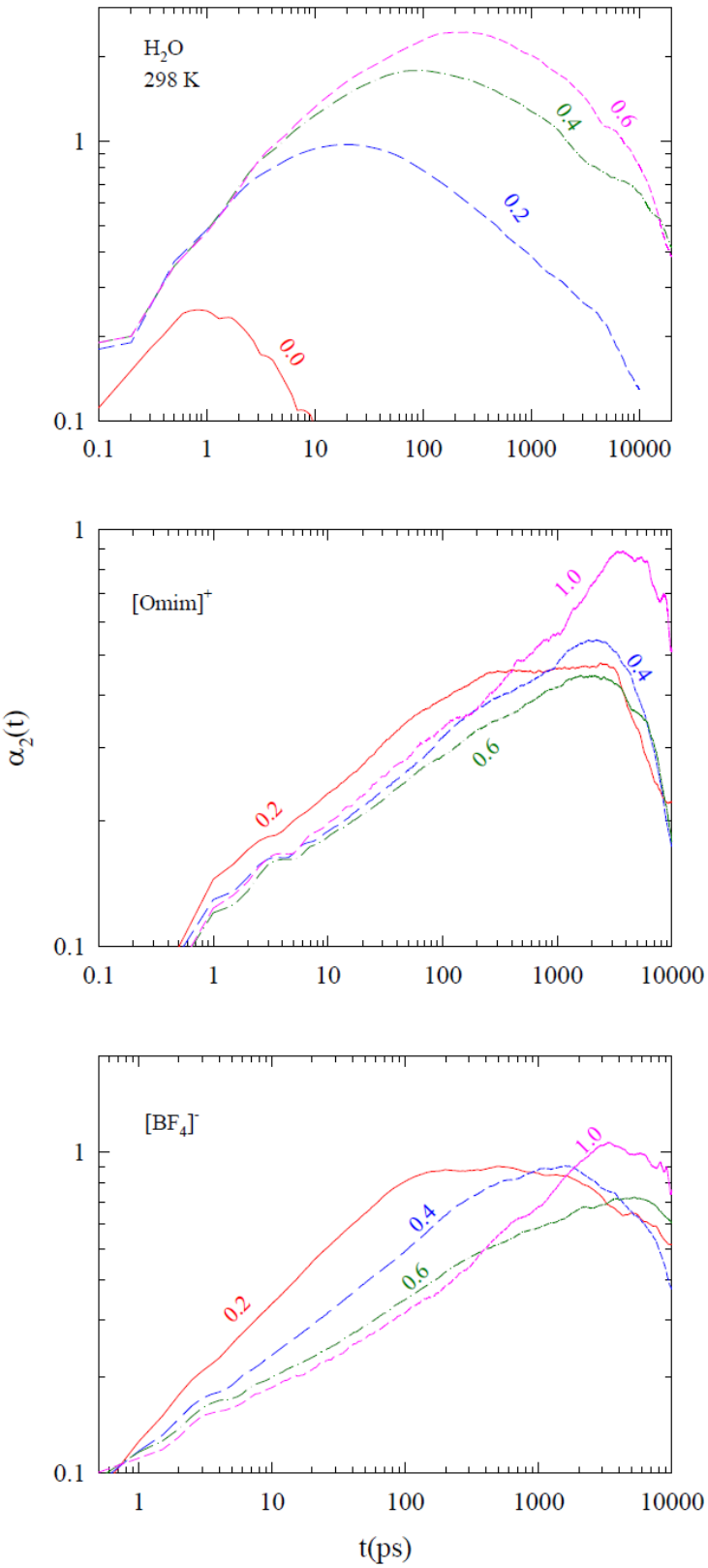

Figure Ad.4. Mixture composition dependence of the simulated non-Gaussian parameter for water (upper panel) , cation (middle panel), and anion(lower panel) at 298 K .

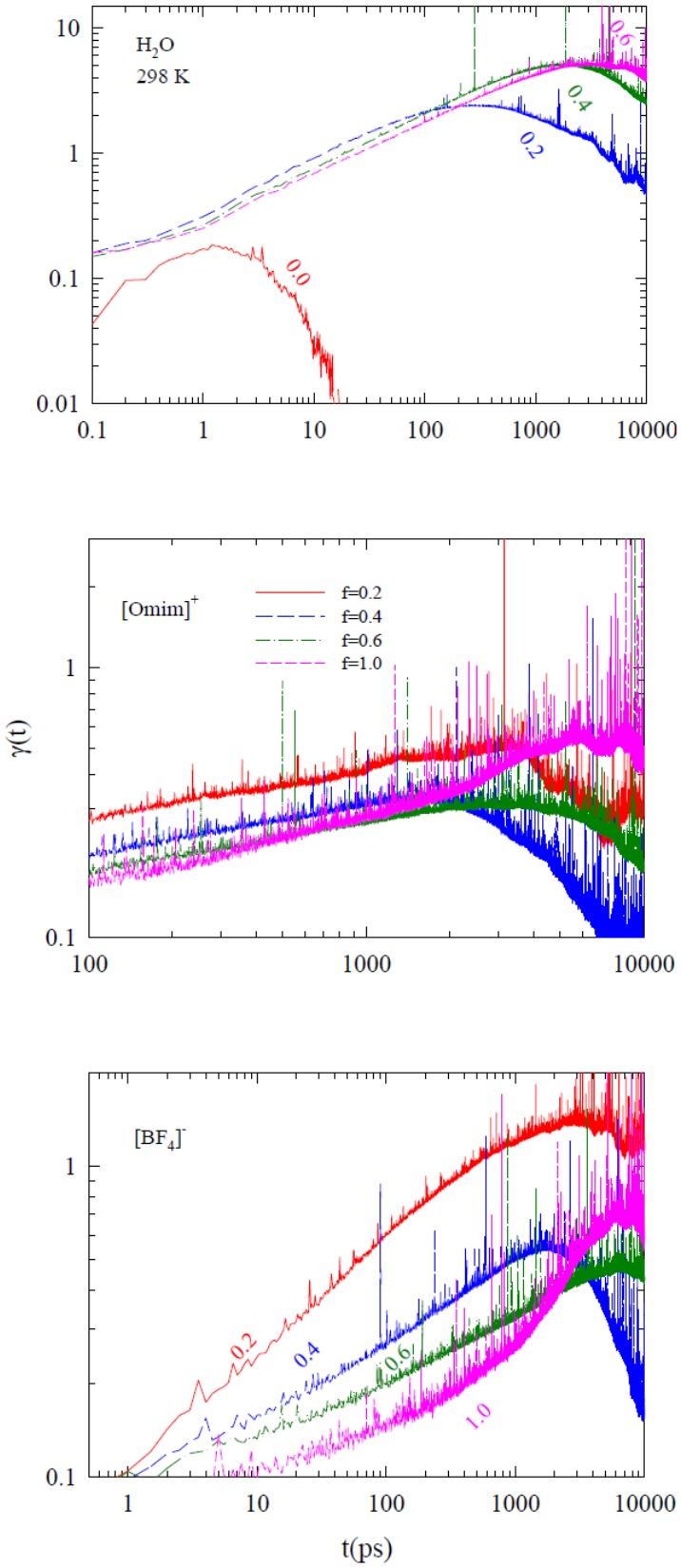

Figure Ad.5. Composition dependence of the simulated new non-Gaussian parameter for water (upper panel) , cation (middle panel), and anion(lower panel) at 298 K.

References :

1. Y. Wang and G. A. Voth, J. Am. Chem. Soc. **127**,12192(2005).
2. J. Dupont , J. Braz. Chem. Soc. **15**, 341 (2004).
3. Triolo, O. Russina, B. Fazio, R. Triolo, and E. D. Cola, Chem. Phys. Lett. **467**,362(2008).
4. C. Hardacre, J. D. Holbrey, C. L. Mullan, T. G. A. Youngs, and D. T. Bowron, J. Chem. Phys. **133**, 074510 (2010).
5. K. Shimizu , C. E. S. Bernardes and J. N. C. Lopes , J. Phys. Chem. B **118**, 567 (2014).
6. J. N. C. Lopes , M. F. C. Gomes, and A. A. H. Padua , J. Phys. Chem. B. Lett. , **110** , 16816 (2006).
7. W. Jiang , Y. Wang and G. A. Voth , J. Phys. Chem. B. **111** , 4812 (2007).
8. S. N. V. K. Aki , J. Brennecke, and A. Samanta , Chem. Commun. 413 (2001).
9. L. Cammsrata , S. G. Kazarian , P. A. Salter , and T. Welton, Phys. Chem. Chem. Phys. **3** , 5192 (2001).
10. S. R. Rubero and S. Baldelli , J. Am. Chem. Soc , **126**,11788 (2004).
11. P. Yee , J. K. Shah and E. J. Maginn , J. Phys. Chem. B. **117**,12556 (2013).
12. H. V. R. Annapureddy , Z. Hu ,J. Xia and C. J. Margulis , J. Phys. Chem. B,**112** ,1770 (2008).
13. C. G. Hanke and R. M. Lynden-Bell , J. Phys. Chem. B. **107**,10873 (2003).
14. A. R. Porter , S. Y. Liem and P. L. A. Popelier , Phys. Chem. Chem. Phys. , **10** , 4240 (2008).
15. A. L. Sturlaugson , K. S. Fruchey, and M. D. Fayer , J. Phys. Chem. B , **116** , 1777(2012).
16. D. Chakrabarty , A. Chakraborty , D. Seth, and N. Sarkar , J. Phys. Chem. A , **109** , 1764 (2005).
17. A. M. Funston, T. A. Fadeeva, J. F. Wishart, and E. W. Castner, Jr., J. Phys. Chem. B. **111**, 4963 (2007).
18. O. Yamamuro, T. Yamada, M. Kofu, M. Nakakoshi, and M. Nagao, J. Chem. Phys. **135**, 054508 (2011).
19. T. Pal and R. Biswas , J. Chem. Phys.(2014) (submitted).
20. A. P. Lyubartsev and A. Laaksonen, Comput. Phys. Commun. **128** ,565 (2000).

21. W. D. Cornell, P. Cieplak, C. I Bayly, I. R. Gould, K. M. Merz, D. M. Ferguson, D. C. Spellmeyer, T. Fox, J. W. Caldwell, and P. A. Kollman, J. Am. Chem. Soc. **117**, 5179 (1995).
22. Z. Liu, S. Huang, W. Wang, J. Phys. Chem. B **108 ,**12978 (2004) .
23. M. P. Allen and D. J. Tildesley, Computer Simulations of Liquids, Oxford, NY. (1987).
24. H. J. C. Berendsen , J. R. Grigera and T. P. Straatsma, J. Phys. Chem. **91**,6269 (1987).
25. S. Nose, J. Chem. Phys. **81** , 511 (1984).
26. W. G. Hoover, Phys. Rev. A **31** ,1695 (1985).
27. A. Rahman, Phys. Rev. **136**, 405 (1964).
28. T. Pal and R. Biswas, Theor. Chem. Acc. **132**,1348 (2013)
29. E. Flenner and G. Szamel, Phys. Rev. E. **72**, 011205 (2005).
30. K. Kim and S. Saito, J. Chem. Phys. **133**, 044511 (2010).